The Influence of Vertical Reinforcement and Lateral Confinement on the Axial Capacity of Masonry Block Walls

A Thesis
Submitted to the College of Graduate Studies and Research
In Partial Fulfillment of the Requirements
for the
Degree of Master of Science
in the
Department of Civil Engineering
University of Saskatchewan
Saskatoon

by
Anna Paturova

PERMISSION TO USE

The author has agreed that the library, University of Saskatchewan, may make this thesis freely available for inspection. Moreover, the author has agreed that permission for extensive copying of this thesis for scholarly purposes may be granted by the professors who supervised the thesis work recorded herein or, in their absence, by the head of the Department or the Dean of the College in which the thesis work was done. It is understood that due recognition will be given to the author of this thesis and to the University of Saskatchewan in any use of the material in this thesis. Copying or publication or any other use of the thesis for financial gain without approval by the University of Saskatchewan and the author's written permission is prohibited.

Requests for permission to copy or to make any other use of material in this thesis in whole or part should be addressed to:

Head of Department of Civil Engineering
University of Saskatchewan
Engineering Building
57 Campus Drive
Saskatoon, Saskatchewan
Canada, S7N 5A9

ABSTRACT

Concrete masonry is a multi-component structural system. In the case of reinforced concrete masonry, the system includes the concrete units, the mortar, the reinforcing steel and the grout fill. Placing vertical steel reinforcing bars in the cores of the concrete units enhances the flexural strength of the wall. The vertical steel, when subjected to compression at moderate strain levels, must be confined to improve its resistance to buckling and to improve the effectiveness of the grout around the reinforcing bar. Based on the well established behaviour of reinforced concrete systems, it seems reasonable to presume that the primary means of enhancing ductility is to provide lateral confining steel at closely-spaced intervals to effectively increase the ultimate compressive strain in the grout. It may be assumed that transverse reinforcement in concrete masonry provides lateral confinement to the core so that the axial compressive strength of the grout is enhanced and the ductility improved.

The focus of this study was to investigate the effect of vertical reinforcement and lateral confinement on the axial capacity of short partially grouted concrete masonry walls built in running bond. In order to better understand the structural behaviour of both confined and unconfined concrete masonry, it is important to have some knowledge of the load-displacement behaviour, stress-strain behaviour and failure modes of the masonry walls with different configurations of vertical and lateral reinforcement.

An experimental study was performed to investigate the behaviour of partially grouted concrete masonry block walls under axial loading. Three types of test specimens of partially grouted concrete block masonry walls were tested: (1) specimens with a grouted core only; (2) specimens with a grouted core and vertical reinforcement (i.e. no confinement); and (3) specimens with a grouted core, vertical reinforcement and spiral

confinement in the grouted cores. In total, thirty short wall specimens were tested to failure.

The structural behaviour of vertically reinforced, laterally confined walls was compared to vertically reinforced, unconfined walls, as well as to unreinforced, unconfined masonry walls. The test results indicated that vertical reinforcement of the grouted core did not have a significant positive effect on the failure modes and strength of the short masonry walls. Due to problems with adequate compaction, the lateral confinement provided by the spiral reinforcement had a slightly negative effect on the compressive strength of concrete masonry walls built in running bond. Vertical reinforcement and lateral confinement of the grouted core had some positive effect on the ductility. From a comparison of the ductility for all three types of specimens it was found that both the vertical reinforcement and lateral confinement of the core had a beneficial influence on the post-peak ductility.

In general, similar crack patterns and failure modes were observed in all three types of specimens. Vertical cracks that progressed through the end faces of the concrete blocks and mortar joints, suggesting that the lateral expansion of the grouted core contributed to tensile splitting stresses in walls. All walls failed in a compression-tension stress state, which featured spalling away of the block shells and vertical tensile splitting on the end faces.

ACKNOWLEDGEMENTS

The Author wishes to express her deepest gratitude and appreciation to Dr. Bruce Sparling and Dr. Leon Wegner for their patient guidance, endless support and assistance. Their continued constructive comments, suggestions and input have helped to improve and prepare this thesis. They retained a cheerful and very cooperative attitude no matter how many changes were made.

Author's thank you to Dr. Mel Hosain, Dr. Moh Boulfiza and Dr. Gord Putz for their generous support and encouragement.

A special thanks goes to Mr. Dale Pavier, Structural Laboratory technician, for his constant assistance in the experimental work for this thesis.

The Author is also thankful to graduate students Mr. Fazlollah Shahidi, Mr. Gregory Del Frari, Mr. Ziengji Zhou, Mr. Amit Pashan, and Ms. Emma Boghossian for their friendship, encouragement and help in the testing of the specimens.

A very special thank you goes to all of the above for the emotional support and patience during some rough times. Without their help, this work would not have been possible to finish.

Finally, thanks are expressed to the University of Saskatchewan for financial support.

DEDICATION

To my husband ***Mr. Sergey Vladimir Paturov*** and

to my best friend ***Mrs. Bespalko Lubov Petrovna***.

TABLE OF CONTENTS

LIST OF TABLES

LIST OF FIGURES

LIST OF ABBREVIATIONS

A_c = area of the core in masonry wall, mm^2.

A_e = effective cross-sectional area of the masonry wall, mm^2.

A_{face} = face shell area of the masonry wall, mm^2.

A_g = gross cross-sectional area of the masonry wall, mm^2.

A_n = net area of the masonry wall, mm^2.

A_s = area of the reinforcement in the wall, mm^2 .

A_{sp} = area of the spiral reinforcement, mm^2.

ASTM = American Society for Testing and Materials.

b = effective width of masonry wall, mm

CMU = Concrete Masonry Unit

COV = Coefficient Of Variation

CSA = Canadian Standard Association.

d = effective depth of masonry wall, mm.

d_{bar} = diameter of reinforcing bar, mm.

d_s = diameter of spiral reinforcement, mm.

e = eccentricity of axial force, equals 0.1t, mm

E_m = modulus of elasticity of masonry, E_m=850 f_m, MPa.

E_s = modulus of elasticity of steel = 200000 MPa.

Eq = equation.

f_m = compressive strength of masonry, MPa.

f_u = ultimate strength of steel, MPa.

f_y = yield strength of steel, MPa.

Fig. = figure

G = shear modulus, G=0.4 E_m, MPa.

H = effective height of masonry wall, mm.

kN = kilonewtons.

kPa = kilopascals.

L = length of the masonry wall, mm.

L_d = development length, mm.

= compression lap splice, mm.

L_{db} = basic development length, mm.

LC = Level of Confidence

LDS = Linear Displacement Sensor

M = bending moment, kN·m.

= mega, 1,000,000.

max = maximum.

min = minimum.

m = metre.

= milli, 0.001.

n = ratio of modulus of elasticity of steel (E_s) to that of masonry (E_m) and is equal to E_s / E_m.

= number of specimens.

N = Newton, force.

NBC = National Building Code.

P = design axial load in the masonry wall, kN.

P_{br} = bearing load of masonry wall, kN.

Pa = Pascals.

SI = International Systems of Measurements.

t = effective thickness of the masonry wall, mm.

= Student t-test.

U = calibration factor.

V = shear force, kN.

w = uniformly distributed load, kN/m.

= width of masonry wall, mm.

y = distance from centroid of the section to the extreme fibre, mm.

δ = deflection, mm.

ε_m = compressive strain in masonry

ε_{mu} = ultimate strain in masonry

ε_{mt} = masonry strain

ε_c = cracking strain in masonry

ε_u = ultimate strain

ρ = ratio of area of reinforcement to effective masonry area, A_s /bd.

Δ = displacement, mm.

Δ_L = change in length, mm.

μ = ductility of the masonry, is defined by the ratio of the displacement at ultimate load to the yield displacement and is equal to Δ_u / Δ_y.

ϕ_c = resistance factor for concrete materials.

ϕ_m = resistance factor for masonry materials.

ϕ_s = resistance factor for steel materials.

°C = degrees Celsius.

% = percent.

= number.

TERMINOLOGY

ALLOWABLE STRESS: Maximum permissible stress used in the design of members of a structure and based on a factor of safety against rupture or yielding of any type.

ASTM: American Society for Testing and Materials.

AXIAL LOAD: Force applied along the length of a member.

BED JOINT: The horizontal layer of mortar on which a masonry unit is laid.

BOND: (1) Patterns formed by exposed faces of units.
(2) Adhesion between mortar or grout and masonry units or reinforcement.
(3) Tying various parts of a masonry wall by lapping units one over another or by connecting with metal ties.

CAVITY: A hollow area within the body of the masonry block.

COMPONENT MATERIALS: In the case of plane masonry there are the masonry units, the mortar, the reinforcing steel, and the grout fill.

COMPRESSIVE STRENGTH: Measured maximum resistance of a material to axial compressive loading, expressed as force per unit cross-sectional area.

COMPRESSIVE STRESS: Stress that resists a force attempting to crush a body.

CONCRETE BLOCK: Basic modular building material, usually 200 x 200 x 400 mm, made from cement, fine aggregates, and sand.

CONCRETE MASONRY UNIT: Hollow or solid unit made of Portland cement and suitable aggregates.

COURSE: Means to arrange in a row. One of the continuous horizontal layers of units, bonded with mortar in masonry.

DUCTILITY: Property of a material by virtue of which it may undergo large permanent deformation without rupture.

DESIGN STRENGTH: 1. Nominal strength of a member multiplied by a strength reduction factor.

EFFECTIVE AREA: Area of a concrete masonry section assumed to include the mortar bedded area and the area of voids filled with grout.

FAILURE: Breakage, displacement, or permanent deformation of a structural member or connection so as to reduce its structural integrity and its supportive capabilities.

FACE: Exposed surface of a wall or masonry unit.

FACE SHELL: Side wall of a hollow concrete masonry unit.

GROUT: A cementitious compound of high water-to-cement ratio, permitting it to be poured into spaces within masonry walls. Consists of Portland cement, lime, and aggregate to which sufficient water is added to produce pouring consistency without segregation of the constituents.

GROUTED MASONRY: Unit masonry composed of either hollow units, wherein the cells are filled with grout, or multiple wythes, where spaces between the wythes are filled with grout.

GROUTING: Process of filling hollow cores of masonry units with grout.

JOINT: The mortar bond placed between individual masonry units.

MASONRY: Brick, concrete block, stone, etc., or combination bonded with mortar.

MASONRY UNITS: Natural or manufactured building units of burned clay, concrete, stone, glass, gypsum, etc.

MODULUS OF ELASTICITY: 1. A function of two time variables: strain in loaded concrete as a function of the age at which the load is initially applied and the length of time the load is sustained. 2. Ratio of stress for strain for a material that does not deform in accordance with Hooke's law when subjected to applied load.

MOLD: Device containing a cavity into which a fluid or material in suspension can be poured to produce a designed shape.

MORTAR: A pasty building material composed of sand, lime and cement mixed with water and is used as a joining medium in masonry construction. This mixture gradually hardens when exposed to the air.

NOMINAL STRENGTH: Strength of a member or cross section calculated in accordance with provisions and assumptions of the strength design method, before application of any strength reduction factor.

POISSON'S RATIO: Ratio of transverse (lateral) strain to the corresponding axial (longitudinal) strain resulting from uniformly distributed axial stress below the proportional limit of the material.

PRISM: A small masonry assemblage made with masonry units and mortar. Primarily used to predict the strength of full-scale masonry members.

REINFORCED MASONRY: Masonry units, grout and/or mortar, reinforcing steel combined to act together in resisting forces.

REINFORCEMENT RATIO: Ration of the effective area of reinforcement to the effective area of concrete at any section of a structural member.

RUNNING BOND: Each head joint (vertical mortar joint) is positioned one-half over the unit below and eliminates continuous vertical joints.

SLUMP: Measure of consistency or fluidity of concrete. Equal to the measured subsidence of a truncated cone of concrete released immediately after molding in a standard slump cone.

STACK BOND: Units are positioned directly above one another.

STRENGTH: Ability of a member to sustain stress without a failure.

STRESS: 1. Load that is applied to a material object. 2. Force of resistance within any solid body against alteration of form.

STRESS CRACKING: Long hairline cracks in hardened concrete due to premature loading.

STRESS-STRAIN: Relationship of force and deformation of a unit area of a body during compression, extension, or shear.

STRESS-STRAIN CURVE: Curve plotting test results in which strains are plotted against stresses.

STRETCHER: 1. The long face of a masonry unit. 2. Masonry unit laid flat with the long face parallel to the wall face.

TENSILE STRENGTH: Strength of material, as measured by attempting to pull apart a specific amount of the material.

TENSILE STRESS: Maximum unit stress that a material is capable of resisting under axial loading, based on the cross-sectional area of the specimen before loading.

CHAPTER ONE

INTRODUCTION

1.1 Background

The use of masonry, brickwork and blockwork for buildings and civil engineering structures has a long history going back to ancient times. For many thousands of years, masonry structures were built using elements such as walls, arches, vaults, and domes. These elements were constructed using thick, plain, unreinforced masonry blocks. Over the years, significant improvements in masonry materials, construction skills, and design abilities have changed masonry construction from massive gravity-type structures to competitive and cost-efficient structural types seen in modern buildings. However, because of the way that masonry has historically been used, brickwork and blockwork are often still seen as just infill material for steel framed or reinforced concrete buildings.

With the introduction of other materials, including concrete, and the advent of reinforced masonry, increasingly complex structures became a possibility. Furthermore, there is an increasing requirement to assess the strength of masonry structures in a rational manner and to determine suitable means of improving masonry performance in order to exploit masonry to its full potential.

Common masonry walls are made of hollow-core concrete block, mortar, grout and reinforcement. Some or all cores can be filled with grout to enhance the compressive strength of the wall. Partially grouted masonry is a masonry assembly in which only cores containing reinforcement are grouted. Placing vertical steel reinforcing bars in

cores enhances the flexural strength of the wall. It has been hypothesized that if the grouted and reinforced masonry core could be confined (e.g. with a ring, comb, cage or spiral), this would delay the failure of the grouted core, making the wall more ductile and stronger in axial compression. An example of a portion of such a reinforced and confined partially grouted concrete masonry wall built in running bond (for definitions of common masonry terms, refer to the Terminology list on pg. xviii), as used in present study, is illustrated in Fig. 1.1.

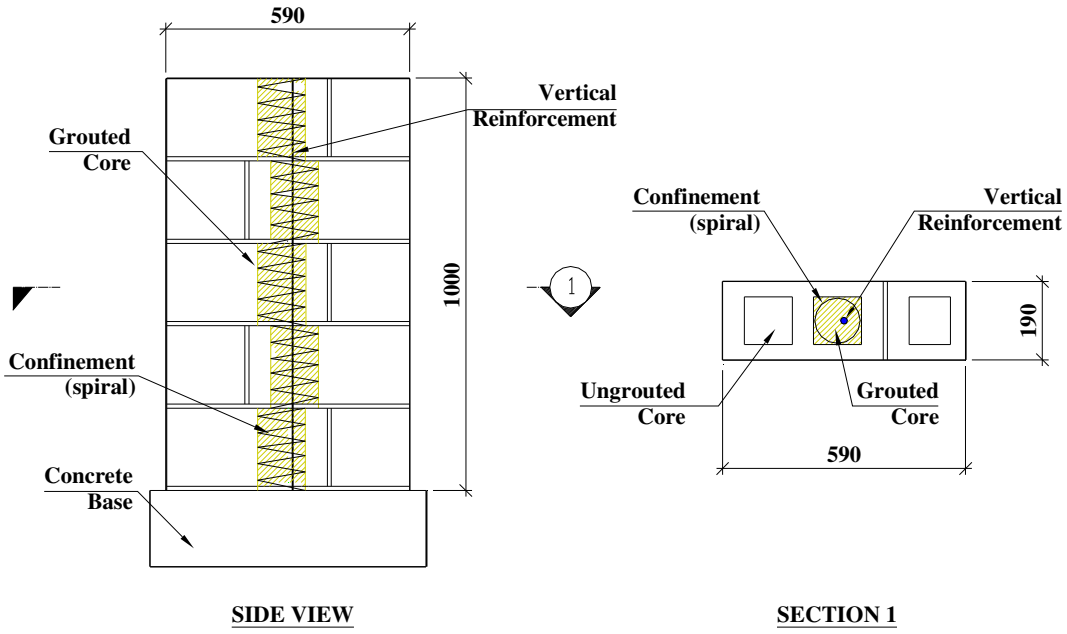

Fig. 1.1. Reinforced and confined partially grouted concrete masonry wall specimen.

One consequence of the running bond configuration for the concrete units is that the hollow cores of the blocks are *shifted horizontally* relative to adjacent courses. This shift has significant influence on the grouted column formed within the wall: the vertical grout column is *not straight*, but rather features an alternating offset at every course level. The presence of offsets in the grout column will inevitably reduce its capacity for carrying axial load.

The study of the compressive strength of partially grouted reinforced concrete masonry is important because, generally, the compressive strength of masonry is one of the most important parameters in the design of masonry structures. Knowledge of the limits within which different grouted core spacings, vertical reinforcement configurations and confinement of the grouted cores can influence the compressive strength is useful for the design of structures. As a result, the study of the effect of vertical reinforcement and confinement on the axial capacity of partially grouted concrete masonry walls is desirable and timely.

1.2 Objectives

The main objective of this study was to investigate the effect of vertical reinforcement and lateral confinement of the grouted cores on the axial capacity of partially grouted concrete masonry walls.

Specific primary objectives were as follows:

- To compare the axial compressive strength of partially grouted concrete masonry walls with and without vertical reinforcement in order to investigate the effectiveness of vertical reinforcement for increasing axial capacity; and
- To investigate the influence of lateral confinement of the grouted core on the strength and ductility of concrete masonry walls with vertical reinforcement.

Other sub-objectives were:

- To investigate the load-displacement and stress-strain behaviours of axially loaded partially grouted concrete masonry walls which were unreinforced, vertically reinforced and vertically reinforced with lateral confinement; and
- To study the post-failure behaviour of axially loaded concrete masonry walls.

1.3 Scope

This study focused on the effect of vertical reinforcement and confinement on the axial capacity of partially grouted concrete masonry block walls. Testing was designed to evaluate the change in compressive resistance and ductility of short concrete masonry walls with vertical reinforcement and lateral confinement of the grouted core and to measure the vertical and horizontal deformation of the short masonry walls. The structural behaviour of vertically reinforced, laterally confined walls was compared to vertically reinforced, unconfined walls, as well as with unreinforced, unconfined masonry walls.

1.4 Methodology

An experimental study was performed to investigate the behaviour of partially grouted concrete masonry block walls under axial loading. In total, thirty short wall specimens were tested to failure. To study the influence of vertical reinforcement and confinement of the grouted cores, three sets of ten short wall specimens were considered:

- Unreinforced walls with no lateral confinement of the grouted cores;
- Walls with vertical reinforcement in the grouted cores, but no lateral confinement; and
- Walls with vertical reinforcement and lateral confinement of the grouted cores.

All wall specimens were made from the same batch of standard concrete masonry blocks. The axial compressive capacity, post-failure strength and ductility, failure modes and load-displacement behaviours of the three wall types were investigated.

1.5 Thesis Overview

This thesis consists of six chapters, plus references and appendices. Chapter one presents an introduction, objectives, scope and methodology of the thesis.

Chapter two provides a literature review regarding the influence of confinement in partially grouted masonry walls, the influence of confinement in concrete columns and a discussion of some research results found in the literature.

Chapter three describes the experimental program. It covers the specimen designation, component materials used in the study, description of test specimens, specimen construction and test procedures.

Chapter four contains a presentation of the important test results for component materials, masonry prisms and masonry walls. A complete listing of all test data is presented in the appendices.

Chapter five presents an analysis of the test data, including a comparison and discussion of the test results. It covers the behaviours of the component materials, prisms and walls, including failure modes, crack patterns, limit states and post failure inspection. Also included is a comparative analysis of unconfined and confined test specimens.

Chapter six presents the conclusions of the study and recommendations for future research.

CHAPTER TWO

LITERATURE REVIEW

2.1 Introduction

In general, an extensive review of masonry literature indicates that there is little experimental data available directly concerning the effect of confinement in reinforced partially grouted concrete masonry under axial compression. However, the literature addresses many relevant aspects which are of interest, including the structural performance of confined concrete columns, grouted masonry walls and partially grouted concrete masonry walls. The durability and serviceability of these columns and walls, as compared to concrete columns and masonry walls, has received some attention.

Comparison of data from many different sources is complicated in the field of masonry research due to the tremendous diversity in specimen shape, size, construction and test procedures. However, there is a body of published material that is of particular significance to this study dealing with the behaviour of unconfined and confined concrete masonry walls under various load conditions.

The majority of experimental studies on the effect of confinement of partially grouted masonry walls have been done on concrete prisms laid in stack bond. Most work has been purely experimental, with limited analytical studies. The observations and conclusions in these studies had an influence on the selection of the type, size and confinement of wall specimens to be tested in the current program.

2.2 Confinement in concrete columns

It is well known that confining the core of a reinforced concrete column with lateral reinforcement will significantly increase the strength and the ductility of the column. Confinement reduces the loss of strength due to spalling of the concrete cover and increases the ability of the concrete core to sustain large deformations without a dramatic loss in strength. The increase in strength and especially in ductile behaviour due to confinement is extremely important for reinforced concrete building columns. The degree of confinement is related to the configuration, size and longitudinal spacing of the lateral reinforcement in the column. Considerable research has been done to investigate the behaviour of confined concrete columns under axial compression; short reviews of some important studies are presented here.

2.2.1 Confinement by crossties or hoops

Studies of the effects of steel ties, hoops or hooks on column confinement have been reported for more than half a century (Richart et al. 1929; Pallewatta et al. 1996). The focus has been on specific requirements for the configuration of the confining system: for example, each tie, hoop or hook must be bent to particular design specifications.

Moehle and Cavanagh (1984) conducted an experimental study of the confinement effectiveness of crossties in reinforced concrete columns subjected to monotonically increasing axial compression. Ten large-scale concrete columns (eight reinforced and two plain concrete) with two types of crossties (180° hooks at both ends; 90° and 135° hooks at the ends) were tested to failure. The ratio of longitudinal reinforcement for reinforced specimens was 2.44% and the ratio of transverse reinforcement was either 1.21% or 2.07% (the ratio was defined as area of steel divided by gross column cross-sectional area). Spalling of the concrete shells in the reinforced columns was noted at the peak stresses and columns maintained the load carrying

capacity beyond the spalling. Buckling of longitudinal bars, the fracture of hoops and ties, and the pullout of tie hooks was observed in all reinforced columns.

The laterally reinforced columns had greater (14%) load and deformation capacities than plain concrete columns. Analytical stress-strain relationships for confined concrete columns were comparable to measured stress-strain relationships. A general finding was that the concrete stress and strain capacity increased with: increasing amounts of transverse steel; decreasing longitudinal spacing of transverse steel; and an increase in the number of longitudinal bars tied by a hoop. The columns with 135°and 90° hooked crossties were less ductile than columns with 180° hooks. Transverse reinforcement was capable of delaying buckling of the main longitudinal reinforcement in the concrete columns.

Abdel-Halim and Abu-Lebdeh (1990) used non-linear finite element analysis to study confinement in reinforced concrete columns. The theoretical results were compared with experimental results. Eight large-scale concrete columns (450 x 450 x 1200 mm) reinforced with 8 or 12 longitudinal bars and square or octagonal steel ties were analyzed under axial compression until failure. Three-dimensional truss elements were used to represent the lateral ties and longitudinal bars and three-dimensional solid elements were used to represent the concrete. The volumetric ratio of lateral ties varied with the spacing and size of the ties.

The strength and ductility of tied concrete columns was found to increase with an increase in the volumetric ratio of lateral ties. Lateral confinement had no effect on the behaviour of the columns at load levels less than 70% of ultimate load. In addition, the larger the number of longitudinal reinforcing bars the better the concrete confinement. For rectangular or square columns, the increased axial strength was expressed in terms of the volumetric ratio of the lateral ties, the yield stress of the tie steel, and the unconfined compressive strength of the concrete.

2.2.2 Confinement by Welded Wire Fabric (WWF)

Welded wire fabric (WWF) as confining transverse reinforcement in columns is an alternative to conventional steel ties. The WWF may be placed transversely in the core of the concrete column in parallel stack with a uniform longitudinal spacing or it may be wrapped around the column in addition to conventional ties.

Grira and Saatcioglu (1996) tested full-size concrete columns under seismic conditions featuring four corner bars for longitudinal reinforcement and transversely oriented WWF instead of lateral ties. An axial compressive force of 20% and 40% of the expected peak compressive load was applied and the columns were loaded laterally in cycles similar to the lateral drift of an earthquake. They concluded that the WWF performed much better than transverse ties.

Mau et al. (1997) performed small-column tests using WWF with different diameters of wires and different gages of wire mesh for lateral confinement. The longitudinal spacing of the parallel WWF layers varied between 0.1 and 0.3 of the width of the column. The study was performed to determine the influence of volumetric ratio of WWF, longitudinal spacing of WWF and grid types of WWF. The peak stresses were reached when columns experienced clear cover failure. Specimens failed suddenly in a two-dimensional (the failure surface was inclined perpendicular to a pair of opposite column surfaces) fashion with failure planes occurring in the middle regions of the test specimens.

Test results showed that the higher the level of confinement, the higher the strength of the specimens. The strength increased (as high as 40%) with increasing volumetric ratio of WWF and decreasing longitudinal spacing of WWF. The type of grid had no effect on strength of the specimens.

2.2.3 Confinement by spirals

Lateral confinement provided by spiral reinforcement greatly improves the strength and ductility of concrete columns. The spirals confine concrete in circular columns much more effectively than ties, hoops or WWF. The increased axial compressive strength of the concrete core for circular columns with spiral lateral reinforcement, due to its geometry, can be expressed as a function of the lateral confining stress and a longitudinal spacing factor.

Martinez et al. (1984) investigated the response of high-strength concrete columns confined with steel spirals under short-term compression. They tested 94 short columns with diameters of 102 mm, 127 mm and 152 mm reinforced only by spirals varying in wire diameter and spacing. Columns were made from lightweight and normal weight concrete; 78 of them did not have a protective cover of concrete over the spiral steel and 16 columns featured a protective cover.

The most important conclusions concerning the spiral reinforcement were: (1) the compressive strength of the concrete core increased with an increase in confinement stress, regardless of concrete strength; (2) the modulus of elasticity for confined and unconfined columns was found to be the same; and (3) spirals provided strength gain to compensate for spalling of protective cover.

Pessiki and Pieroni (1997) tested eight large-scale (559 mm in diameter, 2235 mm in height) circular concrete columns under concentric axial compression. Columns were longitudinally reinforced with 8 No. 8 bars to produce a reinforcement ratio of 1.65%, as well as 16 No. 9 bars to produce a reinforcement ratio of 4.20%. Transverse reinforcement was provided by spirals (wire No. 3, 4 and 5) with pitches of 41 mm and 64 mm. Columns were cast with concrete compressive strengths ranging from 34.5 MPa to 69 MPa. The influence of concrete strength, longitudinal reinforcement (number of bars) and lateral reinforcement (spiral size and pitch) on the column strength and ductility were investigated.

Spalling of the concrete cover, fracture of the spiral reinforcement and buckling of longitudinal reinforcement were observed. The following conclusions were made: (1) increasing the compressive strength of concrete decreased the column's ductility; (2) the initial spiral fracture corresponded to 85% of failure load on average; (3) columns with less longitudinal reinforcement showed greater ductility and more longitudinal bars placed a greater demand on the spiral; (4) a decrease in the pitch and size of the spiral reinforcement decreased the ductility of the column; and (5) first cracking in the concrete cover was observed at relatively lower peak load in columns with higher concrete strength then in low-strength columns.

2.3 Concrete masonry walls

The effect of reinforcement and confinement of grouted cores on the strength and ductility of masonry walls has been a subject of research for a long time. Many experimental programs have been performed to study the effect of various parameters on the strength and ductility of reinforced masonry walls under axial loading.

2.3.1 Compressive strength of masonry

The compressive strength of a masonry wall depends on the strength of its component materials (concrete units, mortar, grout and reinforcement) as well as the interaction between its components. The different types of mortar and grout, different shapes and dimensions of concrete units, the presence and configuration of vertical and lateral reinforcement (number of bars, shape and size), and whether walls are ungrouted, partially grouted or fully grouted have all been the subject of research studies.

Drysdale and Hamid (1979) presented the results of an experimental study on the behaviour of concrete masonry under axial compression. They tested 146 three course high prisms (half block, full block, one full and two half blocks in length) using different bond patterns (stack and running bond), grouted and ungrouted prisms with two types of mortar and five types of grout.

The results showed that the failure mode for all prisms featured vertical tensile splitting which initiated in the end flange shells of the central (middle course) block. The bond pattern did not have any effect on the strength or failure mode for both types of masonry specimens (ungrouted and grouted). The mortar type did not affect the strength of the grouted prisms significantly. Ungrouted prisms showed greater average compressive strength than grouted, due to the large lateral expansion of the grout under axial compression, which led to a premature tensile splitting of the block's shells. The grout strength did not affect the masonry compressive strength.

In the same experimental study, Hamid and Drysdale (1979) suggested failure criteria for grouted concrete masonry under axial compression. The criteria were based on a strength approach using properties that were determined from standard strength tests of the individual component materials. Vertical cracking was attributed to the lateral tension induced in the block by the mortar and grout, which exhibit larger lateral strains at lower axial strains than does the block. It was shown that the compressive strength of grouted concrete masonry, based on the net cross-sectional area, could be significantly less than that for similar ungrouted masonry, even though the grout is much stronger than the block. Two failure conditions were found to be possible for grouted masonry under axial compression, depending on which component reached its unconfined compressive strength first, the shell (the block and mortar joints) or the grouted cores.

Axial compression tests of grouted concrete masonry prisms showed that failure occurs in the block due to a tension-compression state. When the grout has a lower strain level at the maximum stress than the shell, its unconfined compressive strength will be reached first. The shell will tend to confine the grout, generating a bursting pressure exerted by the grout on the block and causing a premature splitting failure of the block shell under a compression-tension state of stress. If the block shell reaches its maximum compressive stress at a lower strain than the grout, then the grout is not confined and the capacity will be controlled by either the failure of the block under a compression-tension

state of stress or the capacity of the grouted core under axial compression after failure of the shell.

Formulations of the failure criteria were developed in a generalized form to be able to account for any strength or geometric characteristic, such as the net to gross area ratio of the block, tapering of the grout cores, joint thickness, and even ungrouted masonry. The predicted ultimate strengths using the proposed criteria were compared with experimental results for ungrouted and grouted prisms, incorporating a wide range of mortar and grout strengths, and were found to produce good agreement.

Hamid and Chandrakeerthy (1992) presented part of a then on-going comprehensive research program at Drexel University aimed at developing a design methodology for reinforced concrete masonry structures. The study consisted of testing 15 wall specimens ranging from ungrouted, partially grouted to fully grouted configurations along with control tests on units, mortar, and grout.

Three-course prisms were used in the study using nominal 150 mm prototype units, which gave a height to thickness ratio of approximately four. The height to thickness ratio of the prism was found to influence compressive strength considerably. Grout spacings of 200 mm for a fully grouted wall, as well as 400 mm, 600 mm, 800 mm and infinite spacings for ungrouted walls were considered, while all other parameters were held constant. For each grout spacing configuration, three replicates were tested. These were obtained by constructing a long wall and subsequently cutting it appropriately to obtain the required wall specimens.

Vertical tensile splitting and spalling away of the block shells were observed. The ratio of load at first crack to ultimate load varied from 0.85 to 1.0 and was a maximum for fully grouted specimens, progressively decreasing as grout spacing increased. Failed specimens were inspected and found to be free from flaws such as formation of grout bridges, voids and shrinkage cracks at the grout-block interface.

The following conclusions were made from this study: (1) the ultimate compression load per unit length of partially grouted masonry walls increases as grout spacing decreased; (2) the compressive strength based on gross area was more suited for use with partially grouted concrete masonry than that based on net area, since stresses are not distributed uniformly over the net area; (3) the compressive strength of partially grouted concrete masonry could be expressed in terms of unit strength, grout strength, percent solid and extent of grouting using the proposed formulas; and (4) the variation of compressive strength based on gross area was linear with grout spacing within the range of 200 mm to 800 mm.

2.3.2 Confinement in mortar beds

Pristley (1981) presented a seismic design philosophy for masonry shear walls and demonstrated the ability of masonry shear walls to exhibit considerable ductility. In the design of reinforced concrete structures, detailed design rules for plastic hinge regions have been developed and incorporated in design codes, which ensure the design level ductility can be obtained without requiring the designer to perform a ductility capacity check. For columns and shear walls, the primary means of ensuring ductility is to provide lateral confining steel at closely-spaced centres to effectively increase the ultimate concrete compression strain, and hence the ultimate curvature and ductility.

The same approach can be, at least in theory, adopted for masonry structures. However, confining reinforcement is difficult to provide and can only be easily incorporated within mortar beds. For concrete masonry block construction with standard size blocks, this means spacing the confining steel at 200 mm centres (the distance between mortar beds), which reduces the efficiency of confinement and the support against compression bar buckling at high strains. It was shown that many masonry shear walls could develop the desired level of ductility without exceeding compression strains that can be sustained by unconfined masonry.

Pristley (1981) presented results of a computer sensitivity analysis for grouted concrete masonry prisms confined with 3 mm thick stainless steel plates within the mortar beds. The plates were cut to the net shape of the masonry units so that there was no interference with the grouted cores, with a 5 mm edge allowance for pointing. Six masonry prisms (five courses high and one full block wide) were also tested in the laboratory under axial compression. Confined prisms showed increased strength, higher strains at peak load, and a much flatter falling branch of the stress-strain curves. A safe ultimate compression strain for concrete masonry confined in this fashion was estimated to be 0.008.

For unconfined masonry an effective ultimate strain of 0.0025 was recommended, because of the potential instability of the compression zone under combined axial force and shear, after formation of extensive vertical splitting. The tests indicated that the peak stress occurred at a strain of approximately 0.0015 as a result of premature formation of vertical cracking of the concrete masonry face shells, caused by lateral expansion of the crushing mortar. This vertical splitting propagated into the grout core and caused a fairly steep falling branch of the stress-strain curves.

Pristley developed a simple method to check the available ductility of masonry shear walls of rectangular section. Results were presented in graphical form indicating that: (1) the available ductility decreases with increasing axial load, reinforcement and yield stress; and (2) the available ductility increases with increasing masonry crushing strength and with confinement.

Pristley and Elder (1983) reported the results of an experimental investigation of the compressive stress-strain characteristics of grouted concrete masonry prisms. The test program investigated the influence of block width, confining plates, strain rate and vertical reinforcement on the failure mechanism and complete stress-strain curves for five-course masonry prisms.

Visual observations revealed that the failure of the unconfined prisms conformed to the mechanism suggested by Drysdale and Hamid (1979) and involved premature failure of the masonry unit/mortar by vertical splitting initiated by high lateral expansion of the crushing mortar. This occurred before grout crushing, lowering the strain at peak stress to approximately 0.0015. There was no significant influence of block width on behaviour, despite the different net/gross area ratios of the blocks. In addition, the presence of vertical reinforcing bars in the grout cores did not significantly influence masonry behaviour. Increasing the strain rate from 0.0005 to 0.5 percent/sec resulted in an average 17 percent increase in strength and a steepening of the falling branch in stress-strain curves for confined prisms.

Stainless steel confining plates in the mortar beds changed the failure mechanism from one initiated at mortar beds by vertical splitting to a shear/crushing failure largely within one course of the blocks and resulted in a more gradual falling branch to the stress-strain curve. These tests indicated that the falling branch was similar to results obtained for reinforced concrete; therefore, it was suggested that it may be appropriate to describe the behaviour of masonry using existing theoretical models for reinforced concrete stress-strain curves.

2.3.3 Confinement of grout cores

Hart et al. (1988) presented the results of Phase I of a two-phase program, which was conducted to study confinement of vertical flexural steel in concrete masonry shear walls. Phase I involved conducting compression tests on prisms to evaluate different types and quantities of confinement. A total of 71 prisms were tested, in which all prisms were constructed with standard concrete block units. The prisms were 4 units high and were laid in stack bond with Type S mortar and grouted with a pea gravel grout. A comprehensive test program was conducted to investigate different types of confinement such as wire mesh, a modified “Pristley Plate” (as described in Section 2.3.2), hoops and spirals. In order to maintain consistent vertical reinforcing throughout all prism tests, one No. 6 bar was provided in each cell.

The stress-strain curves obtained from tests of concrete masonry prisms define the basic information on the performance of prisms at different compressive strain values. Hart et al. (1988) found that these curves could be divided into four distinct strain regions, which were denoted as behaviour states. These (and their corresponding limit states) are defined as follows:

1. Behaviour State 1 – in this behaviour state, prisms under compression show no significant signs of physical damage and there is no benefit associated with using the confining steel.

   Limit State 1 exists when the compressive strain is equal to the strain at which first cracking occurs in the masonry. Beyond this point, which defines the serviceability limit state, confinement steel is recommended.
2. Behaviour State 2 – the compressive strain exceeds Limit State 1; strain in the wall exceeds the cracking strain, but is less than the strain at ultimate strength.

   Limit State 2 exists when the compressive strain in masonry is equal to the strain at ultimate strength. This is a structural damage limit state.
3. Behaviour State 3 – the compressive strain exceeds the strain at ultimate strength and the stress decreases in value from its maximum.

   Limit State 3 exists when the compressive stress has fallen to 50% of its maximum value. This is defined to be the Design Strength Limit State.
4. Behaviour State 4 – the prism experiences a strain greater than that at a stress value that is 50% of its maximum value, and even though it exhibits significant physical distress it is capable of carrying compressive load which is equal to or greater than 20% of its maximum value.

   Limit State 4 corresponds to the end of the fourth behaviour state. This limit state exists when the compressive stress has fallen to 20% of its maximum value. This is the strength limit state of the prism.

The tests conducted by Hart et al. (1988) produced all of the above noted limit states for all of the tested prisms. The role of confinement on each limit state was quantified in this research by comparing limit state values for confined prisms with values for unconfined prisms. The conclusions were: (1) unreinforced and vertically

reinforced unconfined prisms behaved identically and failed in a brittle manner; (2) all types of confinement had a negligible effect on the ascending portion of the stress-strain curve up to and including the second limit state; (3) all types of confinement had a positive effect on the descending portion of the stress-strain curve in that they increased the strain at Limit States 3 and 4, thus increasing the area under the stress-strain curve; (4) the Pristley Plate provided the greatest confinement; and (5) the open wire mesh confinement type performed very well.

Hart et al. (1989) presented the results of Phase II of the same two-phase program, which provided experimental data on various schemes of lateral confinement reinforcement designed specifically for use in reinforced concrete masonry.

In the first part of the experimental effort, 106 prisms were tested, including unreinforced prisms, vertically reinforced unconfined prisms, and vertically reinforced laterally confined prisms using seven different confinement schemes. For each configuration of lateral confinement, two volumes of steel were tested. “Type 1” had a confinement steel volume essentially equivalent to the minimum requirement (#3 bars at 203 mm on center specified by UBC, Section 2412, 1988). The confinement denoted “Type 2” was typically double the steel volume of Type 1 confinement.

In the second part of Phase II, two different mathematical models – a simple model and a more complex model – were developed for stress-strain curves from unreinforced and several varieties of confined prisms. Each model consisted of two mathematical functions: one for the rising branch of the stress-strain curve and one for the falling branch. The simple model – the Acceptable Fit model - required only one shape parameter and two material parameters to completely describe the stress-strain curve. The more complex model – the Best Fit model - more appropriate for research or computer analysis, required three shape parameters in addition to two material parameters.

The experimental evidence showed that analytical curves developed to model the behaviour of concrete in compression were not appropriate for masonry. The falling branch of the stress-strain curve was steeper for masonry than for concrete immediately following maximum stress. Furthermore, the effect of confinement reinforcing on the stress-strain curve was different for the two materials: the increases in strength and strain at maximum stress caused by the presence of confinement were less for masonry than for concrete. Further experimental work was necessary to establish the behaviour of masonry under stress.

To provide quantitative information on the effectiveness of different confining schemes and to present a general analysis tool that could be used to evaluate the flexural strength and ductility of confined and unconfined masonry shear walls, an experimental study was conducted by Shing et al. (1993). To study the influence of various confinement schemes on the flexural response of masonry shear walls, a total of six confined wall specimens were tested. The specimens were constructed with 150 x 200 x 400 mm hollow concrete blocks and were fully grouted. All vertical and horizontal reinforcing bars were uniformly spaced with a centre-to-centre distance of 400 mm. Three of the specimen types had ring, horizontal comb (ladder) and spiral-cage types of confinement, respectively. All three specimens were subjected to a constant axial compressive stress of 690 kPa based on the net area. In-plane cyclic displacement reversals were applied laterally at the top of each wall.

Based on the prism test data, formulas were developed and calibrated to account for the influence of confining steel on the compressive stress-strain relation of masonry. These formulas have been incorporated into an analysis model to evaluate the flexural response of confined and unconfined masonry wall sections. In addition, the modeling parameters introduced provided a quantitative means for comparing the effectiveness of different confinement schemes.

It was shown that the confinement schemes considered in this study had a beneficial influence on flexural ductility. As in reinforced concrete, the compressive strain-softening behaviour of confined masonry depended on the volumetric ratio of the

confining steel and the ratio of the least dimension of the confined area to the spacing of confining steel. Furthermore, based on the data obtained from prism tests, the degree of this influence depended very much on the type of confinement used. Both the experimental and numerical results indicated that the comb (ladder) confinement was most effective among the three confinement schemes considered. The proposed analysis method yielded reasonably reliable results, and appeared to be close to experimental data.

2.4 Summary

Based on the considerable amount of test data summarized in this chapter, several conclusions can be made.

The most important conclusions concerning the lateral reinforcement in concrete columns are presented below.

- Laterally reinforced columns have much greater load and deformation capacities than plain concrete columns.
- The degree of confinement is related to the configuration, size and longitudinal spacing of the lateral reinforcement in the column.
- Spirals confine concrete in circular columns much more effectively than ties, hoops or WWF.
- Confining the concrete core of a column with lateral reinforcement will significantly increase the strength and the ductility of the column.

The preceding studies clearly demonstrate that there are a multitude of parameters that affect the compressive strength and ductility of partially grouted concrete masonry. These include the following.

- The failure mode for unconfined prisms is typically governed by vertical tensile splitting, which is initiated in the shells of the block. Research has shown that large lateral expansion of the grout leads to a premature tensile splitting of the block's

shells and that increasing the grout strength is not an efficient means for increasing the masonry compressive strength. Confining plates in the mortar beds can change the failure mechanism to a shear/compression type of failure limited to one course with more gradual falling branch in stress-strain curve.

- Unreinforced and vertically reinforced unconfined prisms tend to behave identically and fail in a brittle manner. The mortar joint does not affect the strength of grouted prisms.
- Based on the net area, the average compressive strength for grouted prisms is less than for similar ungrouted prisms, which indicates that the incompatibility of the deformation characteristics of the grout and the block limits the utilisation of both materials.
- All confinement types for grouted cores have a negligible effect on the ascending portion of the stress-strain curve and have a positive effect on the descending portion of the stress-strain curve. Stress-strain curves for confined prisms show increased strength, higher strains at peak load and a much flatter falling branch. The confinement increases the area under the stress-strain curve when compared to unconfined specimens.

It can be concluded that there is very little data available on running bond configurations of masonry walls and the effectiveness of heavy confinement of grouted cores using spirals has not been adequately studied. As a result of these observations, the study of the effect of vertical reinforcement and spiral confinement on the axial capacity of partially grouted concrete masonry walls built in running bond is desirable and timely.

CHAPTER THREE

EXPERIMENTAL PROGRAM

3.1 Introduction

The focus of this study was to investigate the effect of vertical reinforcement and lateral confinement on the axial capacity of partially grouted concrete block masonry walls built in a running bond configuration. A partially grouted concrete block wall is a masonry assemblage in which only some of the cores, either with or without reinforcement, are grouted. In this study, thirty partially grouted (middle core only) short masonry walls were built and tested. Details of a partially grouted wall specimen laid in running bond are shown in Fig. 3.1.

Three types of masonry wall specimens were investigated: (1) specimens with a grouted middle core only; (2) specimens with a grouted middle core and vertical reinforcement, but no lateral confinement of the grouted core; and (3) specimens with a grouted middle core, vertical reinforcement and spiral reinforcement to confine the grouted core. All specimens were made from standard 190 x 190 x 390 mm concrete masonry blocks and 190 x 190 x 190 mm half block units and were five courses high with nominal dimensions of 590 x 1000 x 190 mm (width x height x thickness). The height of the test specimens was chosen 1000 mm as short wall ($H/t<10$) that slenderness did not have to be considered. Ten walls of each type of test specimen were constructed and tested.

The three types of specimens were selected for the following reasons:

- The first type without vertical reinforcement was a control set, so that all results could be compared to a case that was unaffected by the presence of reinforcing bars;
- The second type of specimens used the standard vertical reinforcement to provide a case that corresponded to a condition normally encountered in practice; and
- The third type was tested to determine if large amounts of lateral confinement of the grouted cores, as provided by spirals, was able to increase the load capacity and ductility of the specimens.

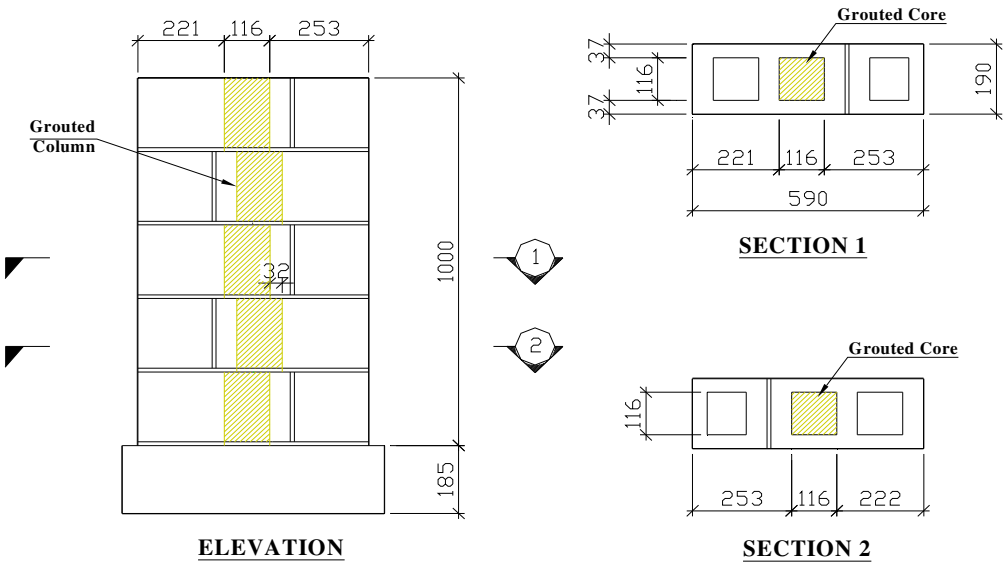

Figure 3.1. Dimensions and configurations of partially grouted concrete block wall specimens.

All masonry specimens were constructed and tested to failure in axial compression in the Structural Laboratory of the College of Engineering, University of Saskatchewan. Standard material samples were made during the specimen construction to determine the mechanical properties of the component materials (concrete prisms, mortar, and grout).

Prior to testing of the specimens, one load cell (LC) and fourteen linear displacement sensors (LDS), which were used to measure load and displacements, were calibrated. Details of the calibration are presented in Appendix G.

3.2 Experimental Design

The number of test specimens of each type (ten) was selected as being the minimum required to statistically differentiate between two hypothetically distinct populations. More specifically, ten samples would enable the differentiation of sample means that differed by at least 10% at the 90% confidence level, based on a two-sided Student t-test (Wine 1998). For this purpose, a coefficient of variation (C.O.V.) of 12.7% was assumed based on previous experimental studies of similar specimens at the University of Saskatchewan (Qi Hu 2004). Details of the statistical design analysis are presented in Appendix A.

3.3 Specimen Designation

A two-part system was developed to identify each specimen. The first letter in the system illustrates the type of the specimen:

- type ***A*** represents ***unreinforced, unconfined*** test specimens with grouted middle core only;
- type ***B*** represents ***reinforced, unconfined*** test specimens with grouted middle core and reinforced with vertical rebar; and
- type ***C*** represents ***reinforced, confined*** test specimens with grouted middle core, reinforced with vertical rebar and confined with a spiral.

The second part of the specimen designation is a number, from 1 to 10, indicating the number of the individual specimen in a particular series of specimens. For example, specimen ***B-8*** refers to the eighth of ten nominally identical specimens in series ***B***, which featured vertical reinforcement but no lateral confinement in the core.

3.4 Component Materials

3.4.1 General

To better understand the structural behaviour of the masonry wall it is important to have some knowledge of the properties of the component materials. Masonry is a multi-component assembly; in the current study, the wall specimens consisted of the concrete masonry units themselves, the mortar, the grout and the reinforcing steel. The compressive strength of a masonry wall is known to depend on the strength of its component materials as well as the interaction between components.

The main purpose of testing the component materials was to characterize the materials, to facilitate comparisons with other published results and design standards, and to ensure that the quality of materials was being maintained. All component materials used in the program were obtained from local suppliers in the Saskatoon area. Further details are described below.

3.4.2 Concrete masonry block units

Standard full block units with dimensions of 190 x 190 x 390 mm (width x height x length) and half block units with dimensions of 190 x 190 x 190 mm (width x height x length) were used in the study, supplied by Cindercrete Products Ltd. of Saskatoon. Pallets of plastic wrapped concrete blocks were delivered to the Laboratory. The nominal compressive strength of the concrete masonry units, as provided by the supplier, was 15 MPa. Actual test results of the compressive strength of the concrete blocks were not available due to the limited capacity of the Amsler Beam Bender machine used in the tests. Figure 3.2 shows the concrete masonry block dimensions for the units used in the study.

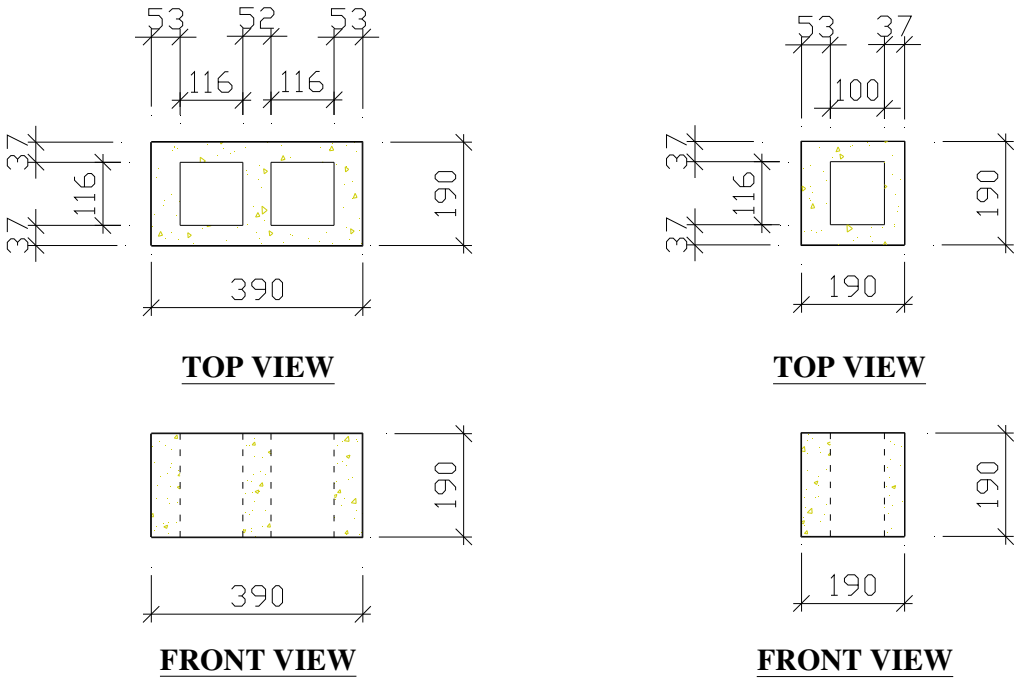

Figure 3.2. Standard full block and half-block concrete units (dimensions in mm).

3.4.3 Mortar

Mortar is composed of sand, lime, and cement mixed with water. The purpose of mortar is to provide a uniform bed for laying the masonry units, and to bond the units together. Type S mortar is permitted by CSA Standard S304.1-94 (CSA 1994) for structural applications and is commonly used for all engineered masonry. Ready for use, type S mortar was supplied by La Farge Canada Inc. (Saskatoon) and was delivered to the laboratory in covered bins.

Ten cylindrical mortar control specimens, 75 mm in diameter and 150 mm in height, were cast in plastic moulds during construction of the wall specimens. These mortar specimens were tested to determine actual material properties. The cylinders were poured in three layers and were well consolidated using a 6 mm diameter rod in

accordance with CSA Standard A179-94 (Mortar and Grout for Unit Masonry, CSA 1994).

All mortar control specimens were removed from moulds after thirty days and subsequently air cured along with the walls in the Structural Laboratory. Half of the specimens were tested in October, 2001, and the rest in August, 2002, at the beginning and at the end of the wall testing program.

3.4.4 Grout

The purpose of grout is to fill the cores, increasing the effective cross-sectional area of the masonry for load resistance, and to permit the bonding of reinforcing bars to the concrete masonry blocks. La Farge Canada Inc. (Saskatoon) supplied fine grout with a maximum aggregate size of 10 mm and a minimum slump of 250 mm, and delivered it to the laboratory in covered bins. The grout was poured into the middle cells of grouted walls seven days after construction of the walls. It was well vibrated using an electrical needle vibrator.

Two types of material control specimens were made at the same time as the walls were grouted. First, ten cylindrical grout specimens, 75 mm in diameter and 150 mm in height, were cast in non-absorbent plastic moulds. In addition, ten prismatic specimens with dimensions of 100 x 100 x 190 mm were cast in absorbent moulds. To make the absorbent moulds, concrete blocks were placed together, and the stretcher faces of the blocks were placed over a non-absorptive base to form a mould space of 100 x 100 x 190 mm, as shown in Fig. 3.3. Paper towels were used to line the mould so that the specimens could be de-moulded easily. Both cylinder and prismatic specimens were poured in three layers and were well consolidated using a 6 mm diameter rod.

All control grout specimens were removed from moulds after thirty days and air cured along with the walls in the Structural Laboratory. Half of the test specimens were tested in October 2001 and the rest in August 2002, at the beginning and at the end of the wall testing program.

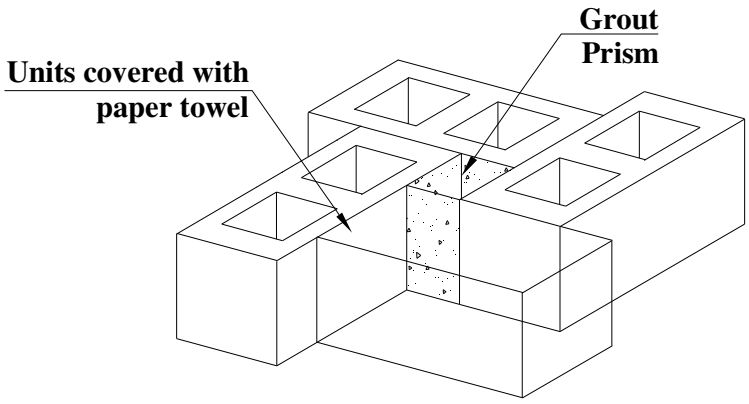

Figure 3.3. Preparation of grout prismatic specimen.

3.4.5 Reinforcing steel

The reinforcement used in the walls consisted of: (a) joint reinforcement; (b) vertical reinforcement; and (c) spirals.

(a) The joint reinforcement was of a ladder type that consisted of two parallel longitudinal wires welded to perpendicular wires, as shown in Fig. 3.4.

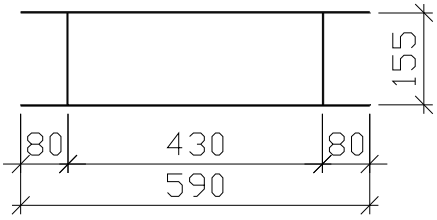

Figure 3.4. Joint reinforcement (ladder type).

Joint reinforcement was purchased from a local supplier (National Concrete Accessories) in 2438 mm (eight foot) lengths and was made from No. 8 (4.1 mm diameter) wire in accordance with CSA Standard G30.5-M1983(R1991) (Welded Steel Wire Fabric for Concrete Reinforcement, CSA 1991). In the Structural Laboratory, it

was cut into 590 mm long segments using a cut-off saw. The joint reinforcement was placed in every bed joint of the wall specimens.

(b) No. 15 deformed steel reinforcing bars were used as the main vertical reinforcement in walls of type ***B*** and ***C***. The No. 15 bar size was selected as a representative size used on the construction site and also to conform to the minimum area of vertical reinforcement required for masonry walls in Clause 5.2.1.2 of CSA Standard S304.1-94 (CSA 1994). The specified yield strength of the rebar was 400 MPa.

As shown in Fig. 3.5, the vertical bar had a bearing plate (66 x 66 x 20 mm) welded to its top surface to ensure the transfer of the load from the loading head of the machine to the bar, thereby making the bar fully effective for its entire length.

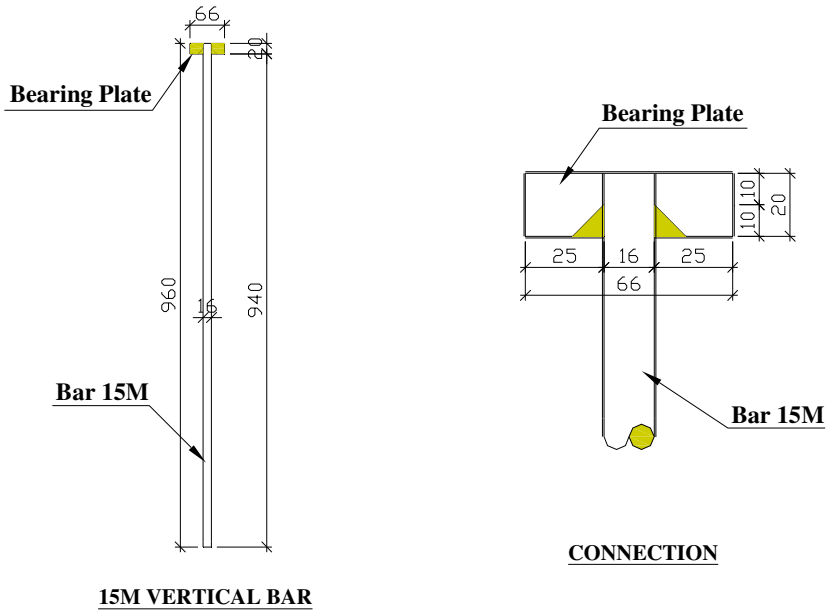

Figure 3.5. Vertical bar with bearing plate (dimensions in mm).

The dimensions of the bearing plate (four diameters of the bar) were chosen to accommodate the required yield strength of the bar. The bar and the bearing plate were made at the Engineering Shops in the College of Engineering at the University of

Saskatchewan. Design calculations relating to the vertical reinforcement, bearing plate and weld size are presented in Appendix A.

(c) Figure 3.6 shows details of spirals, which were made at the Engineering Shops, College of Engineering from No. 9 (4.78 mm diameter) wire and 1018 steel with a nominal yield strength of 400 MPa. The spiral diameter of 110 mm was chosen to accommodate the size of the hollow core (116 x 116 mm). The length of 200 mm was chosen to accommodate the height of the concrete block (190 mm) plus one mortar joint (10 mm). The pitch of the spiral of 15 mm was chosen due to aggregate size of the fine grout (max 10 mm). The spiral reinforcement ratio was 0.02 in accordance to Clause 5.2.1.2 of CSA Standard S304.1-94 (CSA 1994). Design calculations related to the spiral are presented in Appendix A.

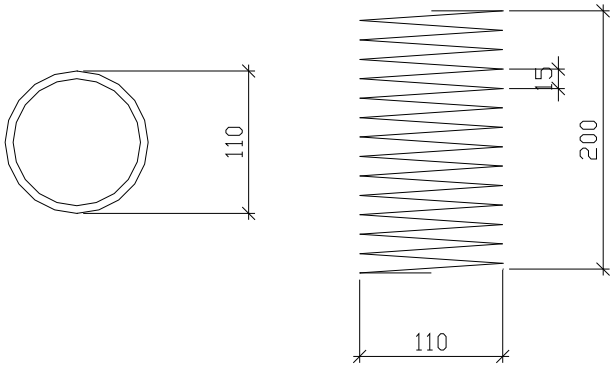

Figure 3.6. Details of a spiral (dimensions in mm).

3.4.6 Supporting Bases

Concrete bases, used for the support, lifting and moving of the test specimens, were reused from a previous study and were 670 x 345 x 185 mm (length x width x height) in dimensions. Figure 3.7 gives the details of the bases.

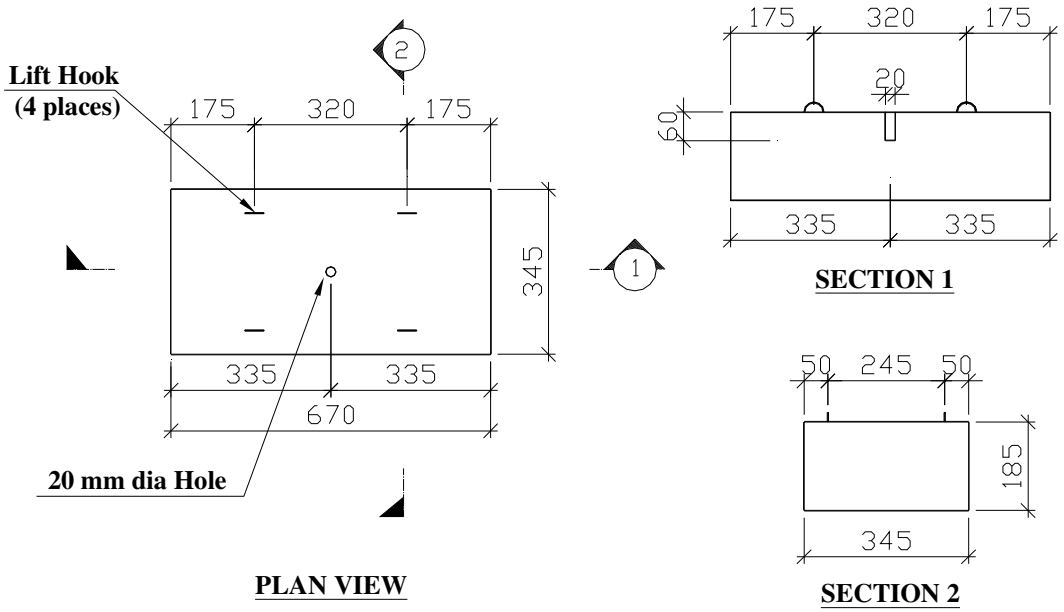

Figure 3.7. Details of the supporting concrete base (dimensions in mm).

To transfer load from the vertical reinforcement to the base, dowels had to be installed in the bases. To install the dowels, holes 20 x 60 mm (diameter x depth) were drilled using a heavy drill set. The dowels were then installed into the bases and secured with epoxy gel, which was purchased from Wallace Construction Specialties Ltd. The dowels formed a lap splice with vertical reinforcement to ensure that the vertical reinforcement was fully effective at the base of the wall specimen.

A No. 15 deformed steel reinforcing bar was chosen for the dowel to match the vertical reinforcement. To assist in the transfer of forces into the base, a bearing plate was welded to the dowel, which would rest directly on the base when the dowel was installed (see Fig. 3.8). The dimensions of the bearing plate were selected to provide the needed bearing area to transfer load from the dowel into the concrete base without crushing the concrete. The dowel and the bearing plate were made at the Engineering Shops in the College of Engineering at the University of Saskatchewan.

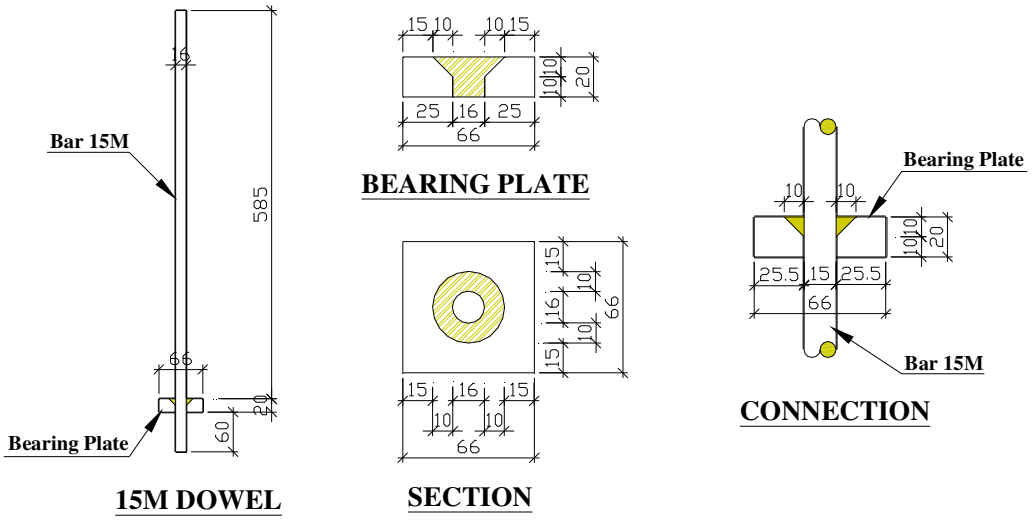

Figure 3.8. Details of the dowel and bearing plate (dimensions in mm).

The calculations relating to the bearing plate and required weld size are presented in Appendix A.

3.5 Prisms

Ten three-block-high plain prisms were made to determine the ultimate compressive strength and modulus of elasticity of the masonry assembly in accordance with Clause 9.2.2.2 of CSA Standard S304.1-94 (CSA 1994). All prisms were laid using only full size block units; dimensions of the prisms are shown in Fig. 3.9. All prism specimens were air cured along with the walls in the Structural Laboratory. Half of the test specimens were tested in February 2002 and the rest in August 2002, at the beginning and at the end of the wall testing program, respectively.

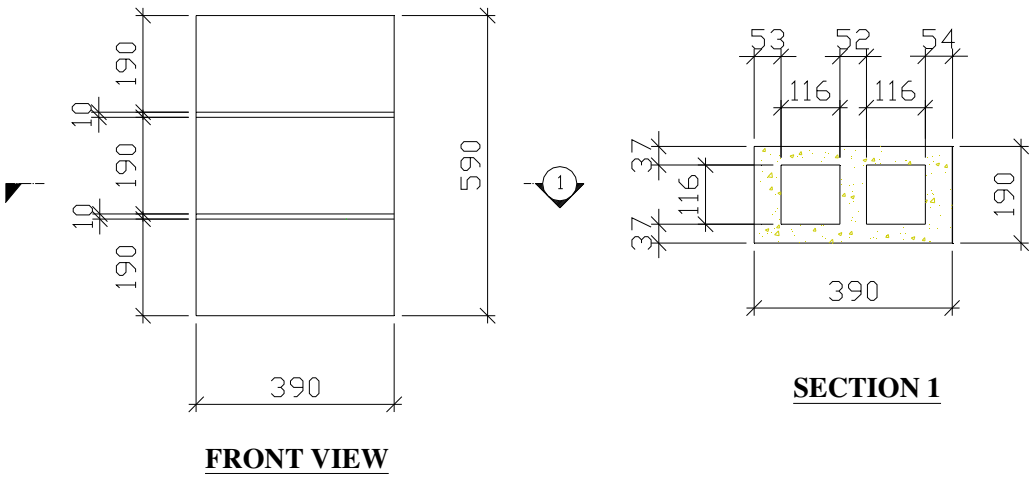

Figure 3.9. Concrete prisms (dimensions in mm).

3.6 Wall test specimens

3.6.1 General

As shown in Fig. 3.10, all wall specimens were five courses high with nominal dimensions of 590 x 1000 x 190 mm (width x height x thickness), and constructed with standard full block and half block concrete units. As was mentioned before, the specimens were partially grouted (middle core only) and were laid in running bond.

One consequence of the running bond configuration for the concrete units is that the hollow cores of the blocks are *shifted horizontally* by 32 mm relative to adjacent courses, as illustrated in Figure 3.10. This shift has significant influence on the grouted column formed within the wall: the vertical grout column is *not straight*, but rather features an alternating offset at every course level. Section dimensions of the hollow core are 116 x 116 mm; however, because of the 32 mm shift at each course level, the

straight section of the column is effective only 84 x 116 mm. The presence of offsets in the grout column will inevitably reduce its capacity for carrying axial load.

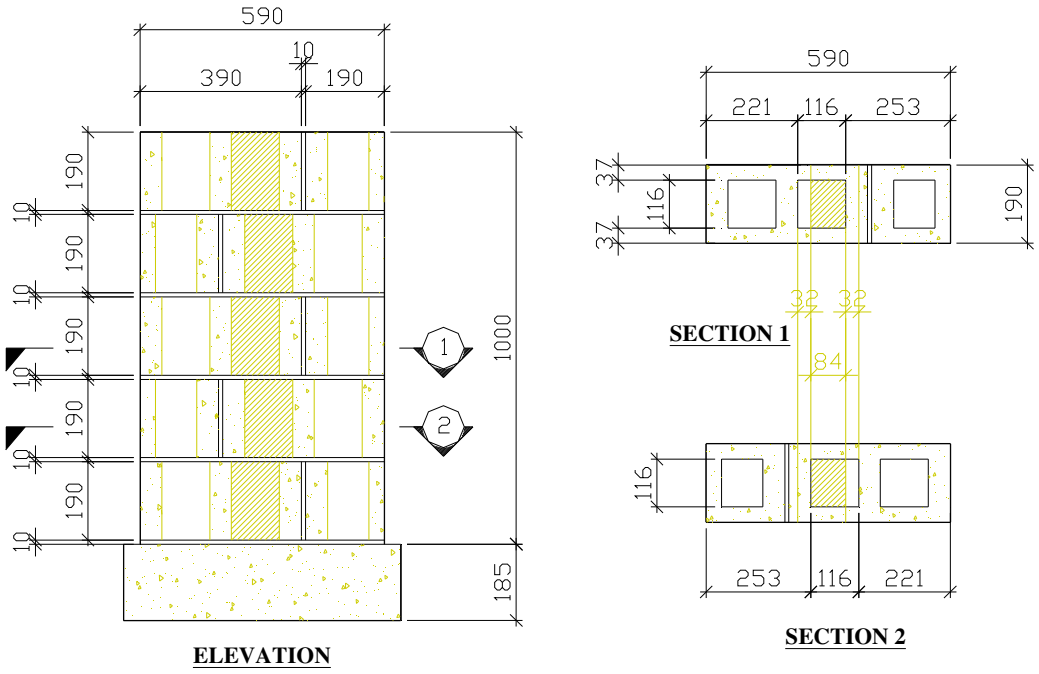

Figure 3.10. Elevation and cross-sections of a wall specimen, showing the shifted hollow cores (dimensions in mm).

To mitigate the effects of the offsets in the grout column, it was decided to place lateral joint reinforcement (ladder type) in every course for all three types of test specimens as described previously. Design calculations relating to the short walls are presented in Appendix A.

3.6.2 Test specimens of type *A*

Type ***A*** test specimens (***unreinforced, unconfined***) featured a plain unreinforced grouted core. The wall elevation and the major wall dimensions for type ***A*** specimens are shown in Figure 3.11. The walls had joint reinforcement (ladder type), placed in the mortar bed of every course.

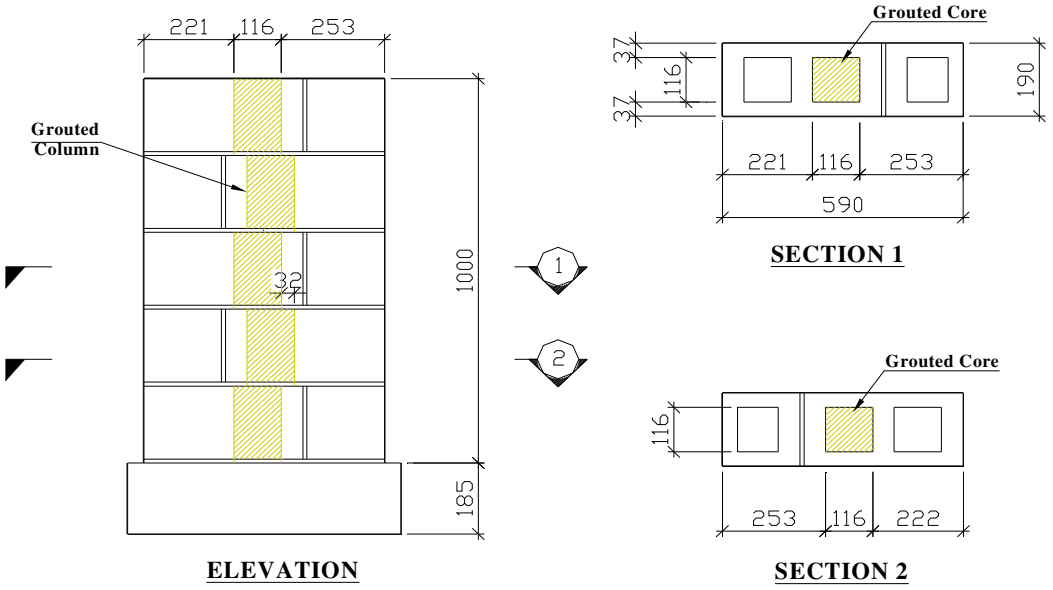

Figure 3.11. Type ***A*** wall test specimens (dimensions in mm).

3.6.3 Test specimens of type ***B***

Type ***B*** test specimens (***reinforced, unconfined***) featured a grouted core that was reinforced with a No. 15 vertical bar and contained joint reinforcement in the mortar bed in every course, as described previously. No. 15 dowels were aligned with the vertical reinforcement and installed into the concrete bases. Figure 3.12 shows the wall elevation and significant wall dimensions.

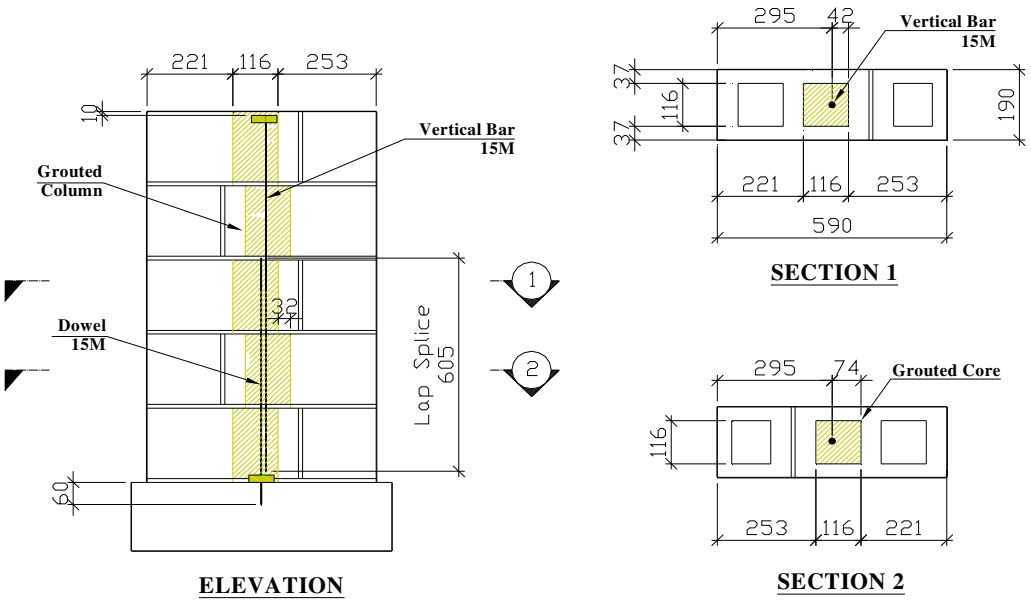

Figure 3.12. Type ***B*** wall test specimens (Dimensions in mm).

3.6.4 Test specimens of type ***C***

Type ***C*** test specimens (***reinforced and confined***) were similar to type ***B***, except that, in addition, they featured grouted cores confined with spirals 200 mm length and 110 mm diameter in every course. The spiral provided lateral confinement to the grouted core; in addition, the spiral was intended to improve the resistance of the vertical reinforcement to buckling. As discussed in Chapter 2, the spirals were designed to restrain the lateral expansion of the column core under axial load, inducing a triaxial state of stress in the grout; in doing so, the column core was made more ductile and potentially stronger. The spirals were made in segments of 200 mm in length to accommodate the block height, and were placed in every course (five per specimen). As indicated in Fig. 3.13, spirals 110 mm in diameter that ran the entire height of the wall could not be installed due to the offsets in the grouted core. Figure 3.13 shows the wall elevation and significant wall dimensions.

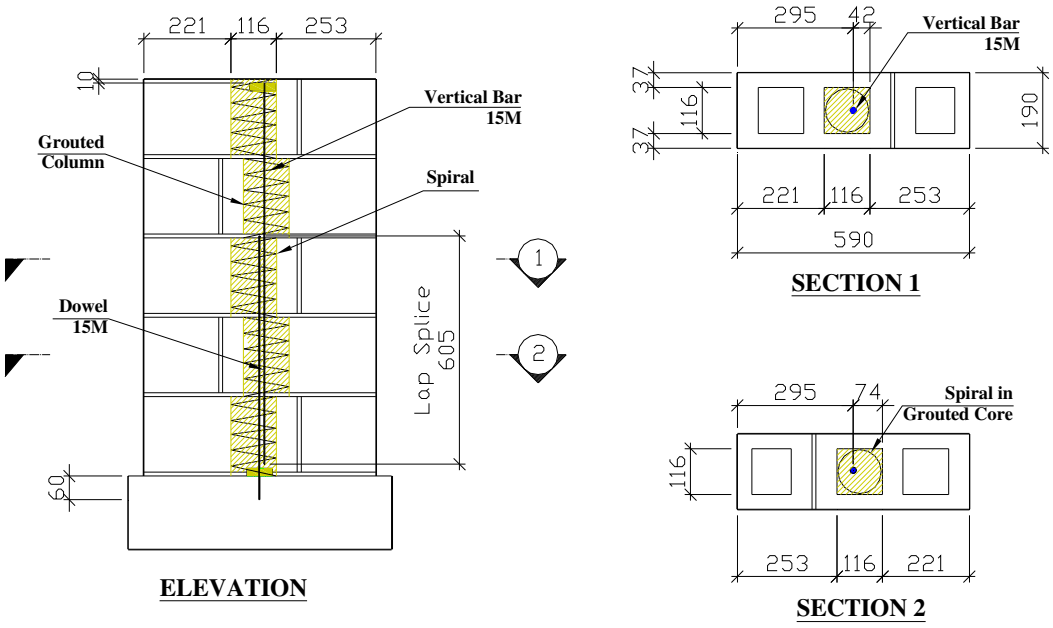

Figure 3.13. Type ***C*** wall test specimens (Dimensions in mm).

3.6.5 Wall specimen construction

The wall specimens were carefully built on the floor of the Structural Laboratory at the University of Saskatchewan. Two qualified masons from Gracom Masonry Northern (Saskatoon) constructed the walls and test prisms. The three types of walls (Types ***A***, ***B*** and ***C***) were constructed at one time. First, the bases were arranged in two lines, and blocks were laid course by course, as can be seen in the photograph of Figure 3.14. Care was taken to ensure that corresponding courses for all wall specimens in a line were level in order to promote uniformity between specimens.

Figure 3.14. First course of the Type ***A*** wall test specimens.

Second, the joint reinforcement (ladders) was placed in every mortar joint between courses in accordance with Clause 5.1.4 and Clause 5.2.4 of CSA Standard S304.1-94 (CSA 1994), as is shown in Figure 3.15.

Third, as the walls were being built, spirals for Type ***C*** test specimens were placed into middle core of the walls in every course in preparation for grouting. Construction of all walls and prisms was completed in one day.

Grouting of the specimens took place one week after construction of the wall specimens. The grout was placed into middle core of the constructed walls and vibrated using an electrical needle vibrator. Care was taken to ensure that the grout filled the bottom core and was adequately vibrated. The grout was placed one course at a time and vibrated until the first sign of bleeding was detected. After filling and compacting of the top core, the grout was levelled and the wall specimens were left to cure. The completed wall specimens and prisms are shown in Figure 3.16.

Figure 3.15. Placement of the joint reinforcement.

Figure 3.16. Completed wall test specimens (background) and test prisms (foreground).

Some difficulty was encountered in grouting the Type ***C*** specimens, as it was very difficult to ensure that the grout reached the bottom of the wall. The vertical bars spliced with dowels, as well as the spirals in every course, occupied a significant portion of the cores and left very little space for the grout and needle vibrator. Grout was forced to the bottom of the middle core with No. 10 rod and rodded 30 times. With much effort, though, Type ***C*** specimens were eventually grouted and vibrated.

Walls were air cured for at least one month at a temperature of 22°C in the Structural Laboratory, until the specimen strength was assumed to be appropriate for testing. In total, thirty short masonry walls and ten test prisms were constructed and tested.

3.7 Test Procedures

3.7.1 General

All test specimens (walls, prisms, cubes and cylinders) were subjected to monotonically increasing quasi-static axial compressive loading until ultimate failure. The test set-up consisted of a testing machine, a load cell, a data acquisition system and linear displacement sensors.

All masonry specimens (walls and prisms) were tested using the Amsler Beam Bender machine in the Structural Laboratory, University of Saskatchewan, having a capacity of 3000 kN. Grout and mortar control specimens were tested using a universal testing machine (A.H. Emery Co., New Canaan, Conn.) with capacity of 1335 kN. Both machines were hydraulically operated.

One load cell (Model 1100/200-K, Artech Industries, CA) with capacity of 1120 kN was used for the testing to measure the vertical compressive load. The load cell was placed between the crosshead of the testing machine and a steel distribution beam,

which was placed atop the specimen. The load cell was connected to the data acquisition system, which was controlled by LabVIEW™ (1999) software to record the load readings. Specific test set-ups for wall and prism tests are discussed in detail in subsequent sections.

Fourteen linear displacement sensors (Models HS10 and HS50, Measurement Group Inc., Releigh, NC), with strokes of 10 and 50 mm, were used to measure displacements during the loading of the specimens.

Prior to testing of the specimens, the linear displacement sensors (LDS) were calibrated to read increments of ± 0.0001 mm.

The load cell and linear displacement sensors were powered by a common six-volt power supply that produced output in the range of ± 6 volts. The readings from the load cell and all linear displacement sensors were recorded at two-second intervals using the data acquisition system controlled by LabVIEW™ (1999) software. After completion of the tests, the data were imported into an electronic spreadsheet for further processing. During the tests, it was noted that some of the LDS's did not work properly for unknown reasons, or exceeded their working range, so the data from those LDS's were not considered in the subsequent analyses.

3.7.2 Prisms

The three-block prisms were tested in two batches, with five prisms tested just prior to the start of the wall tests and two prisms tested just after the wall tests were completed (three prisms were broken during transport). The prism specimens were carefully lifted using a ten ton capacity crane and placed on the bearing beam of the testing machine. The standard test set-up for prism tests is illustrated in Fig. 3.17.

Steel angles were glued on the middle of the top and bottom courses of front and back faces of the prisms where the displacement measurements were to be taken. The bearing beam of the machine then was carefully moved into place at the appropriate testing position. Four LDS's were supported independently from the prism specimens and carefully positioned to measure the vertical displacements at the locations of the supporting angles. Figure 3.18 shows a typical prism specimen that had been prepared for a test.

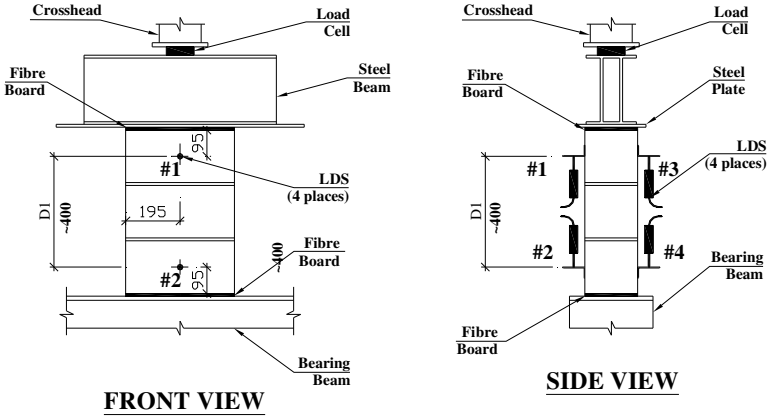

Figure 3.17. Prism test set-up.

Figure 3.18. Prism test specimen prepared for the test.

As shown in Figures 3.17 and 3.18, a pair of fibre boards (10 mm thick) was placed at the top and bottom of the prism to make the applied vertical load more uniform. A 20 mm thick steel plate and a 700 x 245 x 175 mm (length x height x width) load distribution beam were placed on top of the prism; these were used to transfer load from the crosshead and distribute it uniformly across the whole sectional area of the prism.

Prism specimens were tested to failure under monotonically increasing quasi-static load applied at a rate of approximately 2 kN per minute. During the tests, first cracking loads and failure loads were recorded; in addition, appearance and growth of cracks, as well as the splitting of the shells were noted and photographed periodically throughout the tests.

3.7.3 Walls

Wall specimens were tested in five series, each consisting of six specimens. The order of testing within each series was as follows: two specimens of type ***A*** were tested, followed by two specimens of type ***B***, and finally by two specimens of type ***C***.

The wall specimens were carefully lifted using a ten ton capacity crane and were placed on the bearing beam of the Amsler Beam Bender testing machine. In this position, walls were prepared for the test: four steel angles were glued to each side of the wall where the displacement measurements were to be taken. Four LDS's (on each side of the wall) were supported on the bearing beam independently from the wall specimens and carefully positioned to measure the vertical displacements at the locations of the supporting angles. Fourteen linear displacement sensors were placed at various locations on the test specimens, as can be seen in Fig. 3.19. The arrangement and orientation of the LDS's are described below:

- Sensors #1 and #2 were mounted on the top of the steel plate under the steel beam to measure vertical displacements (D1 and D2) between the steel plate and

the bearing beam of the machine (these were used principally to provide an indication of total deformation near ultimate, when the remaining sensors were removed to avoid damage to the instruments);

- Eight LDS's (#3 - #10) were mounted on the front and back faces of the masonry specimen (four on each side: two on the top course and two on the bottom course) to measure vertical displacement (D3 – D6) between the top and bottom courses (these were used to provide accurate load-deformation data at lower load levels); and
- Four LDS's (#11 - #14) were mounted on horizontal arms attached to the middle of the walls on the front side of the masonry specimen (on the second and fourth courses) to measure lateral displacements (D7) and twist of the specimens.

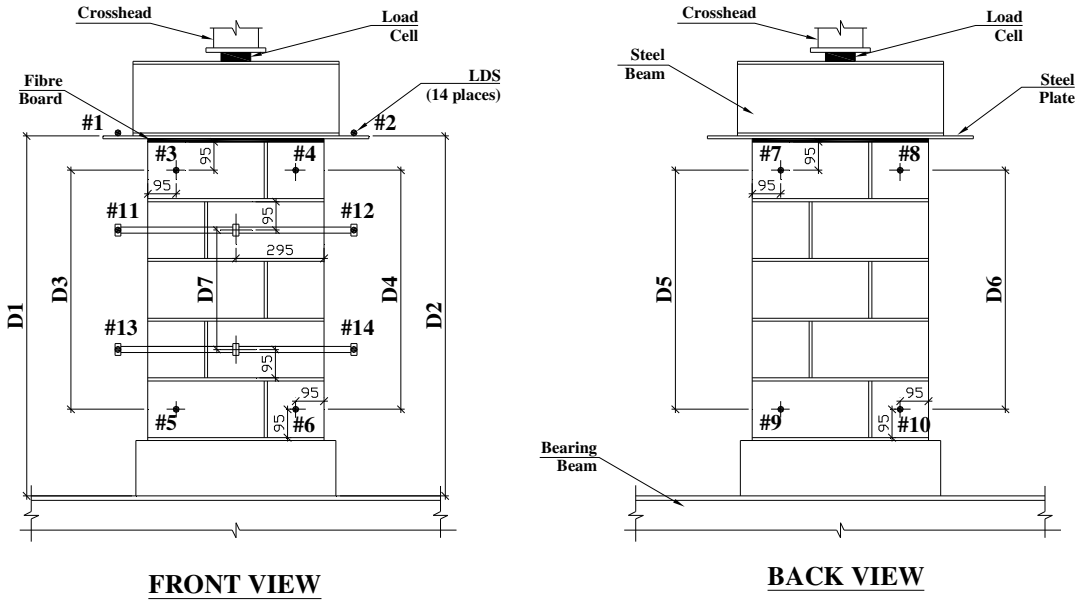

Figure 3.19. Wall test set-up (Dimensions in mm).

The bearing beam of the machine then was carefully moved into the test position. Figure 3.20. shows a test specimen prepared for the test.

Figure 3.20. Masonry test specimen prepared for the test (back side).

As shown in Figures 3.19 and 3.20, a piece of fibre board (10 mm thick) was placed at the top end of the specimen to distribute the applied vertical load more uniformly. Also, a 20 mm thick steel plate and a 700 x 245 x 175 mm (length x height x width) load distribution beam were placed on top of the specimen; these were used to transfer load from the crosshead, distributing it uniformly to the whole cross-sectional area of the specimen.

All specimens were tested under monotonically increasing quasi-static load to failure at a rate of approximately 5 kN per minute. The Amsler Beam Bender testing machine was operated in load control mode (i.e. the applied load level was monitored and controlled). Load and deflection readings were obtained for the entire test, including the post-peak region. During the tests, cracking loads and failure loads were recorded; the appearance and growth of cracks and splitting of shells were photographed. After full failure of the specimen, the remaining grouted column was uncovered and photographed.

3.7.4 Mortar cylinders

Mortar cylinders were tested in two batches, with five cylinders tested before the wall tests (October 26, 2001) and five cylinders tested after the wall tests (August 22, 2002). Fig. 3.21 shows a schematic of the cylinder test set-up.

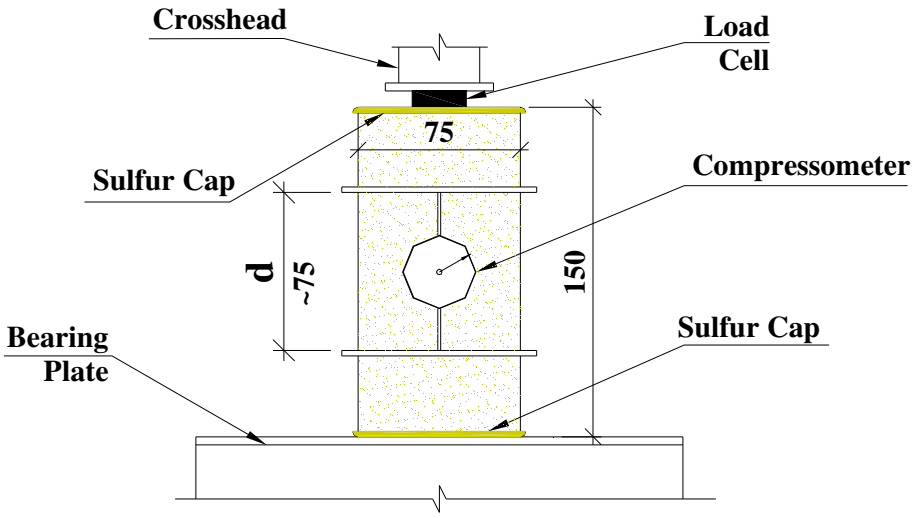

Figure 3.21. Cylinder test set-up (Dimensions in mm).

All mortar cylinders were capped with sulfur in accordance with CSA Standard A179-94 (CSA 1994) at least one day before they were tested. Compression tests were conducted using a universal testing machine (A.H. Emery Co., New Canaan, Conn.) with capacity of 1335 kN at a load rate of 2.5 kN per minute. To measure the displacement over a gauge length, **d**, a compressometer was used. During tests, all loads and displacements were recorded manually until the failure of the mortar cylinders.

3.7.5 Grout cylinders and prismatic specimens

Grout prismatic specimens and cylinders were tested in two batches, with five cubes and five cylinders tested before the wall tests (October 26, 2001) and five prisms and five cylinders tested after the wall tests (August 22, 2002). A schematic of the cylinder test set-up is shown in Fig. 3.21. A schematic of prism specimens test set-up is shown in Fig. 3.22.

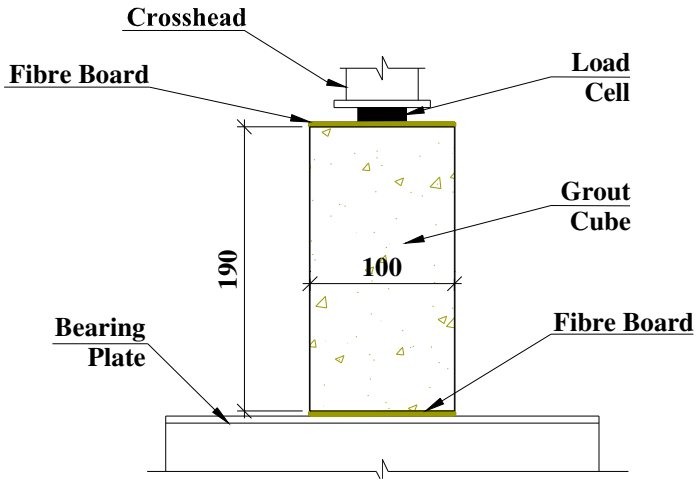

Figure 3.22. Prismatic specimen test set-up (Dimensions in mm).

All grout cylinders were capped with sulfur in accordance with CSA Standard A179-94 (CSA 1994) at least one day before they were tested. A pair of fibre boards (10 mm thick) was placed at the top and bottom of the grout prismatic specimens to make the applied vertical load more uniform. Compression tests were conducted using a universal testing machine (A.H. Emery Co., New Canaan, Conn.) with a capacity of 1335 kN at a load rate of 5.0 kN per minute and 12.5 kN per minute for cylindrical and prismatic specimens, respectively. To measure displacement over gauge lengths, **d** which permitted calculation of the strain in grout cylinders, a compressometer was used. During tests, all loads and displacements were recorded manually until failure of the grout prismatic and cylindrical specimens.

CHAPTER FOUR

TEST RESULTS

4.1 Introduction

The results and observations obtained during the wall test program are presented in this chapter. As was discussed in Chapter Three, the objectives of this program were to study the effect of the confinement of grouted and reinforced cells on the strength, stiffness, ductility and failure mode of short, partially grouted concrete masonry specimens subjected to axial load. In the current study, three types of short masonry walls were investigated: (1) specimens with a grouted middle core only; (2) specimens with a grouted middle core and vertical reinforcement (i.e. no confinement); and (3) specimens with a grouted middle core, vertical reinforcement and spiral confinement of the grouted core. In an attempt to make statistically reliable conclusions, each type of test specimen featured of ten masonry walls.

All three types of specimens were loaded with monotonically applied uniform axial compression. Cracks, crushing of the mortar, and spalling of blocks were monitored during the testing. The readings from the load cell and linear displacement sensors were used to measure the load versus displacement behaviour and thereby to investigate the stress-strain characteristics of the specimens.

The test results are illustrated in tabular as well as graphical form, including load versus time, load versus deflection and stress versus strain curves. Typical curves of

each type of test specimen are presented in this chapter. A complete listing of test data for all test specimens is provided in Appendices B, C, D and E. More detailed discussion of the results is presented in Chapter 5.

4.2. Component Materials

Mechanical properties of component materials were determined in the Structural Laboratory at University of Saskatchewan. The main purpose of the testing of component materials was to ensure that the specified quality was being maintained, and to characterize the material behaviour to facilitate comparisons with other published material. A summary of properties of the component materials is presented in Table 4.1. Representative stress-strain curves for each component material are presented in Fig. 4.1.

Table 4.1 Compressive strengths of component materials.

Component Material	No. of Specimens	Max. Value (MPa)	Min. Value (MPa)	Mean Value (MPa)	C.O.V.
Prisms	**7**	11.55	8.08	**10.28**	12.60%
Mortar	**10**	16.23	5.99	**12.37**	26.58%
Grout (cylinders)	**10**	19.68	12.25	**17.11**	11.96%
Grout (prismatic specimens)	**10**	23.77	17.54	**20.62**	11.01%

More detailed information on the component material tests is provided in subsequent sections.

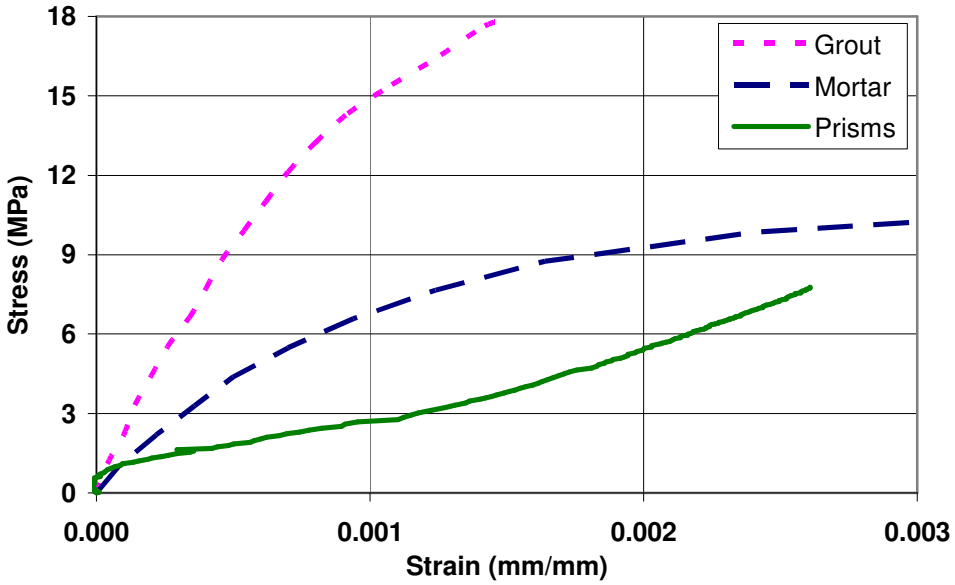

Fig. 4.1. Representative stress-strain curves for component materials.

4.2.1 Mortar cylinders

Ten 75 mm diameter by 150 mm high mortar cylinders were tested under compressive loading. The maximum, minimum and average values of compressive strength and strain at ultimate load (over a gauge length of approximately 75 mm), and coefficient of variation for each set are presented in Tables 4.2 and 4.3, respectively.

Table 4.2. Compressive strength of mortar cylinders.

Set No.	No. of Specimens	Max. Strength (MPa)	Min. Strength (MPa)	Mean Strength (MPa)	C.O.V.
Set #1	5	12.18	5.99	**9.78**	23.29%
Set #2	5	16.23	12.75	**14.97**	10.12%

Table 4.3. Compressive strain at ultimate load of mortar cylinders.

Set No.	No. of Specimens	Max. Strain (mm/mm)	Min. Strain (mm/mm)	Mean Strain (mm/mm)	C.O.V.
Set #1	5	0.0042	0.0018	**0.0028**	32.41%
Set #2	5	0.0029	0.0020	**0.0025**	15.49%

The results for Set #1 and Set #2 differ significantly due to the difference in the age of the specimens at testing. Five of the mortar cylinders (Set #1) were tested before the wall tests at an age of approximately fifty days and five (Set #2) were tested after wall tests were completed, at an age of approximately one year. Comparing the average compressive strengths of the two sets, Set #2 had a 53.9% higher compressive strength than Set #1. In accordance with Clause 9.2.2.5 of S304.1-94, the mortar compressive strength should be taken as the average compressive strength of all the specimens tested, which was found to be 12.37 MPa.

Stress versus strain curves representing the typical behaviour of each of the two sets of mortar cylinder tests are shown in Fig. 4.2. The modulus of elasticity for mortar cylinders, as calculated from the secant modulus at approximately 40% of ultimate compressive stress (in accordance with Clause 8.6.2.1 of A23.3-94), was found to be 8.8 GPa for Set #1 and 8.9 GPa for Set #2. The average measured modulus of elasticity was therefore found to be 8.8 GPa.

The test data for the mortar test specimens and a summary are presented in Appendix E.

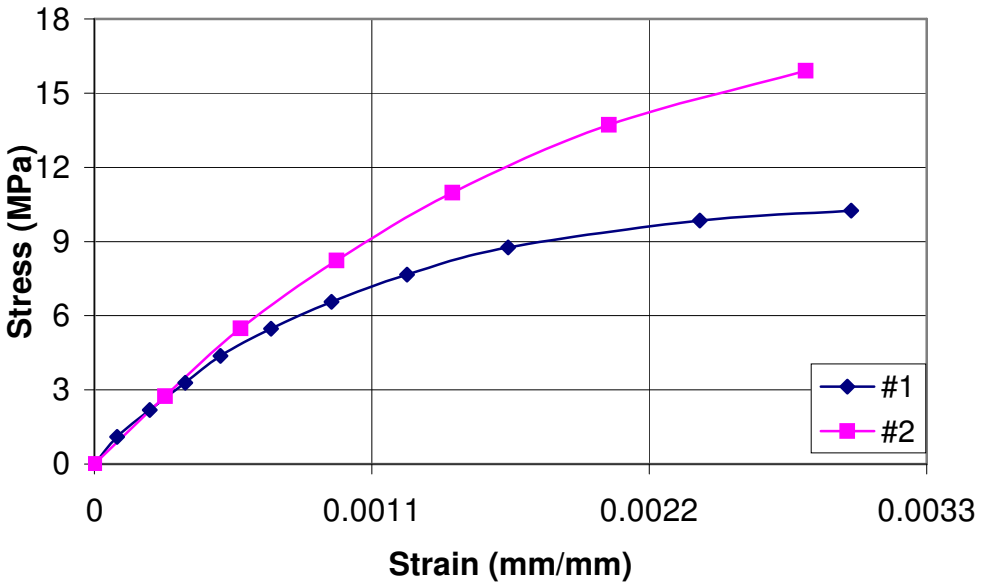

Figure 4.2. Representative stress-strain curves for mortar cylinders.

4.2.2 Grout prismatic specimens and cylinders

Ten grout prismatic specimens with dimensions of 100 x 100 x 190 mm were loaded to failure in compression in order to measure the stress-strain behaviour of the grout. Five of the grout cubes (Set #1) were tested before wall tests at an age of approximately fifty days and five (Set #2) were tested after wall tests at an age of approximately one year. The maximum, minimum and average values of compressive strength and coefficient of variation for each set are presented in Table 4.4.

Comparing the compressive strengths of grout prismatic specimens there is a very little difference between Set #1 and Set #2 test results. The average compressive strength of all grout prismatic specimens was found to be 20.6 MPa.

Table 4.4. Compressive strength of grout prismatic specimens.

Set No.	No. of Specimens	Max. Strength (MPa)	Min. Strength (MPa)	Mean Strength (MPa)	C.O.V.
Set #1	5	23.65	17.73	**20.30**	10.47%
Set #2	5	23.77	17.54	**20.93**	12.47%

In addition to the prismatic specimen tests, ten 75 mm diameter by 150 mm high grout cylinders were tested under compressive load. The maximum, minimum and average values of compressive strength, strain at ultimate load, and coefficient of variation for each set are presented in Tables 4.5 and 4.6.

Table 4.5. Compressive strength of grout cylinders.

Set No.	No. of Specimens	Max Strength (MPa)	Min Strength (MPa)	Mean Strength (MPa)	C.O.V.
Set #1	5	19.68	12.25	**17.03**	16.46%
Set #2	5	18.57	15.79	**17.20**	7.25%

Table 4.6. Compressive strain at ultimate load of grout cylinders.

Set No.	No. of Specimens	Max Strength (MPa)	Min Strength (MPa)	Mean Strength (MPa)	C.O.V.
Set #1	5	19.68	12.25	**17.03**	16.46%
Set #2	5	18.57	15.79	**17.20**	7.25%

The results for Set #1 and Set #2 do not differ significantly. In accordance with Clause 9.2.2.6 of S304.1-94, the grout compressive strength should be taken as the

average compressive strength of all the specimens. The average compressive strength for all grout cylinders was found to be 17.1 MPa. Comparison of the average compressive strength for grout prismatic specimens, presented in Table 4.4, and the average compressive strength for grout cylinders, presented in Table 4.5, shows that the average strength of the prismatic specimens was approximately 20% greater than that of the cylinders.

Stress versus strain curves from grout cylinder tests are shown in Fig. 4.3. The modulus of elasticity for grout cylinders, as calculated from the secant modulus at approximate 40% of ultimate compressive strength of the stress-strain relationships, was found to be 19.3 GPa for Set #1 and 22.9 GPa for Set #2. The average measured modulus of elasticity was found to be 21.1 GPa.

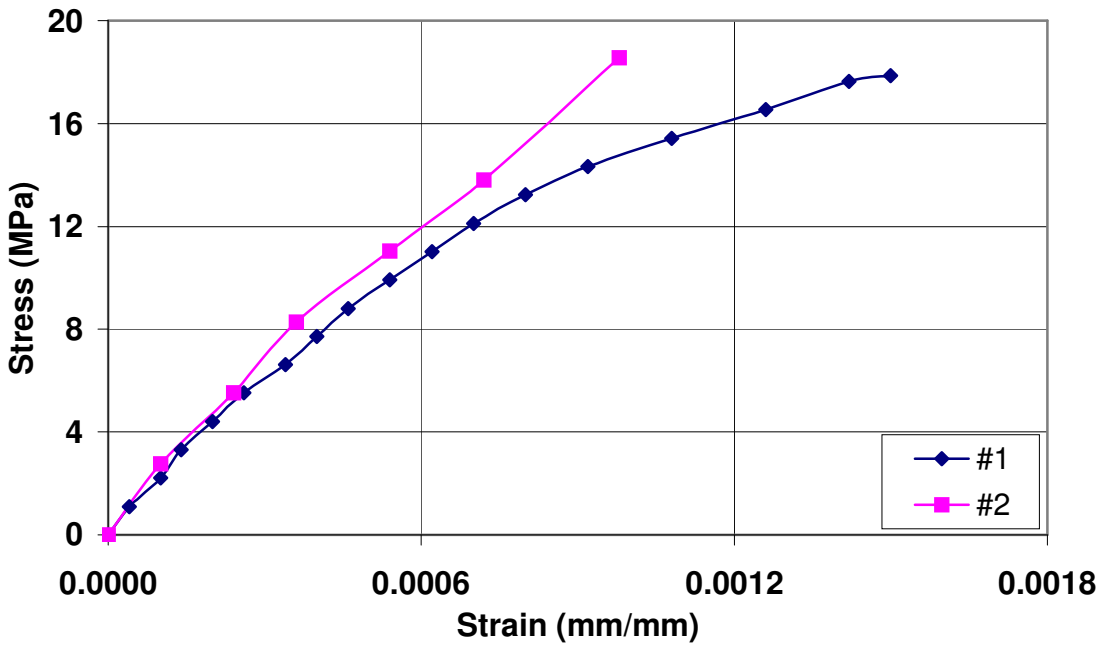

Figure 4.3. Representative stress-strain curves for grout cylinders.

Test data for all grout test specimens are presented in Appendix E.

4.3 Masonry Prisms

4.3.1 Test results

A total of ten prisms, each three courses high, were constructed in stack bond and were tested under axial compression to determine the compressive strength and modulus of elasticity of the masonry assembly. Five prisms (Set #1) were tested at the same time as the first six walls at the age of approximately six months and two (Set #2) were tested after the wall tests were completed at the age of approximately one year. Unfortunately, three prisms from Set #2 were broken during movement and the displacement data for the last two of concrete prisms were lost due to problems with the linear displacement sensors. The average compressive strength was calculated by dividing the peak load obtained during the tests by the effective cross-sectional area (the area of mortar bed, which is equal to area of the face shells only) of the prism (29,406 mm^2).

The results for all masonry prism tests are summarised in Table 4.7, including the ultimate axial loads reached during the tests, calculated ultimate strength, calculated ultimate strain, design compressive strength and modulus of elasticity. Discussions regarding the design compressive strength, modulus of elasticity, load-time relationship, load-deflection relationship and stress-strain relationship are presented in the following sections.

The detailed test data for the concrete prisms, including load-time curves, load-deflection curves and stress-strain curves, and its summary are presented in Appendix E.

Table 4.7. Summary of test results for masonry prisms.

Set No.	Failure Load (kN)	Failure Stress (MPa)	Failure Strain (mm/mm)	Design* Compressive Strength (MPa)	Modulus of Elasticity (GPa)
Set #1 (five specimens)	273.7	9.31	0.00272	7.86	2.99
C.O.V.	10.37%	10.37%	18.37%	6.67%	14.49%
Set #2 (two specimens)	330.6	11.24	n/a	10.58	n/a
C.O.V.	3.86%	3.86%	0%	6.60%	0%
Mean	**302.2**	**10.28**	**0.00272**	**9.22**	**2.99**

***** Calculated in accordance with CSA S304.1-94 Clause 9.2.2.2.

4.3.2 Loading history

The load versus time histories for the two sets of prisms are presented in Fig. 4.4. The load was recorded electronically at two-second intervals using a computer based data acquisition system. The appearance of the first cracks (at approximately 200 kN), the behaviour of the prisms before and after failure, and the ultimate loads can be clearly identified on the graph.

From a comparison of the two curves, it can be seen that the Set #2 prisms exhibited very rapid failure, which can be explained by the increased amount of handling experienced by these specimens prior to testing.

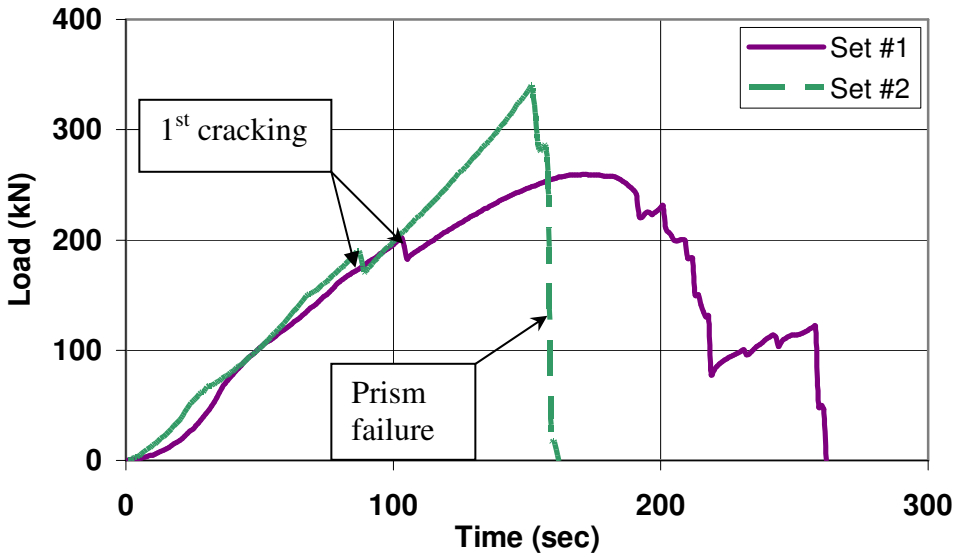

Figure 4.4. Representative time-load curves for concrete prisms.

4.3.3 Stress-strain relationship

The stress-strain curves for tested concrete masonry prisms are presented in Fig. 4.5. Strain values were derived from the average of four linear displacement sensors readings, taken at various locations on the face of the prisms (see Section 3.6.2). To avoid damaging the linear displacement sensors, strains were measured only to load levels of approximately 75% of the ultimate load.

The average compressive strength of the concrete prisms was obtained by dividing the ultimate load for all the prism specimens by the net area of the prism (29406 mm²). The average compressive strength was found to be 10.28 MPa.

For comparative purposes, the design compressive strength, f_m, was calculated in accordance with Clause 9.2.2.2 of the Canadian Design Standard CSA S304.1-94 (CSA 1994). In this clause, the design compressive strength is defined as the average

value of at least five test specimens less 1.5 times the standard deviation of the specimen strengths. As shown in Table 4.7, the average design strength for both sets was 9.22 MPa. Detailed calculations for compressive strength of masonry are presented in Appendix A.

In accordance with Clause 8.3.1.4 of CSA S304.1-94 (CSA 1994), the average modulus of elasticity was found to be 2.99 GPa with a coefficient of variation of 14.49%. The modulus of elasticity was based on the secant modulus of the five prisms tested under compression, measured over a stress range from 0.05 to 0.33 of the measured mean prism compressive strength (9.22 MPa).

The secant moduli for all specimens in Set #1 are presented in Table A.1. in Appendix A. Unfortunately, due to technical difficulties with the displacement transducers, there were no strain data available for Set #2.

A comparison of the measured value to suggested value (Clause 8.3.1.2 of S304.1-94) of $E_m = 850 f'_m = (850)(9.22) = 7837$ MPa indicates that the tested modulus of elasticity of concrete masonry prisms was 61.8% lower than the code value. Possible reasons for the low measured values include excessive handling of the specimens prior to testing and limited data due to problems with linear displacement sensors.

The initial response of all Set #1 specimens was quite similar (see. Fig. 4.5). At about 75% of the peak stress, vertical cracks began to open in the side webs and the stiffness dropped rapidly. Large cracks appeared (Fig. 4.6) just prior to failure. In general, the prisms failed from tensile splitting along the end face, eventually leading to crushing and spalling of the face shells, as can be seen in Fig. 4.7.

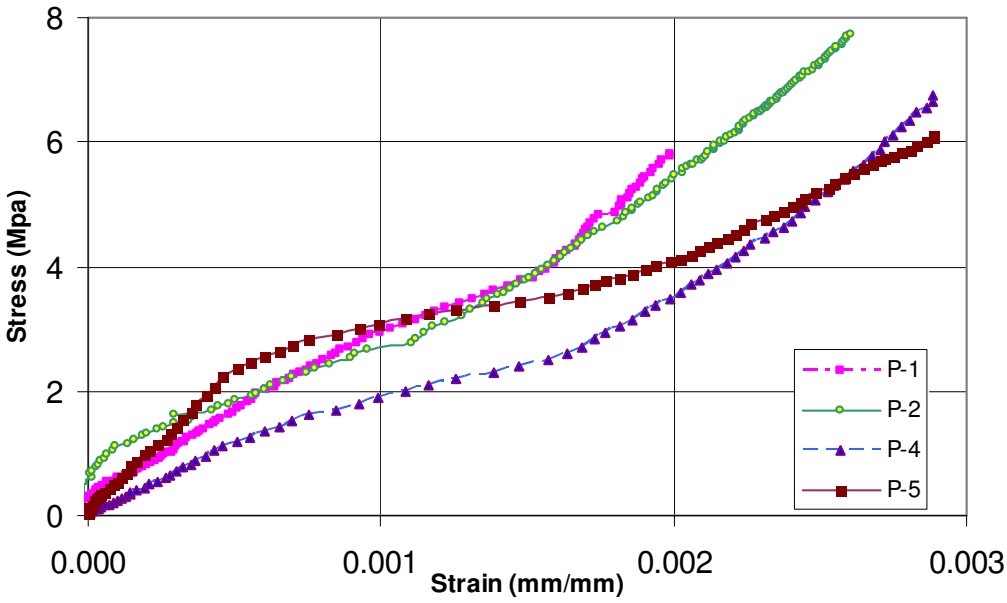

Figure 4.5. Stress-strain curves for four of the Set #1 concrete prisms.

Figure 4.6. Widening of the side crack in the prism.

Figure 4.7. Tensile splitting failure of the prism, combined with crushing and spalling of the face shells.

4.4 Masonry Walls

4.4.1 Overview

As was described in Section 3.6, three types of short masonry walls were tested in this study: (1) specimens with a grouted middle core only (Type ***A***); (2) specimens with a grouted middle core and vertical reinforcement (i.e. no confinement – Type ***B***); and (3) specimens with a grouted middle core, vertical reinforcement and spirals used to confine the grouted core (Type ***C***). All masonry walls were tested to failure under monotonically increasing axial load. During the tests, cracking loads, spalling loads and ultimate (maximum applied) loads were recorded. The appearance of the first cracks, the widening of the cracks and spalling of face shells were recorded and photographed. After full failure (collapse), the specimens were inspected and photographed. The summaries of experimentally obtained results for concrete masonry walls are presented

in tables, load history curves, load-deflection curves, stress-strain curves and photographs.

4.4.2 Cracking and failure behaviour

The summary of the applied loads at first cracking obtained from the wall tests for all three types of masonry specimens are presented in Table 4.8 and Fig. 4.8. The table and the bar graph give a good visual comparison of the maximum, minimum and mean first crack loads for the three types of masonry walls along with the corresponding standard deviations and coefficients of variation.

Table 4.8. Summary of loads at first cracking.

	Max. (kN)	Min. (kN)	Mean (kN)	St. Dev.	C.O.V. (%)
Type "A"	646.7	320.4	484.7	107.0	22.1
Type "B"	640.2	330.2	504.8	94.2	18.7
Type "C"	551.6	271.0	394.8	92.2	23.3

As can be seen from Table 4.8, type ***B*** specimens ***(reinforced, unconfined)*** had the highest average first crack load of 504.8 kN with a coefficient of variation of 18.7%. The lowest average first crack load of 394.8 kN (coefficient of variation of 23.3%) was observed for type ***C*** (***reinforced, confined***), suggesting that the presence of confinement lowered the resistance to initial cracking, which can be explained by a poor quality of grouting as discussed in Chapter 5. It was determined that the difference in the average first crack load for types ***C*** and ***B*** walls was statistically significant at the 90% level of confidence. The difference in average first crack loads between types ***A*** and ***B*** was 4.0%, which was not statistically significant at the 90% level of confidence, suggesting that the

presence of reinforcement in type ***B*** walls has no significant influence on first crack loads.

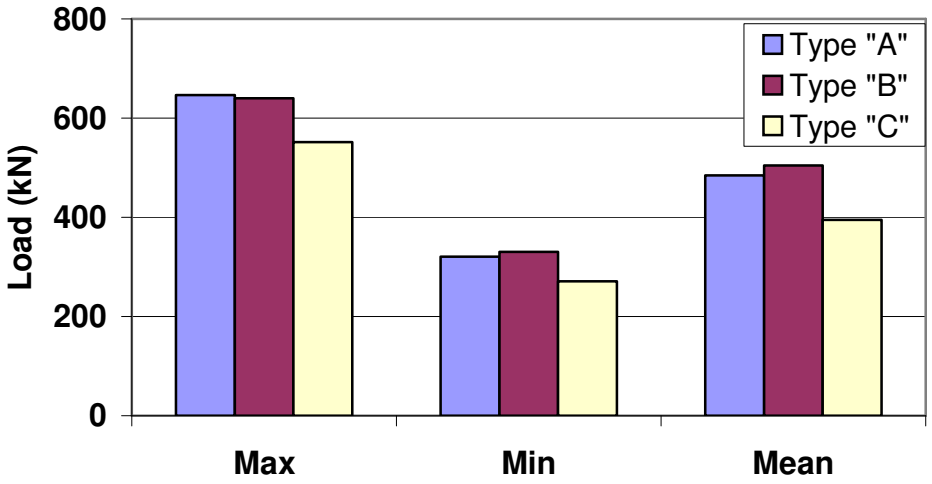

Figure 4.8. First crack loads for the three types of wall specimens.

The summary of spalling loads (the first observation of material becoming loose from face shells) obtained from walls tests for all three types of masonry specimens is presented in Table 4.9 and Fig. 4.9. The table and the bar graph give a good visual comparison of the maximum, minimum and mean spalling loads for the three types of masonry walls along with corresponding standard deviations and coefficients of variation.

Table 4.9. Summary of spalling loads for three types of specimens.

	Max (kN)	Min (kN)	Mean (kN)	St. Dev.	C.O.V. (%)
Type "A"	797.0	520.8	681.7	102.9	15.1
Type "B"	949.5	641.7	752.3	102.3	13.6
Type "C"	935.7	336.0	642.1	156.9	24.4

As can be seen from Table 4.9, type ***B*** specimens ***(reinforced, unconfined)*** had the highest maximum, minimum and average spalling loads with an average spalling load of 752.3 kN (coefficient of variation of 13.6%). The lowest average spalling load of 642.1 kN (coefficient of variation of 24.4%) was observed for the specimens of type ***C*** (***reinforced, confined***), suggesting that the presence of confinement lowered the spalling loads; however, considerable variation was observed, as indicated by the high and low values for the maximum and minimum spalling loads, respectively, for type ***C*** specimens. The difference in average spalling loads between types ***A*** and ***B*** was 9.4%, while that between types ***B*** and ***C*** was 14.6%. These differences were both found to be statistically significant at the 90% level of confidence.

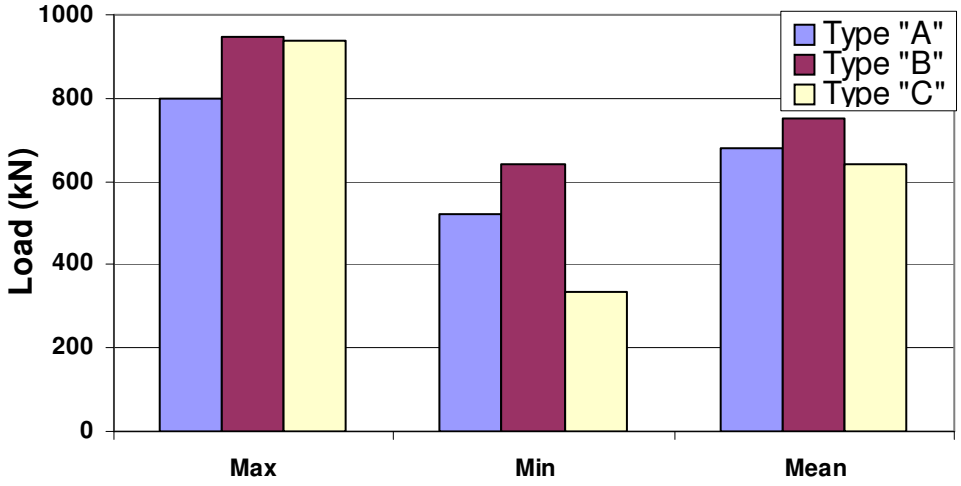

Figure 4.9. Spalling loads for the three types of wall specimens.

The summaries of failure loads obtained from walls tests for all three types of masonry specimens are presented in Table 4.10 and Fig. 4.10. The table and the bar graph give a good visual comparison of the maximum, minimum and mean failure loads for the three types of masonry walls along with the corresponding standard deviations and coefficients of variation.

Table 4.10. Summary of failure loads for three types of specimens.

	Max (kN)	Min (kN)	Mean (kN)	St. Dev.	C.O.V. (%)
Type "A"	934.8	647.0	800.6	99.9	12.5
Type "B"	949.5	650.3	792.9	96.6	12.2
Type "C"	1031.1	538.3	725.7	138.8	19.1

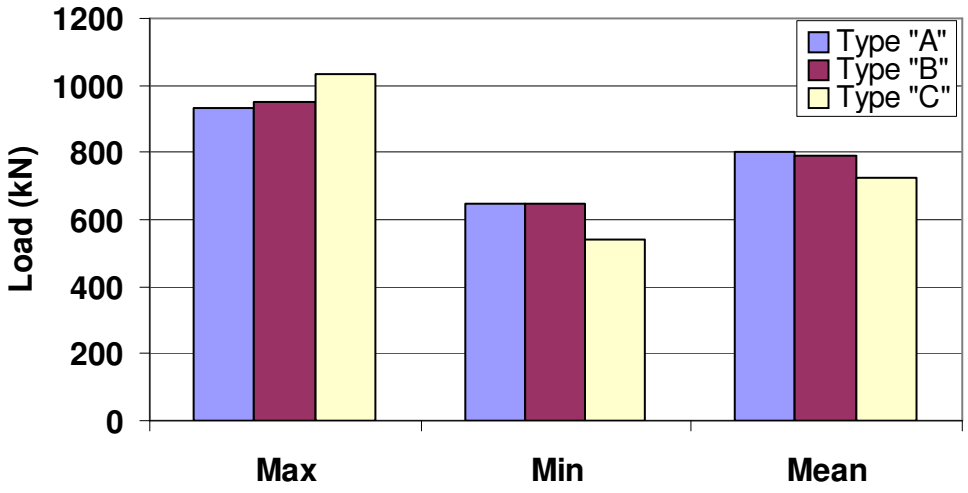

Figure 4.10. Failure loads for the three types of wall specimens.

As can be seen from Table 4.10, type ***A*** specimens ***(unreinforced, unconfined)*** exhibited the highest average failure load of 800.6 kN (coefficient of variation of 12.5%). The lowest average failure load of 725.7 kN (coefficient of variation of 19.1%) was observed for the specimens of type ***C*** (***reinforced, confined***), suggesting that the presence of confinement lowered the failure loads. However, type ***C*** specimens also exhibited the highest maximum load, the lowest minimum load, and the highest coefficient of variation. This high level of variability again suggests that the quality of workmanship for specimen preparation was lower than it should have been. The

difference in average failure loads between types ***A*** and ***B*** was 1.0% while that between types ***B*** and ***C*** was 8.5%. The 1% difference between walls ***A*** and ***B*** was not statistically significant at the 90% level of confidence, suggesting that the two types of walls had essentially the same axial strength. The 8.5% difference between wall types ***B*** and ***C*** was also not statistically significant at the 90% level of confidence, although it is large enough to suggest that some differences existed.

Further discussion of these results is provided in Chapter 5.

4.4.3 Loading history

The short masonry walls were tested under monotonically increasing axial loads. The applied load versus time histories for the three types of wall specimens are presented in Fig. 4.11, Fig. 4.12 and Fig. 4.13 for types ***A***, ***B*** and ***C***, respectively. The load was recorded electronically at two-second intervals using a computer-based data acquisition system.

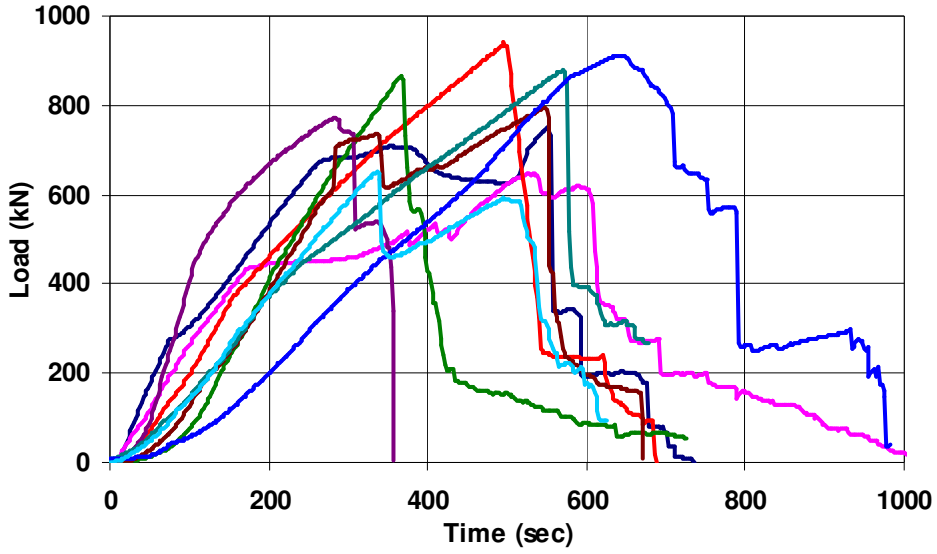

Figure 4.11. Load versus time histories for type ***A*** wall specimens.

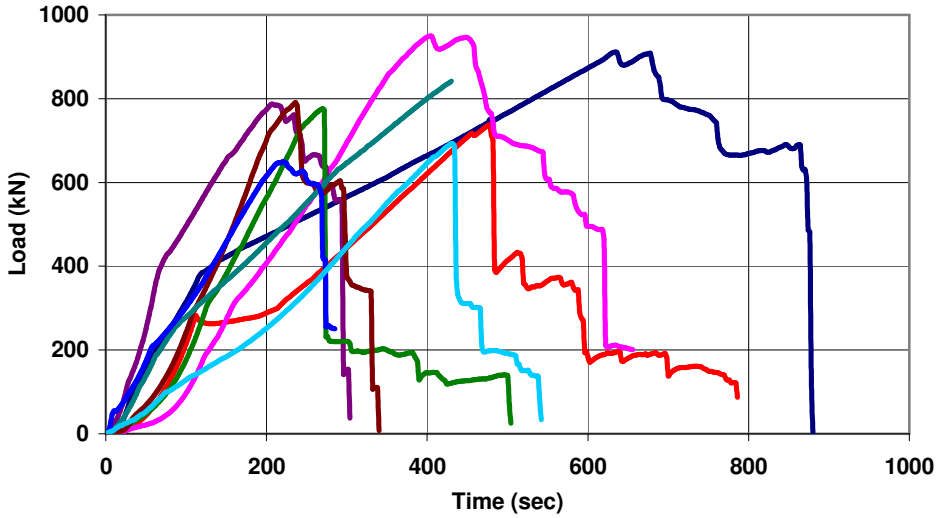

Figure 4.12. Load versus time histories for type ***B*** wall specimens.

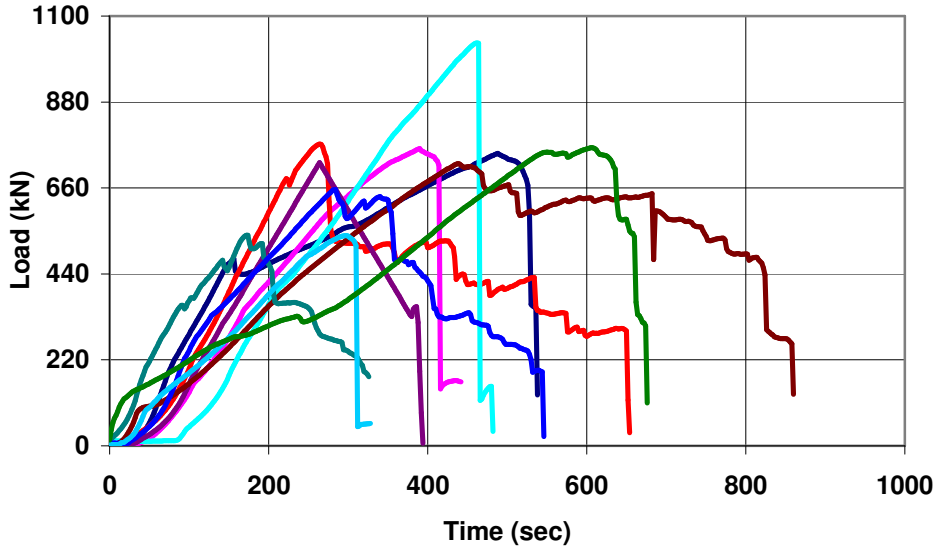

Figure 4.13. Load versus time histories for type ***C*** wall specimens.

The failure loads and the behaviour of the walls before and after failure may be clearly identified on the graphs. It is apparent that there is a similar behaviour in all three types of walls, both before and after failure. Once the failure loads were reached, there were sharp drops in load carrying capacity, resulting in steeply falling branches of the

graphs (after failure). Most walls exhibited brittle failure modes, as indicated by the steep, short descending branch. Some of the walls, though, in all three types of specimens, showed good ductility, which is indicated by the extended falling branches of the curves. Individual graphs for the load versus time histories for all three types of specimens are presented in Appendix B.

4.4.4 Load-displacement behaviour

Vertical strains along the height of the wall, as well as load-deflection curves derived using displacements measured at the top of the walls at the load points, represent the principal results obtained from the wall specimens tested under axial compression. The deflections were derived using readings from the linear displacement sensors installed on the top of the specimens (see Section 3.6.3 for location of sensors). These displacements include the crushing of the fibre board, which explains the initial apparent stiffening of the walls with increasing load, as seen in subsequent graphs. These displacements were used to show total deformation of the wall specimens to the end of the test, long after the other sensors attached to the face of the specimens had been removed to avoid damage to the instruments. The load-deflection curves for axially compressed concrete masonry walls are presented in Fig.4.14, Fig. 4.15 and Fig. 4.16.

Fig. 4.14 represents the load-displacement curves for type ***A*** (***unreinforced, unconfined***) specimens, showing that all walls exhibited similar behaviour before failure. The rising branches of the curves (before failure) are nearly coincident; in addition, very little difference in the falling branches of the curves (after failure) is apparent. This suggests that all type ***A*** wall specimens were of a consistent quality.

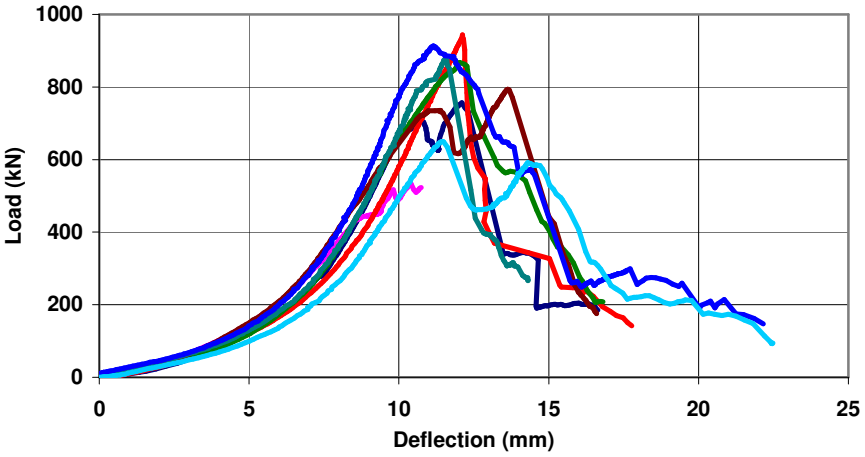

Figure 4.14. Load-deflection curves for test specimens of type ***A.***

Fig. 4.15 represents the load-displacement curves for type ***B*** (***reinforced, unconfined***) specimens. Once again, these plots suggest that all walls of this type exhibited similar behaviour before failure, although there is more variation in stiffness than was seen for type ***A*** specimens. In the descending branches of the curves (after failure), however, type ***B*** specimens exhibited a wider variety of behaviour, ranging from sudden declines and brittle failures to more gradual declines and ductile failures. Comparing Figs. 4.14 and 4.15, it can be deduced that the presence of vertical reinforcement in walls increased the variability of behaviour of the walls after failure to some extent and possibly enhanced ductility in some cases.

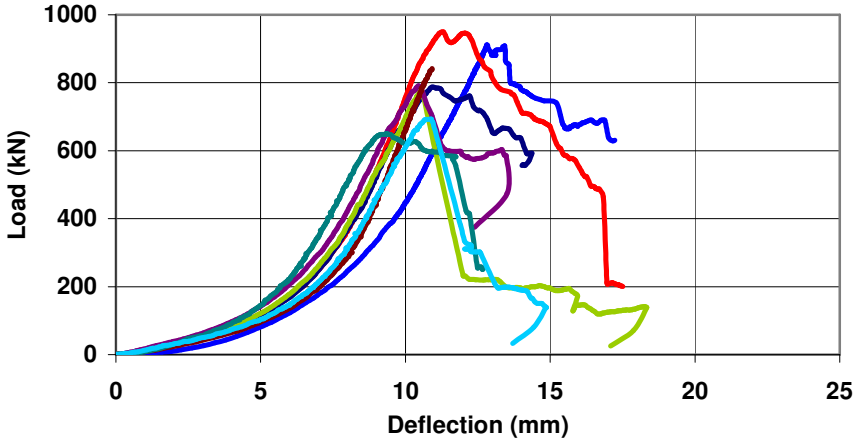

Figure 4.15. Load-deflection curves for test specimens of type ***B.***

Fig. 4.16 represents the load-displacement curves for type ***C*** (***reinforced, confined***) specimens. These curves, unlike those in Figs. 4.15 and 4.16, show a wide variety in behaviour both before and after failure. As can be seen from Fig. 4.16, only three of seven of the walls (the three plots with the lowest values in the ascending region) plotted had some similarities in behaviour. It can be concluded that the presence of vertical reinforcement and confinement (spirals) in the walls very much influenced the behaviour of the walls in all stages of loading. A visual inspection after failure suggested that the presence of vertical reinforcement and spiral confinement in the core decreased the quality of the grouted columns (introducing voids) and, in doing so, degraded the stiffness and load carrying capacity of that type of concrete masonry wall. However, there is some evidence to suggest an increase in ultimate ductility as compared to types ***A*** and ***B*** walls, as several type ***C*** specimens exhibited more gradual descending branches.

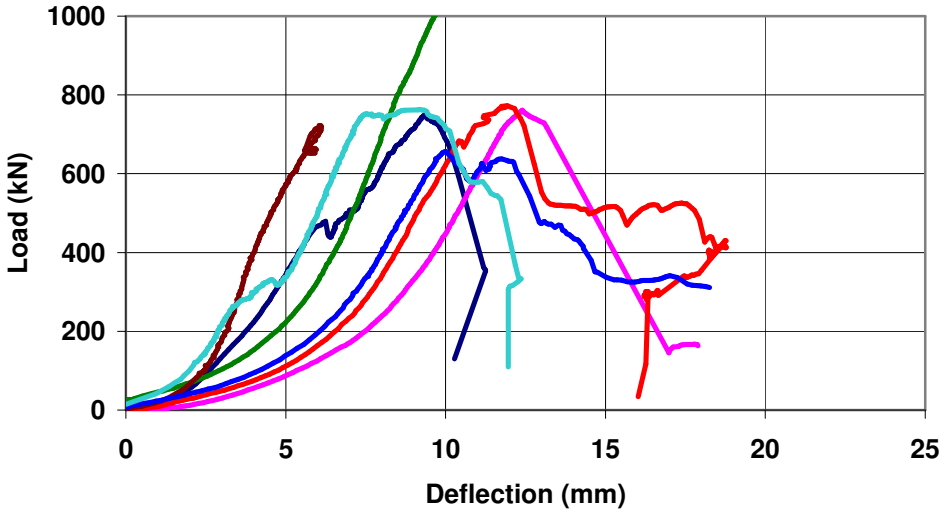

Figure 4.16. Load-deflection curves for test specimens of type ***C.***

For several of the wall tests (A-5, A-10, B-2, B-7, C-5, C-7 and C-9), the linear displacement sensors and load cell did not work properly for unknown reasons, or were operated beyond their functional range; as a result, the data from those tests were not included in the previous three figures and were not considered in the subsequent analyses of test results. More detailed data (individual graphs) for the load-displacement

relationships for all three types of specimens are presented in Appendix C. A more comprehensive comparison between the specimen types and a further discussion of the load-displacement results for the three types of walls are presented in Chapter Five.

4.4.5 Vertical stress-strain behaviour

As was mentioned previously, the stress-strain relationships within the wall describe the relationship between the load and the deformation within the wall. To be able to predict the ultimate strength of masonry structures it is necessary to have detailed information on the complete stress-strain characteristics of masonry in compression.

As discussed in Chapter 3, eight LDS's were mounted on the front and back faces of the masonry specimen to measure vertical displacements between the top and bottom courses, which were used to provide accurate load-deformation data. The strain values were derived as the ratio of relative vertical displacement between sensors mounted at the mid-height of the top course (on both the front and back faces of wall specimens) to that at sensors mounted at mid-height of the bottom course, divided by the vertical distance between those sensors. Four average strain measurements (front-top, front-bottom, back-top and back-bottom) for each wall specimen, along the specimen height, were calculated at each load level. For these tests, the average compressive stress of the concrete masonry walls was obtained by dividing the applied load by the effective area of the wall.

The detailed calculations of the compressive stresses and strains for each type of wall are presented in Appendix A. The stress-strain curves for all of the axially compressed concrete masonry walls are presented in Fig.4.17, Fig. 4.18 and Fig. 4.19.

Fig. 4.17 represents the stress-strain curves for type ***A*** (***unreinforced, unconfined***) specimens, suggesting that several of type ***A*** walls showed fairly linear behaviour at low strain levels. Interestly, several exhibited an apparent "hardening" behaviour, becoming stiffer at higher strain levels. These tests indicated that first crack

stresses occurred at strains of approximately 0.0014, and were limited by the premature formation of vertical cracking of the concrete masonry face and end shells, caused by lateral expansion of the grouted core. This vertical splitting of the walls made it necessary to remove the sensors (to avoid damage to the instruments). Type ***A*** masonry specimens showed the ability to support load up to strains as high as 0.0036 before spalling of face shells.

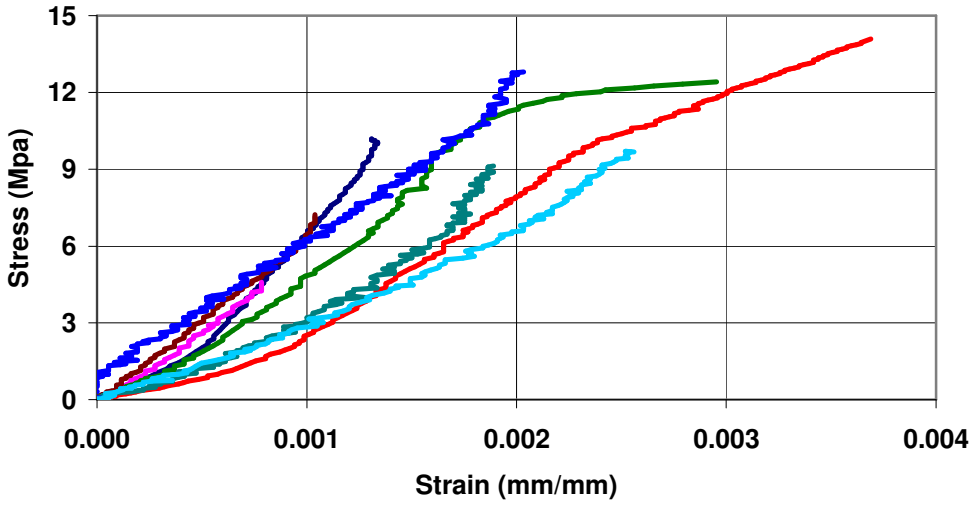

Figure 4.17. Stress-strain curves for type ***A*** wall specimens.

Fig. 4.18 represents the stress-strain curves for type ***B*** (***reinforced, unconfined***) specimens. These plots show that these walls exhibited similar behaviour in terms of initial slopes and some variability after first cracking in the non-linear regions; once again, both softening (reduction in slope) and hardening behaviour was observed at high strain levels. The tests indicate that first cracking stresses occurred at strains of approximately 0.0015 as a result of premature formation of vertical cracking of the concrete masonry face and end shells, caused by lateral expansion of the grouted core. In comparison, the same level of stress (which was assumed to be approximately 6 MPa) occurred at strains that ranged from 0.0006 to 0.0016 for type ***B*** walls and from 0.0009 to 0.0018 for type ***A*** walls. Type ***B*** masonry specimens showed the ability to support loads up to strains as high as 0.004 before spalling of face shells.

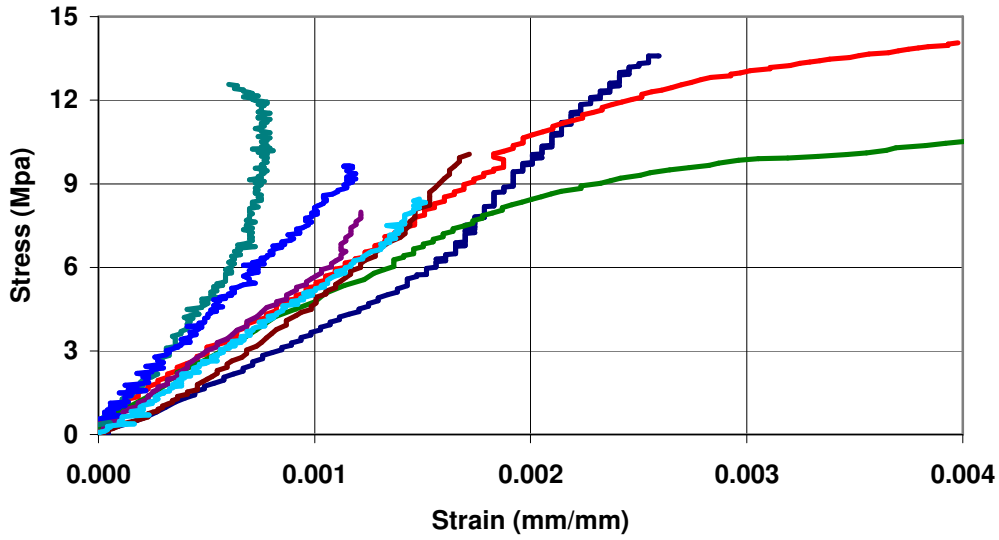

Figure 4.18. Stress-strain curves for type ***B*** of wall specimens.

Fig. 4.19 represents the stress-strain curves for type ***C*** (***reinforced, confined***) specimens and shows that the behaviour of the walls was somewhat more varied than those in series ***A*** and ***B***. The tests indicated that the first crack stresses occurred at strains of approximately 0.0011, as a result of premature formation of vertical cracking of the concrete masonry face and end shells, caused by lateral expansion of the grouted core. In comparison, the same level of stress (which was assumed to be approximately 6 MPa) occurred at strains that ranged from 0.0006 to 0.0017 for type ***C*** walls. The presence of the vertical reinforcement and confinement (spirals) in grouted cores very much influenced the strains. As mentioned previously, a visual inspection after failure suggested that the presence of vertical reinforcement and spiral confinement in the core decreased the quality of the grouted columns (introducing voids). The post-failure inspections revealed that crushing of the concrete masonry shells occurred precisely at locations where voids were apparent in grouted cores. Nonetheless, some type ***C*** masonry specimens showed the ability to support loads up to strains as high as 0.0035.

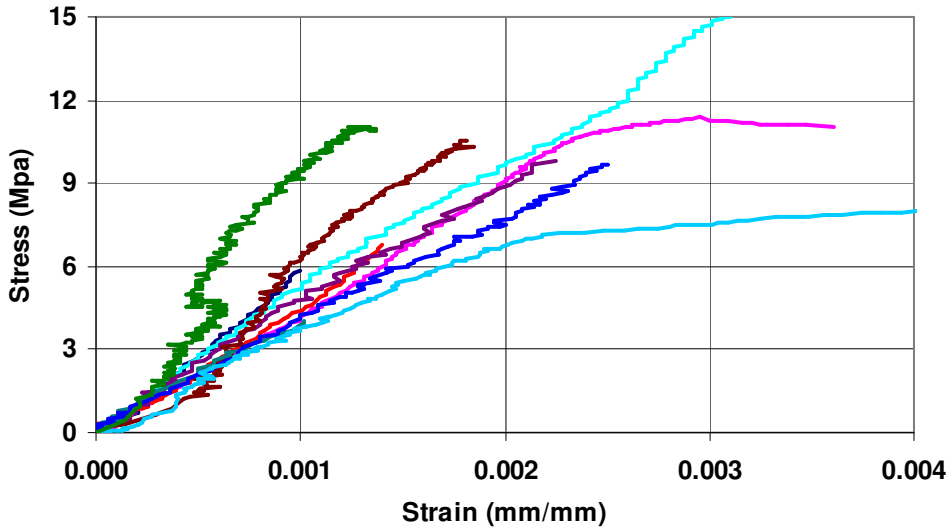

Figure 4.19. Stress-strain curves for type ***C*** of wall specimens.

Fig. 4.20 represents the average stress versus strain curves for all three types of wall specimens. The similarity in the slopes of all curves shows that there was little difference between the behaviours of three types of short walls before failure, although type C walls appeared to exhibit softer behaviour at strains above 0.001. All walls experienced the formation of vertical cracking of the concrete masonry faces and end shells, caused by lateral expansion of the grouted cores.

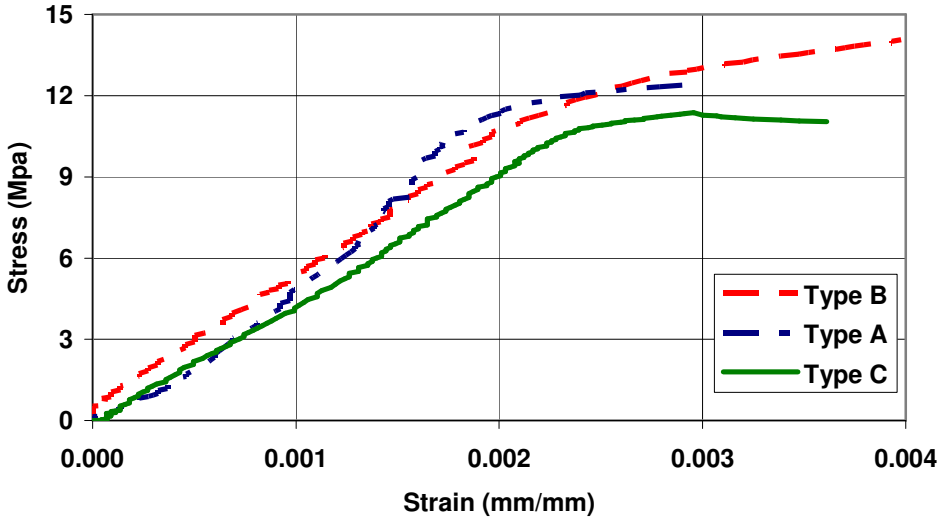

Figure 4.20. Average stress-strain curves for each wall type.

The areas under stress-strain curves may be taken as representing of the "toughness" of the walls: the larger the area, the better the toughness. From a comparison of the three types of walls, as can be seen on Fig. 4.20, type ***B*** (***reinforced, unconfined***) walls typically exhibited larger areas under the stress-strain curves and so demonstrated higher levels of toughness.

More detailed data (individual graphs) for the stress-strain relationships for all three types of specimens are presented in Appendix D.

4.3 Summary

The primary objectives of this program were to study the effect of vertical reinforcement and lateral confinement in grouted cores on the strength, deflection, ductility and failure modes of partially grouted concrete masonry walls. In addition, the mechanical properties of the component materials of the walls (concrete prisms, grout and mortar) were investigated.

In general, it was concluded that physical properties of the concrete blocks, mortar, grout and steel in the masonry walls were within expected ranges. The average compressive strengths were 12.4 MPa for mortar cylinders and 18.9 MPa for grout test specimens; these are within the expected ranges. The average compressive strength calculated for concrete masonry prisms was 9.22 MPa and average modulus of elasticity for concrete masonry prisms was 2.99 GPa; these values were lower than expected, based on provisions given in the CSA Standard S304.1-94 (CSA 1994).

The maximum and average values of ultimate loads (failure, spalling, and first crack), vertical displacements, compressive stresses and strains, standard deviations and coefficients of variations for component materials and short masonry walls were summarised in tabular and graphical form in this chapter.

Load-displacement curves were used to summarize the principal results obtained from the specimen tests under axial compressive load. It can be concluded that all three types of walls exhibited similar behaviour before failure, but varied significantly after failure. The presence of vertical and lateral spiral reinforcement had a positive influence on the wall's behaviour and failure modes (from sudden and brittle to more gradual and ductile).

From the stress-strain curves, it appeared that the presence of vertical and lateral spiral reinforcement in the grouted cores significantly influenced the levels of strains at given levels of stresses. A visual inspection after failure suggested that the presence of vertical reinforcement and spiral confinement in the core decreased the quality of the grouted columns (introducing voids). The post-failure inspections revealed that crushing of the concrete masonry shells occurred precisely at locations where voids were apparent in grouted cores.

A more comprehensive discussion and comparison of the behaviour of the short masonry walls, including crack patterns, failure modes and ductility of these walls, are presented in Chapter Five.

CHAPTER FIVE

DISCUSSION OF TEST RESULTS

5.1 Introduction

The discussion of the test results and behaviour of the short concrete masonry walls are presented in this chapter. Also presented are observations regarding the crack patterns, the failure modes, the ductility and results from the post-failure inspections of the short concrete masonry walls.

As was discussed in previous chapters, the objectives of this study were to study the effect of confinement on the strength, stiffness, ductility and failure modes of partially grouted concrete masonry specimens. In the current study, three types of short masonry walls were investigated: (1) specimens with a grouted middle core only; (2) specimens with a grouted middle core and vertical reinforcement (i.e. no confinement); and (3) specimens with a grouted middle core, vertical reinforcement and spirals (i.e. confined). During the tests, the appearance and widening of cracks, as well as spalling of the shells were photographed; in addition, after failure of the specimens, the remaining grouted columns were inspected and photographed. Due to the considerable number of these photographs, only a representative sample is provided in this chapter; the remainder are presented in Appendix F.

5.2 Behaviour of the short masonry walls

5.2.1 General observations

The behaviour of the walls is discussed with respect to load-deflection behaviour, stress-strain behaviour, ductility and strength. The overall behaviour of all masonry specimens can be illustrated by a set of average stress-strain relationships obtained for three types of short masonry walls, which are shown in Fig. 5.1. For this figure, the axial stress values were calculated by dividing the load by the effective cross-sectional area of the walls, while the strain values were derived from the average of the readings from two linear displacement sensors, which were mounted on top of the steel plate above the walls (see Fig. 3.19 for sensor arrangement). Displacements plotted in Fig. 5.1 include the crushing of the fibre board, which explains the initial apparent stiffening of the walls with increasing stress.

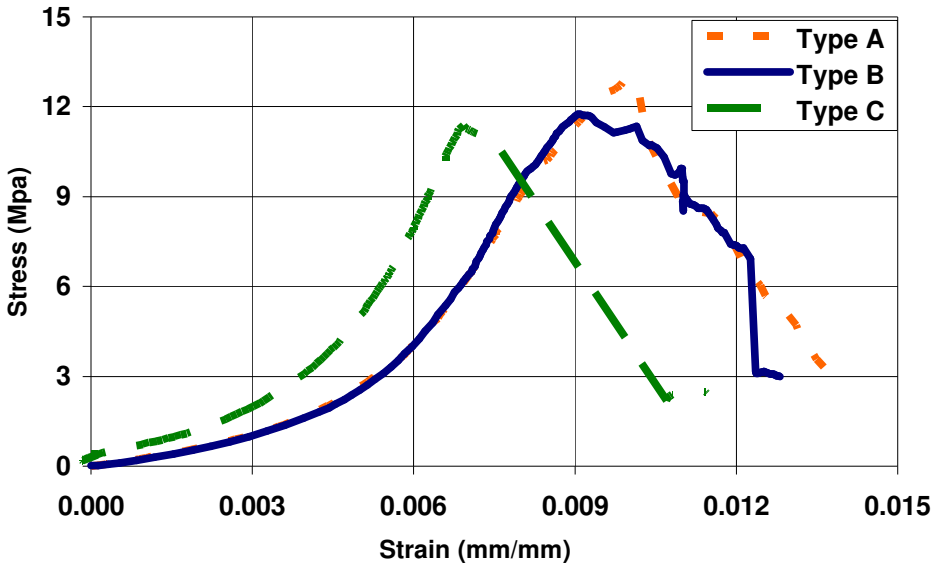

Fig. 5.1. Average stress-strain curves for type ***A***, ***B*** and ***C*** specimens.

Stress-strain curves for types ***A*** (grouted only) and ***B*** (vertical reinforcement but no confinement) are seen to be nearly coincident in the initial portion of the load-

deformation history. Type ***C*** (vertical reinforcement plus spiral confinement) specimens behaved in a less ductile manner with slightly lower strength, possibly due to the incomplete grouting of the cores that was observed when inspecting the failed samples.

At about 55% - 65% of the peak stress for all specimen types, the first cracks became visible on the side face of the wall, as shown in Fig. 5.2. The peak stress was reached when one or more surfaces of the wall showed clear signs of wide cracks, sometimes accompanied by a loud sound of fracture, often with only partial failure in the block shells, as seen on Fig. 5.3. The post-peak load-carrying capacity began to decrease either abruptly or gradually with more visible signs of cracks and the spalling of shells until a residual strength level was reached, and the failure was stabilized. The tests were terminated after substantial post-peak deformation, after which the failure surface of the grouted core was made visible by removing the loose face shells of concrete blocks, as illustrated on Fig. 5.4.

Fig. 5.2. First crack appearance.

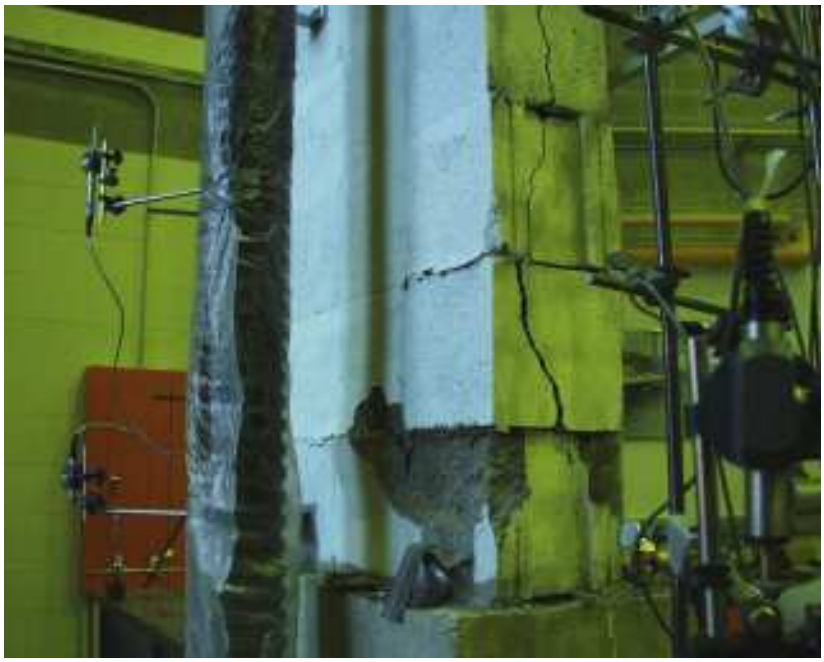

Fig. 5.3. Widening of cracks and crushing of mortar and block shells.

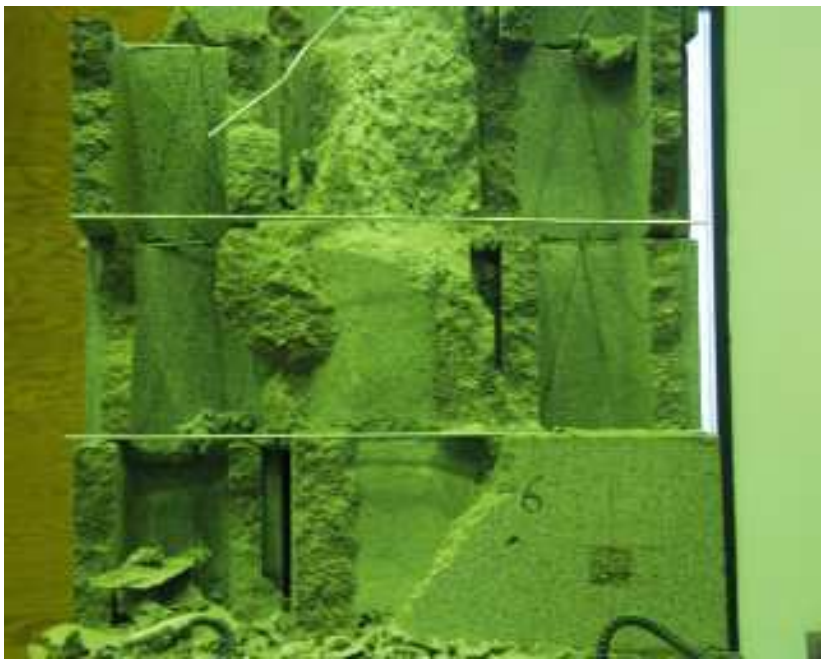

Fig. 5.4. Failure of the specimen.

On the basis of these observations it was concluded that partially grouted concrete masonry walls progressed through several specific stages of behaviour. As suggested by Hart et al. (1988), the behaviour of the short axially loaded specimens

could be described by four limit states (shown in Fig. 5.5). These stages are discussed further below.

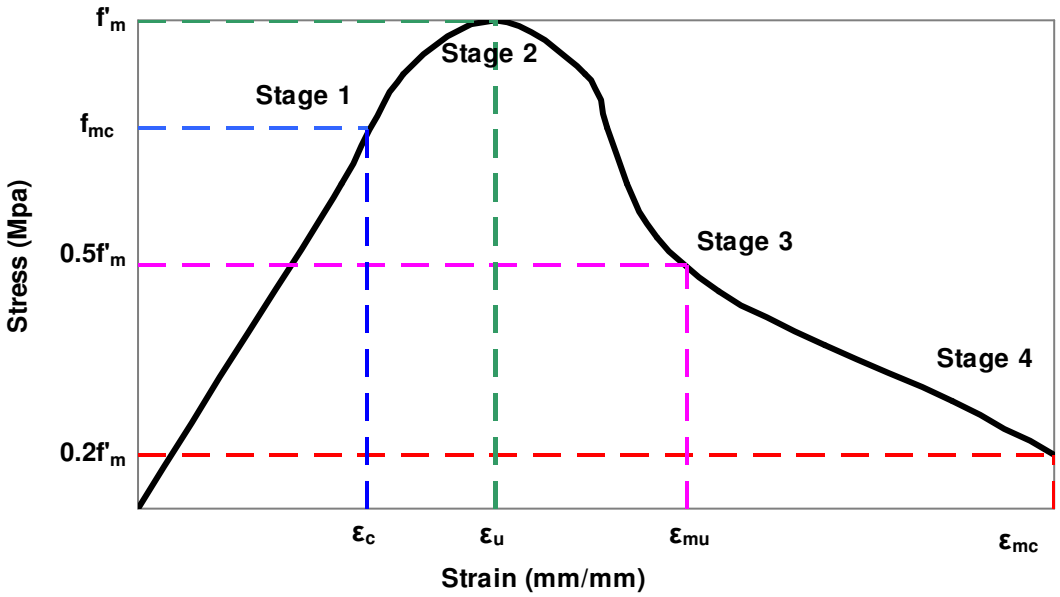

Fig. 5.5. Typical stress-strain curve for masonry walls by Hart et al. (1988).

5.2.2 Behaviour Stage I

Prior to reaching limit state 1, the walls were uncracked and the stress level was less than the first cracking stress. The first cracks were noted as soon as they were visible on the side faces of wall specimens. The average first cracking stresses ($f_m = f_{mc}$), marking the end of Stage 1, for each type of wall are presented in Table 5.1. The average compressive strains corresponding to limit state 1 for each type of wall also presented in Table 5.1. These strains include deformations in the fibre board and therefore are not representative of the actual strains in the walls but may be used for rough comparison of the behaviour of different wall types.

Table 5.1. Summary of first cracking stresses and strains for three types of specimens

Stage I	Type "A"	Type "B"	Type "C"
Mean Stress (MPa)	7.31	**7.53**	6.40
C.O.V.	20.15%	18.63%	18.14%
Mean Strain (mm/mm)	0.00672	**0.00749**	0.00532
C.O.V.	23.96%	9.77%	38.52%

As can be seen, the type ***B*** walls experienced the highest first crack stresses and highest first crack strains on average, while type ***C*** walls experienced the lowest first crack stresses and lowest first crack strains.

5.2.3 Behaviour Stage II

Behaviour stage II is an ultimate structural damage stage, ending at the ultimate limit state. The ultimate loads calculated on the basis of the CSA Standard S304.1-94 (CSA 1994), with no material resistance factors included, and average measured ultimate loads (respectively) were found to be: 502.5 kN and 800.6 kN for type ***A*** walls, 582.5 kN and 792.9 kN for type ***B*** walls and 589.7 kN and 725.7 kN for type ***C*** walls (detailed calculations of the predicted maximum axial loads for three types of short masonry walls are presented in Appendix A). All three types of walls experienced higher ultimate loads than were predicted. The average ratios of measured to calculated values were found to be 1.6 for type ***A*** walls, 1.4 for type ***B*** walls and 1.2 for type ***C*** walls.

In this behaviour stage, the walls were cracked and the compressive stress in the walls exceeded the first cracking stress. At the ultimate limit state, the applied compressive stress was equal to its maximum compressive stress ($f_m = f'_m$). The

compressive strength of masonry walls, marking the end of Stage 2, for each type of wall are presented in Table 5.2. The average compressive strains corresponding to the ultimate limit state are also presented in Table 5.2. As described in the previous section, the strains include some crushing of the fibre board but are useful for a rough comparison of the behaviour of different wall types.

Table 5.2. Summary of ultimate cracking stresses and strains for three types of specimens

Stage II	Type "A"	Type "B"	Type "C"
Mean Stress (MPa)	**11.96**	11.83	11.08
C.O.V.	12.54%	12.21%	17.80%
Mean Strain (mm/mm)	**0.00899**	0.00859	0.00782
C.O.V.	22.37%	17.30%	23.29%

As can be seen, the type ***A*** walls produced the highest compressive strength and highest strains, while type ***C*** walls experienced the lowest ultimate strength and lowest ultimate strain. This result was unanticipated as the lateral confinement in type ***C*** specimens was expected to increase the strength marginally, at least, and the ultimate deformation substantially. However, incomplete compaction may have decreased the ultimate capacity of type ***C*** walls. The average compressive strength of concrete masonry prisms, which was discussed in Chapter 4.3.3, was found to be 10.28 MPa. It can be concluded that all three types of walls experienced higher stresses than indicated by the prism tests.

5.2.4 Behaviour Stage III

In Stage III, the walls were cracked and the compressive strains exceeded the strain at ultimate strength; however, the stress decreased in value due to cracking and crushing of wall shells. The third limit state was deemed to be reached when the compressive stress in the masonry has been reduced by 50% from its maximum value. This stage is defined as the design strength limit stage.

The calculated average loads at limit state 3 were 400.3 kN for type ***A*** walls, 396.5 kN for type ***B*** walls and 362.9 kN for type ***C*** walls. Design compressive stresses and compressive strains at this limit state are presented in Table 5.3.

Table 5.3. Summary of design cracking stresses and strains for three types of specimens

Stage III	Type "A"	Type "B"	Type "C"
Mean Stress (MPa)	5.65	6.28	**3.85**
C.O.V.	32.84%	31.99%	51.30%
Mean Strain (mm/mm)	0.01118	0.01060	**0.01043**
C.O.V.	15.98%	33.76%	43.16%

As can be seen, the type ***C*** walls produced the lowest design stress and the lowest design strain, which can suggest that lateral confinement did not have a positive influence at this stage.

5.2.5 Behaviour Stage IV

In Behaviour Stage IV, the walls had essentially failed, with compressive strains exceeding that at limit state 3. In this stage, the walls exhibited significant physical distress, but were capable of carrying at least 20% of the peak compressive load. The calculated average loads defined at the end of Stage IV were 160.1 kN for type ***A*** walls, 158.6 kN for type ***B*** walls and 145.1 kN for type ***C*** walls.

The stress-strain behaviour of all three types of wall specimens was seen to follow the typical stress-strain curve suggested by Hart et al. (1988). It can be concluded that all three types of masonry walls followed similar response patterns and were substantially stronger than predicted by design equations in CSA Standard S304.1-94 (CSA 1994), (presented in Appendix A). It appears that vertical reinforcement had, perhaps, a slightly positive effect and lateral confinement did not have an observable positive effect on the rising branch of the stress-strain curve. The lateral confinement also appeared to be detrimental to the falling branch of the stress-strain curve, likely due to the resulting incomplete compaction.

5.3 Crack patterns

Cracks were monitored during the testing of each specimen in the experimental program. With the load maintained at some level, any observed cracks were traced and marked with the current load magnitude and then photographed. All cracks were monitored up to specimen failure, with detailed post-failure observations made at the completion of the test. The following observations were made.

- The first visible vertical cracks were observed on the sides of the test specimens at about 55 % of average ultimate load for type ***A*** specimens, at about 64 % for type ***B*** specimens and about 55 % for type ***C*** specimens, an example of which can be

seen in Fig. 5.2. In most cases, cracks were initiated at the mortar joints between courses of the walls. These cracks gradually penetrated into the wall.

- After the initial cracks appeared, additional cracks appeared in other courses, widening as the load increased. At about 85 % of the average ultimate load for type ***A*** specimens, about 95 % for type ***B*** specimens and about 88 % for type ***C*** specimens, local crushing in the most severely compressed faces of the specimens occurred. At this point, the walls were separating into two halves, with face-shell spalling and mortar crushing taking place (Fig. 5.3).

- Failure occurred when the splitting cracks in the end faces joined together over the height of the wall and the bond between grout and masonry blocks was lost (Fig. 5.4).

While some slight differences in performance between the three types of specimens were observed, no marked differences in cracking behaviour were observed. It can be concluded that the crack patterns of all types of walls were similar to those described in the literature (Hart et al. (1988). All walls failed under a compression-tension stress state, which produced spalling away of block shells and vertical tensile splitting on the end faces.

5.4 Failure modes

Compression tests of all three types of masonry wall specimens produced a combined tension-compressive failure, as was reported by Hamid and Drysdale (1979), Hart et al. (1988) and Hamid and Chadrakeerthy (1992). The typical failure mode included tensile splitting parallel to the line of application of load along end faces, followed by compressive face-shell spalling and mortar crushing. Failure was gradual and occurred in a ductile manner, as reported by Hart et al. (1988). A typical tensile splitting crack is shown on Fig. 5.6, which was similar to that observed in all three types

of masonry specimens. Variations in the actual location of the crack were attributed, in part, to imperfections or voids in the grouted column.

When the load applied above the grouted columns reached the ultimate value, the face shells of the concrete blocks attached to the grouted columns split away and the remaining grouted columns in the central core picked up the load. The spalling away of the block face shells was observed in all specimens, with variations observed in the actual spalling location. The opening-up of the vertical cracks on the sides of the masonry specimens, and the simultaneous elongation of the joint reinforcement caused by high lateral expansion of the wall, can be seen in Fig. 5.7. The observed deformation of the joint reinforcement suggests that increased lateral confinement from stiffer joint reinforcement may be effective in delaying the formation of splitting cracks in the end faces. Similar observations have been reported by Pristley (1981).

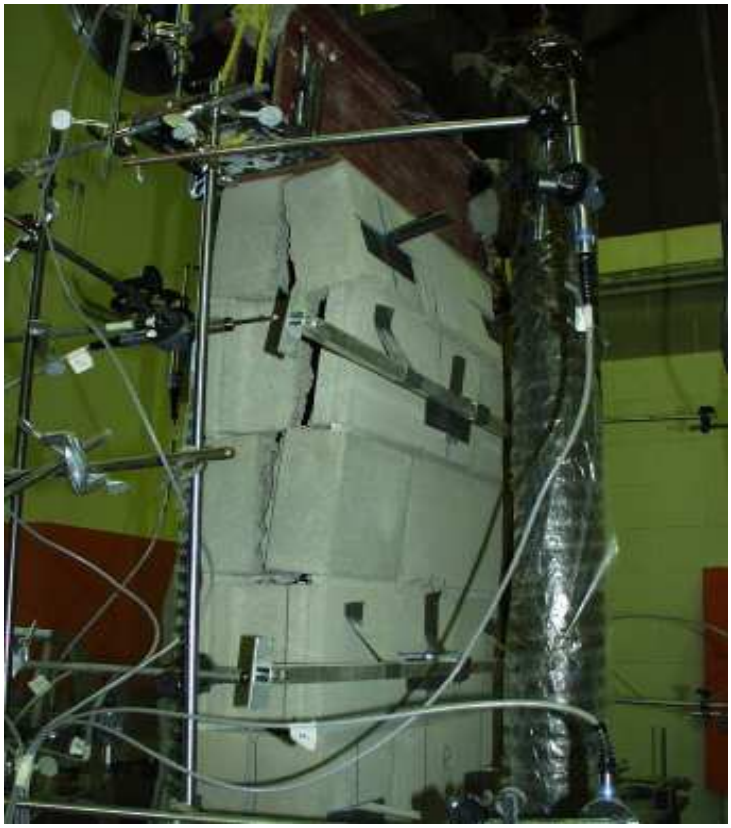

Fig. 5.6. Typical tensile splitting of the wall.

Fig. 5.7. Typical opening-up of the side crack and crushing.

To compare the behaviour of short masonry walls under axial compression, average first crack loads, average spalling loads and average ultimate loads for all three types of masonry walls are presented in Table 5.4.

Table 5.4. Summary of average first crack, spalling and ultimate loads for three types of specimens

	Type "A"	**Type "B"**	**Type "C"**
First Crack Load (kN)	484.70	504.84	394.82
C.O.V.	22.08%	18.65%	23.34%
Spalling Load (kN)	681.67	752.27	642.13
C.O.V.	15.09%	13.60%	24.43%
Ultimate Load (kN)	800.56	792.95	725.73
C.O.V.	12.48%	12.18%	19.13%

The ratio of the average first crack load to the average ultimate load varied from 0.61 for type ***A*** specimens, to 0.64 for type ***B*** specimens, and 0.54 for type ***C*** specimens. It was determined that the difference in the average first crack load between types ***C*** and ***B*** walls was statistically significant at the 90% level of confidence. The difference in average first crack loads between types ***A*** and ***B*** was 4.0%, which was not statistically significant at the 90% level of confidence, suggesting that the presence of reinforcement in type ***B*** walls did not have significant influence on first crack loads.

The ratio of average spalling load to average ultimate load varied from 0.85 for type ***A*** specimens, to 0.95 for type ***B*** specimens, and 0.88 for type ***C*** specimens. The difference in average spalling loads between types ***A*** and ***B*** was 9.4%, while that between types ***B*** and ***C*** was 14.6%. These differences were both found to be statistically significant at the 90% level of confidence.

The difference in average failure loads between types ***A*** and ***B*** was 1.0% while that between types ***B*** and ***C*** was 8.5%. The 1% difference between walls ***A*** and ***B*** was not statistically significant at the 90% level of confidence, suggesting that the two types of walls had essentially the same axial strength. The 8.5% difference between wall types ***B*** and ***C*** was also not statistically significant at the 90% level of confidence, although it is large enough to suggest that some differences may have existed.

5.5 Ductility

Ductility of partially grouted concrete masonry walls depends on the ultimate compressive strain that can be achieved and the general stress-strain characteristics of masonry in compression. More specifically, the post-peak ductility (denoted here as simply ductility) has been defined as the ratio between the difference of displacements at collapse and ultimate loads to the displacement at ultimate load. It was difficult to determine precisely the collapse displacements since the recordings of the descending branch of the load-displacement curves were incomplete due to movement of the linear

displacement sensors as the walls failed. For simplicity average post-peak load-displacement curves were chosen for each type of masonry wall, as presented in Fig. 5.8.

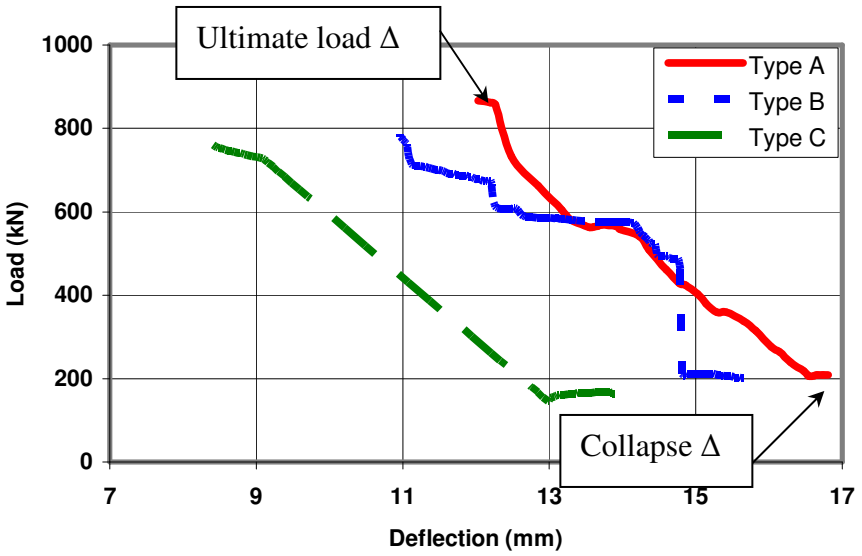

Fig. 5.8. Post-peak average load-deflection curves for three types of walls.

For ductility calculations, average displacements at ultimate and collapse were measured off the graph. More specifically, the difference between average displacements at collapse and ultimate loads was divided by ultimate load displacement to estimate the ductility. The average ductility for the concrete masonry walls was found to be 39.7% for type ***A*** specimens, 42.9% for type ***B*** specimens and 63.0% for type ***C*** specimens. Detailed calculations of the ductility for all three types of masonry walls are presented in Appendix A. These results indicate that the vertical reinforcement and lateral confinement had a positive effect on the ductility.

5.6 Summary

Based on the test data, it appears that three types of short partrially grouted concrete masonry walls - (a) ***unreinforced***, ***unconfined***; (b) ***reinforced***, ***unconfined***; (c) ***reinforced***, ***confined*** - behaved in a comparable manner with regard to crack patterns,

modes of failure and ductility. The test results indicated that vertical reinforcement of the grouted core did not have a significant positive effect on the failure modes and strength of the short masonry walls. Due to problems with adequate compaction, the lateral confinement provided by the spiral reinforcement had a slightly negative effect on the compressive strength of concrete masonry walls built in running bond. Vertical reinforcement and lateral confinement of the grouted core had some positive effect on the ductility.

Similar crack patterns and failure modes were observed in all three types of specimens. Vertical cracks that progressed through the end faces of the concrete blocks and mortar joints, suggesting that the lateral expansion of the grouted core contributed to tensile splitting stresses, as was reported by Hamid and Drysdale (1979), Hart et al. (1988) and Hamid and Chadrakeerthy (1992). Local failure of the grouted cores was found in some type ***C*** specimens due to incomplete compaction in the grouted columns. Post-failure inspection revealed voids in these grouted columns, resulting from poor consolidation during vibration.

From a comparison of the ductility for all three types of specimens it was found that both the vertical reinforcement and lateral confinement of the core had a beneficial influence on the post-peak ductility. Type ***B*** specimens were approximately 7% more ductile than type ***A*** specimens, while type ***C*** specimens were 32% more ductile than type ***B*** specimens. These differences were found to be statistically significant.

CHAPTER SIX

CONCLUSIONS AND RECOMMENDATIONS

6.1 Summary

Historically, concrete masonry walls have been used extensively to form structural load bearing systems. These walls are made of concrete blocks, mortar, grout and reinforcement; therefore, their strengths depend on the strength of each material itself, the interaction between the materials, and on the workmanship and construction of the walls. An experimental study was conducted in order to determine the effect of vertical reinforcement and horizontal confinement on the compressive strength of short partially grouted concrete masonry walls laid in running bond.

Three types of test specimens of partially grouted concrete block masonry walls were tested: (1) specimens with a grouted core only; (2) specimens with a grouted core and vertical reinforcement (i.e. no confinement); and (3) specimens with a grouted core, vertical reinforcement and spiral confinement in the grouted cores. Ten specimens of each type were tested in an attempt to make statistically reliable conclusions.

Test results for all three types of test specimens were presented and discussed in previous chapters. The following sections present the conclusions based on the information obtained in this program. It should be recognized that the conclusions are restricted to the conditions considered in this study. More research is needed to confirm and extend the conclusions to represent all general situations. Some recommendations for future studies are also presented.

6.2 Conclusions

6.2.1 Compressive strength

Specimens of type ***B*** - with grouted core and vertical reinforcement only (i.e. no confinement) - exhibited a slightly higher average stress at the first crack appearance and at spalling of the shells than those of type ***A*** (without reinforcement) and of type ***C*** (reinforced with vertical bar and confined with spirals). Type ***A*** specimens exhibited the highest average ultimate strength, exceeding that of type ***B*** walls by 1.0%, and that of type ***C*** walls by 6.3%. These differences were not statistically significant at the 90% level of confidence, suggesting that the three types of walls had essentially the same axial strength. However, the 6.3% difference between wall types ***B*** and ***C*** is large enough to suggest that some differences may have existed. Contrary to expectations based on design calculations, it was found that type ***C*** specimens, which were reinforced with a vertical bar and confined with spirals, exhibited the lowest average stress at the first crack appearance, at spalling of the shells and at failure of the specimens.

The strength of masonry depends not only on the quality of the component materials, but also on the quality of construction, especially of the grouting. It was found that incomplete grouting in type ***C*** specimens, which resulted in incomplete bonding between concrete blocks, grout and reinforcement, reduced the average strength of these specimens. It also led to greater variability in the ultimate strengths. The difference between the maximum and minimum ultimate strengths among the ten walls of each type was: (1) for type ***A*** walls – 30.4 %; (2) for type ***B*** walls – 31.5 %; (3) for Type ***C*** walls – 46.8 %.

In general, it appeared that vertical reinforcement had a small positive effect but the lateral confinement did not have an observable positive effect on the compressive

strength of short masonry walls. The lateral confinement also appeared to be detrimental to these walls in the sense that it made proper compaction of the grout difficult to achieve.

6.2.2 Failure modes

The failure modes of the three types of specimens were virtually identical. Specimens failed in a splitting manner with vertical cracks starting on the end faces of the two top courses, followed by a progressive widening and lenghtening of these cracks and spalling of the front shells. Variations in the actual locations of the cracks were attributed, in part, to imperfections or voids in the grouted columns. The post-failure inspections revealed that crushing of the concrete masonry shells occurred precisely at locations where voids were apparent in grouted cores.

Failure of all three types of walls occurred when the splitting cracks in the end faces joined together over the height of the wall and the bond between grout and masonry blocks was lost. Opening-up of the vertical cracks on the sides of the masonry specimens and simultaneous elongation of the joint reinforcement was noted near ultimate loads. This was accompanied by lateral expansion of the grout and mortar. All walls failed in a compression-tension stress state, which produced spalling away of the block shells and vertical tensile splitting on the end faces.

6.2.3 Ductility

Large deflections were measured after failure of the specimens. All three types of specimens showed ductile behaviour. From a comparison of the ductility for all three types of specimens, it was found that the reinforcement and confinement had a beneficial influence on the post-peak ductility, defined as the ratio between the difference of displacements at collapse and ultimate loads to the displacement at ultimate load. The average post-peak ductility of type ***B*** walls was 3.2% higher than that of type ***A***, while type ***C*** walls were 20.1% more ductile than type ***B***.

The 3.2% difference between wall types ***A*** and ***B*** was not statistically significant at the 90% level of confidence, suggesting that the two types of walls possessed similar levels of ductility and therefore that the presence of vertical reinforcing steel had no significant influence on ductility. On the other hand, the 20.1% difference between wall types ***B*** and ***C*** was statistically significant at the 90% level of confidence, suggesting that horizontal confinement (spirals) had a positive influence on the ductility, perhaps by helping to stabilize the grouted cores. Increased provides the potential for advanced warning of impending failures, and is particular critical for earthquake resistant design before its failure.

In summary, experimental data from this study indicate that vertical reinforcement and lateral confinement of the grouted core in the short masonry walls provided no significant improvement in the failure load or axial strength on the *ascending* portion of the stress-strain curve. However, vertical reinforcement and lateral confinement had a positive effect on the *descending* portion of the stress-strain curve in that they imparted increased ductility to the walls when subjected to axial loads.

6.3 Recommendations for future studies

Future studies should consider different configurations of the specimens to examine the structural behaviour of the reinforced masonry walls constructed in *stack and running bond*.

These may include variations in the dimensions of test specimens (i.e. two, three blocks in length with every other grouted core, etc.), cross section configurations, different materials, various bar sizes, various spiral sizes (i.e. undivided spiral on whole height of the wall , different pitch, etc.), various types of confinement and stiffer joint reinforcement.

These studies will give useful information about the structural behaviour of masonry walls. Although the results from the current study must be confirmed by further testing, there may well be a case to be made for the development of a new configuration for concrete blocks to eliminate offsets in the grouted cores for walls laid in *running bond*).

REFERENCES

Abboud, B.E., Hamid A. and Harris, H.G. ***Flexural Behaviour and Strength of Reinforced Masonry Walls Built with Masonry Cement Mortar.*** TMS Journal, August 1993, pp. 17-24.

Abdel-Halim, M.A.H. and Abu-Lebdeh, T.M. ***Analytical Study for Concrete Confinement in Tied Columns.*** Journal of Structural Engineering, Vol. 111, No. 11, November 1989, pp. 2810-2827.

Abrams, D.P. ***Dynamic and Static Testing of Reinforced Concrete Masonry Structures.*** TMS Journal, January-June 1988, pp. T18-T22.

Atkinson, R.H. ***Tension Stiffening Behaviour of Reinforced Masonry.*** Journal of Structural Engineering, Vol. 23, May 1997, pp. 597-603.

Canadian Standards Association. 1994. ***Design of Concrete Structures (A23.3-94).*** CSA, Etobicoke, ON, Canada.

Canadian Standards Association. 1994. ***Masonry Design for Buildings (Limit States Design). S304.1-94.*** CSA, Etobicoke, ON, Canada.

Canadian Standards Association. 1994. ***Mortar and Grout for Unit Masonry. A179-94.*** CSA, Rexdale, ON, Canada.

Drysdale, R.G. and Hamid A.A. ***Behaviour of Concrete Block Masonry under Axial Compression.*** ACI Journal, June 1979, pp. 707-721.

Drysdale, R.G. and Hamid, A.A. 1994. ***Masonry Structures: Behaviour and Design.*** Prentice-Hall Inc., Englewood Cliffs, NJ, USA.

Fahmy, E.H. and Ghoneim, T.G.M. ***Behaviour of Concrete Block Masonry Prisms Under Axial Compression.*** Can. J. of C. Eng. Vol. 22, January 1995, pp. 898-915.

Grira, M. and Saatcioglu, M. ***Concrete Columns Confined with Welded Reinforcement grids.*** ACI Structural Journal, Vol. 96, No. 1, January 1996, pp. 29-39.

Hamid, A.A. and De S. Chandrakeerthy, S.R. ***Compressive Strength of Partially Grouted Concrete Masonry Using Small Scale Wall Elements.*** TMS Journal, Vol. 11, No. 1, August 1992, pp. 75-85.

Hamid, A.A. and Drysdale, R.G. ***Suggested Failure Criteria for Grouted Concrete Masonry under Axial Compression.*** ACI Journal, October 1979, pp. 1047-1061.

Hart, G. ***Expected Value Wall Performance. .*** TMS Journal, February 1992, pp. 15-28.

Hart, G.C. et al. ***Analytical Stress-Strain Curves for Grouted Concrete Masonry.*** TMS Journal, January-June 1989, T21-T34.

Hart, G.C. et al. ***The Use of Confinement Steel to Increase the Ductility in Reinforced Concrete Masonry Shear Walls.*** TMS Journal, July-December 1988, pp. T19-T42.

Khalaf, F.M. ***Blockwork Masonry Compressed in Two Orthogonal Directions.*** Journal of Structural Engineering, May 1997, pp. 591-596.

LabVIEW™, 1999. ***Version 5.0 Student Edition.*** Addison-Wesley, Boston, MA, USA.

MacGregor J.G. and Bartlett F.M. 2000. ***Reinforced Concrete: Mechanics and Design.*** First Canadian Edition. Prentice-Hall Canada Inc., Scarborough, ON, Canada.

Martinez, S. et al. ***Spirally Reinforced High-Strength Concrete Columns.*** ACI Journal, September 1984, pp. 431-442.

Mau, S.T. and Holland J. ***Small-Column Compression Tests on Concrete Confined by WWF.*** Journal of Structural Eng., Vol. 124, No.3, March 1998, pp. 252-261.

Mau, S.T., Elwi, A.E. and Zhou, Si-Zhu. ***Analytical Study of Spacing of Lateral Steel and Column Confinement.*** Journal of Structural Eng., Vol. 124, No. 3, March 1998, pp. 262-269.

Moehle, J.P. and Cavanagh T. ***Confinement Effectiveness of Crossties in PC.*** Journal of Structural Engineering, Vol. 111, No. 10, October 1985, pp. 2105-2119.

Pessiki, S. and Pieroni, A. ***Strength and Ductility of Laterally Confined Concrete Columns.*** ACI Journal, May-June 1997, pp. 304-314.

Pristley, M.J.N. and Elder, D.M. ***Staess-Strain Curves for Unconfined and Confined Concrete Masonry.*** ACI Journal, May-June 1983, pp. 192-201.

Pristley, M.J.N. ***Ductility of Unconfined and Confined Concrete Masonry Shear Walls.*** TMS Journal, July-December 1981, pp.T28-T39.

Shing, P.B., Carter, E.W. and Noland, J.L. ***Influence of Confining Steel on Flexural Response of Reinforced Masonry Shear Walls.*** TMS Journal, February 1993, pp. 72-85.

Shrive, N.G. ***The Failure Mechanism of Face-shell Bedded (ungrouted and unreinforced) Masonry.*** ACI Journal, Vol. 2, No. 3, 1982, pp. 115-128.

APPENDIX A

Specimen design and details

This appendix describes and illustrates the important design calculations:

1. Number of test specimens
2. Dimensions of the test specimens
3. Maximum axial load on the short wall
4. Minimum area of vertical reinforcement
5. Development length of vertical reinforcement
6. The bearing plate
7. Minimum spiral reinforcement
8. Compressive strength of masonry
9. Modulus of elasticity for masonry
10. Ductility of masonry walls

For axially compressed walls, dimensions of the walls, maximum axial load, minimum area of vertical reinforcement, development length of vertical reinforcement and minimum spiral reinforcement were calculated based on masonry code S304.1-94 (CSA 1994). These theoretical values were summarized and compared with the results obtained from experimental tests of masonry specimens.

1. Number of test specimens

To demonstrate a significant level of confidence, number of test specimens was calculated using a two-sided Student t-test. Relevant calculations are presented below. The expected statistical parameters provided below were based on previous test programs at the University of Saskatchewan (Qi Hu 2004).

- Assumed number of specimens (samples): $n = 10$
- Expected difference between sample means: $d = 10 \cdot \%$
- Expected coefficient of variation: $COV = 12.7 \cdot \%$
- Expected level of confidence: $LC_{expected} = 90\%$
- Degree of freedom: $v = 2 \cdot n - 2$ $v = 18$

$x_1 = 100$ $x_2 = x_1 \cdot (1 + d)$ $x_2 = 110$

$y = x_2 - x_1$ $y = 10$

- Sample standard deviation: $s_1 = COV \cdot x_1$ $s_1 = 12.7$

$s_2 = COV \cdot x_2$ $s_2 = 13.97$

- Combined sample standard deviation:

$$s_c = \left[\frac{s_1^{\,2} \cdot (n-1) + s_2^{\,2} \cdot (n-1)}{v} \right]^{\frac{1}{2}} \qquad s_c = 13.35$$

$$s_y = \left(2 \cdot \frac{s_c^2}{n} \right)^{\frac{1}{2}} \qquad s_y = 5.97$$

- Student t-test: $t = \frac{y}{s_y}$ $t = 1.675$

- Level of confidence: $LC = 1 - 2 \cdot (1 - pt(t, v))$ $LC = 88.877\%$

Ten test specimens provide an 88.9 % level of confidence with coefficient of variation of 12.7 % and a 10 % difference between sample means.

2. Dimensions of the test specimens

To achieve the objectives of the experimental study on partially grouted concrete masonry walls, the wall dimensions were selected as described below.

- The width of the test specimens was chosen to be 590 mm so that the specimens could be considered as a wall - the main difference between a wall and a column is the difference of cross-sectional dimensions in accordance with Standard S304.1-94 (CSA 1994), which defines a column as a vertical member having a width less than three times the thickness; anything wider is considered a wall.

For T = 190 mm; W > 3t then W = 590 mm > 3 x 190 = 570 mm.

- The height of the test specimens was chosen 1000 mm so that they qualified as short walls in which slenderness effects did not have to be considered; also, that size accommodated the working height of the testing machine (Amsler Beam Bender as described in Chapter Three).

3. Maximum axial load on the short wall

In planning the experimental program, the axial capacity of partially grouted concrete masonry walls was calculated in accordance with CSA Standard S304.1-94 (CSA 1994). The unfactored ultimate resistance of the partially grouted wall to axial load is governed by the interaction of material strength and member stability (cross-section). A typical cross section of concrete masonry wall specimen is shown in Fig. A.1.

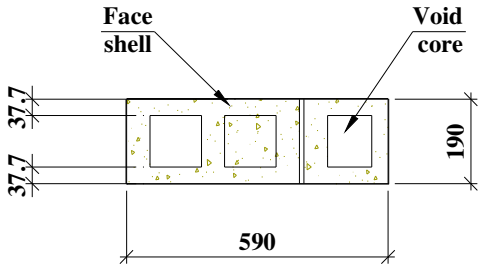

Fig. A.1 Cross section of the short masonry wall

The calculations of the analytical strengths for three types of test specimens, using the Whitney stress block, are given below. From the Table 5 in S304.1-94 (CSA 1994) for a unit compressive strength of 15 MPa, the compressive strength of concrete block masonry would be $f'_m = 7.5$ MPa. Section property and strength calculations are summarised below:

Gross area:	$A_{gross} = W * T$	$A_{gross} = 590 * 190 = 112100 mm^2$
Face shell area:	$A_{face} = W * t * 2$	$A_{face} = 590 * 37.7 * 2 = 44490 mm^2$
Non-bearing area:	$A_v = A_{gross} - A_{face}$	$A_v = 112100 - 44486 = 67610 mm^2$
Grouted area:	$A_{grouted} = 1/3 * A_v$	$A_{grouted} = 0.333 * 67614 = 22520 mm^2$
Effective area:	$A_e = A_{face} + A_{grouted}$	$A_e = 44486 + 22515.5 = 67000 mm^2$

Type *A* $P_A = f'_m * A_e$ $P_A = 7.5 * 67001.5 * 10^{-3} = 502.5kN$

Type *B* - reinforced with one 15M bar $f_y = 400MPa$ $A_s = 200mm^2$

$P_B = f'_m * A_e + f_y * A_s$ $P_B = (7.5 * 67001.5 + 400 * 200) * 10^{-3} = 582.5kN$

Type *C* - reinforced with one 15M bar and spiral $A_s = 200 + 18 = 218mm^2$

$P_c = f'_m * A_e + f_y * A_s$ $P_C = (7.5 * 67001.5 + 400 * 218) * 10^{-3} = 589.7kN$

4. Minimum area of vertical reinforcement

The minimum area of vertical reinforcement in load bearing partially grouted reinforced walls is specified in Clause 5.2.1.2 of S304.1-94 (CSA 1994) as 0.133% of the gross area of the wall. A 15M bar with an area of 200 mm² was chosen to accommodate the required minimum area:

$A_{s-\min} = 0.133\% * A_{gross}$ $A_{s-\min} = 0.00133 * 112100 = 149.1mm^2$

5. Development length of vertical reinforcement

The vertical bars and dowels in type ***B*** and type ***C*** specimens had the same lap splice. The lap splice is seen in Figure 3.11 and Fig. 3.12 in Chapter Three. The design of the lap splice was done in accordance with Standard S304.1-94 (CSA 1994).

- Basic compression development length - Clause 5.5.3.3

$L_{db} = 0.07 * d_{bar} * f_y$ $d_{bar} = 16mm$ $L_{db} = 0.07 * 16 * 400 = 448mm$

- Compression lap splice - Clause 5.5.10.4.1

$L_d = 1.35 * L_{db}$ $L_d = 1.35 * 448 = 604.8mm$

6. The bearing plate

The bearing plate was designed to transfer the full yield load from the loading head of the testing machine to the vertical reinforcing bar, as well as through the dowel to the supporting base. Plates were welded on top of the vertical bar and to the connecting point on the dowel. Calculations for sizing of the plate are presented in below:

1. Fillet Weld Size:

- Vertical reinforcement - 15M bar $d_b = 16 \cdot mm$

$A_b = 200 \cdot mm^2$ $f_y = 400 \cdot MPa$

- Vertical force: $P = A_b \cdot f_y$ $P = 80\,kN$

- Weld length: $L_w = \pi \cdot d_b$ $L_w = 50.27\,mm$

- Factored shear resistance: $\sigma = \frac{P}{L_w}$ $\sigma = 1.59\,\frac{kN}{mm}$

- Fillet weld size (for Electrode E480XX, pg. 3-41, Table 3-24 of Handbook of Steel Construction, Canadian Institute of Steel Construction, 2004):

$D = 10 \cdot mm$

2. Plate Thickness:

- Width of the plate: $w_p = 4 \cdot d_b$ $w_p = 64\,mm$

- Assume $W_p = 65 \cdot mm$

- Area of the plate: $A_p = W_p^2$ $A_p = 4225\,mm^2$

- The bearing strength of concrete: $f = \frac{P}{A_p}$ $f = 18.93\,\text{MPa}$

- Uniformly distributed load on the plate: $q = f \cdot W_p$ $q = 1230.77\,\frac{N}{mm}$

- Length of cantilever: $l_c = \frac{W_p - d_b}{2}$ $l_c = 24.5\,\text{mm}$

- Moment on the cantlever: $M = \frac{q \cdot l_c^{\,2}}{2}$ $M = 0.37\,\text{kN} \cdot \text{m}$

- The thickness of the plate: $\sigma_y = 300 \cdot \text{MPa}$

$$t_p = \sqrt{\frac{4 \cdot M}{d_b \cdot \sigma_y}} \qquad t_p = 17.54\,\text{mm}$$

- Use: $t = 20\text{mm}$

Plate dimensions of 66 x 66 x 20 mm (length x width x thickness) were selected to accommodate the required loading area of the vertical reinforcement. Details of the bearing plate welded to the vertical rebar can be seen in Fig. 3.33, and welded to the dowel in Fig. 3.6.

7. Minimum spiral reinforcement

The spiral acts to restrain the lateral expansion of the grouted column core under axial loading. Documented improvements in the ultimate strength and ductility of reinforced concrete columns with lateral confinement suggests that reinforced masonry walls should contain a certain minimum amount of lateral reinforcement to provide enhanced performance. Figure 3.4 in Chapter Three shows details of the spirals used in this study. A diameter of 110 mm was chosen to accommodate the size of the hollow

core (116 x 116 mm). The length of 200 mm was chosen to accommodate the height of the concrete block (190 mm), plus one mortar joint thickness (10 mm). Supporting calculations of the pitch of the spiral are presented below:

- Diameter of the wire No. 9: $d_s = 4.78 \cdot mm$
- Area of the wire: $A_s = \frac{\pi \cdot d_s^2}{4}$ $A_s = 17.945 mm^2$
- Width of the hollow core: $W_c = 116 \cdot mm$
- Diameter of the spiral: $D_s = W_c - 6 \cdot mm$ $D_s = 110 mm$
- Area of the spiral core: $A_c = \frac{\pi \cdot D_s^2}{4}$ $A_c = 9503.32 mm^2$
- Gross area of the core: $A_g = \pi \cdot W_c^2$ $A_g = 42273.27 mm^2$
- Properties of the grout and the wire: $f_g = 12 \cdot MPa$ $f_y = 400 \cdot MPa$
- Pitch of the spiral: $S_s = \frac{\pi \cdot d_s^2 \cdot f_y}{0.45 \cdot D_s \cdot f_g \cdot \left(\frac{A_g}{A_c} - 1 \right)}$ $S_s = 14.02 mm$
- Choose the pitch of the spiral: $S_s = 15 \cdot mm$
- The ratio of the spiral reinforcement: $\rho_s = \frac{A_s \cdot \pi \cdot d_s}{A_c \cdot S_s}$ $\rho_s = 0.0019$

The 15 mm pitch of the spiral was chosen to accommodate the maximum aggregate size of the fine grout (max 10 mm).

8. Compressive strength of masonry

The Canadian Masonry Standard Design (CSA 1994 Clause 9.2.2.2) requires that when prism test results are used for determining the design compressive strength, a minimum of five prisms should be tested. The prism compressive strength should than be obtained by multiplying the resulting average compressive stress by the following coefficient:

$$1-\frac{1.5}{\bar{x}}\sqrt{\frac{\sum(x-\bar{x})^2}{n-1}}$$

Calculations of the compressive strength of the masonry prisms in this program are presented below:

1. Set #1

- The average strength for set #1: $\chi_1 = 9.31$ MPa $\quad n = 5$

- The individual strengths for set #1: $x_{11} = 9.11$ MPa $\quad x_{12} = 10.03$ MPa

  $x_{13} = 10.50$ MPa $\quad x_{14} = 8.08$ MPa $\quad x_{15} = 8.82$ MPa

- The coeficient for set #1:

$$k_1 = \left[1-\frac{1.5}{\chi_1}\cdot\sqrt{\frac{(x_{11}-\chi_1)^2+(x_{12}-\chi_1)^2+(x_{13}-\chi_1)^2+(x_{14}-\chi_1)^2+(x_{15}-\chi_1)^2}{n-1}}\right]$$

$$k_1 = 0.844$$

- The calculated strength for masonry for set #1:

$$f_1 = \chi_1 \cdot k_1 \qquad f_1 = 7.86 \text{ MPa}$$

1. **Set #2**

- The average strength for set #2: $n_2 = 2$ $\chi_2 = 11.24$ MPa

- The individual strengths for set #2: $x_{21} = 10.93$ MPa $x_{22} = 11.55$ MPa

- The coeficient for set #2:

$$k_2 = \left[1 - \frac{1.5}{\chi_2} \cdot \sqrt{\frac{\left(x_{21} - \chi_2\right)^2 + \left(x_{22} - \chi_2\right)^2}{n_2 - 1}}\right] \qquad k_2 = 0.941$$

- The calculated strength for masonry for set #2:

$$f_2 = \chi_2 \cdot k_2 \qquad f_2 = 10.58 \text{ MPa}$$

- The compressive strength of concrete masonry:

$$f_m = \frac{f_1 + f_2}{2} \qquad f_m = 9.22 \text{ MPa}$$

The final compressive strength of the concrete masonry prisms was therefore found to be 9.22 MPa.

9. Modulus of elasticity of masonry

In accordance with the Clause 8.3.1.4 of S304.1-94 (CSA 1994) the modulus of elasticity of masonry shall be based on the secant modulus of at least five prisms tested under compression and shall be measured over a stress range from 0.05 to 0.33 of the measured mean prism compressive strength; furthermore, shall be based on the average value of these five tests.

As the average compressive strength for the concrete prisms was found to be 9.22 MPa, the values of $0.05 * f'_m = 0.461\,\text{MPa}$ and $0.33 * f'_m = 3.043\,\text{MPa}$ were defined.

The corresponding strains from stress-strain curves for each prism were subsequently determined as an example for prism P-1:

$$E_{m1} = \frac{\sigma}{\varepsilon} = \frac{3.043 - 0.461}{0.00108 - 0.00005} = 2506.80 \text{ MPa}$$

By repeating the above procedure for all prisms of set #1 the secant modulus values were obtained and are presented in Table A.1. Unfortunately, there is no strain data available for set #2.

Table A.1 Modulus of elasticity for concrete prisms

Prism No.	**Calculations:**	**Modulus of Elasticity**
P-1	(3.043-0.461) / (0.00108-0.00005)	**2506.80**
P-2	(3.043-0.461) / (0.00118-0.00202)	**3073.81**
P-4	(3.043-0.461) / (0.00181-0.00108)	**3536.99**
P-5	(3.043-0.461) / (0.00099-0.00008)	**2837.36**
Average:		**2988.74**
STDEV		**433.20**
COVAR		**14.49%**

The average modulus of elasticity was calculated and was found to be 2988.74 MPa, with coefficient of variation of 14.49 %.

10. Ductility of masonry walls

For simplicity in the analysis of the post-peak ductility, average load-displacement curves (after failure) were used for each type of the test masonry walls; these average curves are presented in Fig. A.1. Ductility (μ) is defined by the ratio of the displacement at ultimate load to the yield displacement: $\mu = \frac{\Delta_u - \Delta_y}{\Delta_y}$.

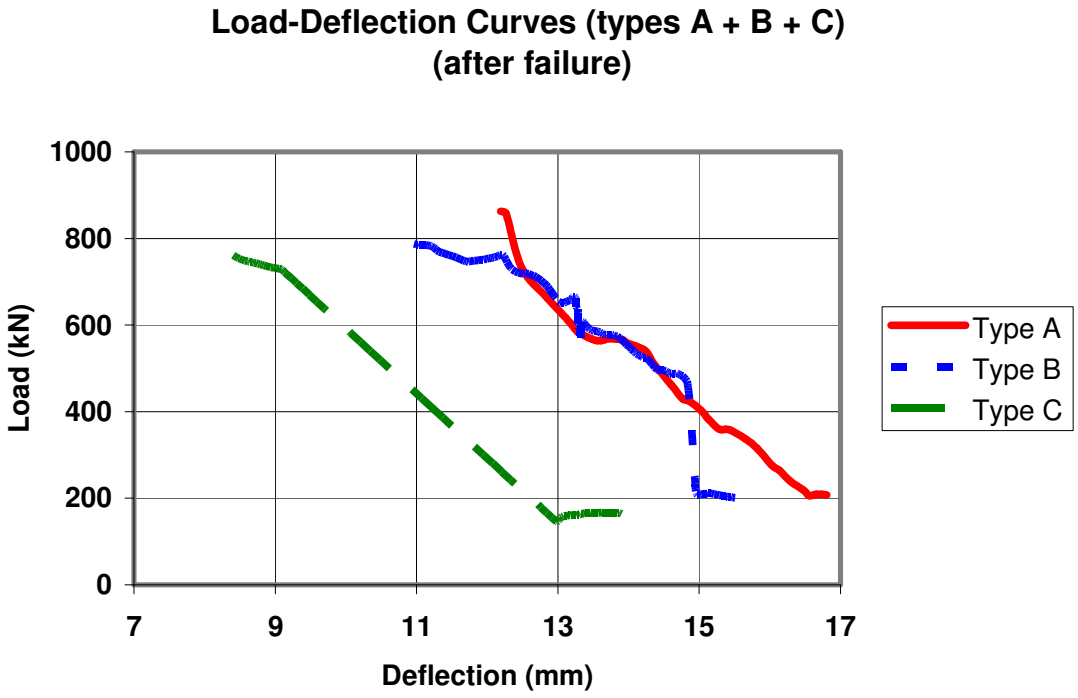

Fig. A.1 Load-deflection curves after failure

Using the values of displacements shown in Fig. A.1, calculations of the ductility of masonry walls are presented below:

- Failure displacement for type A specimens: $\Delta_{fA} = 16.81 \cdot mm$
- Yield displacement for type A specimens: $\Delta_{yA} = 12.03 \cdot mm$
- Ultimate displacement for type A specimens:

$$\Delta_{uA} = \Delta_{fA} - \Delta_{yA} \qquad \Delta_{uA} = 4.78\ mm$$

- Ductility for type A specimens:

$$\mu_A = \frac{\Delta_{uA}}{\Delta_{yA}} \cdot 100 \cdot \% \qquad \mu_A = 39.7\ \%$$

- Yield displacement for type B specimens: $\Delta_{yB} = 10.96 \cdot mm$

- Ultimate displacement for type B specimens:

$$\Delta_{uB} = \Delta_{fB} - \Delta_{yB} \qquad \Delta_{uB} = 4.7\,mm$$

- Ductility for type B specimens:

$$\mu_B = \frac{\Delta_{uB}}{\Delta_{yB}} \cdot 100 \cdot \% \qquad \mu_B = 42.9\,\%$$

- Failure displacement for type C specimens: $\Delta_{fC} = 13.90 \cdot mm$

- Yield displacement for type C specimens: $\Delta_{yC} = 8.53 \cdot mm$

- Ultimate displacement for type C specimens:

$$\Delta_{uC} = \Delta_{fC} - \Delta_{yC} \qquad \Delta_{uC} = 5.37\,mm$$

- Ductility for type C specimens:

$$\mu_C = \frac{\Delta_{uC}}{\Delta_{yC}} \cdot 100 \cdot \% \qquad \mu_C = 63\,\%$$

Based on these calculations the average ductility for the concrete masonry walls was found to be 39.7% for type ***A*** specimens, 42.9% for type ***B*** specimens and 63.0% for type ***C*** specimens.

APPENDIX B

Summation of Test Results

This appendix presents the following data:

1. Summation of test results

2. Test specimens type ***A***

3. Test specimens type ***B***

4. Test specimens type ***C***

1. Summation of test results

Table B.1 Summation of test results for three types of test specimens

First crack	Max	Min	Mean	St. Dev.	C.O.V.
Type "A"	646.7	320.4	484.7	107.0	0.221
Type "B"	640.2	330.2	504.8	94.2	0.187
Type "C"	551.6	271.0	394.8	92.2	0.233

Spalling	Max	Min	(a) Mean	St. Dev.	C.O.V.
Type "A"	797.0	520.8	681.7	102.9	0.151
Type "B"	949.5	641.7	752.3	102.3	0.136
Type "C"	935.7	336.0	642.1	156.9	0.244

Failure Load	Max	Min	Mean	St. Dev.	C.O.V.
Type "A"	934.8	647.0	800.6	99.9	0.125
Type "B"	949.5	650.3	792.9	96.6	0.122
Type "C"	1031.1	538.3	725.7	138.8	0.191

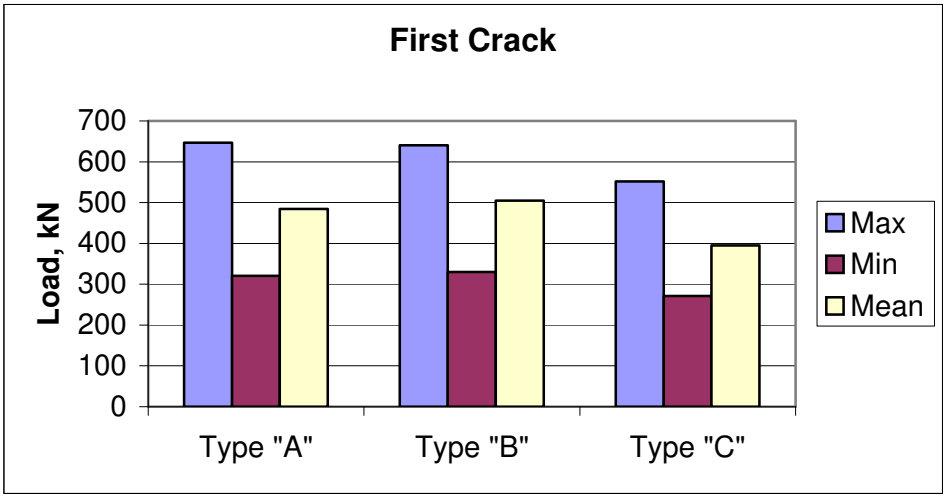

Fig. B.1 First crack appearance load ration by type

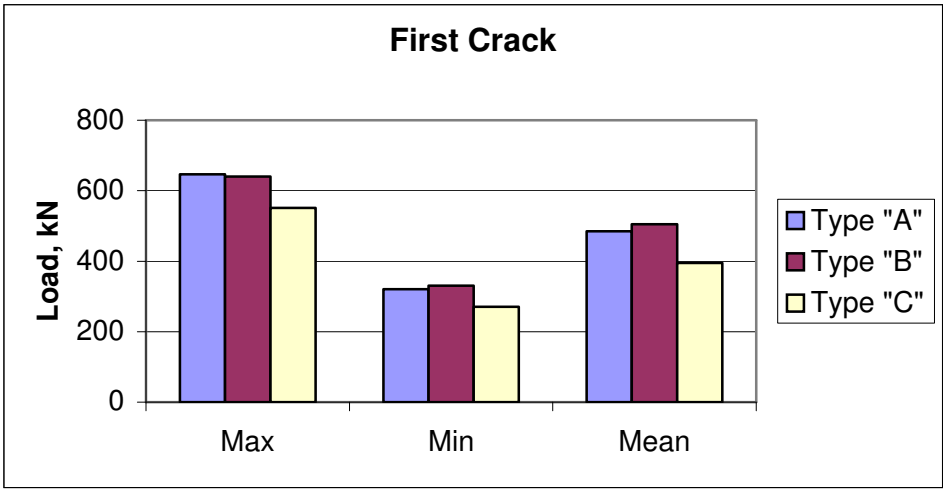

Fig. B.2 First crack appearance load ratio by average

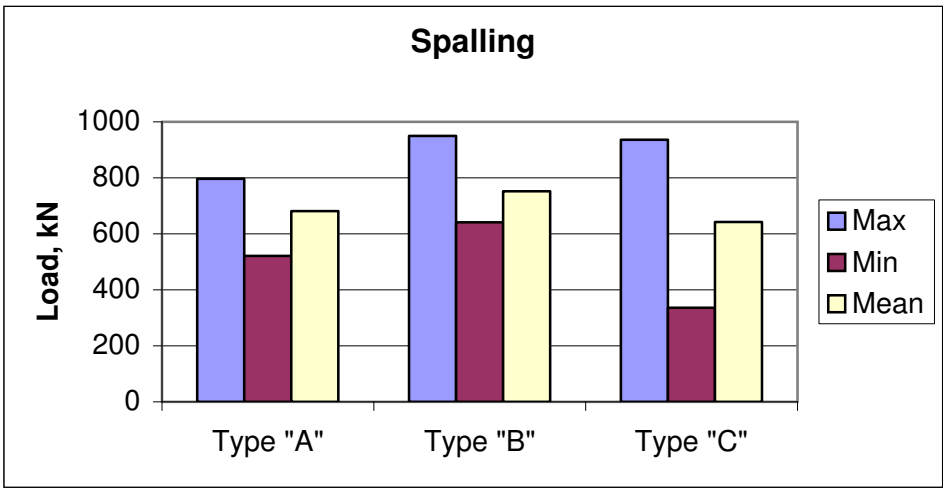

Fig. B.3 Spalling of face shells load ratio by type

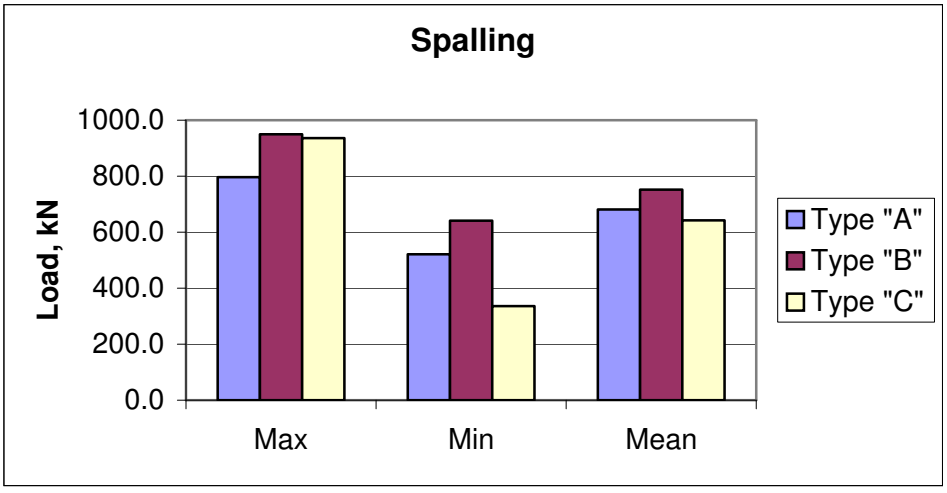

Fig. B.4 Spalling of face shells load ratio by average

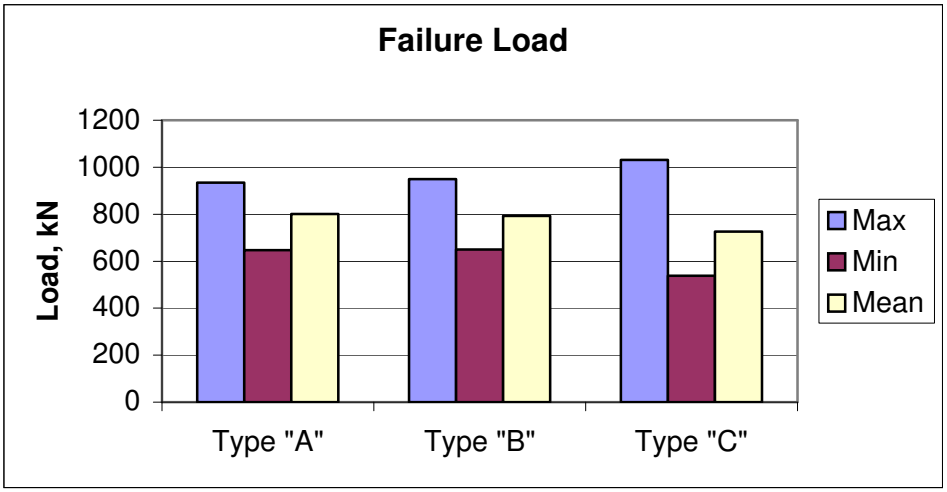

Fig. B. 5 Failure load ratio by type

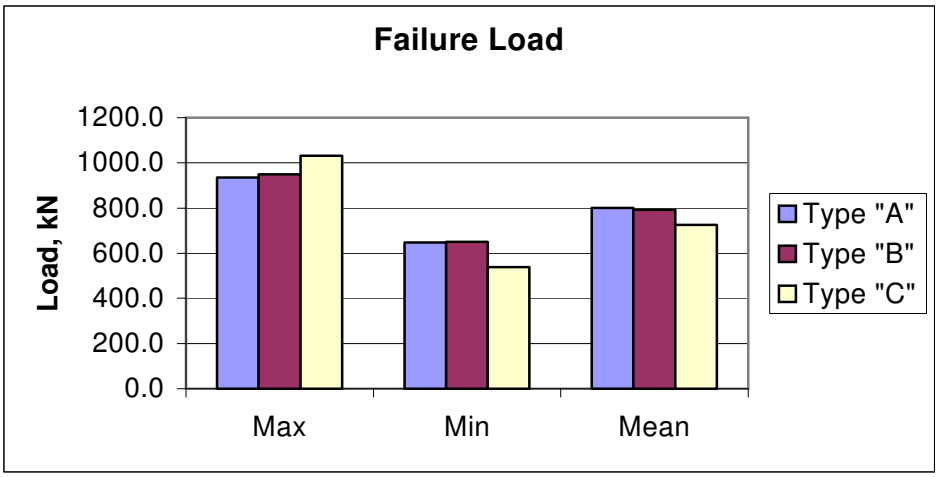

Fig. B. 6 Failure load ratio by average

2. Test specimens type *A*

Table B.2 Summation of test results for type *A* specimens

Type *A*	First crack, kN	Spalling, kN	Failure Load, kN
A-1	646.679	756.273	756.273
A-2	320.436	520.755	647.042
A-3	596.962	743.209	934.820
A-4	470.675	566.479	867.319
A-5	544.822	770.265	770.265
A-6	426.319	724.020	793.388
A-7	375.021	744.261	876.493
A-8	402.479	544.105	912.622
A-9	473.292	650.325	650.325
A-10	590.350	797.009	797.009
Max	**646.679**	**797.009**	**934.820**
Min	**320.436**	**520.755**	**647.042**
Mean	**484.704**	**681.670**	**800.556**
St. Dev.	**107.04**	**102.89**	**99.94**
C.O.V.	**22.08%**	**15.09%**	**12.48%**

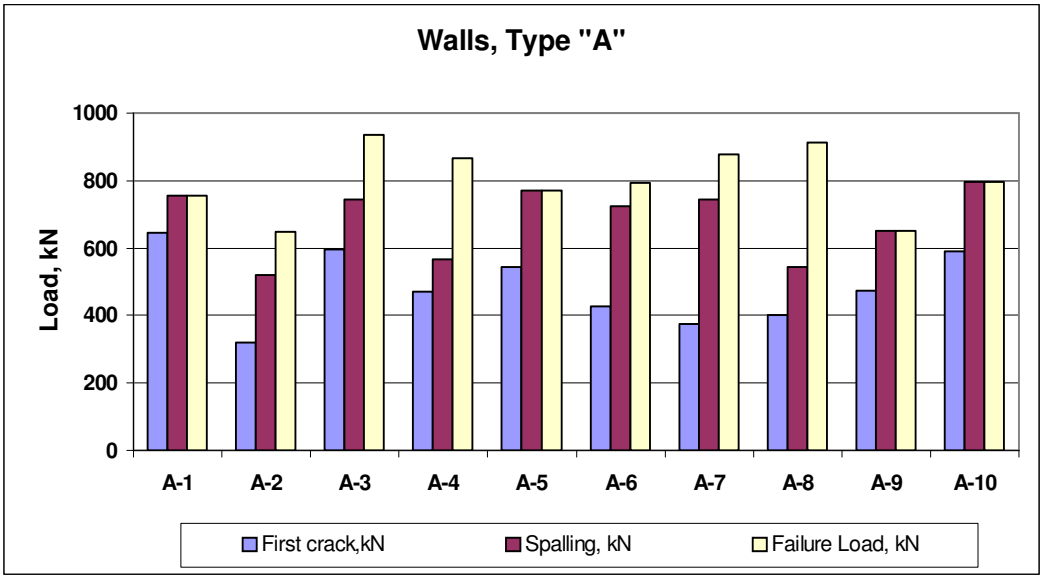

Fig. B.7 First crack, Spalling and Failure loads ratios for type *A* walls

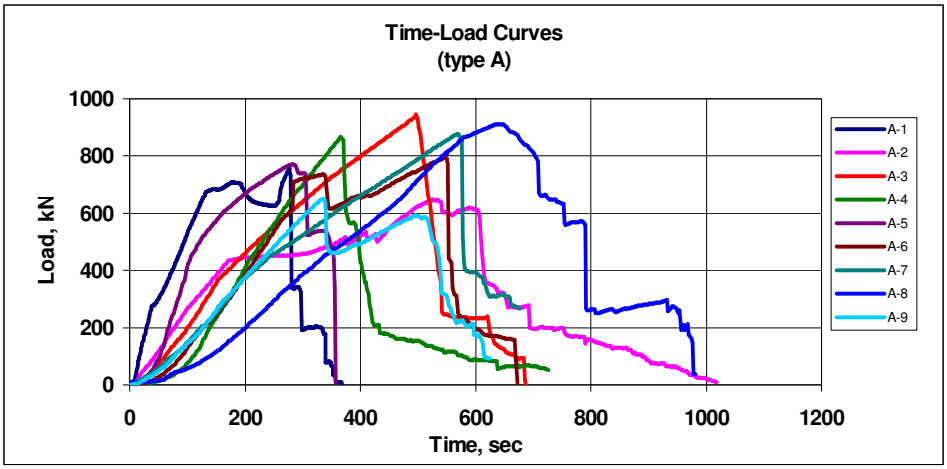

Fig. B.8 Time versus load curves (type **A**)

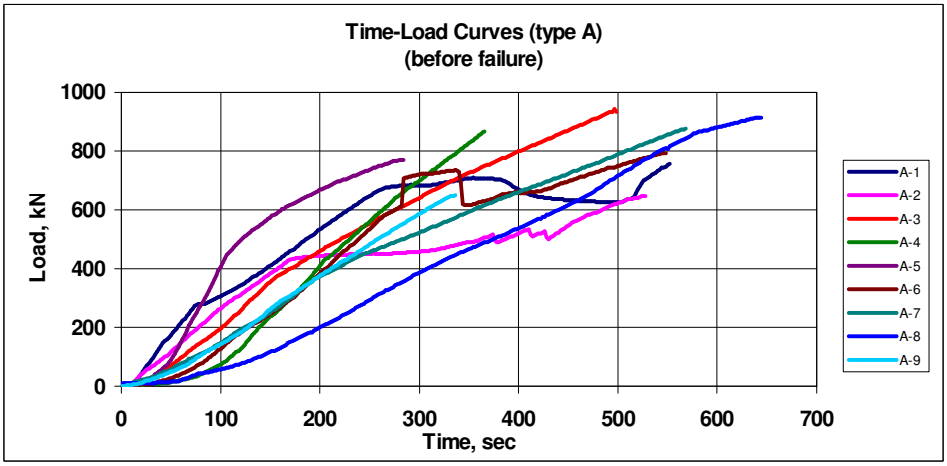

Fig. B.9 Time versus load curves (before failure)

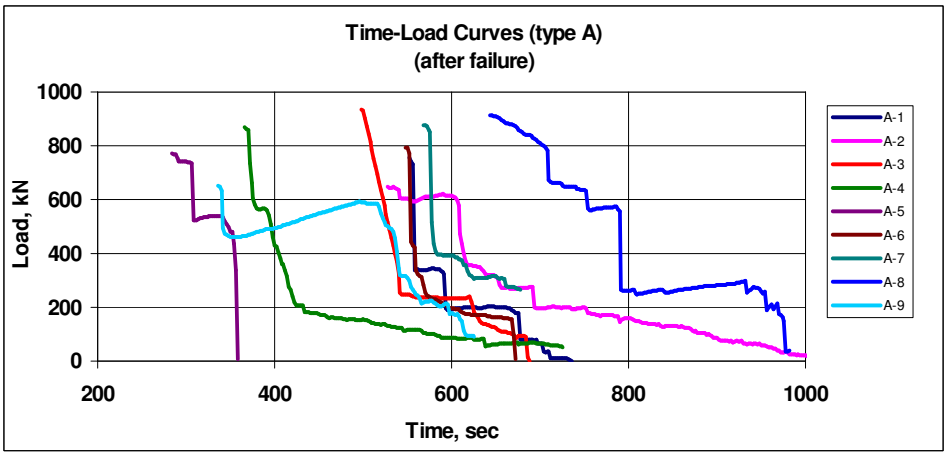

Fig. B.10 Time versus load curves (after failure)

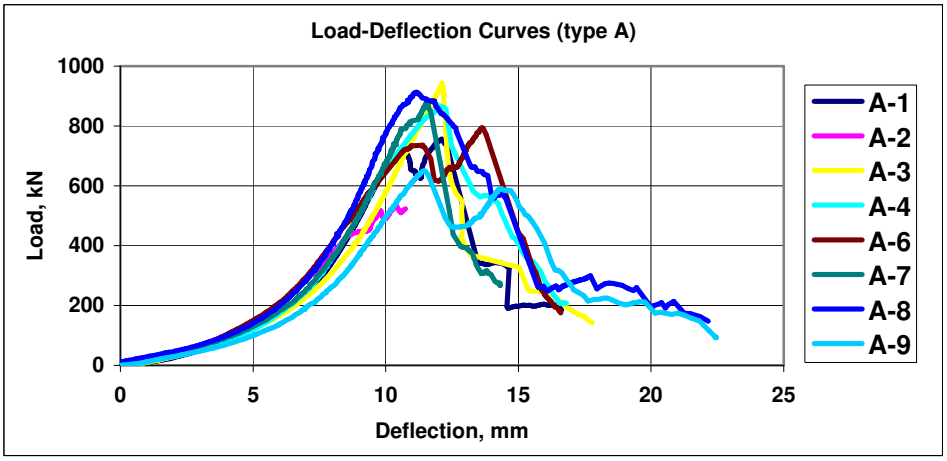

Fig. B.11 Load versus deflection curves (type **A**)

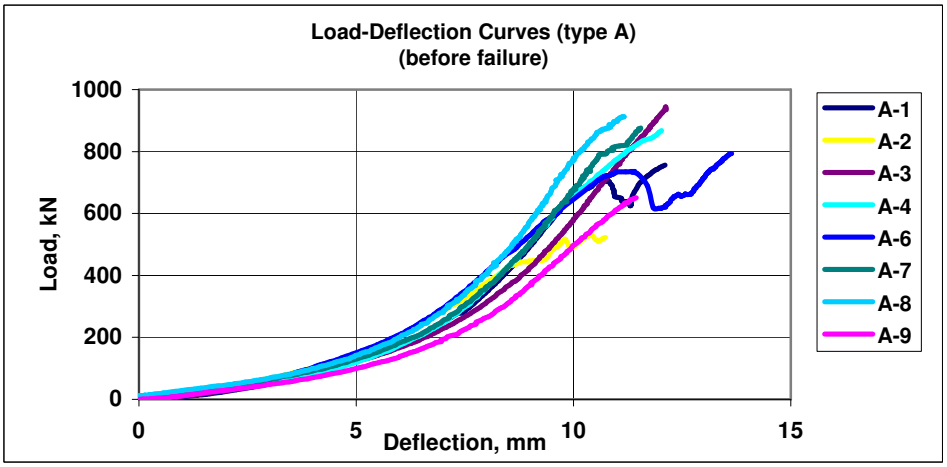

Fig. B.12 Load versus deflection curves (before failure)

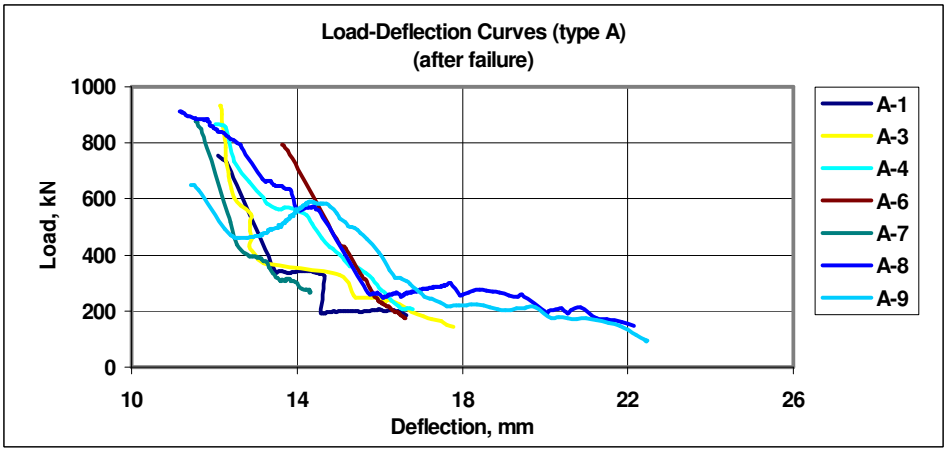

Fig. B.13 Load versus deflection curves (after failure)

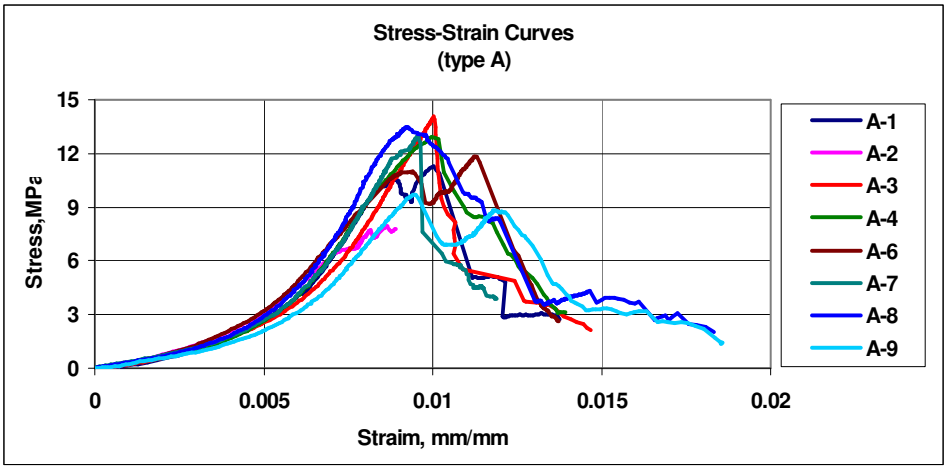

Fig. B.14 Stress versus strain curves (type ***A***)

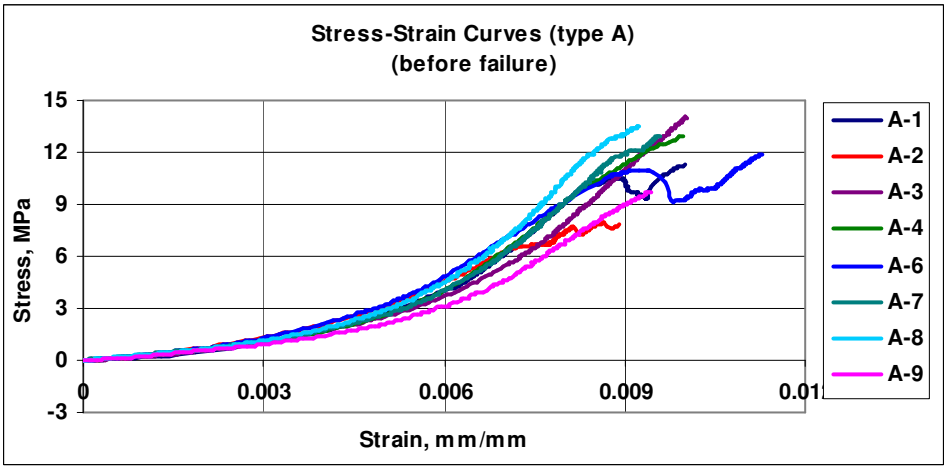

Fig. B.15 Stress versus strain curves (before failure)

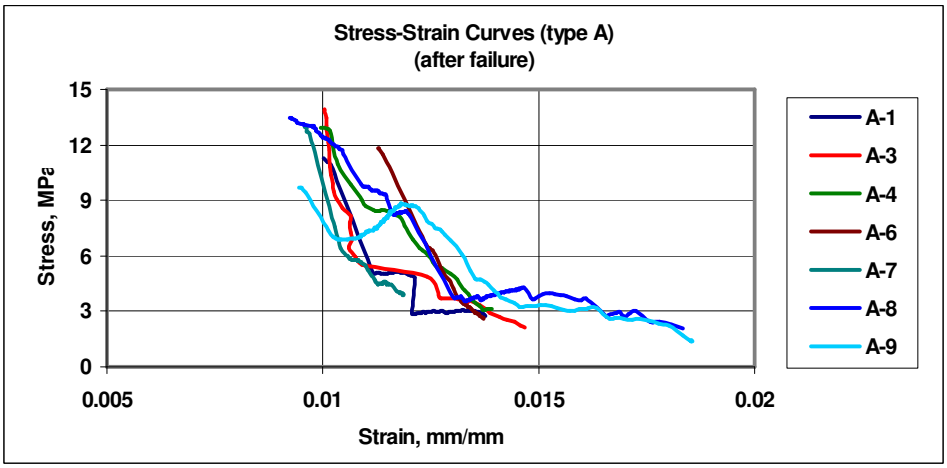

Fig. B.16 Stress versus strain curves (after failure)

3. Test specimens type *B*

Table B.3 Summation of test results for type ***B*** specimens

Type *B*	First crack, kN	Spalling, kN	Failure Load, kN
B-1	533.456	704.379	911.156
B-2	433.297	653.211	737.403
B-3	589.621	949.464	949.464
B-4	453.055	763.039	786.884
B-5	489.183	776.046	776.046
B-6	330.217	790.497	790.497
B-8	492.802	841.809	841.809
B-9	640.209	650.325	650.325
B-10	581.679	641.654	692.957
Max	**640.209**	**949.464**	**949.464**
Min	**330.217**	**641.654**	**650.325**
Mean	**504.835**	**752.269**	**792.949**
St. Dev.	**94.15**	**102.34**	**96.57**
C.O.V.	**18.65%**	**13.60%**	**12.18%**

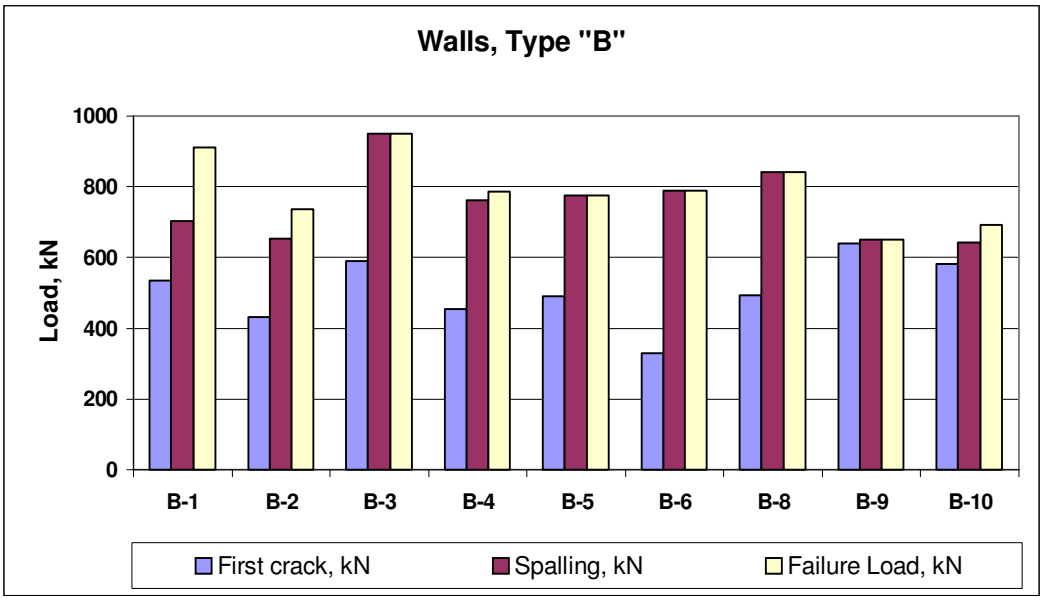

Fig. 17 First crack, Spalling and Failure loads ratios for type **B** walls

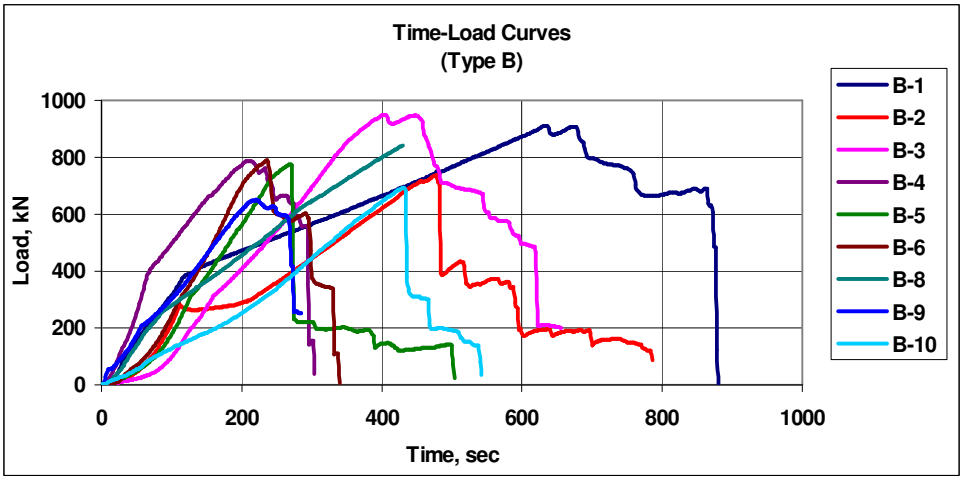

Fig. B.18 Time versus load curves (type **B**)

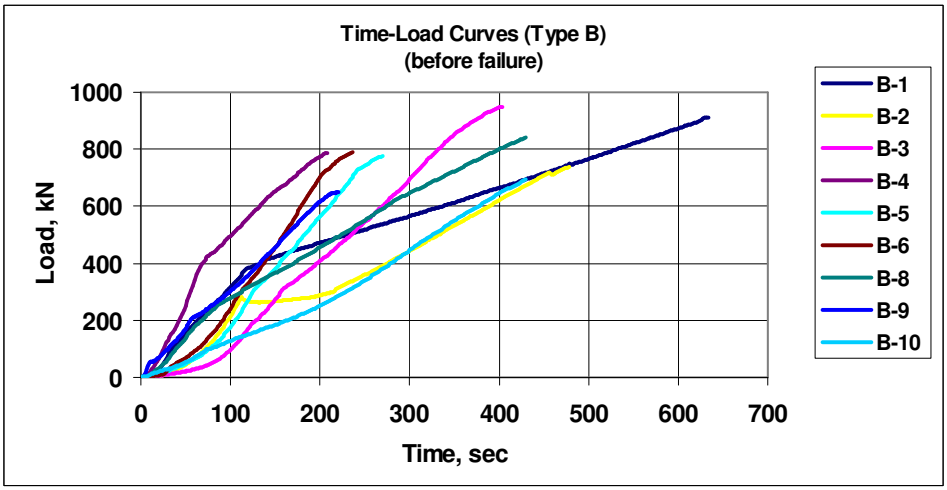

Fig. B.19 Time versus load curves (before failure)

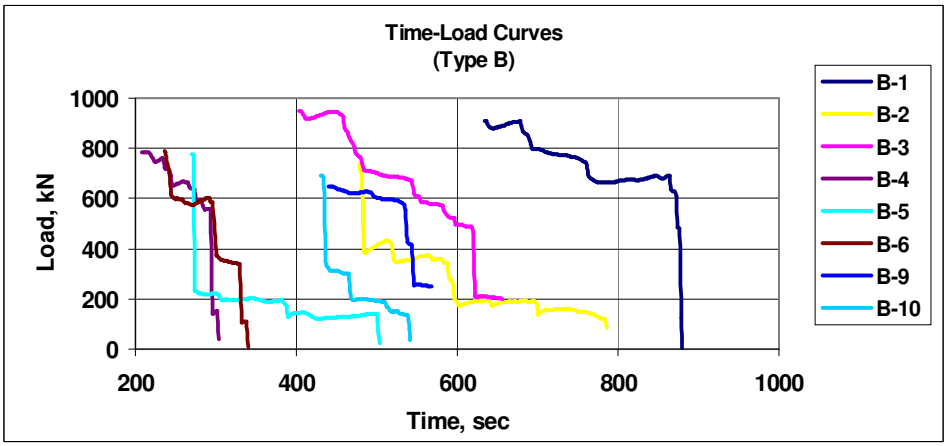

Fig. B.20 Time versus load curves (after failure)

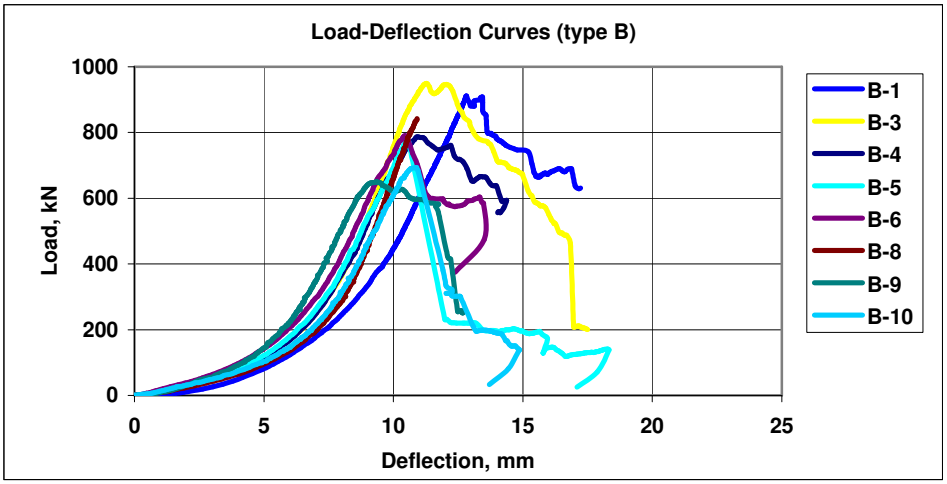

Fig. B.21 Load versus deflection curves (type **B**)

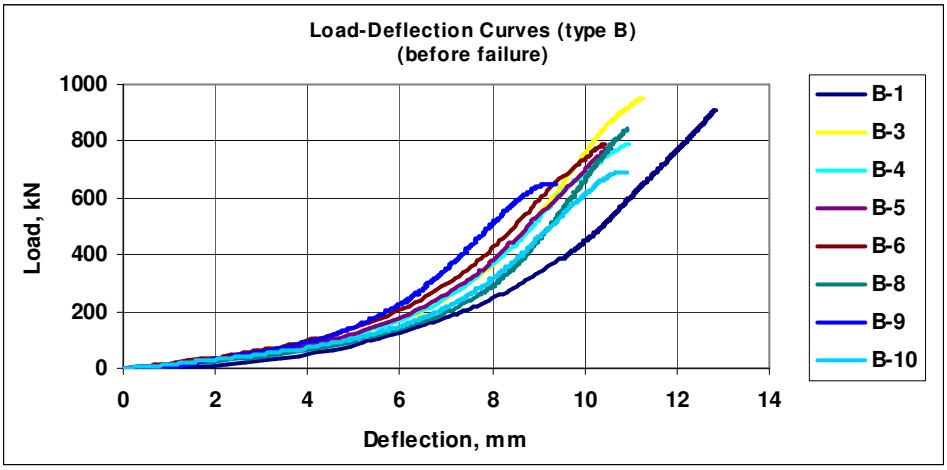

Fig. B.22 Load versus deflection curves (before failure)

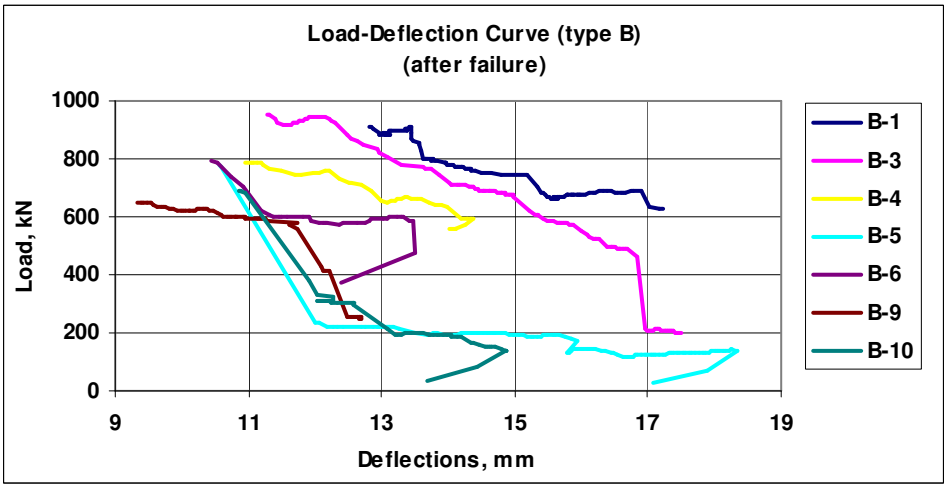

Fig. B.23 Load versus deflection curves (after failure)

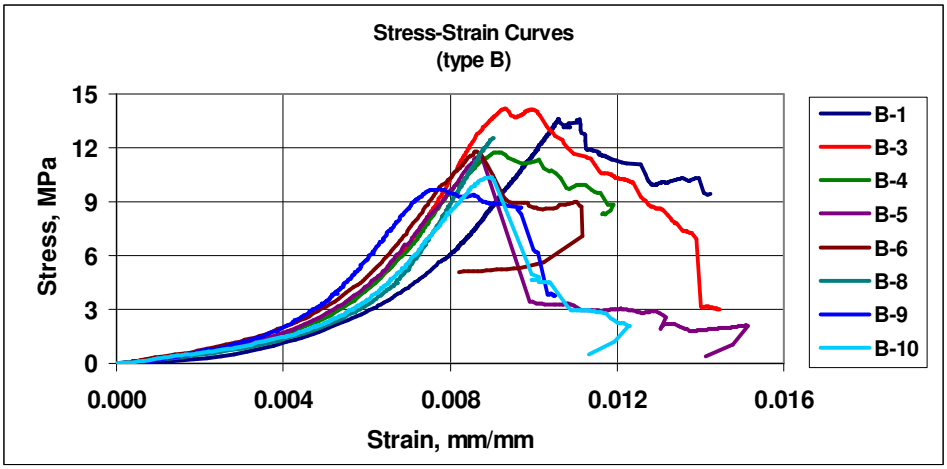

Fig. B.24 Stress versus strain curves (type ***B***)

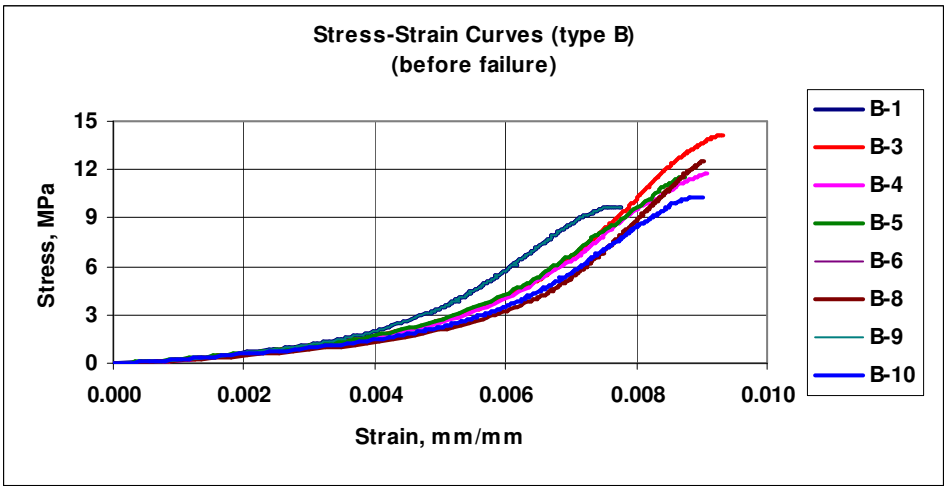

Fig. B.25 Stress versus strain curves (before failure)

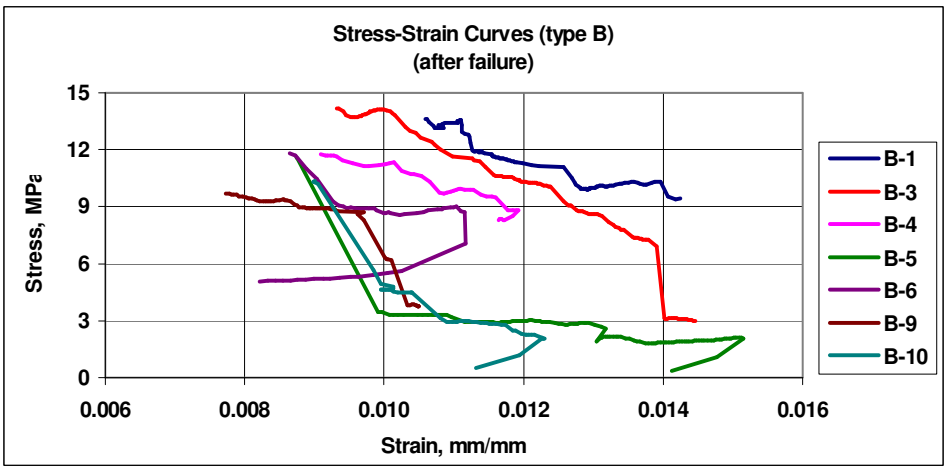

Fig. B.26 Stress versus strain curves (after failure)

4. Test specimens type *C*

Table B.4 Summation of test results for type **C** specimens

Type C	First crack, kN	Spalling, kN	Failure Load, kN
C-1	434.385	739.580	748.653
C-2	551.601	735.226	760.991
C-3	421.261	621.415	772.433
C-4	524.590	935.735	1031.115
C-5	324.055	670.280	724.979
C-6	396.698	679.228	722.583
C-7	312.878	336.001	539.047
C-8	319.382	619.976	656.105
C-9	392.363	531.821	538.324
C-10	270.969	552.053	763.048
Max	**551.601**	**935.735**	**1031.115**
Min	**270.969**	**336.001**	**538.324**
Mean	**394.818**	**642.131**	**725.728**
St. Dev.	**92.16**	**156.86**	**138.82**
C.O.V.	**23.34%**	**24.43%**	**19.13%**

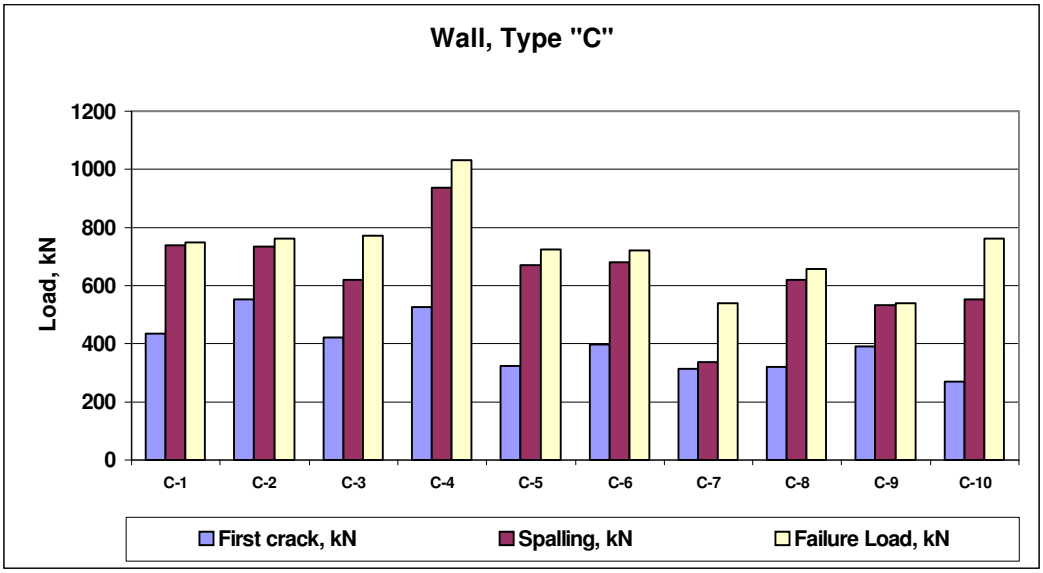

Fig. B.27 First crack, Spalling and Failure loads ratios for type **C** walls

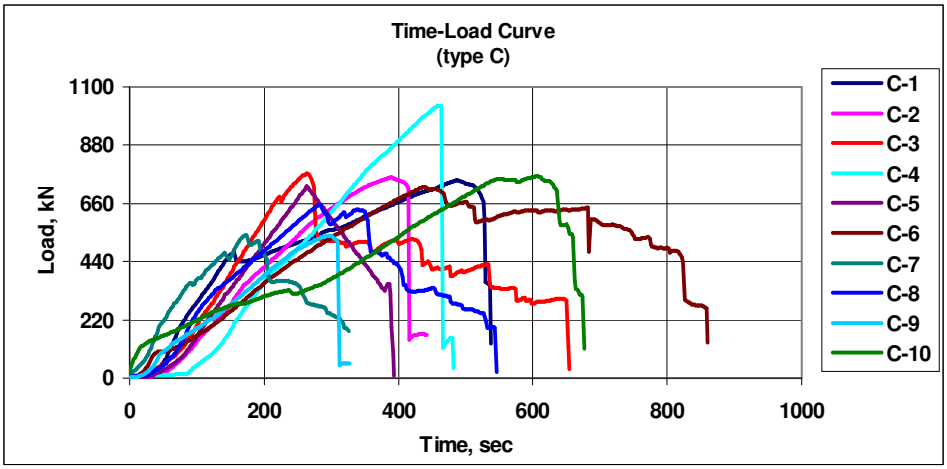

Fig. B.28 Time versus load curves (type **C**)

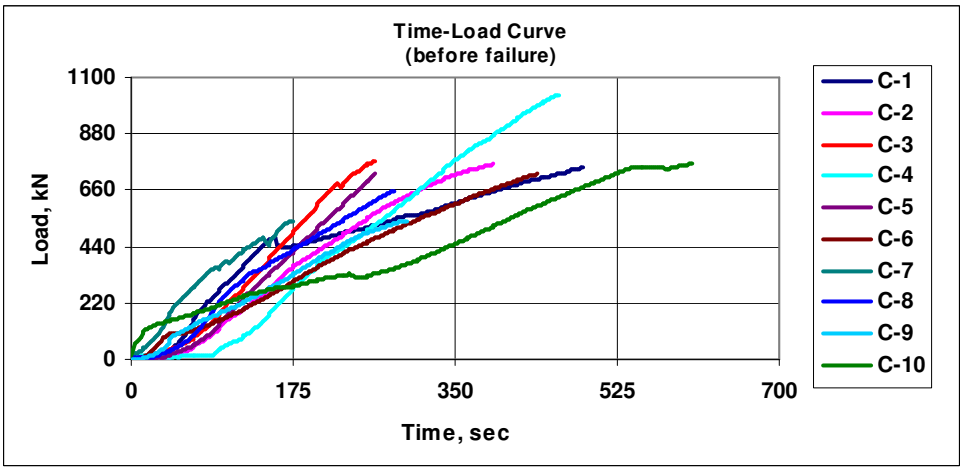

Fig. B.29 Time versus load curves (before failure)

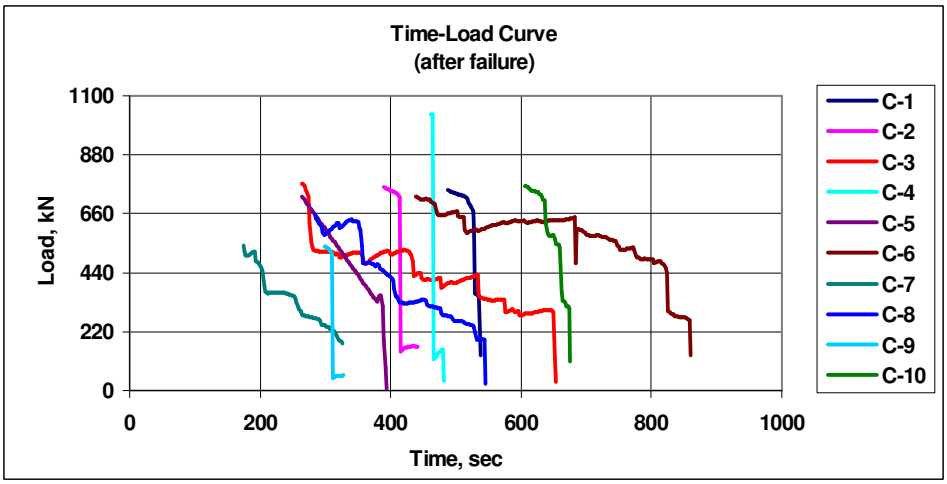

Fig. B.30 Time versus load curves (after failure)

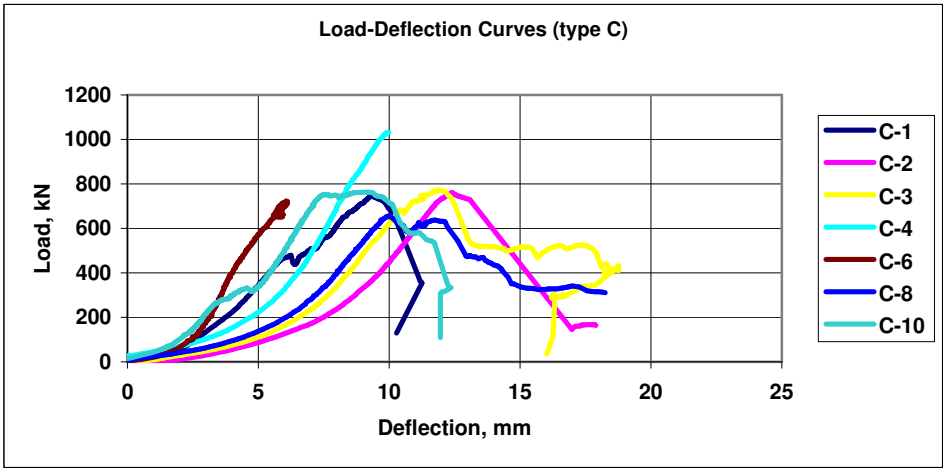

Fig. B.31 Load versus deflection curves (type **C**)

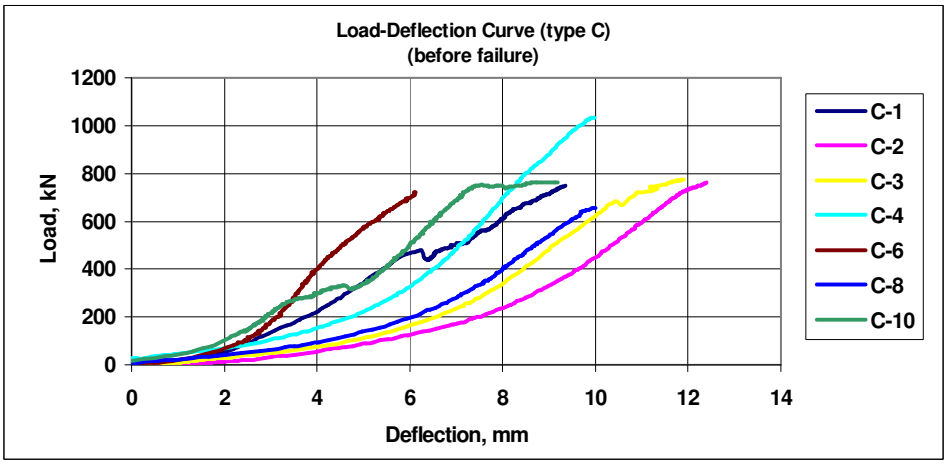

Fig. B.32 Load versus deflection curves (before failure)

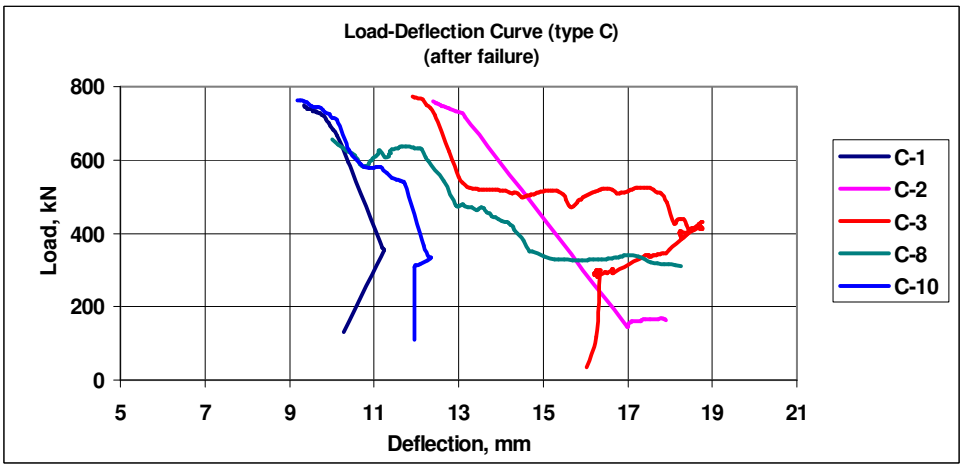

Fig. B.33 Load versus deflection curves (after failure).

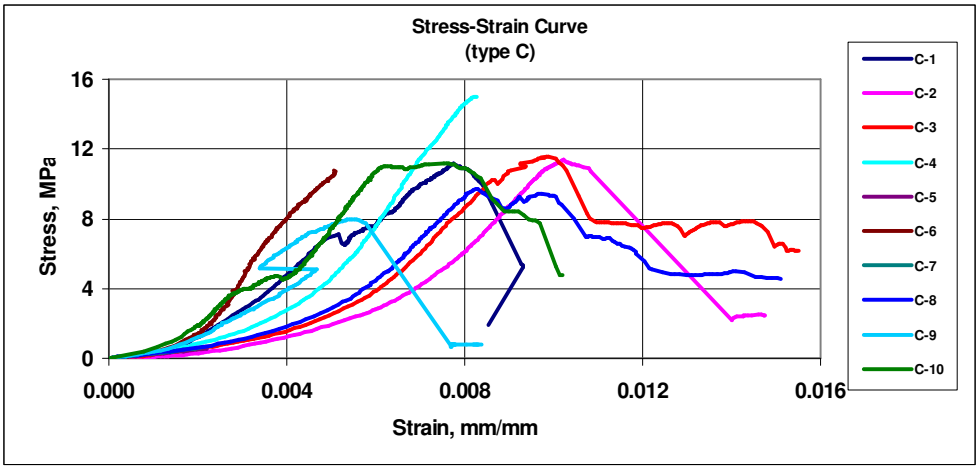

Fig. B.34 Stress versus strain curves (type ***C***).

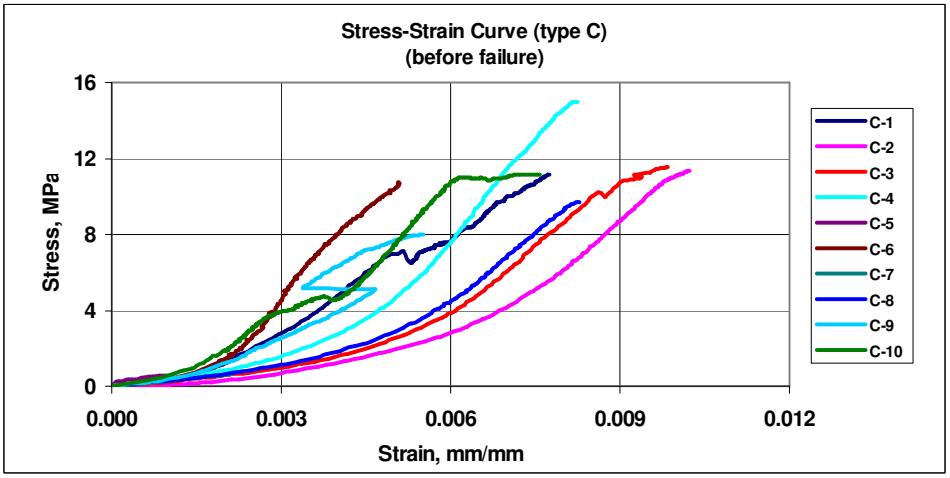

Fig. B.35 Stress versus strain curves (before failure).

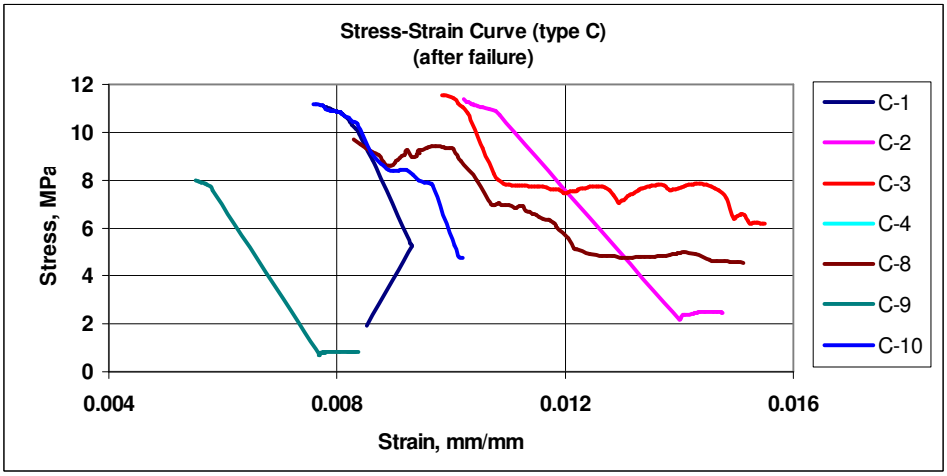

Fig. B.36 Stress versus strain curves (after failure).

APPENDIX C

Load – Deflection Data

This appendix presents sets of important time-load and load-deflection curves.

These curves represent the raw data prior to processing. Some of the curves appear to be reversed because the way that LDS's were mounted.

1. Time versus load, load versus deflection curves for wall specimens of type ***A*** are given in Fig. C.1 to C.69:

- Wall ***A-1***

Fig. C.1 Time versus load curve
Fig. C.2 Load versus deflection curve (LDS #1, LDS #2 and CL)
Fig. C.3 Load versus deflection curve (LDS #3 & #4, LDS #7 & #8 and top CL)
Fig. C.4 Load versus deflection curve (LDS #5 & #6, LDS #9 & #10 and bottom CL)
Fig. C.5 Load versus deflection curve (LDS #3 & #5, LDS #8 & #10 and left CL)
Fig. C.6 Load versus deflection curve (LDS #4 & #6, LDS #7 & #9 and right CL)

- Wall ***A-2***

Fig. C.7 Time versus load curve
Fig. C.8 Load versus deflection curve (LDS #1, LDS #2 and CL)
Fig. C.9 Load versus deflection curve (LDS #3 & #4, LDS #7 & #8 and top CL)
Fig. C.10 Load versus deflection curve (LDS #5 & #6, LDS #9 & #10 and bottom CL)
Fig. C.11 Load versus deflection curve (LDS #3 & #5, LDS #8 & #10 and left CL)
Fig. C.12 Load versus deflection curve (LDS #4 & #6, LDS #7 & #9 and right CL)
Fig. C.13 Load versus deflection curve (LDS #11 & #12, LDS #13 & #14, middle CL)

- Wall ***A-3***

Fig. C.14 Time versus load curve
Fig. C.15 Load versus deflection curve (LDS #1, LDS #2 and CL)
Fig. C.16 Load versus deflection curve (LDS #3 & #4, LDS #7 & #8 and top CL)
Fig. C.17 Load versus deflection curve (LDS #5 & #6, LDS #9 & #10 and bottom CL)
Fig. C.18 Load versus deflection curve (LDS #3 & #5, LDS #8 & #10 and left CL)
Fig. C.19 Load versus deflection curve (LDS #4 & #6, LDS #7 & #9 and right CL)
Fig. C.20 Load versus deflection curve (LDS #11 & #12, LDS #13 & #14, middle CL)

- Wall ***A-4***

- Wall ***A-5***

- Wall ***A-6***

- Wall ***A-7***

- Wall ***A-8***

- Wall ***A-9***

Fig. C.56 Time versus load curve
Fig. C.57 Load versus deflection curve (LDS #1, LDS #2 and CL)
Fig. C.58 Load versus deflection curve (LDS #3 & #4, LDS #7 & #8 and top CL)
Fig. C.59 Load versus deflection curve (LDS #5 & #6, LDS #9 & #10 and bottom CL)
Fig. C.60 Load versus deflection curve (LDS #3 & #5, LDS #8 & #10 and left CL)
Fig. C.61 Load versus deflection curve (LDS #4 & #6, LDS #7 & #9 and right CL)
Fig. C.62 Load versus deflection curve (LDS #11 & #12, LDS #13 & #14, middle CL)

- Wall ***A-10***

Fig. C.63 Time versus load curve
Fig. C.64 Load versus deflection curve (LDS #1, LDS #2 and CL)
Fig. C.65 Load versus deflection curve (LDS #3 & #4, LDS #7 & #8 and top CL)
Fig. C.66 Load versus deflection curve (LDS #5 & #6, LDS #9 & #10 and bottom CL)
Fig. C.67 Load versus deflection curve (LDS #3 & #5, LDS #8 & #10 and left CL)
Fig. C.68 Load versus deflection curve (LDS #4 & #6, LDS #7 & #9 and right CL)
Fig. C.69 Load versus deflection curve (LDS #11 & #12, LDS #13 & #14, middle CL)

2. Time versus load, load versus deflection curves for the wall specimens of type ***B*** are given in Fig. C.70 to Fig. C.132:

- Wall ***B-1***

Fig. C.70 Time versus load curve
Fig. C.71 Load versus deflection curve (LDS #1, LDS #2 and CL)
Fig. C.72 Load versus deflection curve (LDS #3 & #4, LDS #7 & #8 and top CL)
Fig. C.73 Load versus deflection curve (LDS #5 & #6, LDS #9 & #10 and bottom CL)
Fig. C.74 Load versus deflection curve (LDS #3 & #5, LDS #8 & #10 and left CL)
Fig. C.75 Load versus deflection curve (LDS #4 & #6, LDS #7 & #9 and right CL)
Fig. C.76 Load versus deflection curve (LDS #11 & #12, LDS #13 & #14, middle CL)

- Wall ***B-2***

Fig. C.77 Time versus load curve
Fig. C.78 Load versus deflection curve (LDS #1, LDS #2 and CL)
Fig. C.79 Load versus deflection curve (LDS #3 & #4, LDS #7 & #8 and top CL)
Fig. C.80 Load versus deflection curve (LDS #5 & #6, LDS #9 & #10 and bottom CL)
Fig. C.81 Load versus deflection curve (LDS #3 & #5, LDS #8 & #10 and left CL)
Fig. C.82 Load versus deflection curve (LDS #4 & #6, LDS #7 & #9 and right CL)
Fig. C.83 Load versus deflection curve (LDS #11 & #12, LDS #13 & #14, middle CL)

- Wall ***B-3***

Fig. C.84 Time versus load curve
Fig. C.85 Load versus deflection curve (LDS #1, LDS #2 and CL)
Fig. C.86 Load versus deflection curve (LDS #3 & #4, LDS #7 & #8 and top CL)
Fig. C.87 Load versus deflection curve (LDS #5 & #6, LDS #9 & #10 and bottom CL)
Fig. C.88 Load versus deflection curve (LDS #3 & #5, LDS #8 & #10 and left CL)

- Wall ***B-4***

- Wall ***B-5***

- Wall ***B-6***

- Wall ***B-7***

There is no data available for wall test specimens ***B-7*** – the load cell was broken.

- Wall ***B-8***

- Wall ***B-9***

Fig. C.119 Time versus load curve
Fig. C.120 Load versus deflection curve (LDS #1, LDS #2 and CL)
Fig. C.121 Load versus deflection curve (LDS #3 & #4, LDS #7 & #8 and top CL)
Fig. C.122 Load versus deflection curve (LDS #5 & #6, LDS #9 & #10 and bottom CL)
Fig. C.123 Load versus deflection curve (LDS #3 & #5, LDS #8 & #10 and left CL)
Fig. C.124 Load versus deflection curve (LDS #4 & #6, LDS #7 & #9 and right CL)
Fig. C.125 Load versus deflection curve (LDS #11 & #12, LDS #13 & #14, middle CL)

- Wall ***B-10***

Fig. C.126 Time versus load curve
Fig. C.127 Load versus deflection curve (LDS #1, LDS #2 and CL)
Fig. C.128 Load versus deflection curve (LDS #3 & #4, LDS #7 & #8 and top CL)
Fig. C.129 Load versus deflection curve (LDS #5 & #6, LDS #9 & #10 and bottom CL)
Fig. C.130 Load versus deflection curve (LDS #3 & #5, LDS #8 & #10 and left CL)
Fig. C.131 Load versus deflection curve (LDS #4 & #6, LDS #7 & #9 and right CL)
Fig. C.132 Load versus deflection curve (LDS #11 & #12, LDS #13 & #14, middle CL)

3. Time versus load, load versus deflection curves for the wall specimens of type ***B*** are given in Fig. C.133 to Fig. C.202:

- Wall ***C-1***

Fig. C.133 Time versus load curve
Fig. C.134 Load versus deflection curve (LDS #1, LDS #2 and CL)
Fig. C.135 Load versus deflection curve (LDS #3 & #4, LDS #7 & #8 and top CL)
Fig. C.136 Load versus deflection curve (LDS #5 & #6, LDS #9 & #10 and bottom CL)
Fig. C.137 Load versus deflection curve (LDS #3 & #5, LDS #8 & #10 and left CL)
Fig. C.138 Load versus deflection curve (LDS #4 & #6, LDS #7 & #9 and right CL)
Fig. C.139 Load versus deflection curve (LDS #11 & #12, LDS #13 & #14, middle CL)

- Wall ***C-2***

Fig. C.140 Time versus load curve
Fig. C.141 Load versus deflection curve (LDS #1, LDS #2 and CL)
Fig. C.142 Load versus deflection curve (LDS #3 & #4, LDS #7 & #8 and top CL)
Fig. C.143 Load versus deflection curve (LDS #5 & #6, LDS #9 & #10 and bottom CL)
Fig. C.144 Load versus deflection curve (LDS #3 & #5, LDS #8 & #10 and left CL)
Fig. C.145 Load versus deflection curve (LDS #4 & #6, LDS #7 & #9 and right CL)
Fig. C.146 Load versus deflection curve (LDS #11 & #12, LDS #13 & #14, middle CL)

- Wall ***C-3***

Fig. C.147 Time versus load curve
Fig. C.148 Load versus deflection curve (LDS #1, LDS #2 and CL)
Fig. C.149 Load versus deflection curve (LDS #3 & #4, LDS #7 & #8 and top CL)
Fig. C.150 Load versus deflection curve (LDS #5 & #6, LDS #9 & #10 and bottom CL)
Fig. C.151 Load versus deflection curve (LDS #3 & #5, LDS #8 & #10 and left CL)

- Wall ***C-4***

- Wall ***C-5***

- Wall ***C-6***

- Wall ***C-7***

- Wall ***C-8***

1. Test results for wall specimens type *A*

1.1 Wall *A-1*

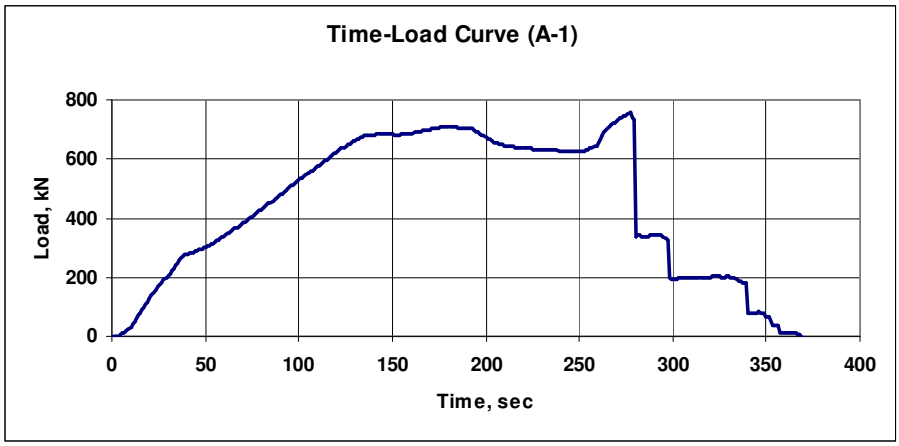

Fig. C.1 Time versus load curve

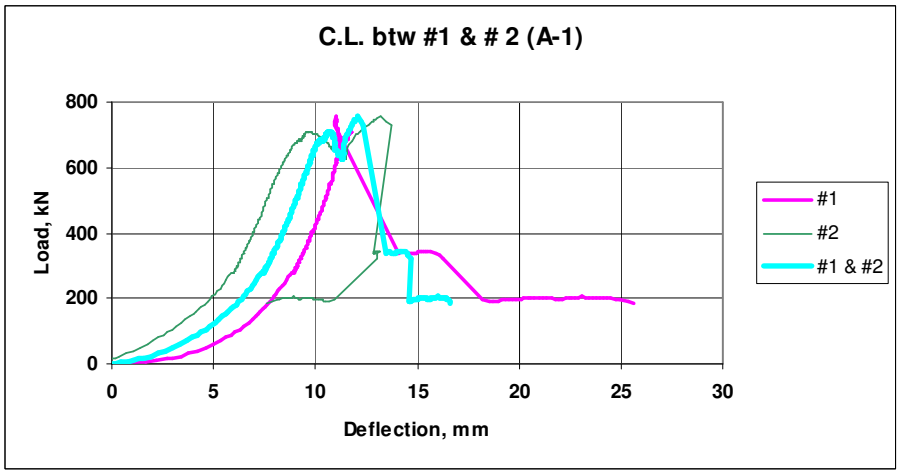

Fig. C.2 Load versus deflection curve (LDS #1, LDS #2 and CL)

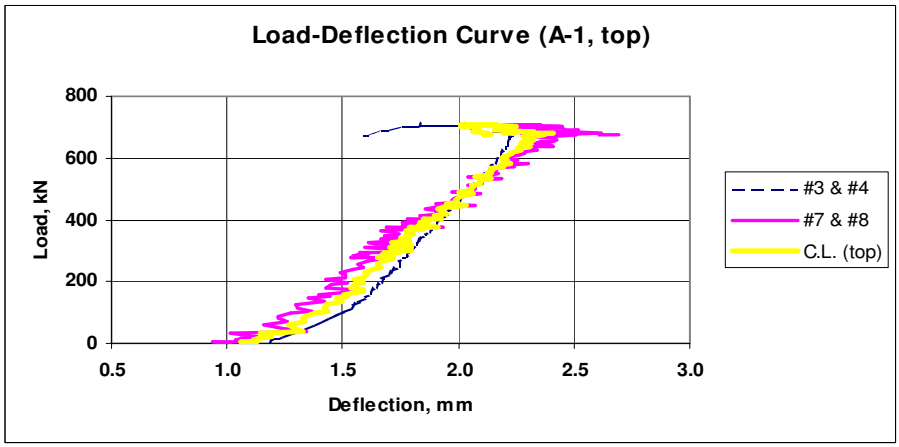

Fig. C.3 Load versus deflection curve (LDS #3 & #4, LDS #7 & #8 and top CL)

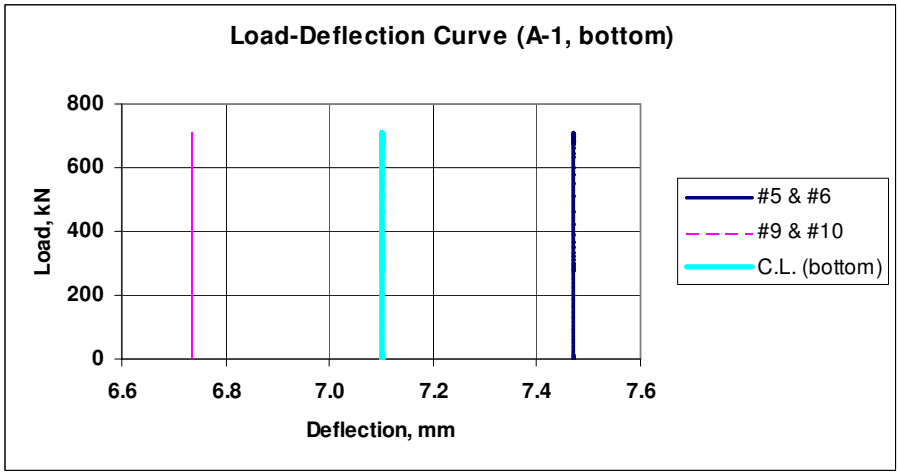

Fig. C.4 Load versus deflection curve (LDS #5 & #6, LDS #9 & #10 and bottom CL)

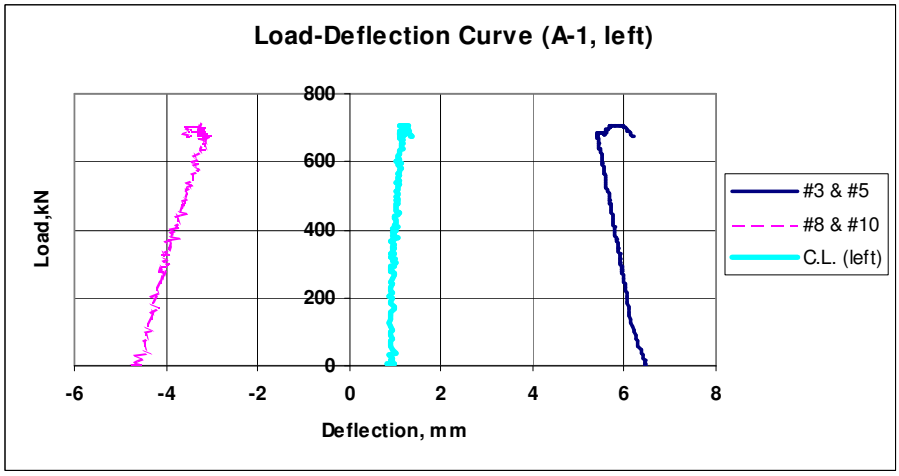

Fig. C.5 Load versus deflection curve (LDS #3 & #5, LDS #8 & #10 and left CL)

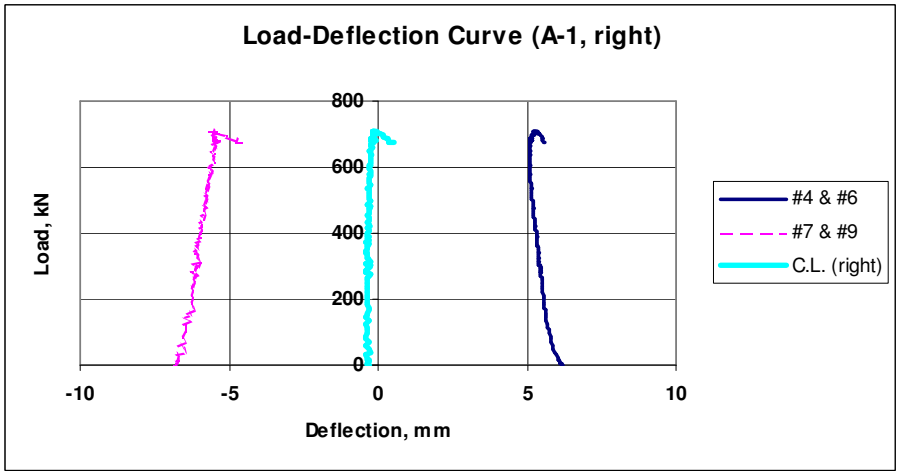

Fig. C.6 Load versus deflection curve (LDS #4 & #6, LDS #7 & #9 and right CL)

1.2 Wall ***A-2***

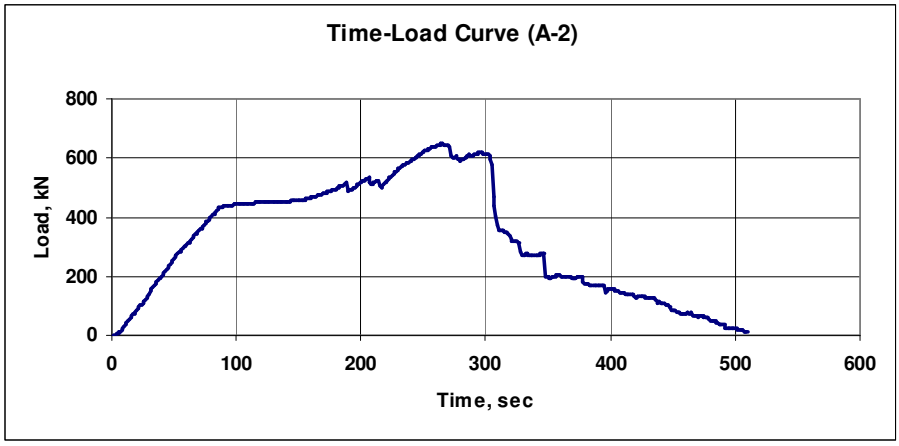

Fig. C.7 Time versus load curve

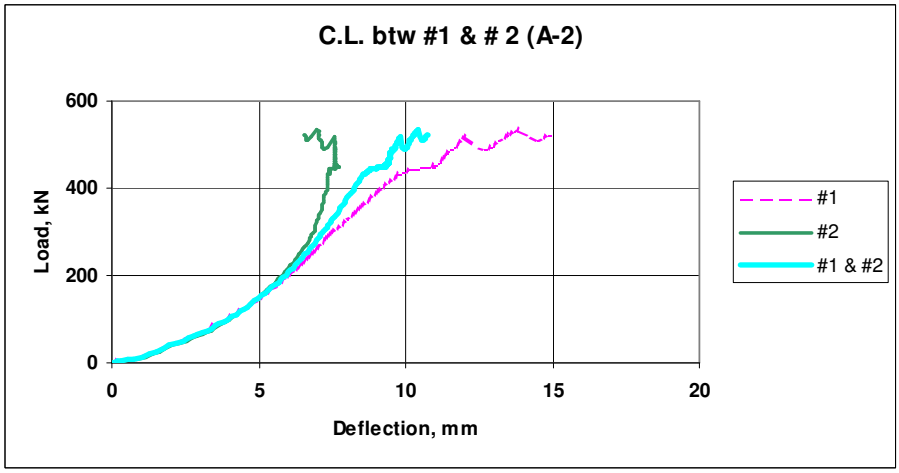

Fig. C.8 Load versus deflection curve (LDS #1, LDS #2 and CL)

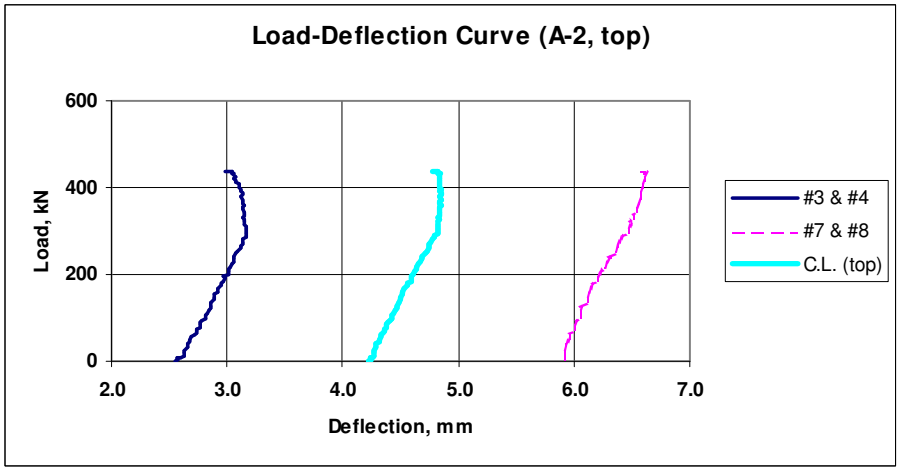

Fig. C.9 Load versus deflection curve (LDS #3 & #4, LDS #7 & #8 and top CL)

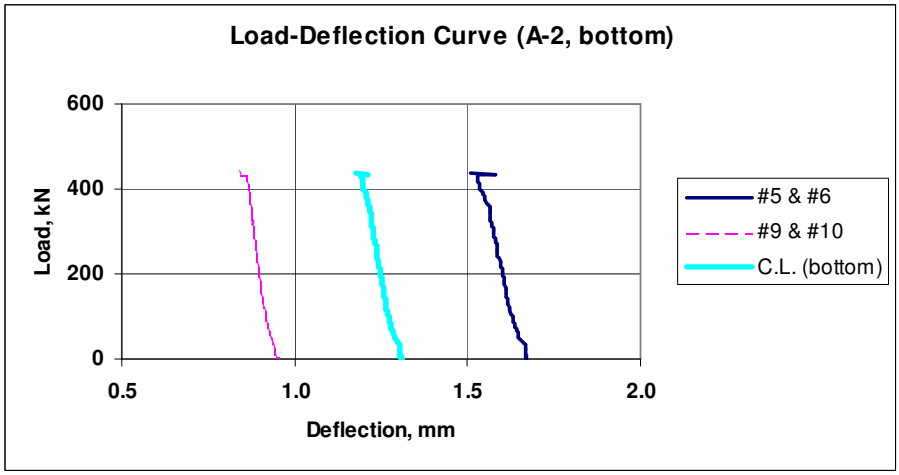

Fig. C.10 Load versus deflection curve (LDS #5 & #6, LDS #9 & #10 and bottom CL)

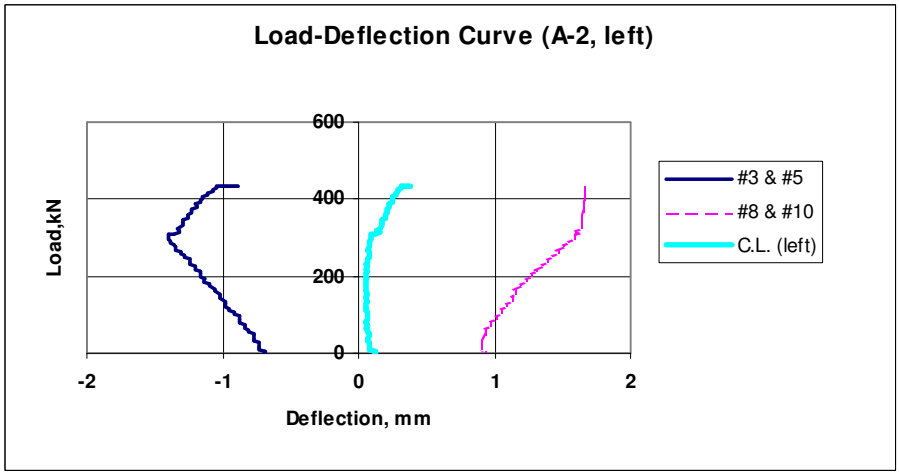

Fig. C.11 Load versus deflection curve (LDS #3 & #5, LDS #8 & #10 and left CL)

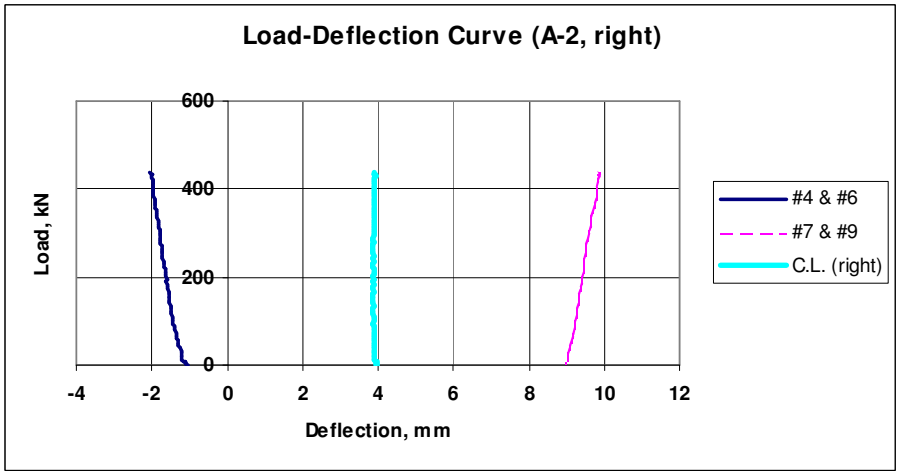

Fig. C.12 Load versus deflection curve (LDS #4 & #6, LDS #7 & #9 and right CL)

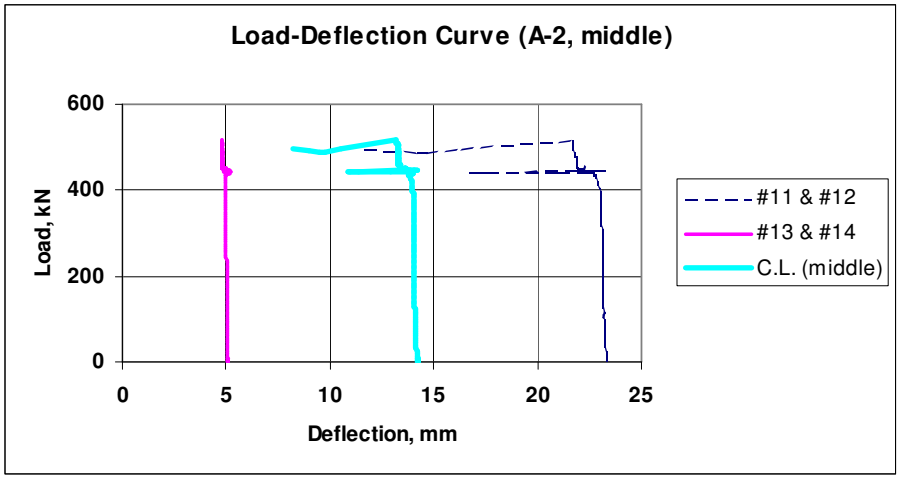

Fig. C.13 Load versus deflection curve (LDS #11 & #12, LDS #13 & #14, middle CL)

1.3 Wall ***A-3***

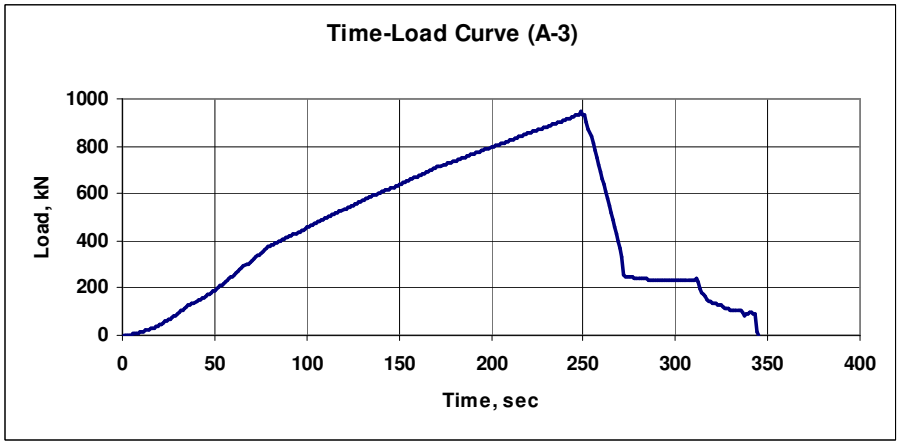

Fig. C.14 Time versus load curve

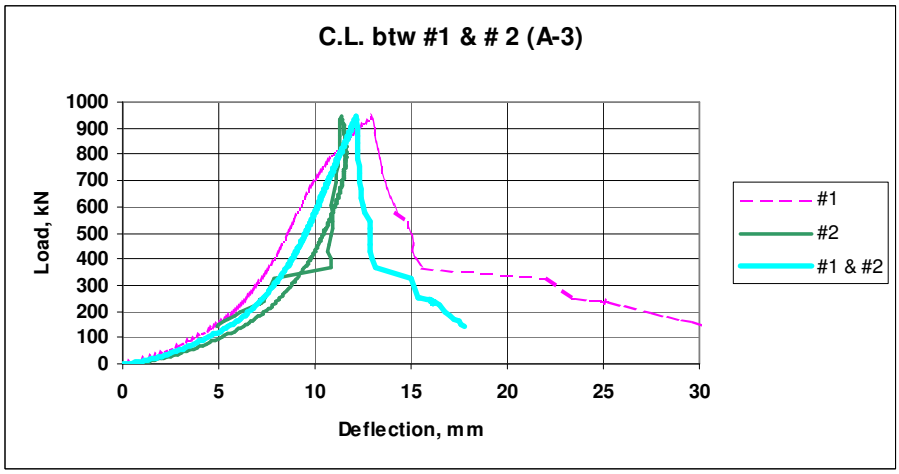

Fig. C.15 Load versus deflection curve (LDS #1, LDS #2 and CL)

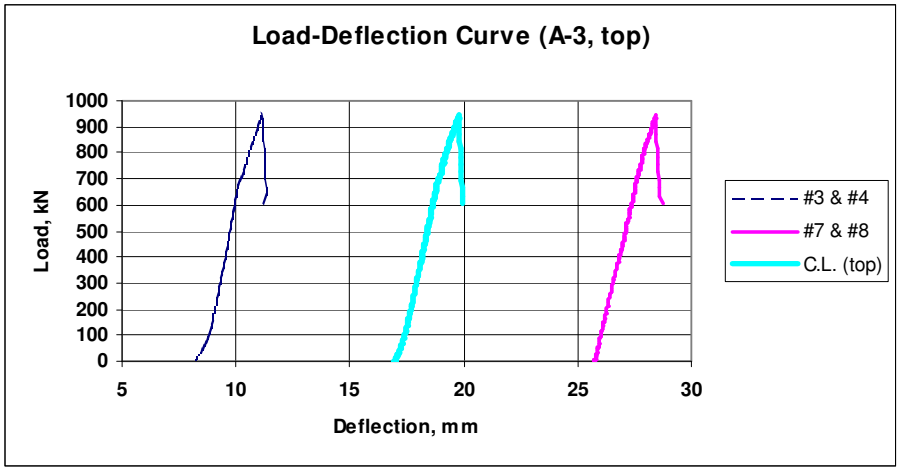

Fig. C.16 Load versus deflection curve (LDS #3 & #4, LDS #7 & #8 and top CL)

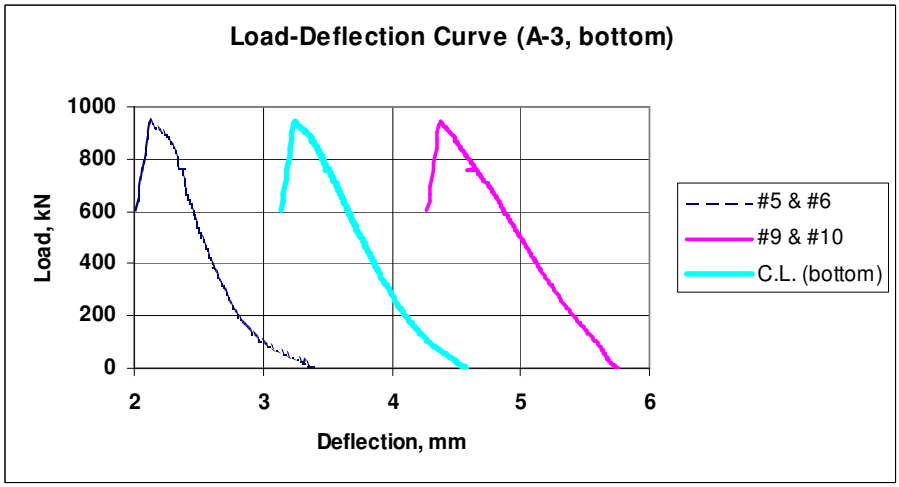

Fig. C.17 Load versus deflection curve (LDS #5 & #6, LDS #9 & #10 and bottom CL)

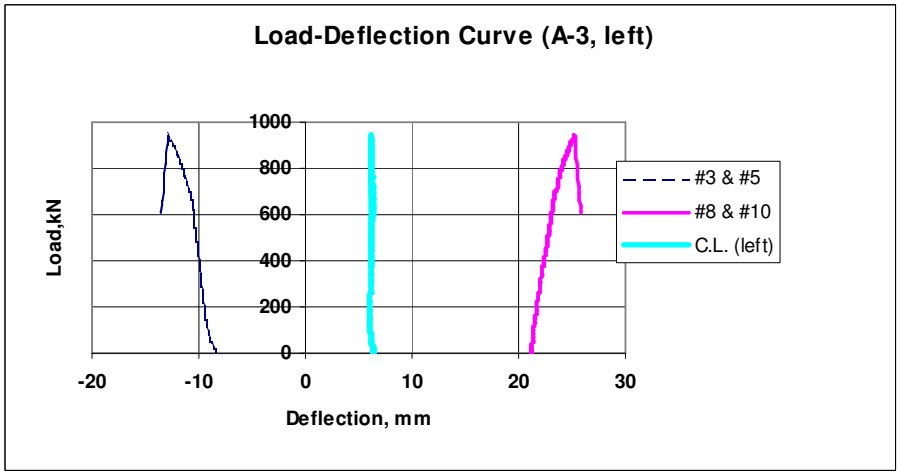

Fig. C.18 Load versus deflection curve (LDS #3 & #5, LDS #8 & #10 and left CL)

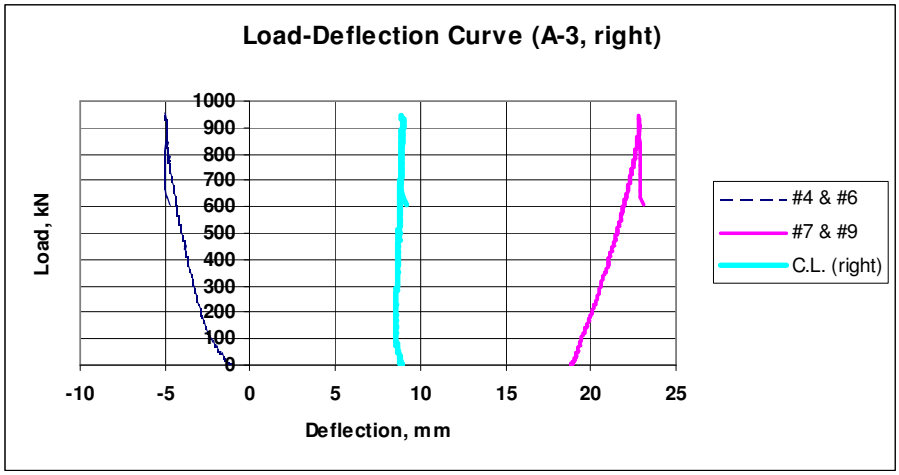

Fig. C.19 Load versus deflection curve (LDS #4 & #6, LDS #7 & #9 and right CL)

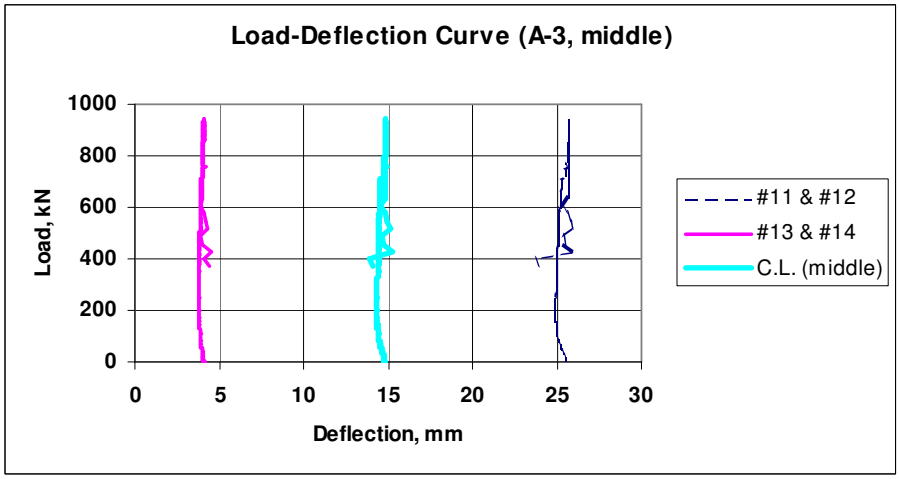

Fig. C.20 Load versus deflection curve (LDS #11 & #12, LDS #13 & #14, middle CL)

1.4 Wall ***A-4***

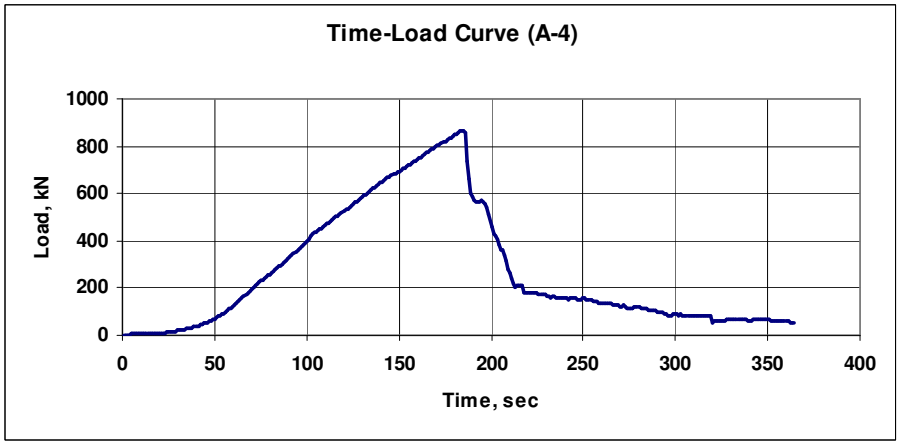

Fig. C.21 Time versus load curve

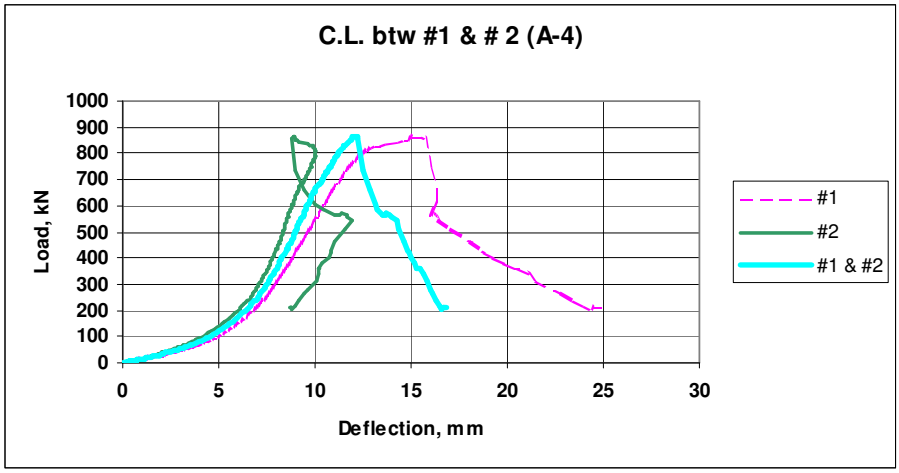

Fig. C.22 Load versus deflection curve (LDS #1, LDS #2 and CL)

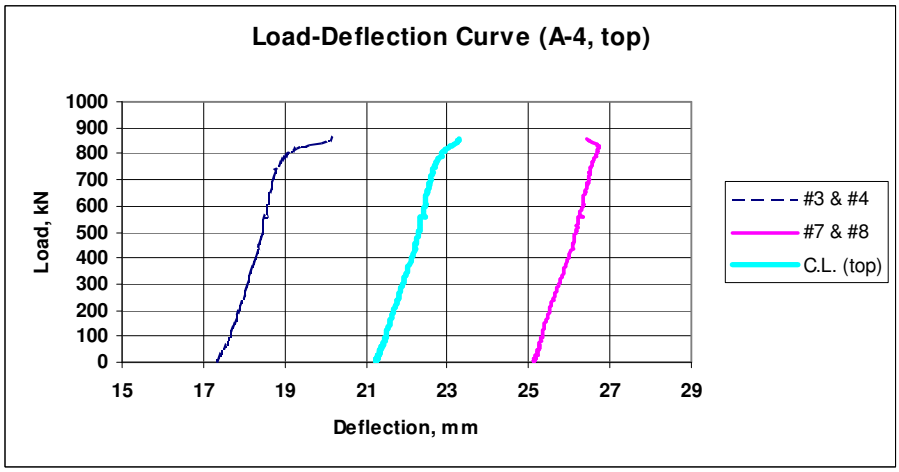

Fig. C.23 Load versus deflection curve (LDS #3 & #4, LDS #7 & #8 and top CL)

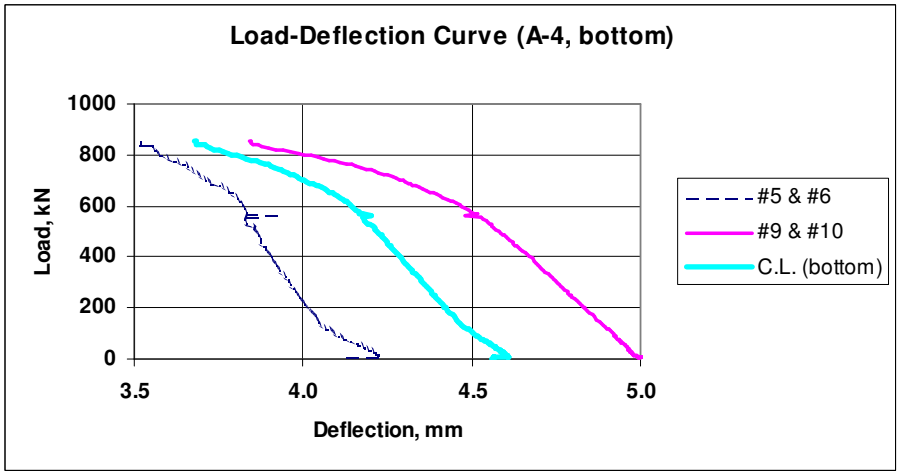

Fig. C.24 Load versus deflection curve (LDS #5 & #6, LDS #9 & #10 and bottom CL)

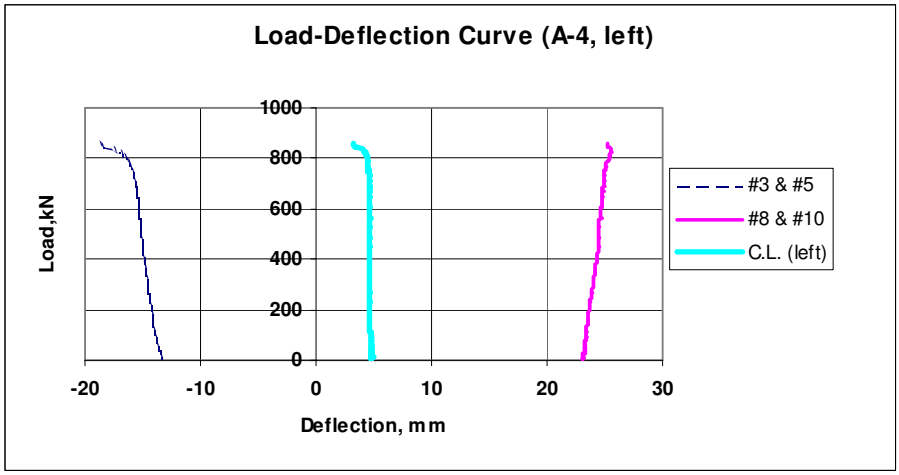

Fig. C.25 Load versus deflection curve (LDS #3 & #5, LDS #8 & #10 and left CL)

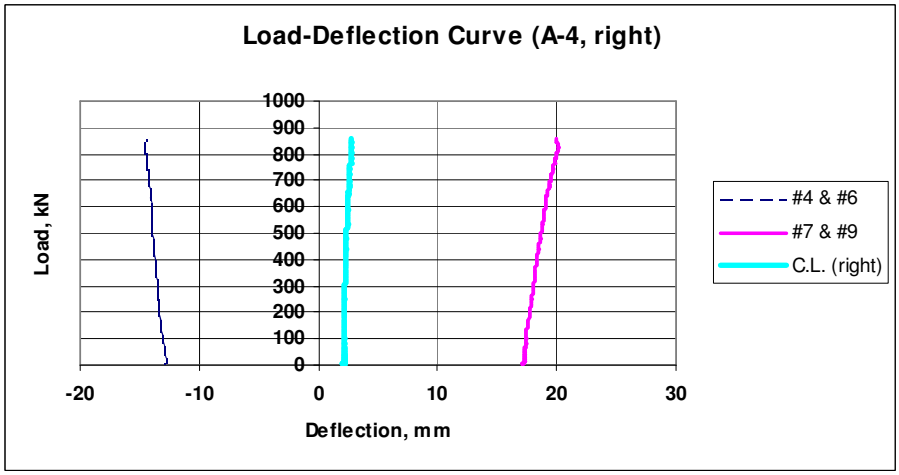

Fig. C.26 Load versus deflection curve (LDS #4 & #6, LDS #7 & #9 and right CL)

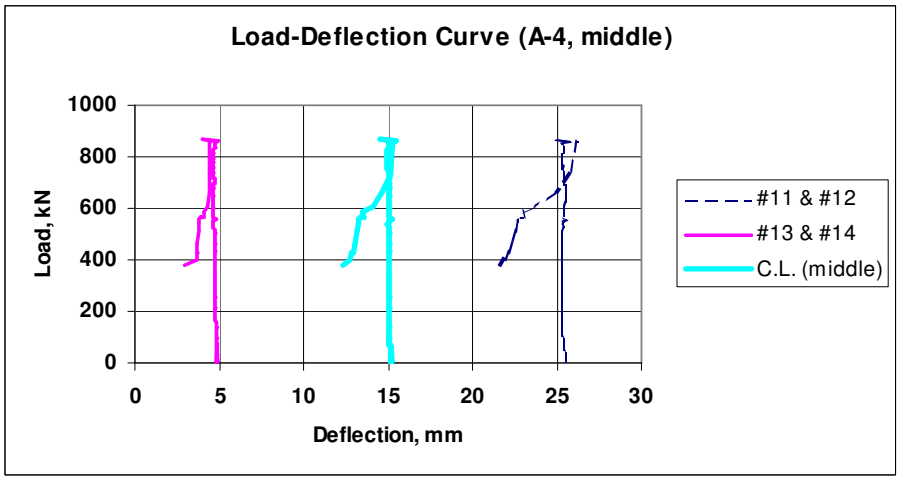

Fig. C.27 Load versus deflection curve (LDS #11 & #12, LDS #13 & #14, middle CL)

1.5 Wall ***A-5***

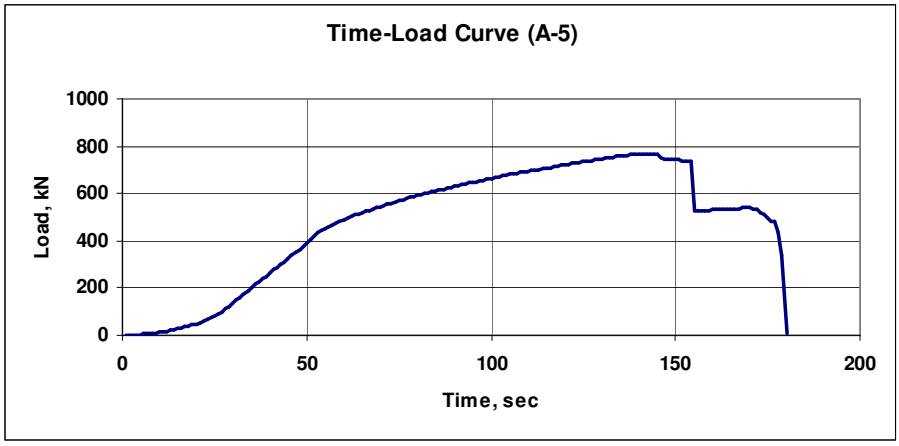

Fig. C.28 Time versus load curve

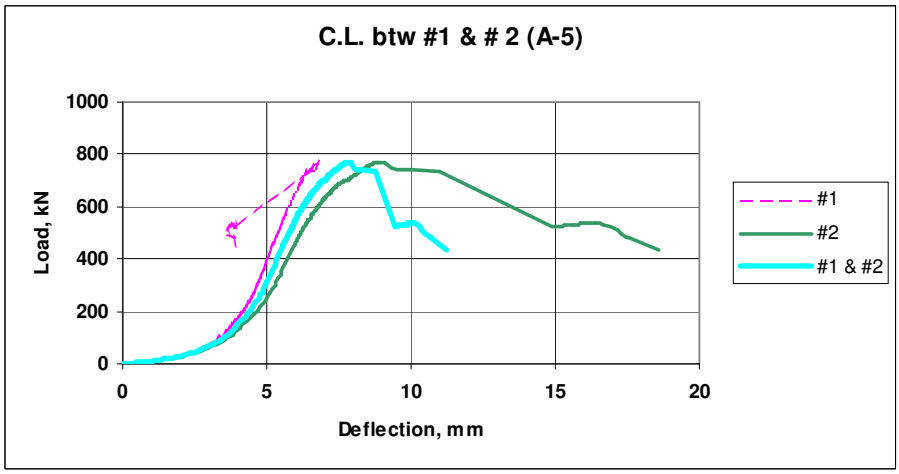

Fig. C.29 Load versus deflection curve (LDS #1, LDS #2 and CL)

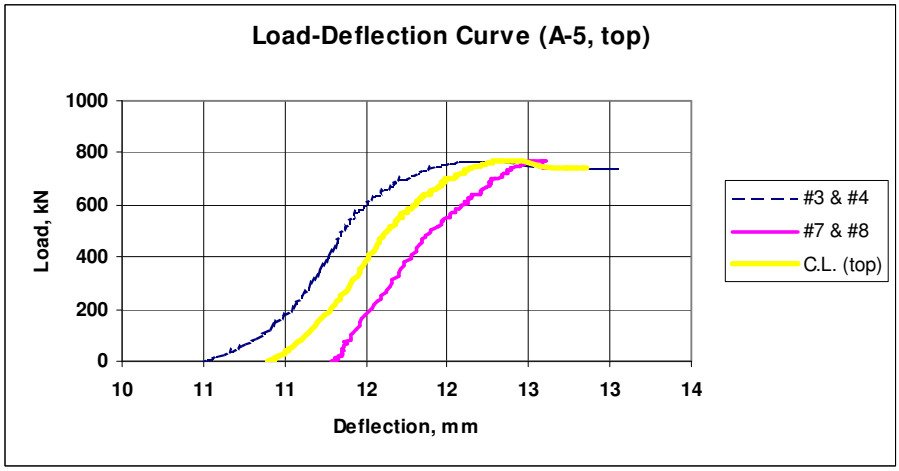

Fig. C.30 Load versus deflection curve (LDS #3 & #4, LDS #7 & #8 and top CL)

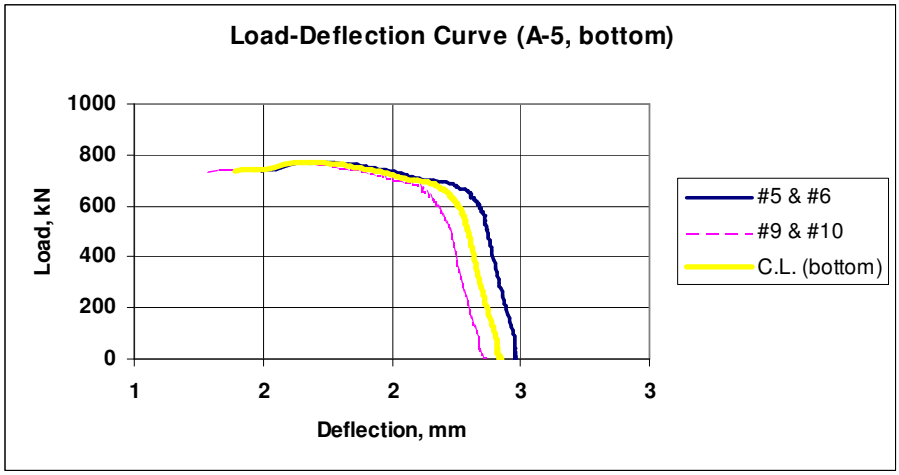

Fig. C.31 Load versus deflection curve (LDS #5 & #6, LDS #9 & #10 and bottom CL)

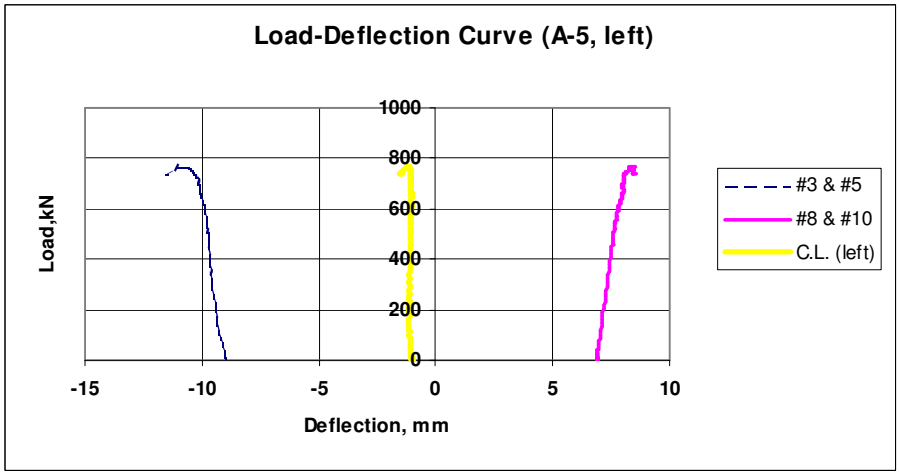

Fig. C.32 Load versus deflection curve (LDS #3 & #5, LDS #8 & #10 and left CL)

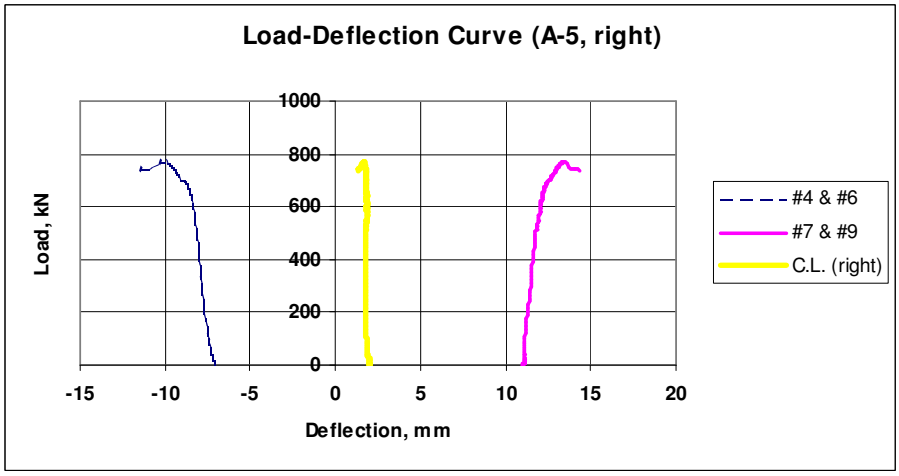

Fig. C.33 Load versus deflection curve (LDS #4 & #6, LDS #7 & #9 and right CL)

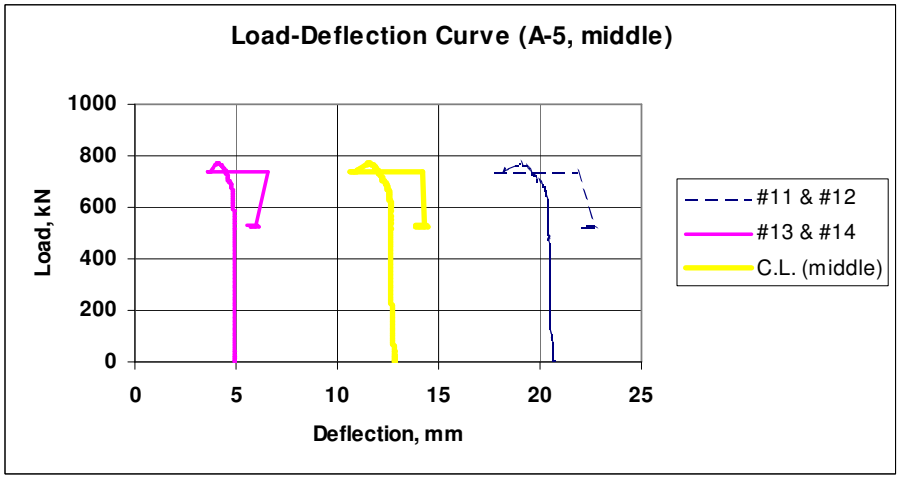

Fig. C.34 Load versus deflection curve (LDS #11 & #12, LDS #13 & #14, middle CL)

1.6 Wall ***A-6***

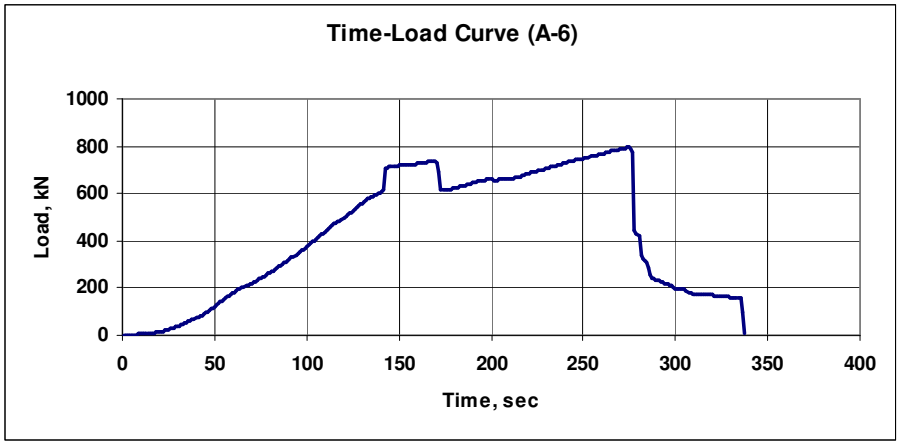

Fig. C.35 Time versus load curve

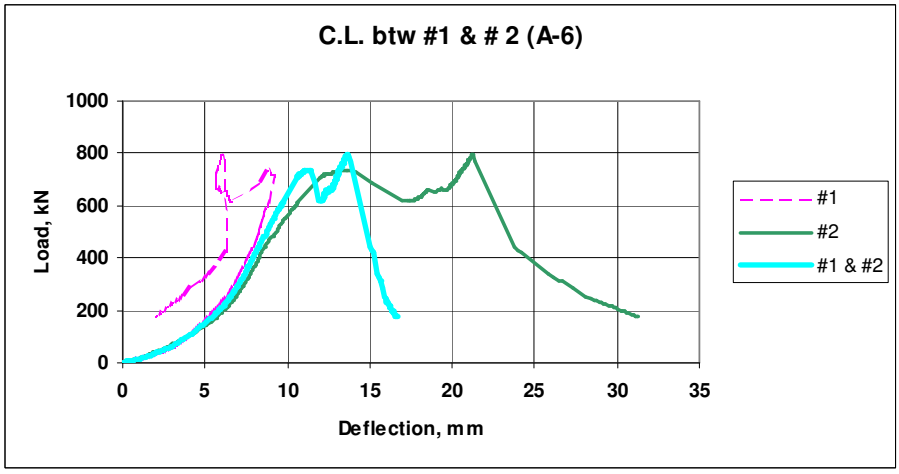

Fig. C.36 Load versus deflection curve (LDS #1, LDS #2 and CL)

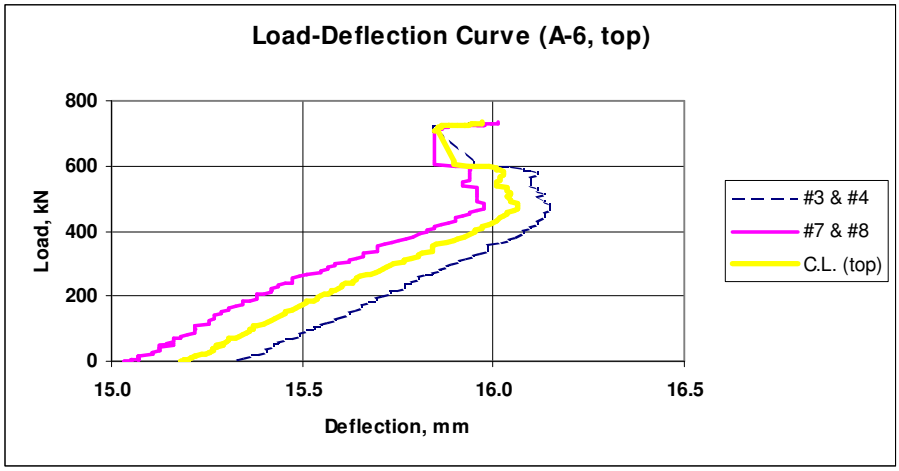

Fig. C.37 Load versus deflection curve (LDS #3 & #4, LDS #7 & #8 and top CL)

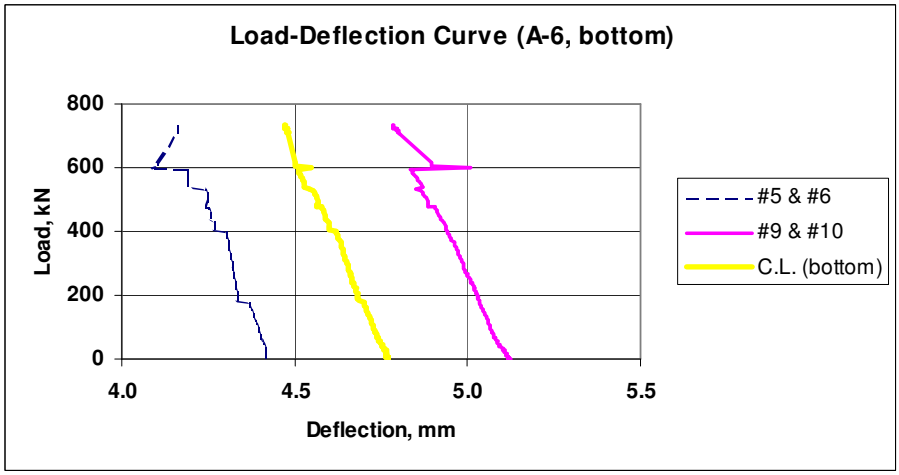

Fig. C.38 Load versus deflection curve (LDS #5 & #6, LDS #9 & #10 and bottom CL)

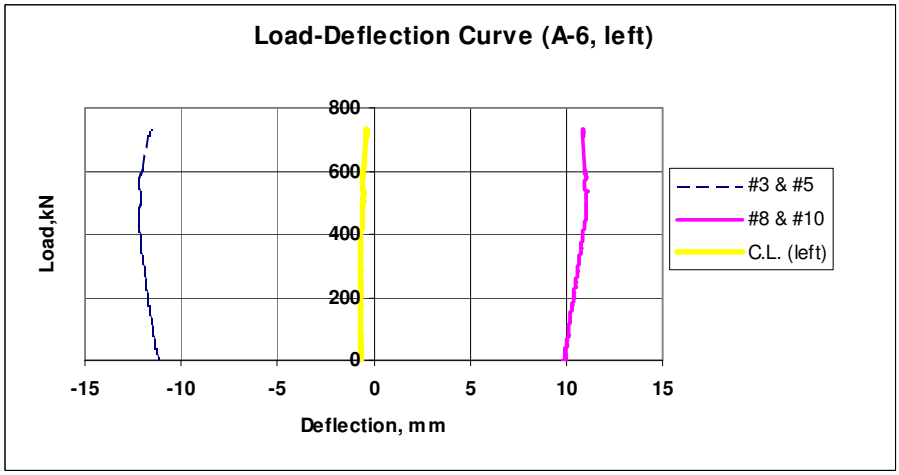

Fig. C.39 Load versus deflection curve (LDS #3 & #5, LDS #8 & #10 and left CL)

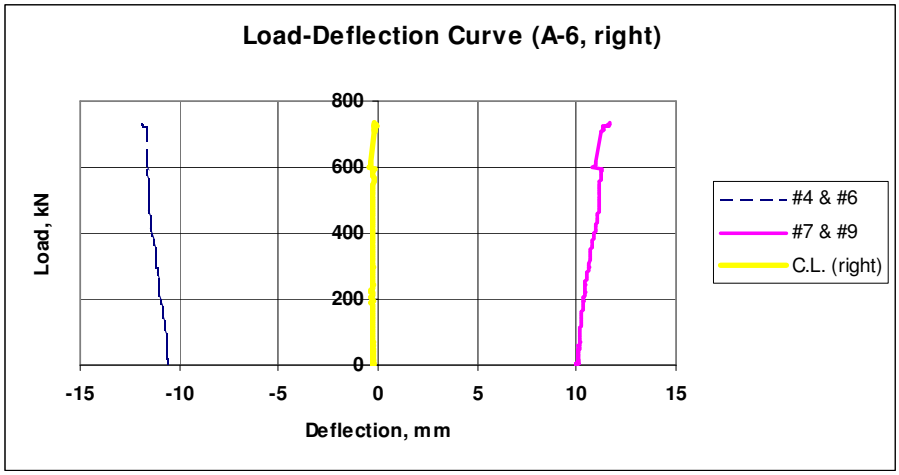

Fig. C.40 Load versus deflection curve (LDS #4 & #6, LDS #7 & #9 and right CL)

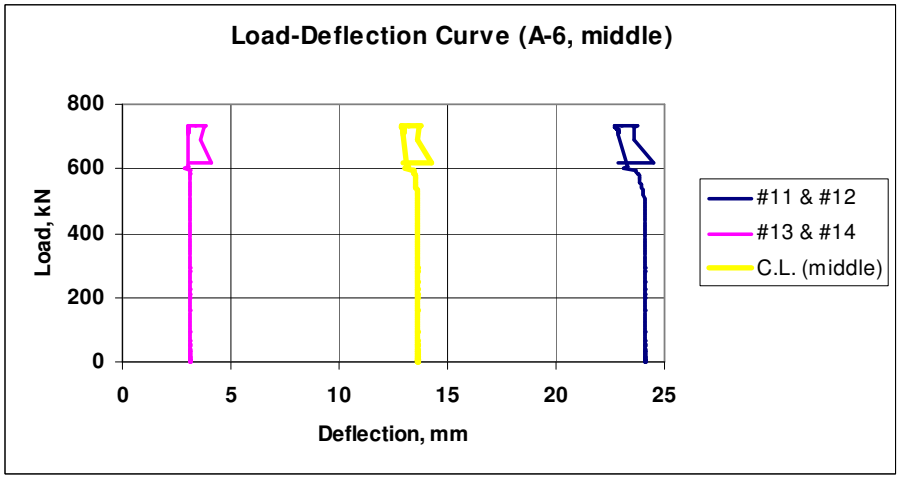

Fig. C.41 Load versus deflection curve (LDS #11 & #12, LDS #13 & #14, middle CL)

1.7 Wall ***A-7***

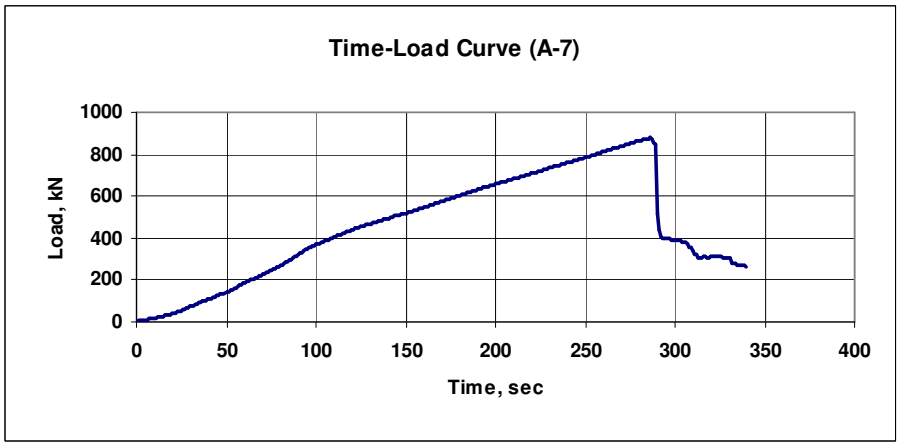

Fig. C.42 Time versus load curve

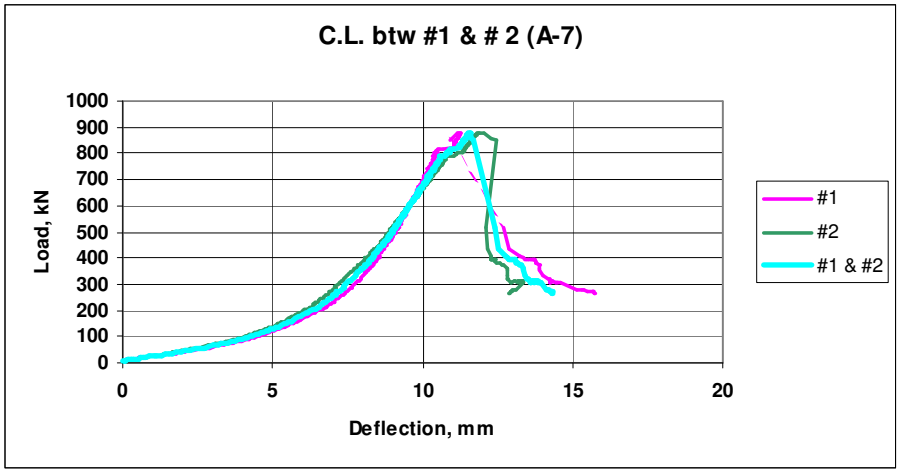

Fig. C.43 Load versus deflection curve (LDS #1, LDS #2 and CL)

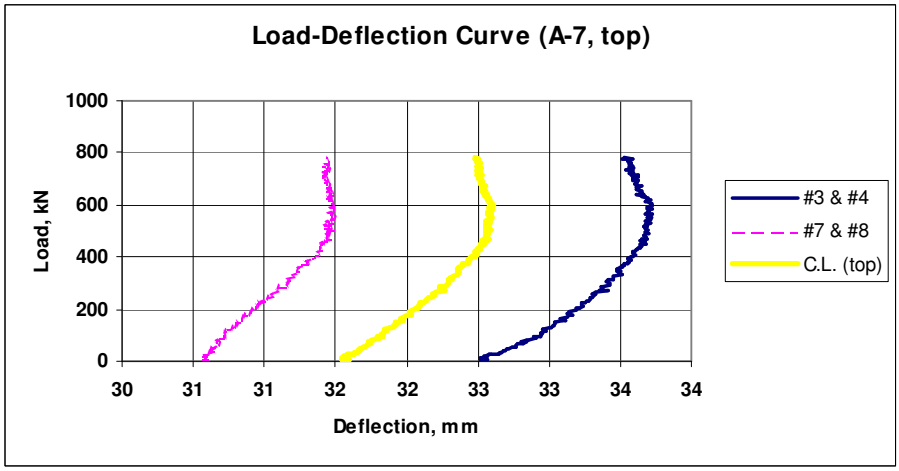

Fig. C.44 Load versus deflection curve (LDS #3 & #4, LDS #7 & #8 and top CL)

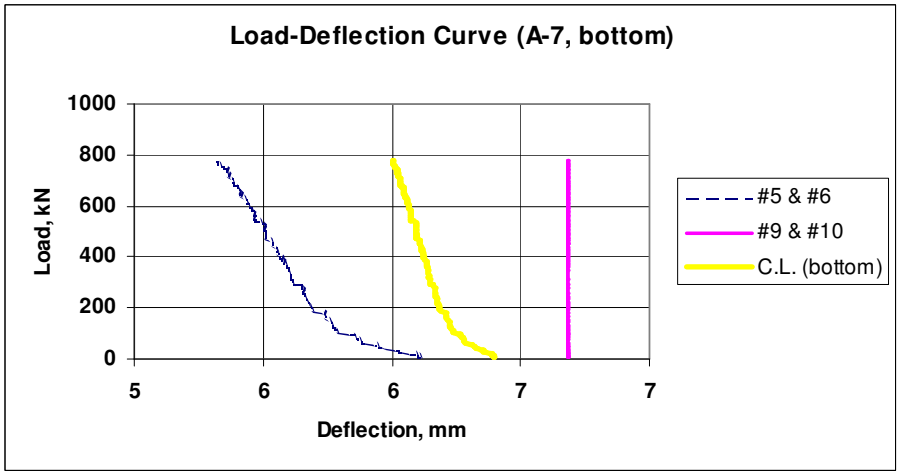

Fig. C.45 Load versus deflection curve (LDS #5 & #6, LDS #9 & #10 and bottom CL)

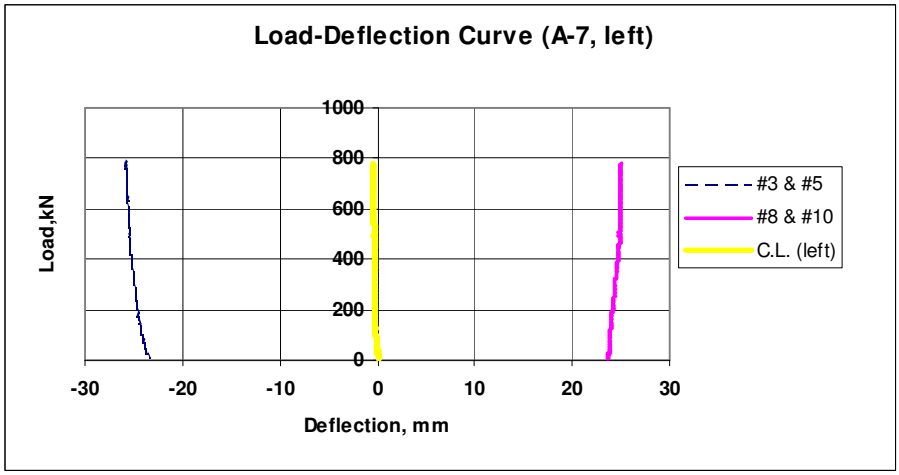

Fig. C.46 Load versus deflection curve (LDS #3 & #5, LDS #8 & #10 and left CL)

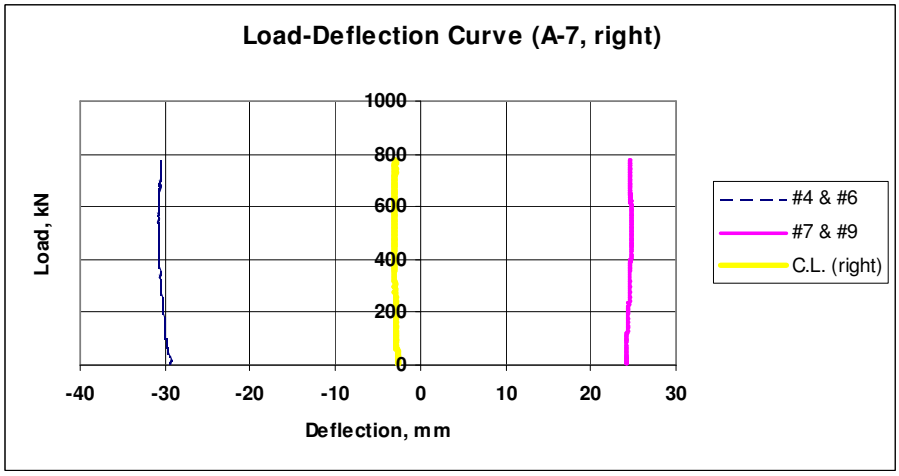

Fig. C.47 Load versus deflection curve (LDS #4 & #6, LDS #7 & #9 and right CL)

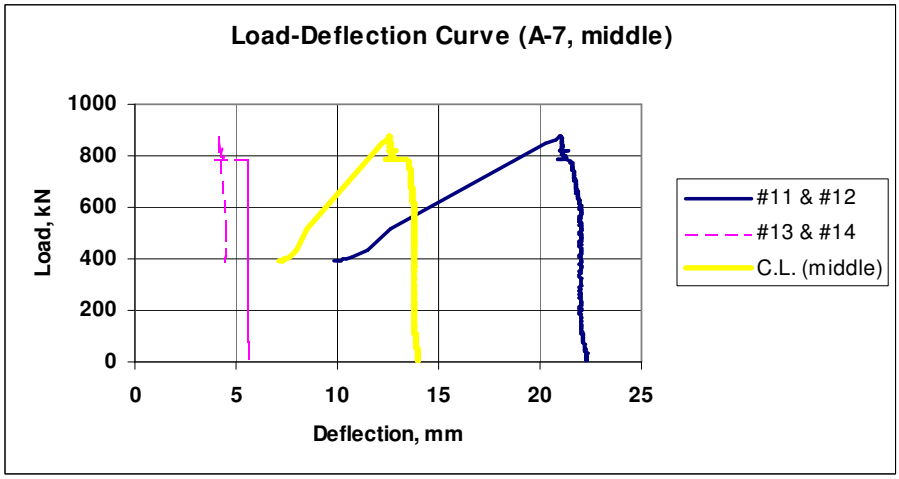

Fig. C.48 Load versus deflection curve (LDS #11 & #12, LDS #13 & #14, middle CL)

1.8 Wall ***A-8***

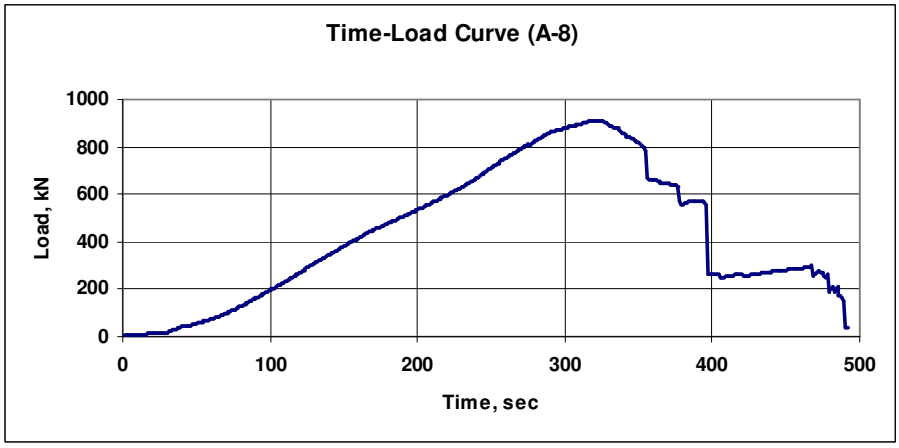

Fig. C.49 Time versus load curve

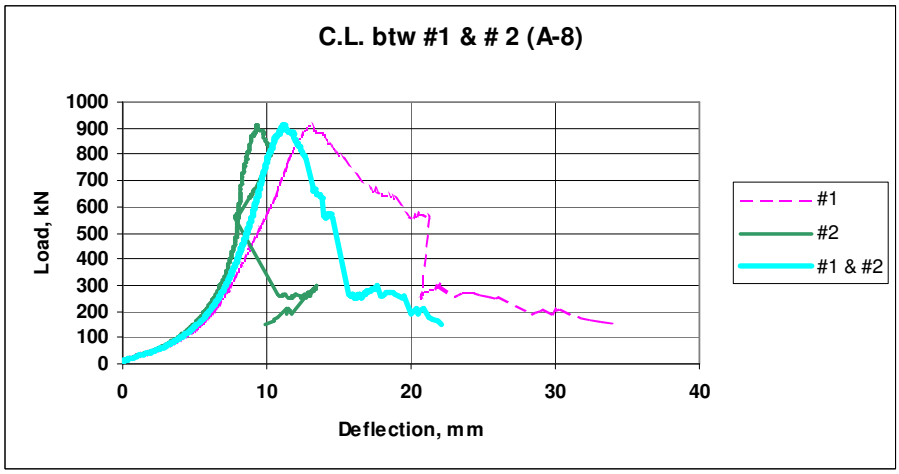

Fig. C.50 Load versus deflection curve (LDS #1, LDS #2 and CL)

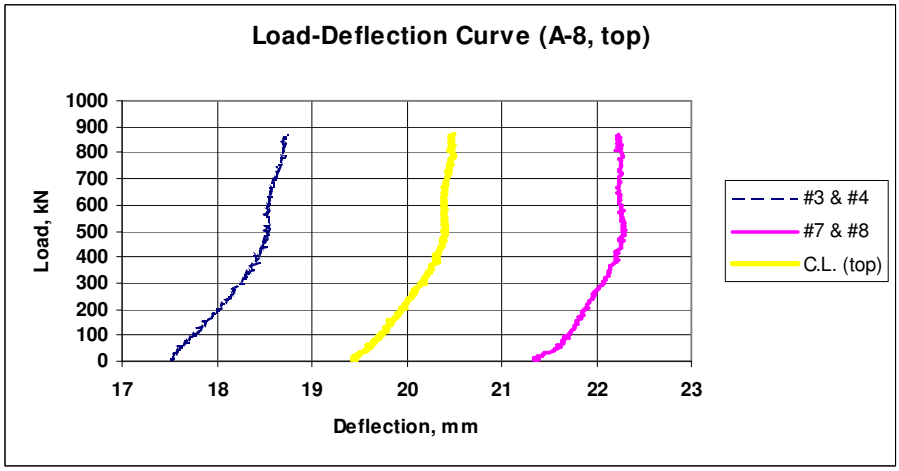

Fig. C.51 Load versus deflection curve (LDS #3 & #4, LDS #7 & #8 and top CL)

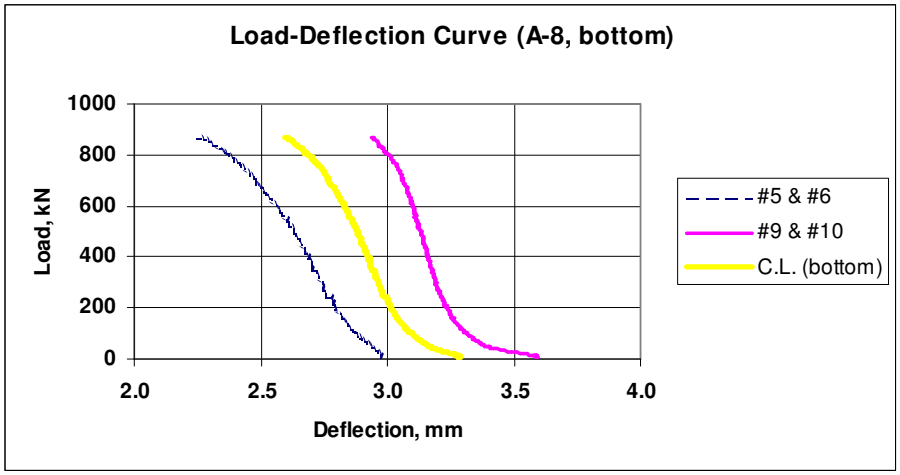

Fig. C.52 Load versus deflection curve (LDS #5 & #6, LDS #9 & #10 and bottom CL)

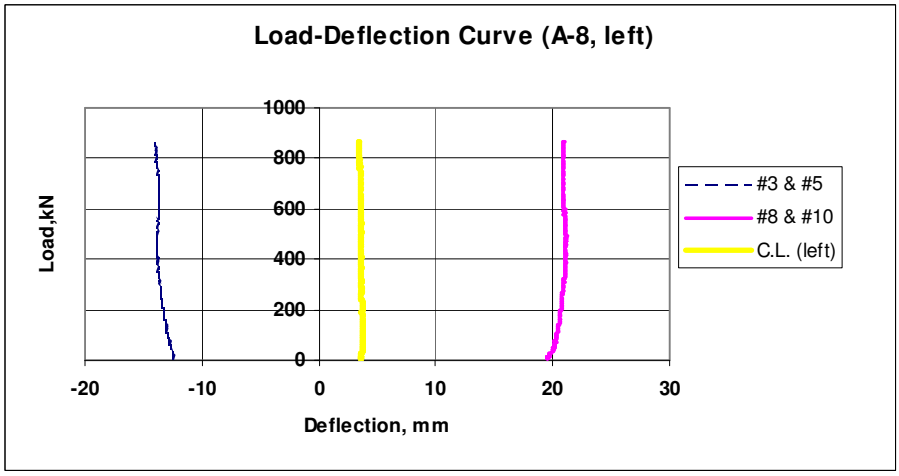

Fig. C.53 Load versus deflection curve (LDS #3 & #5, LDS #8 & #10 and left CL)

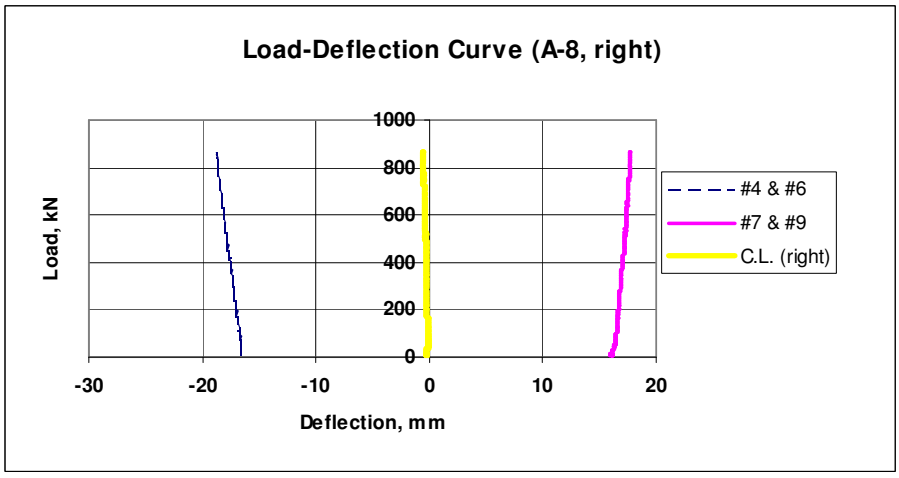

Fig. C.54 Load versus deflection curve (LDS #4 & #6, LDS #7 & #9 and right CL)

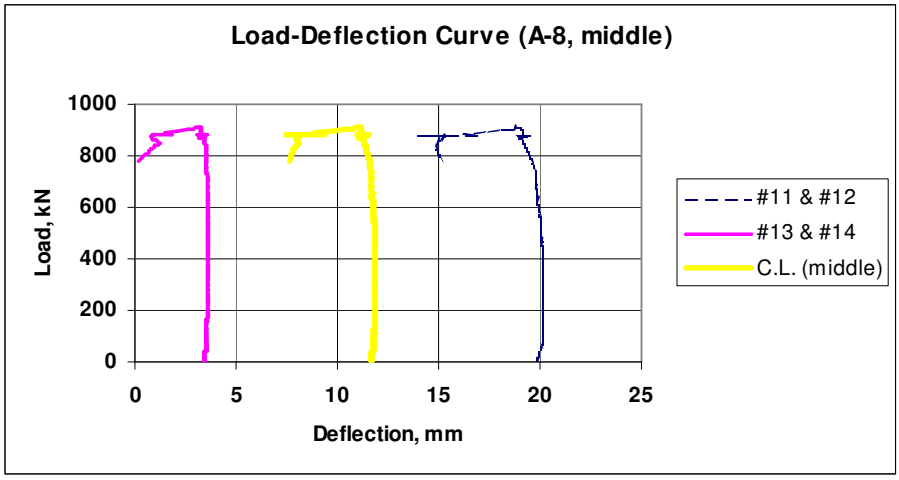

Fig. C.55 Load versus deflection curve (LDS #11 & #12, LDS #13 & #14, middle CL)

1.9 Wall ***A-9***

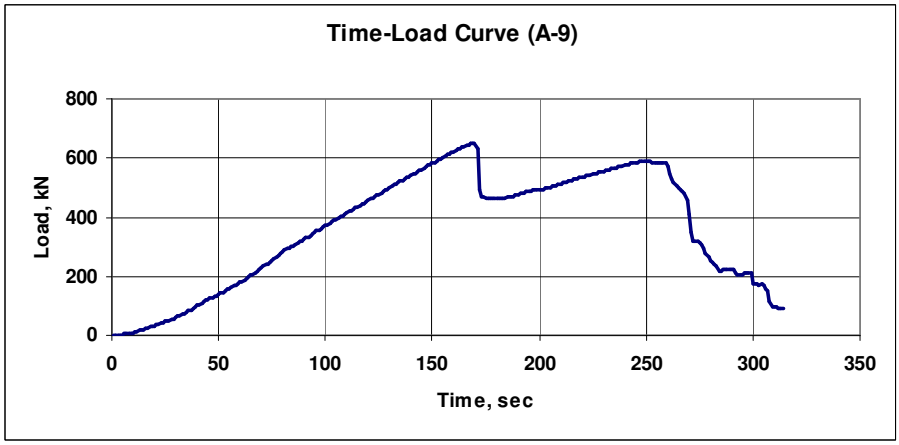

Fig. C.56 Time versus load curve

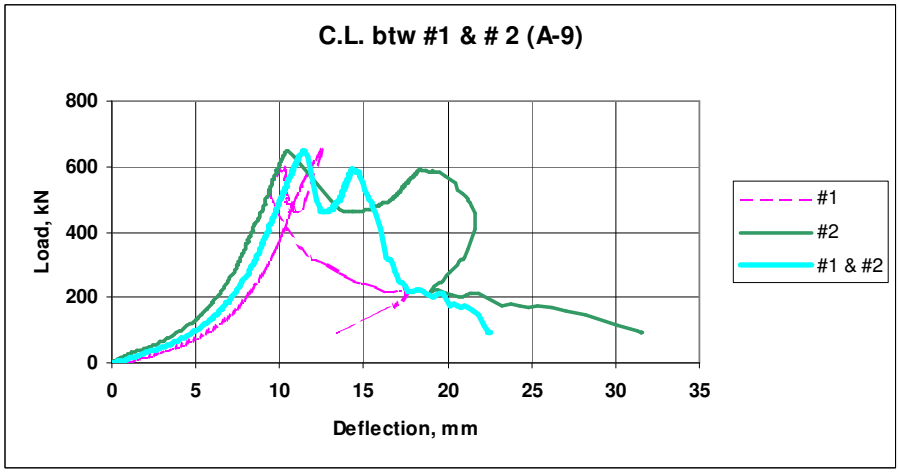

Fig. C.57 Load versus deflection curve (LDS #1, LDS #2 and CL)

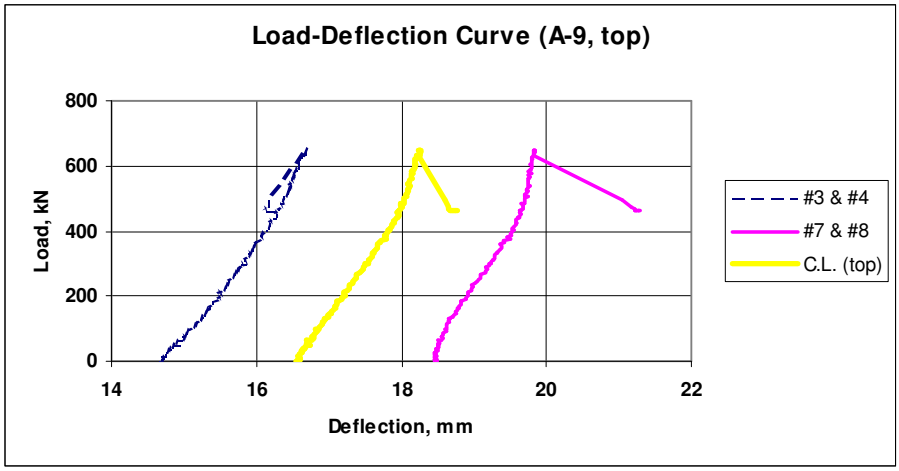

Fig. C.58 Load versus deflection curve (LDS #3 & #4, LDS #7 & #8 and top CL)

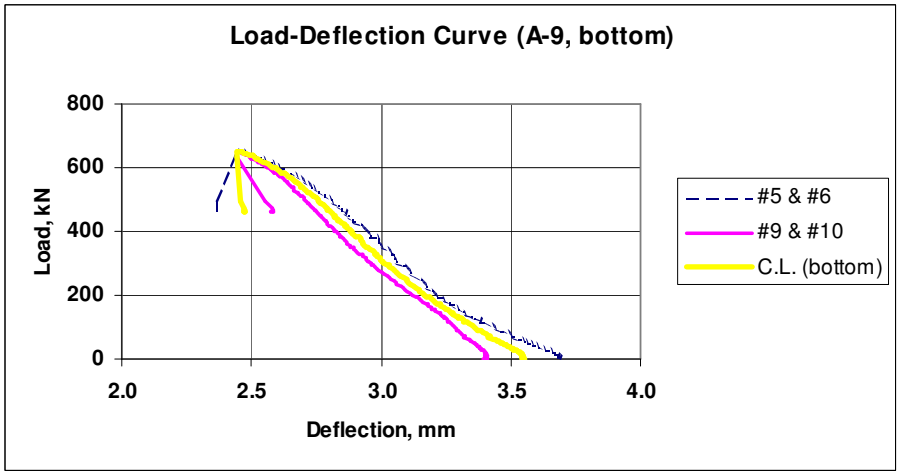

Fig. C.59 Load versus deflection curve (LDS #5 & #6, LDS #9 & #10 and bottom CL)

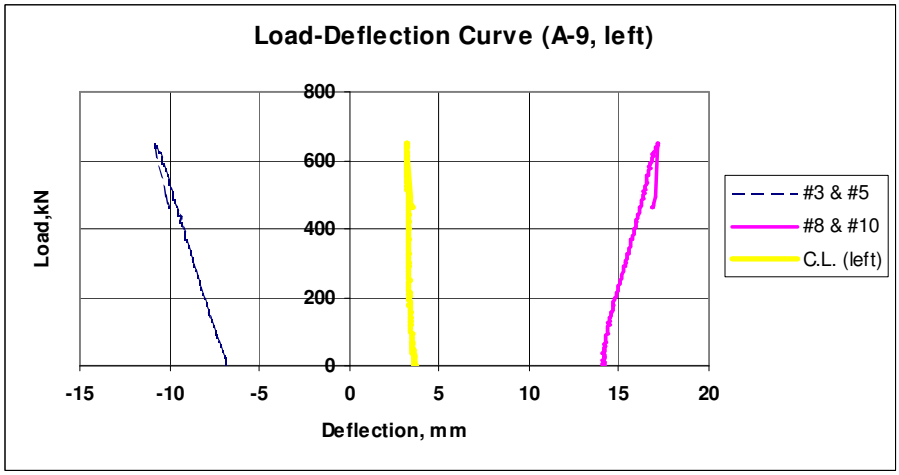

Fig. C.60 Load versus deflection curve (LDS #3 & #5, LDS #8 & #10 and left CL)

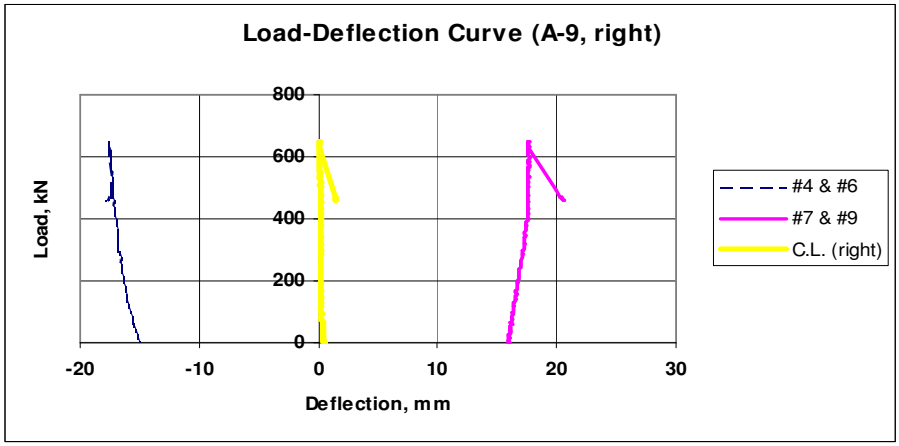

Fig. C.61 Load versus deflection curve (LDS #4 & #6, LDS #7 & #9 and right CL)

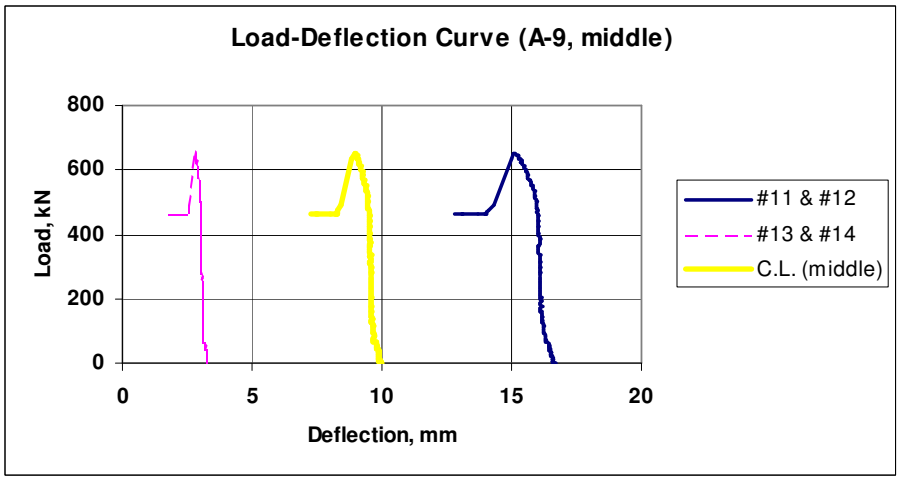

Fig. C.62 Load versus deflection curve (LDS #11 & #12, LDS #13 & #14, middle CL)

1.10 Wall *A-10*

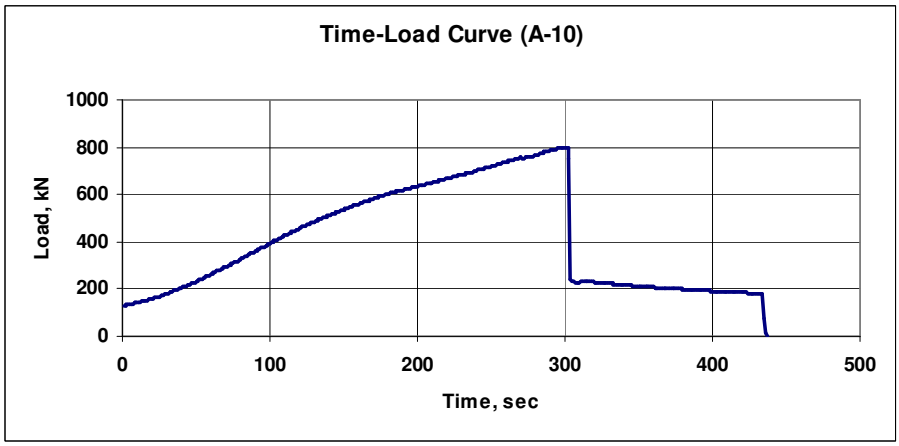

Fig. C.63 Time versus load curve

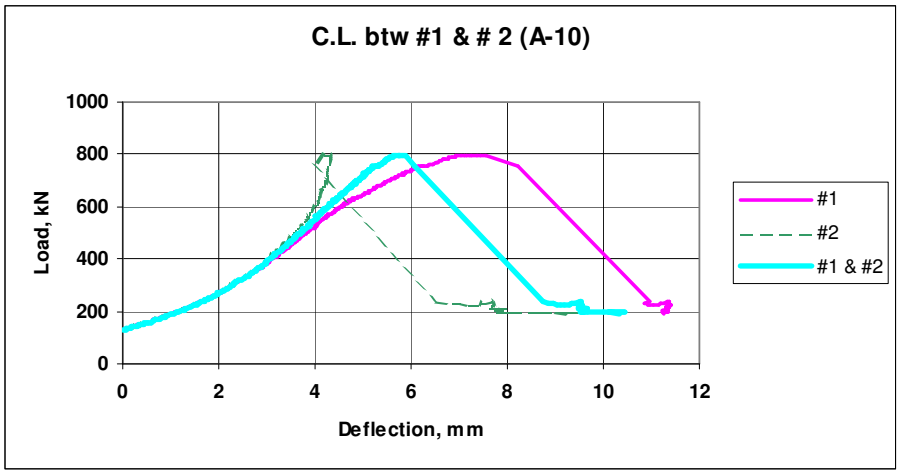

Fig. C.64 Load versus deflection curve (LDS #1, LDS #2 and CL)

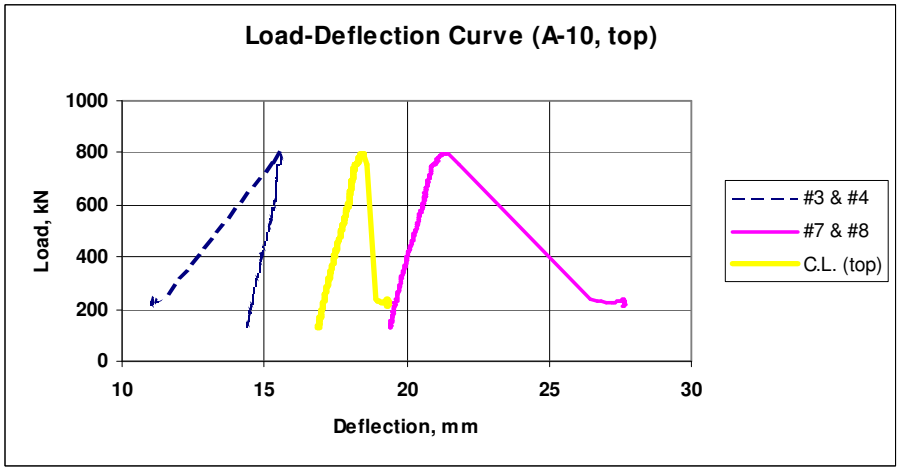

Fig. C.65 Load versus deflection curve (LDS #3 & #4, LDS #7 & #8 and top CL)

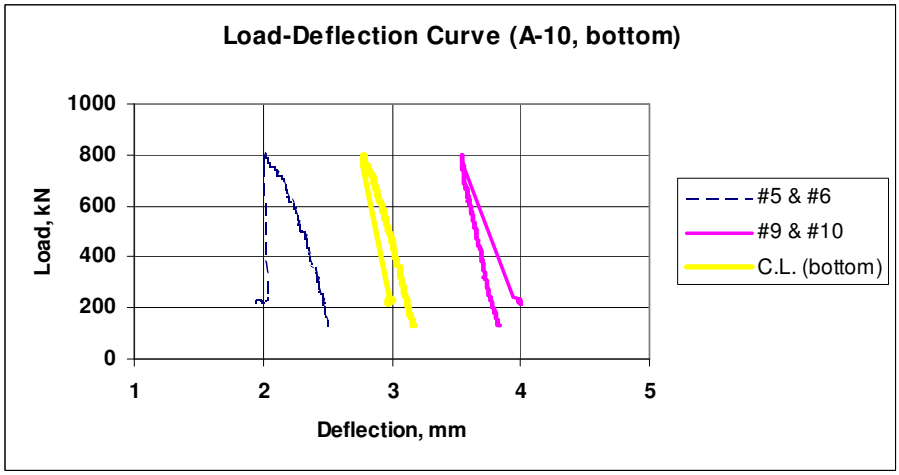

Fig. C.66 Load versus deflection curve (LDS #5 & #6, LDS #9 & #10 and bottom CL)

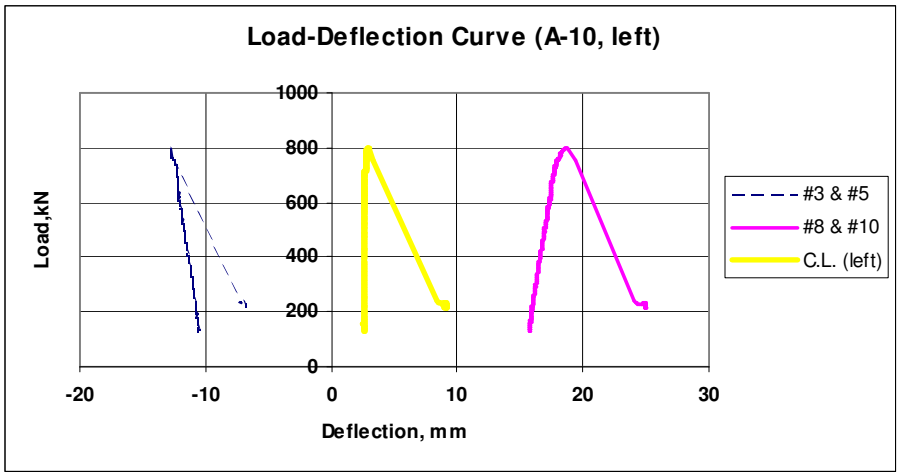

Fig. C.67 Load versus deflection curve (LDS #3 & #5, LDS #8 & #10 and left CL)

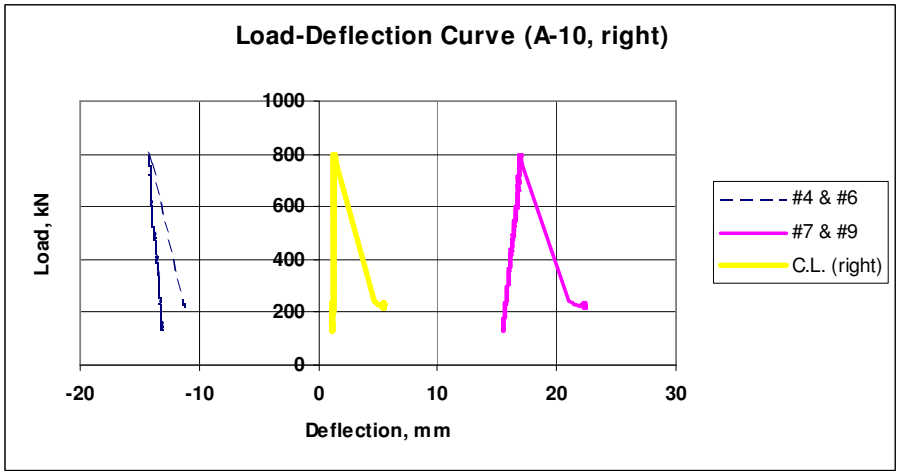

Fig. C.68 Load versus deflection curve (LDS #4 & #6, LDS #7 & #9 and right CL)

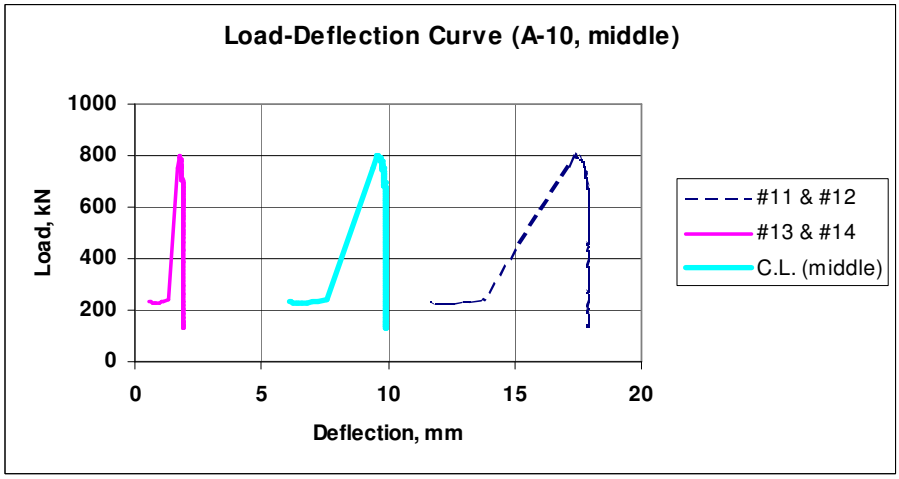

Fig. C.69 Load versus deflection curve (LDS #11 & #12, LDS #13 & #14, middle CL)

2. Test results for wall specimens type *B*

2.1 Wall *B-1*

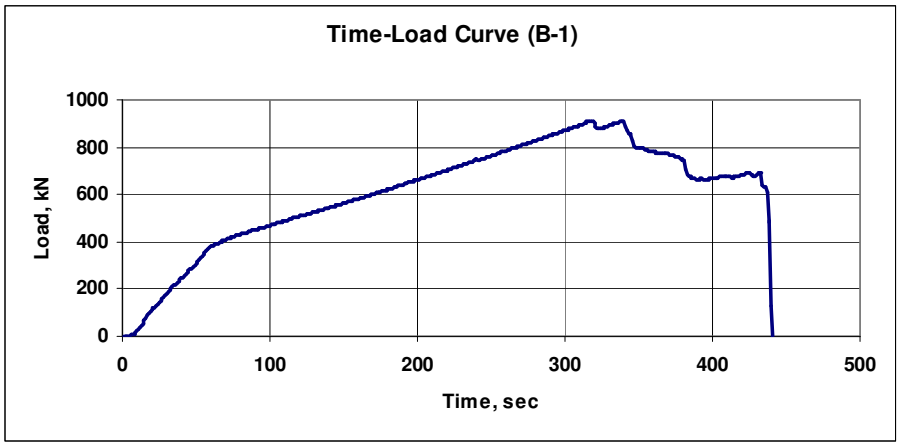

Fig. C.70 Time versus load curve

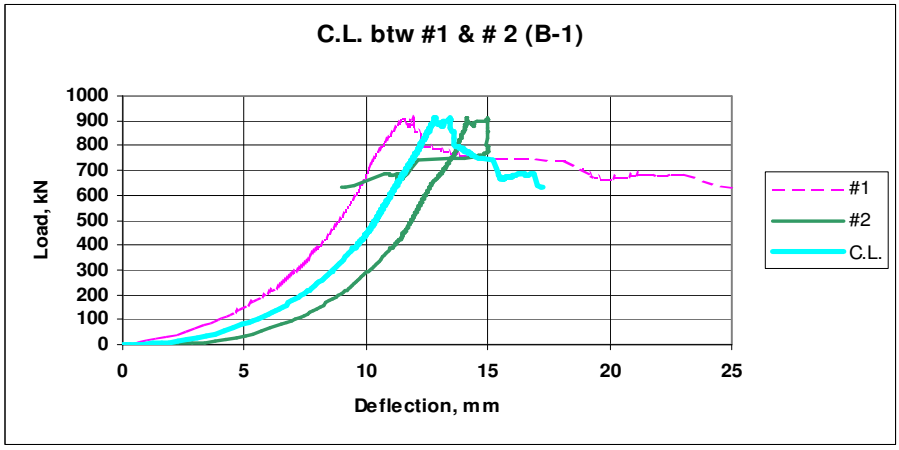

Fig. C.71 Load versus deflection curve (LDS #1, LDS #2 and CL)

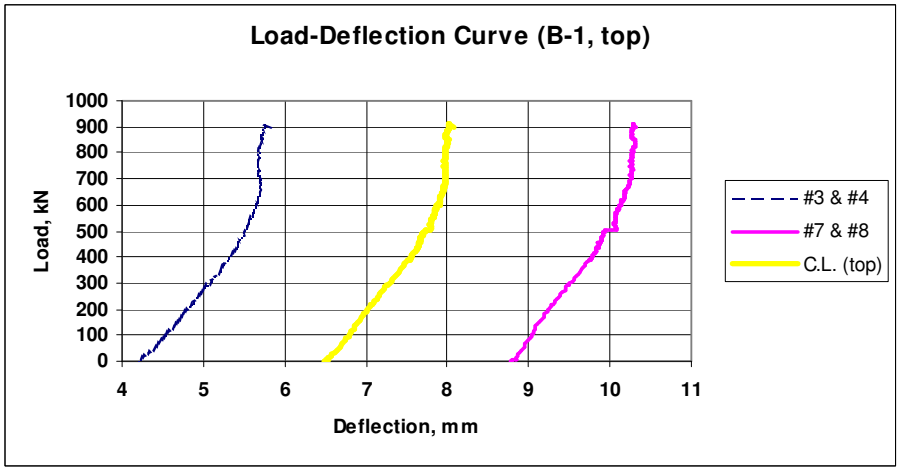

Fig. C.72 Load versus deflection curve (LDS #3 & #4, LDS #7 & #8 and top CL)

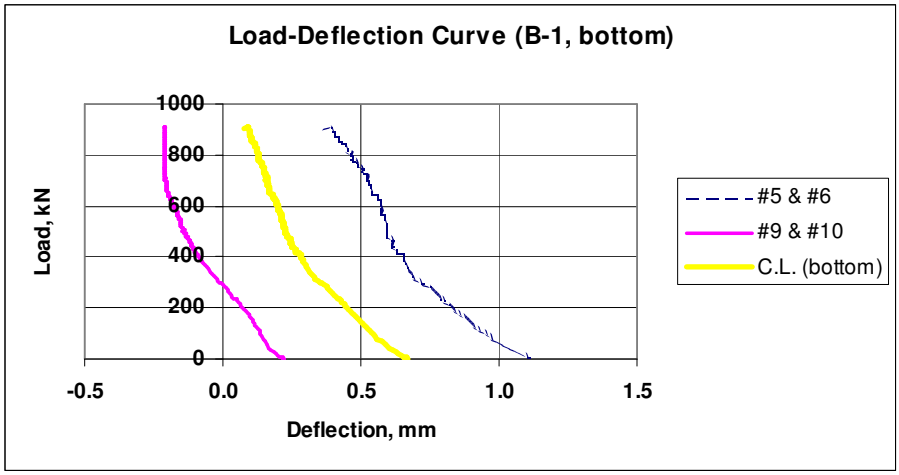

Fig. C.73 Load versus deflection curve (LDS #5 & #6, LDS #9 & #10 and bottom CL)

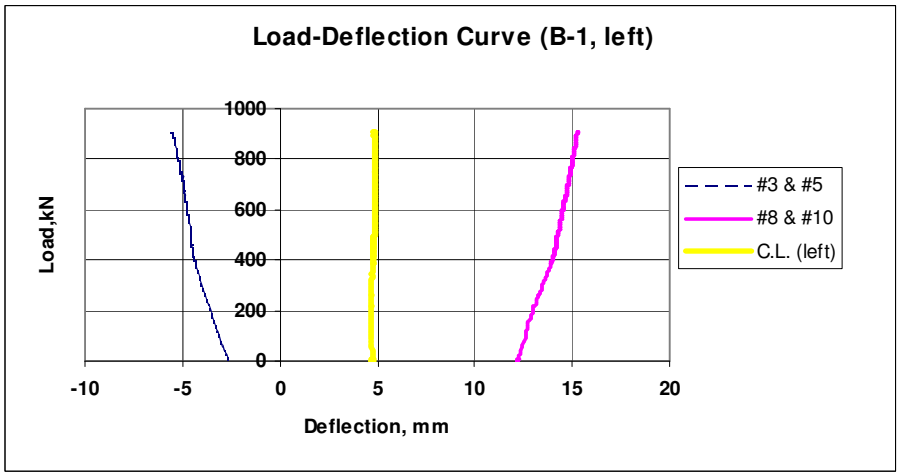

Fig. C.74 Load versus deflection curve (LDS #3 & #5, LDS #8 & #10 and left CL)

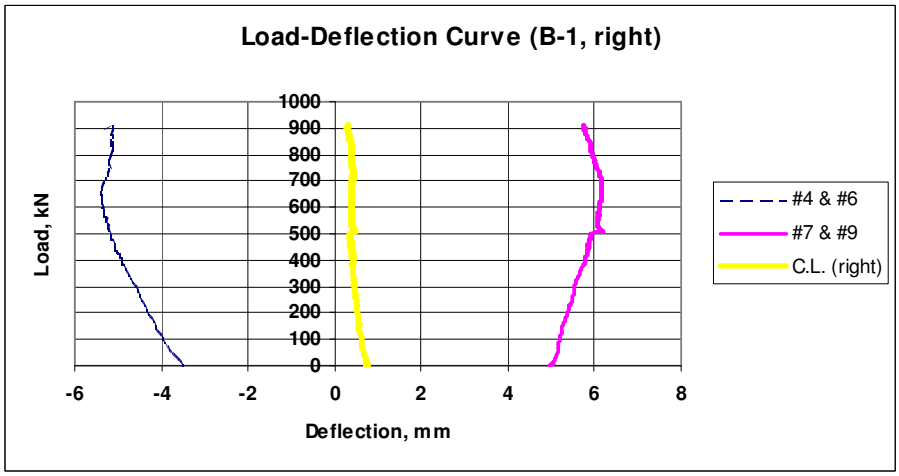

Fig. C.75 Load versus deflection curve (LDS #4 & #6, LDS #7 & #9 and right CL)

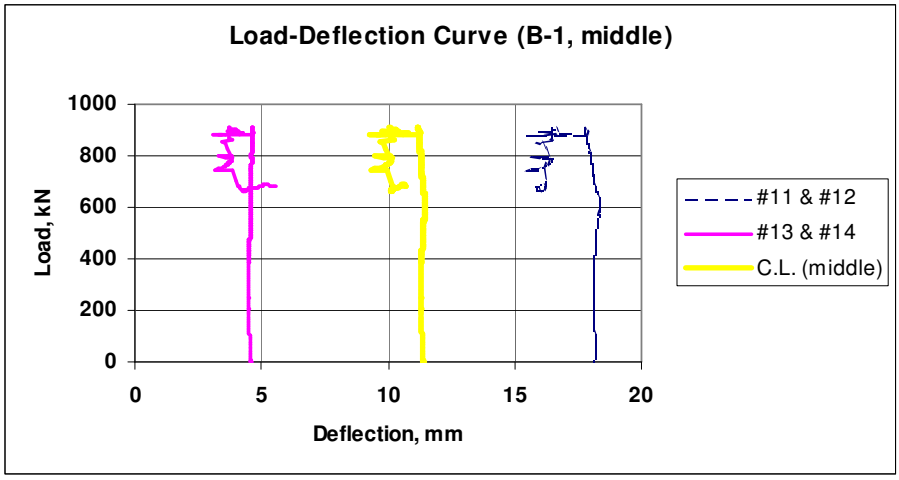

Fig. C.76 Load versus deflection curve (LDS #11 & #12, LDS #13 & #14, middle CL)

2.2 Wall ***B-2***

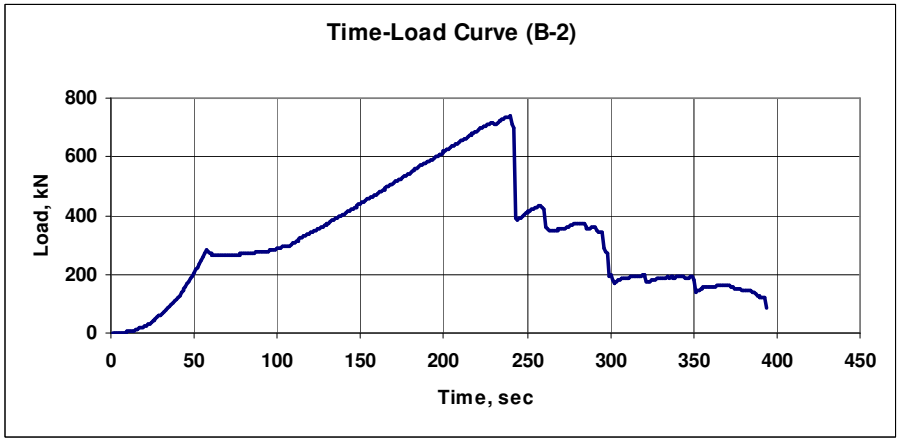

Fig. C.77 Time versus load curve

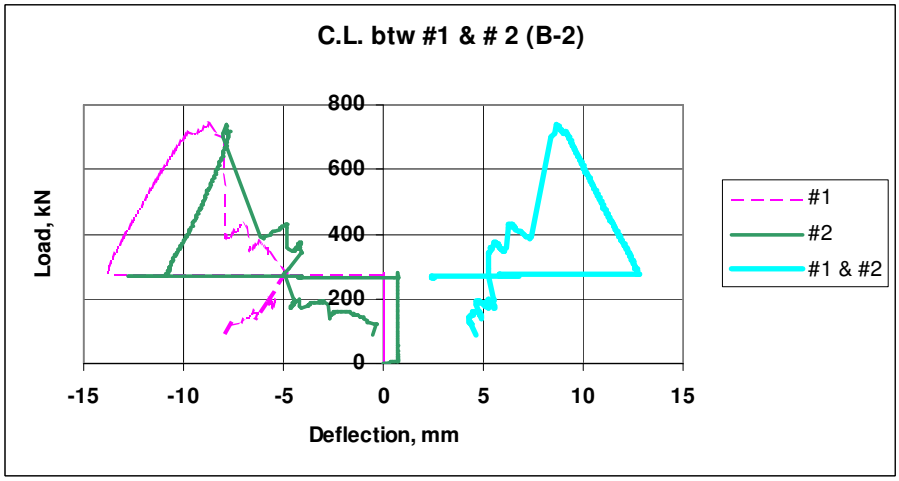

Fig. C.78 Load versus deflection curve (LDS #1, LDS #2 and CL)

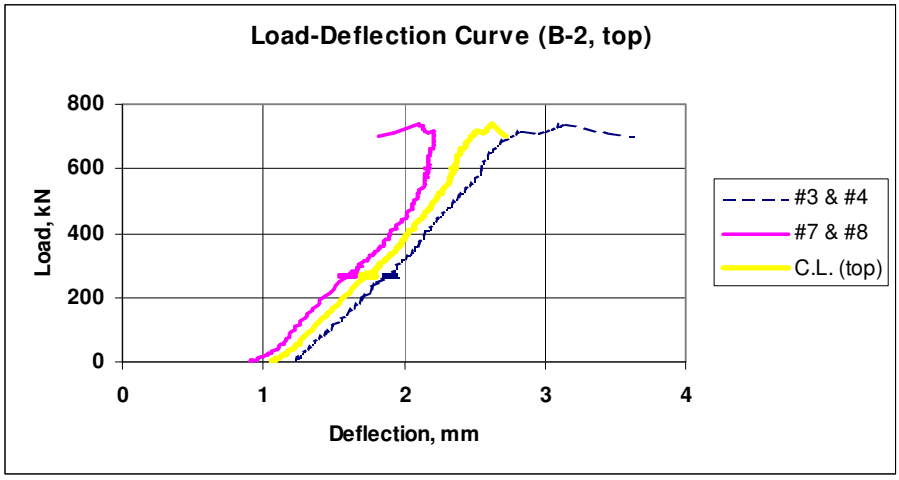

Fig. C.79 Load versus deflection curve (LDS #3 & #4, LDS #7 & #8 and top CL)

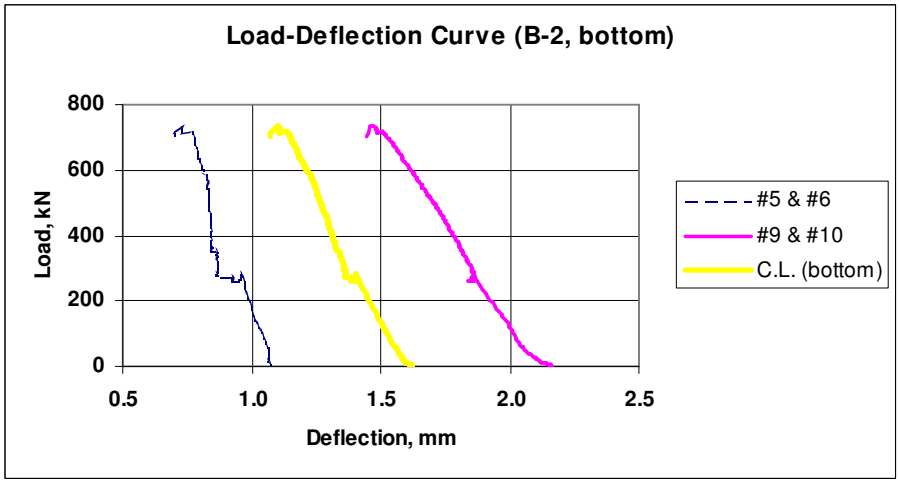

Fig. C.80 Load versus deflection curve (LDS #5 & #6, LDS #9 & #10 and bottom CL)

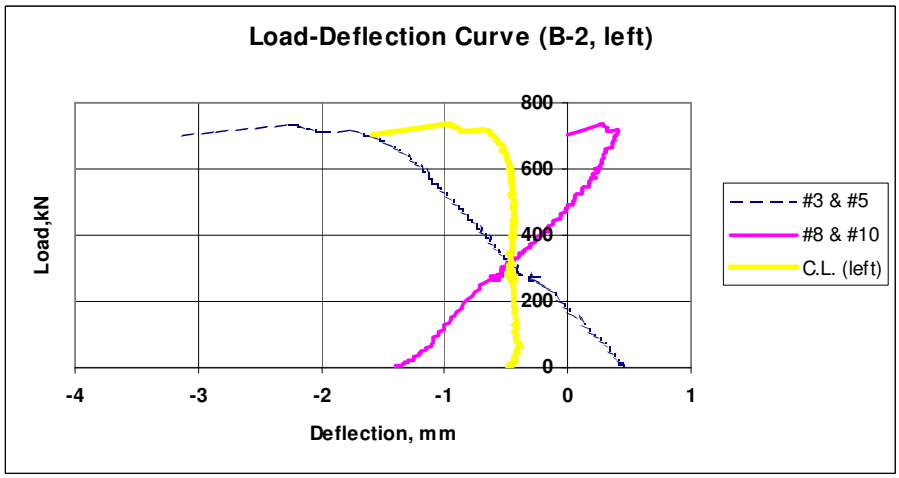

Fig. C.81 Load versus deflection curve (LDS #3 & #5, LDS #8 & #10 and left CL)

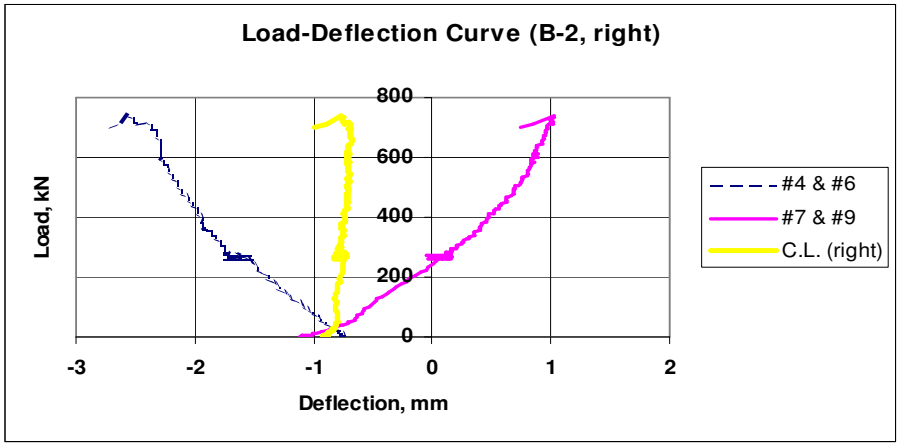

Fig. C.82 Load versus deflection curve (LDS #4 & #6, LDS #7 & #9 and right CL)

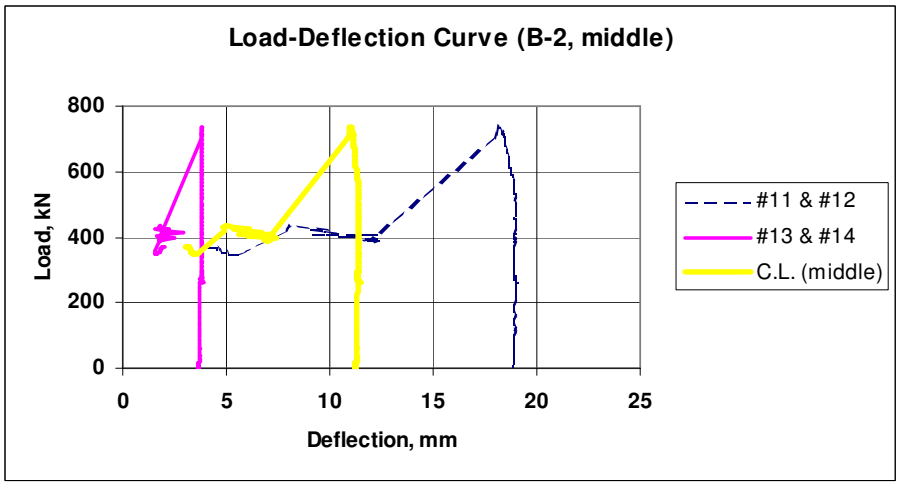

Fig. C.83 Load versus deflection curve (LDS #11 & #12, LDS #13 & #14, middle CL)

2.3 Wall ***B-3***

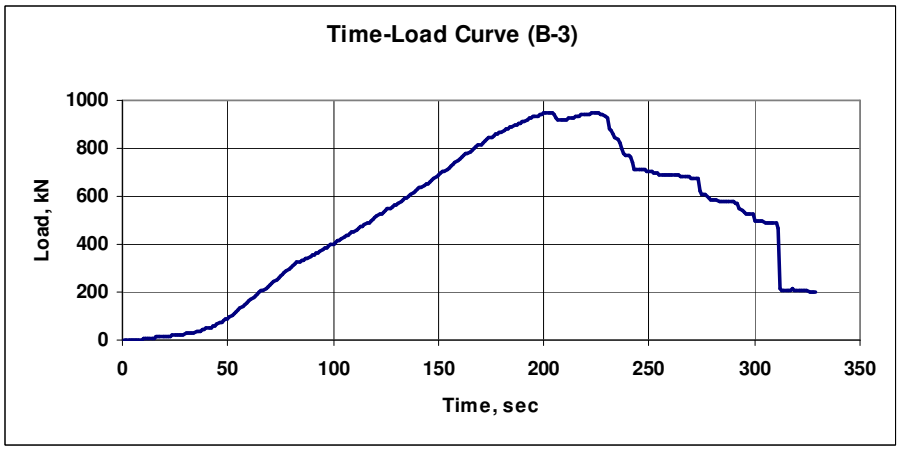

Fig. C.84 Time versus load curve

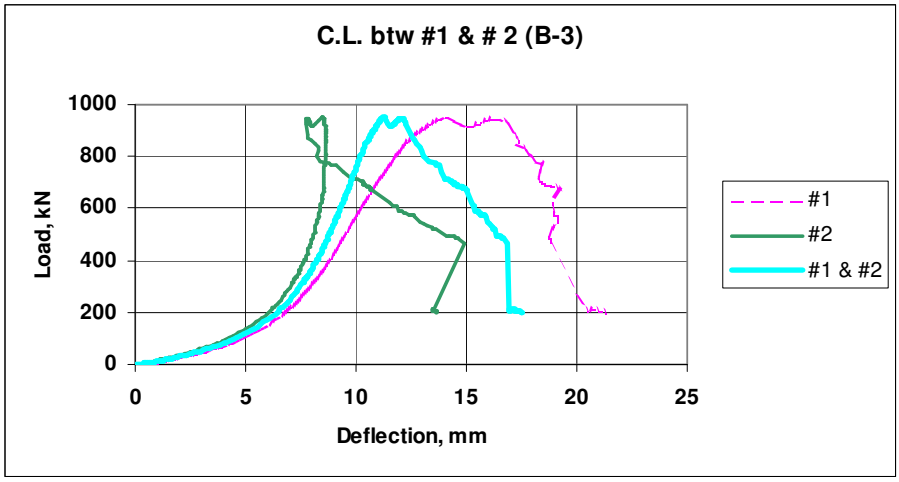

Fig. C.85 Load versus deflection curve (LDS #1, LDS #2 and CL)

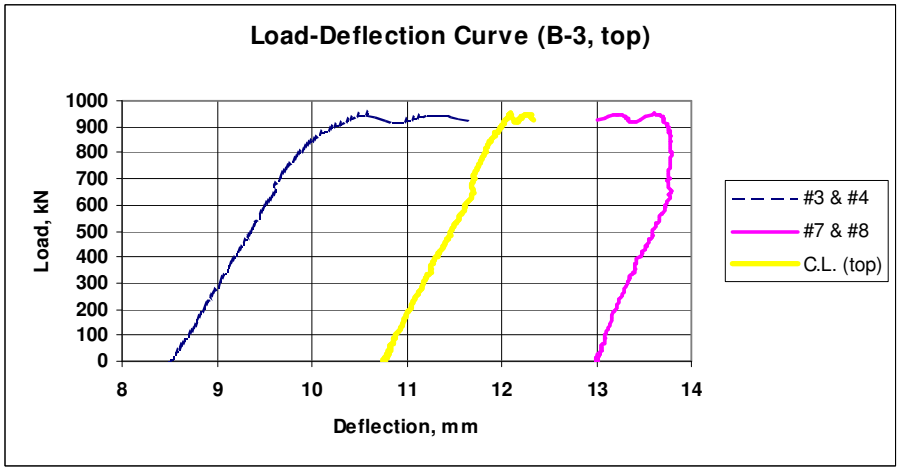

Fig. C.86 Load versus deflection curve (LDS #3 & #4, LDS #7 & #8 and top CL)

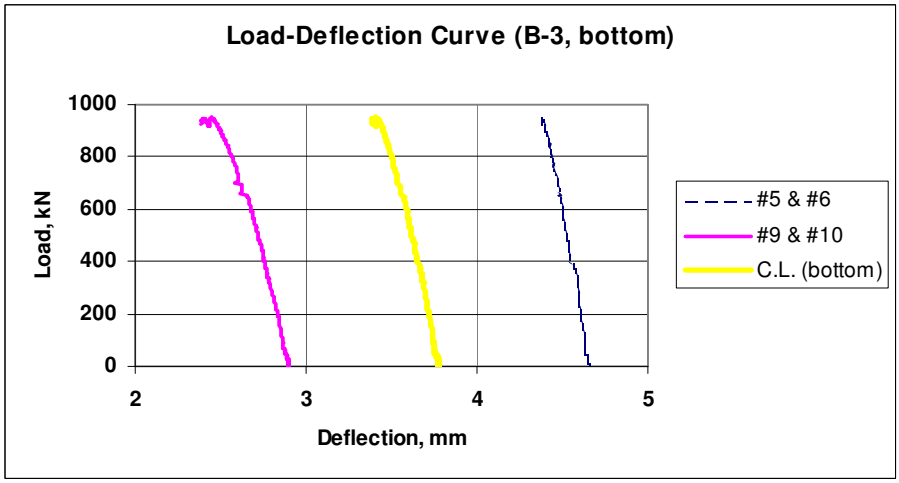

Fig. C.87 Load versus deflection curve (LDS #5 & #6, LDS #9 & #10 and bottom CL)

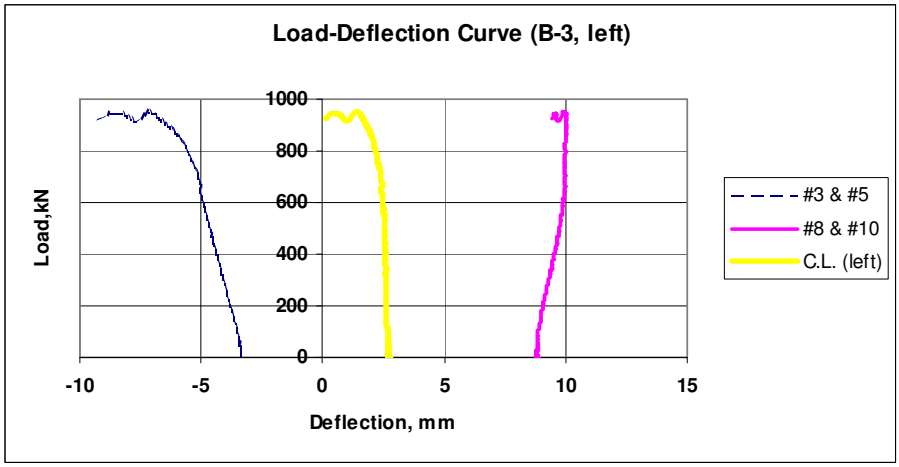

Fig. C.88 Load versus deflection curve (LDS #3 & #5, LDS #8 & #10 and left CL)

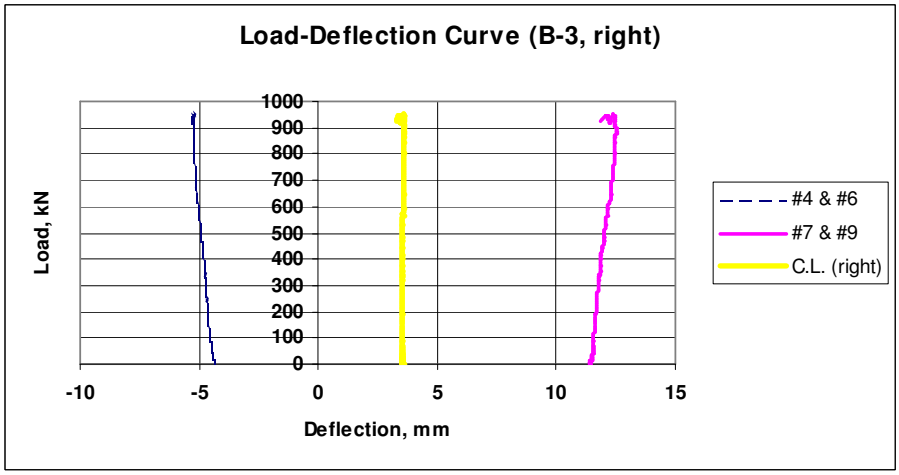

Fig. C.89 Load versus deflection curve (LDS #4 & #6, LDS #7 & #9 and right CL)

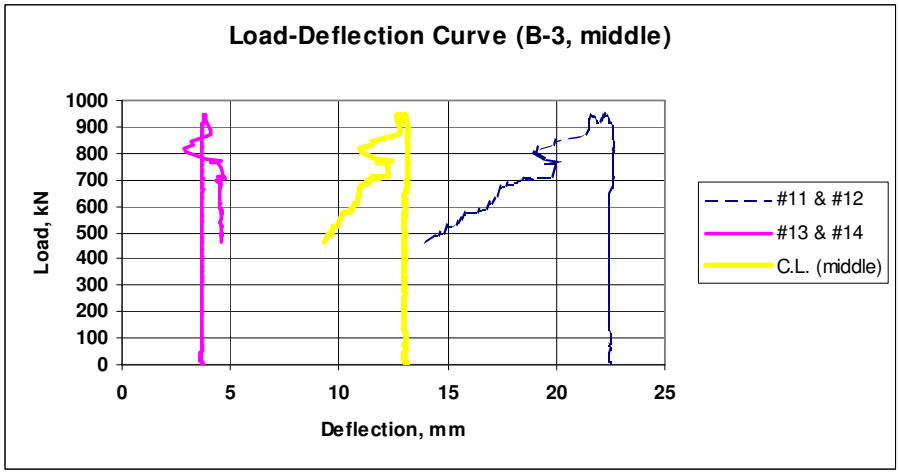

Fig. C.90 Load versus deflection curve (LDS #11 & #12, LDS #13 & #14, middle CL)

2.4 Wall ***B-4***

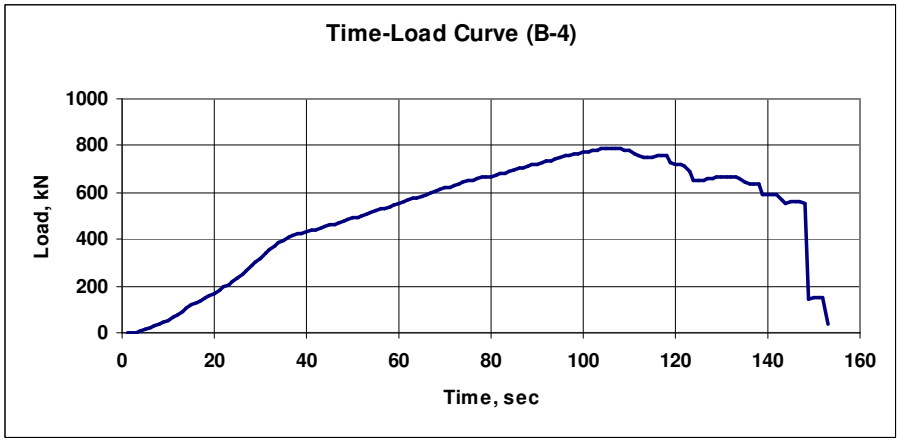

Fig. C.91 Time versus load curve

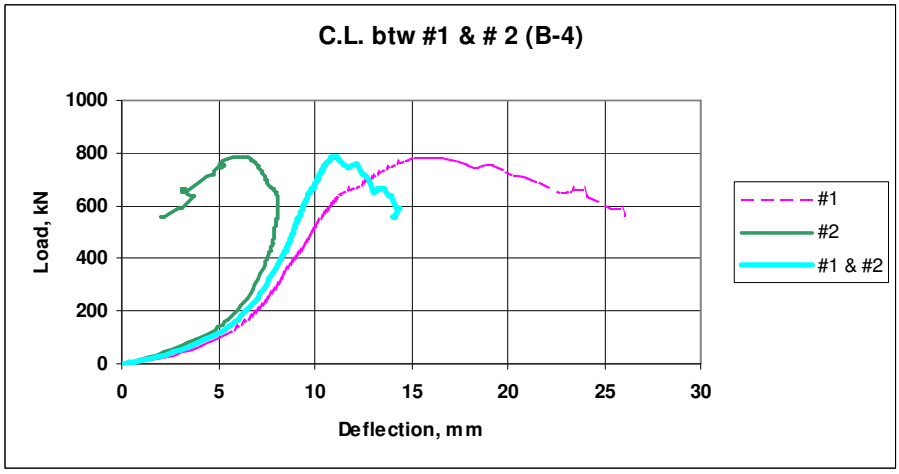

Fig. C.92 Load versus deflection curve (LDS #1, LDS #2 and CL)

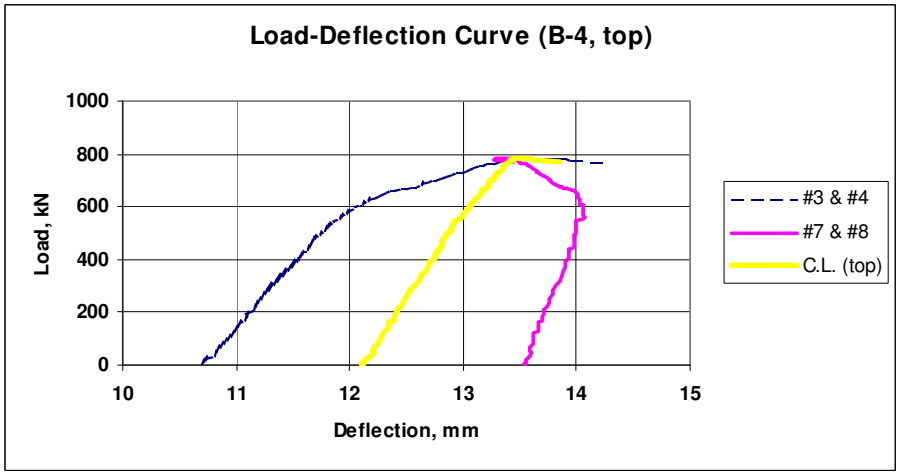

Fig. C.93 Load versus deflection curve (LDS #3 & #4, LDS #7 & #8 and top CL)

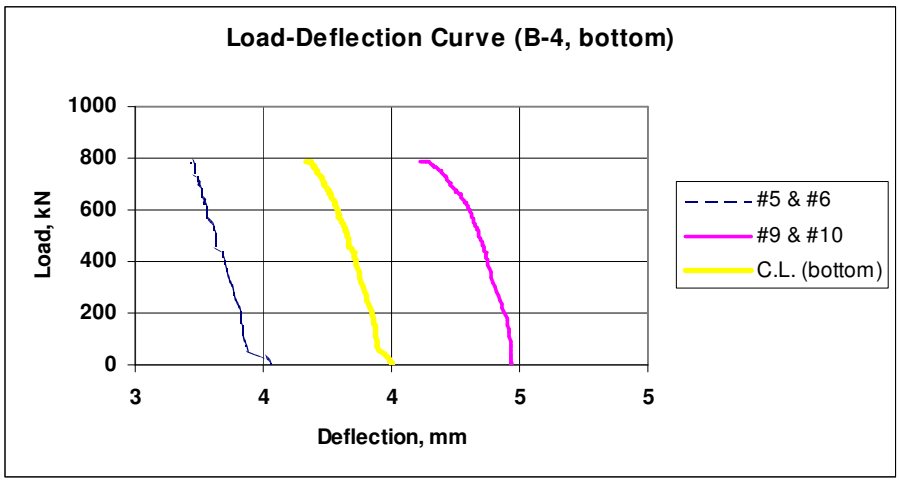

Fig. C.94 Load versus deflection curve (LDS #5 & #6, LDS #9 & #10 and bottom CL)

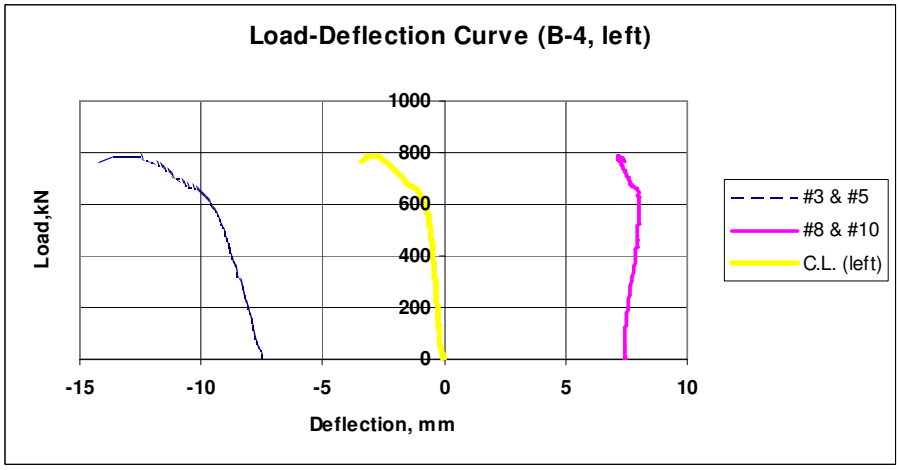

Fig. C.95 Load versus deflection curve (LDS #3 & #5, LDS #8 & #10 and left CL)

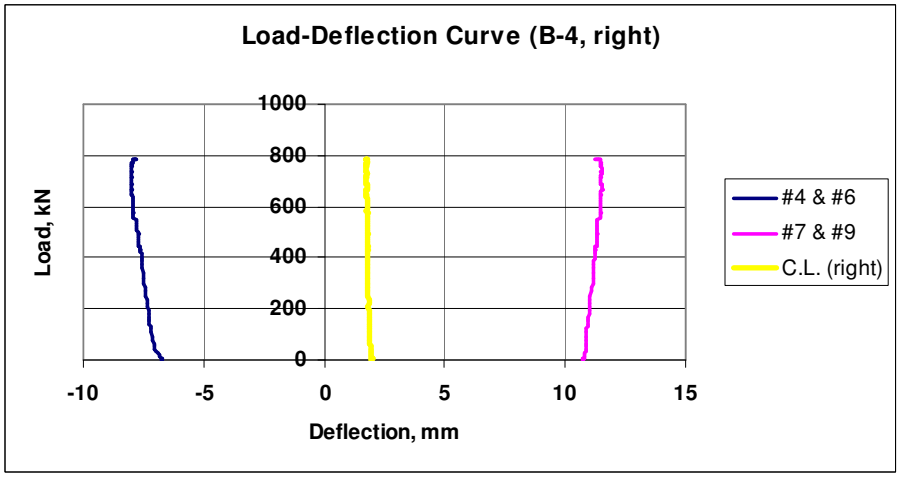

Fig. C.96 Load versus deflection curve (LDS #4 & #6, LDS #7 & #9 and right CL)

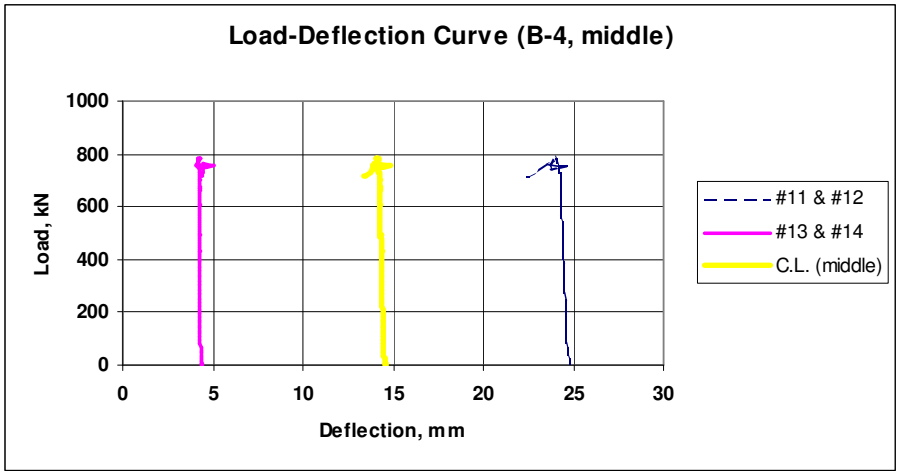

Fig. C.97 Load versus deflection curve (LDS #11 & #12, LDS #13 & #14, middle CL)

2.5 Wall ***B-5***

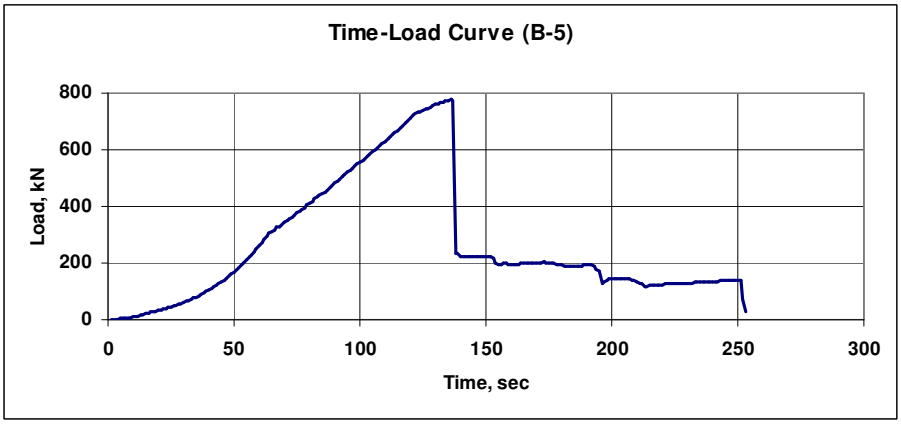

Fig. C.98 Time versus load curve

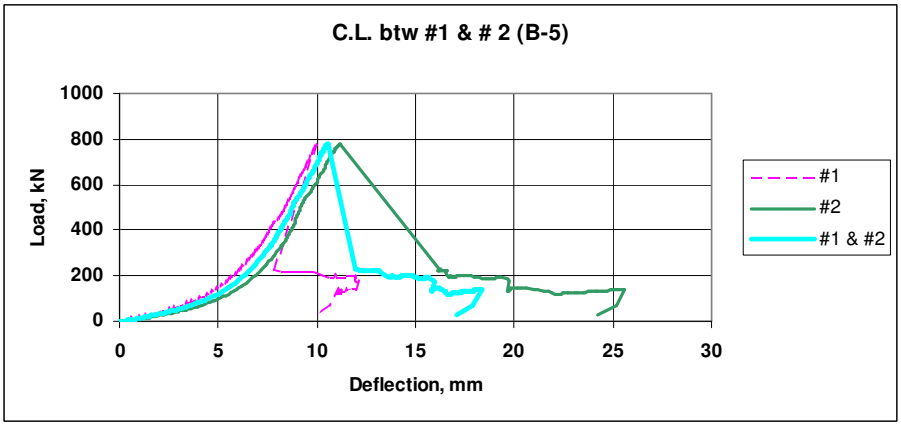

Fig. C.99 Load versus deflection curve (LDS #1, LDS #2 and CL)

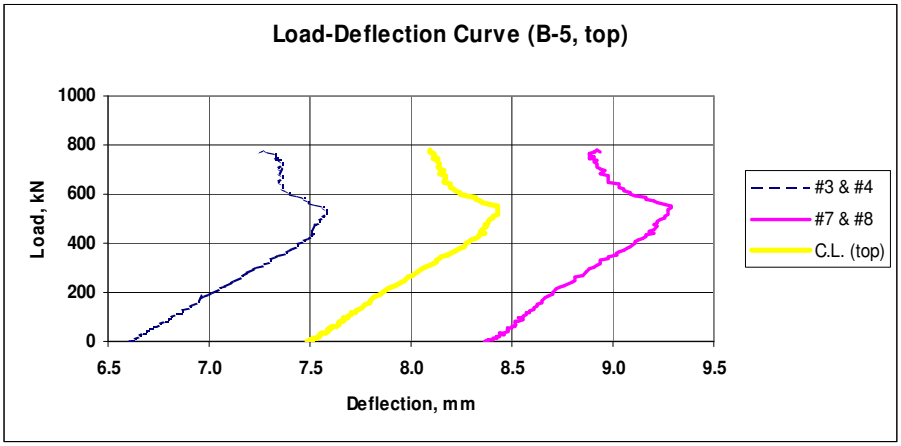

Fig. C.100 Load versus deflection curve (LDS #3 & #4, LDS #7 & #8 and top CL)

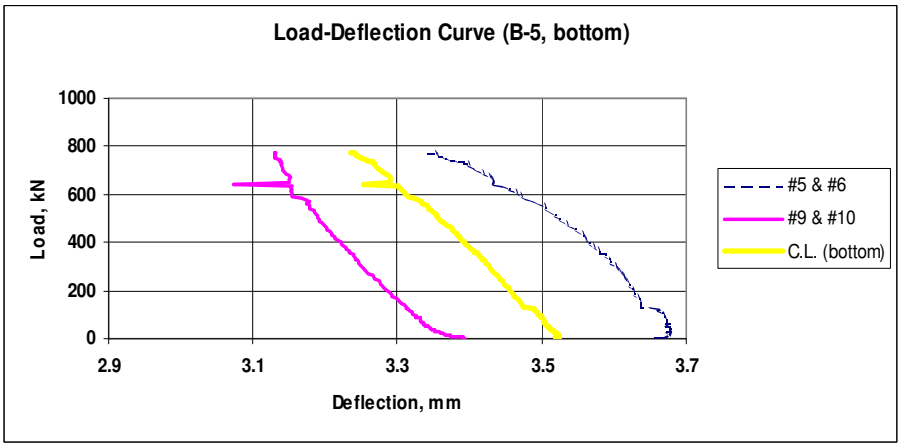

Fig. C.101 Load versus deflection curve (LDS #5 & #6, LDS #9 & #10 and bottom CL)

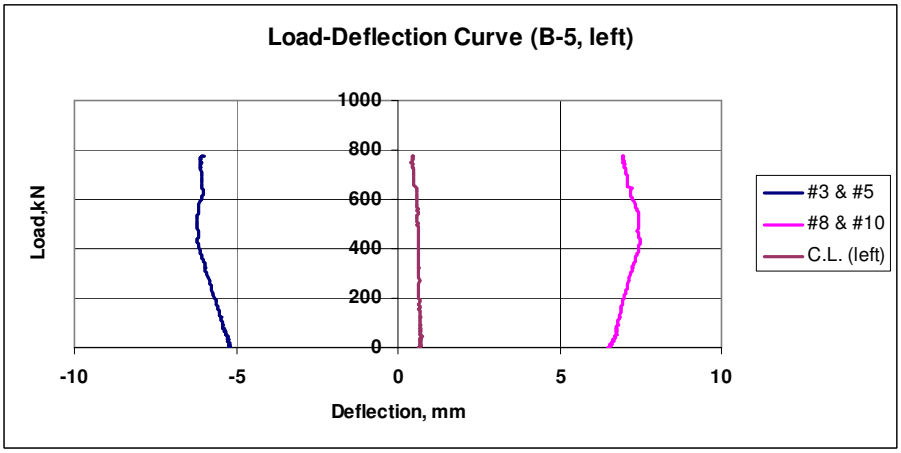

Fig. C.102 Load versus deflection curve (LDS #3 & #5, LDS #8 & #10 and left CL)

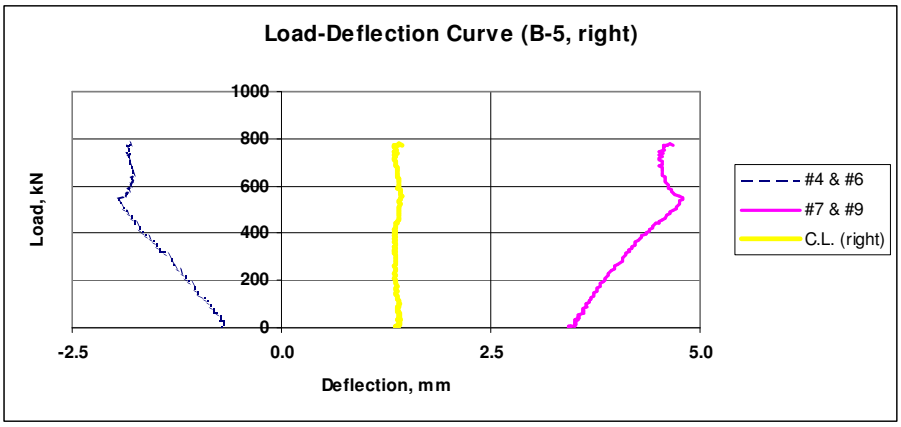

Fig. C.103 Load versus deflection curve (LDS #4 & #6, LDS #7 & #9 and right CL)

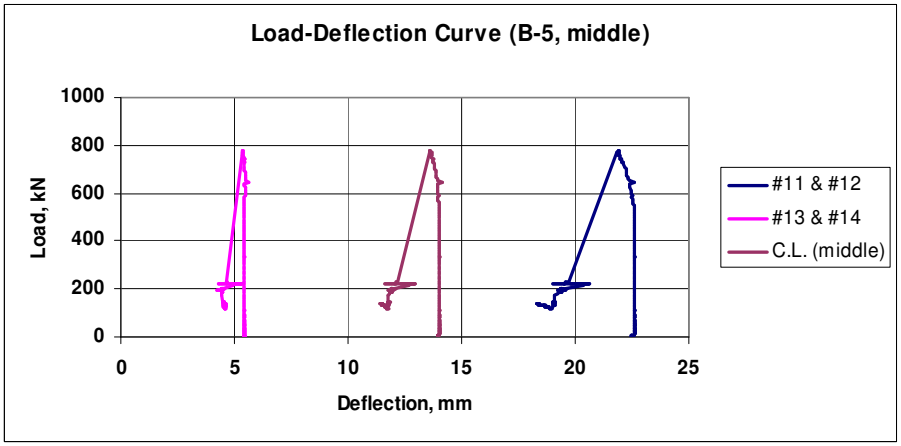

Fig. C.104 Load versus deflection curve (LDS #11 & #12, LDS #13 & #14, middle CL)

2.6 Wall ***B-6***

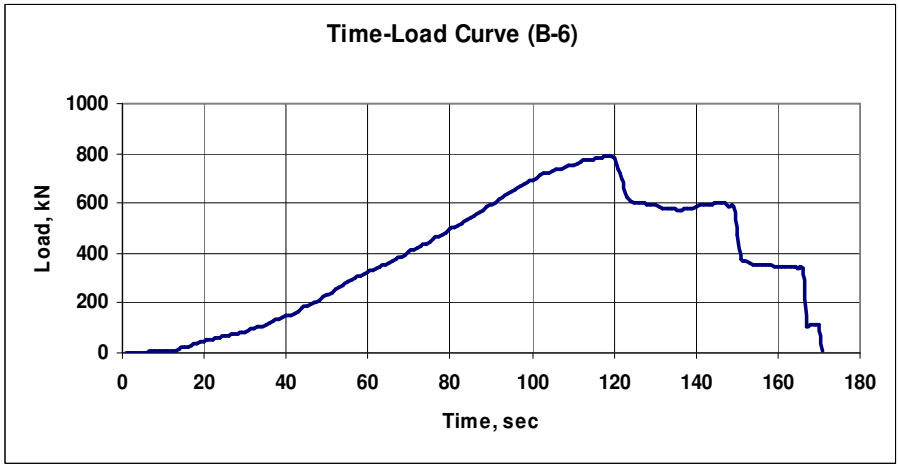

Fig. C.105 Time versus load curve

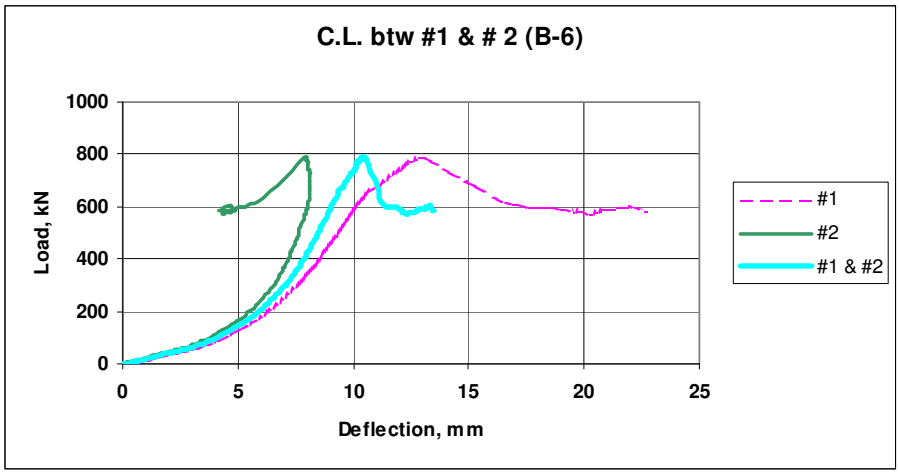

Fig. C.106 Load versus deflection curve (LDS #1, LDS #2 and CL)

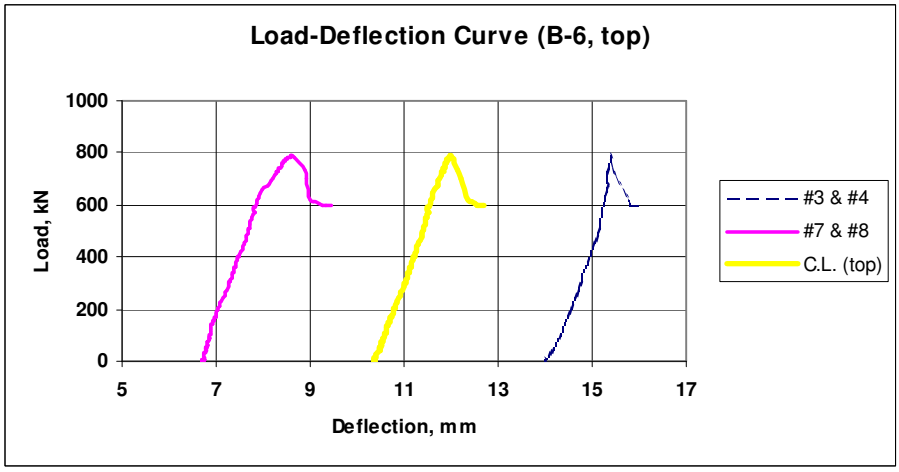

Fig. C.107 Load versus deflection curve (LDS #3 & #4, LDS #7 & #8 and top CL)

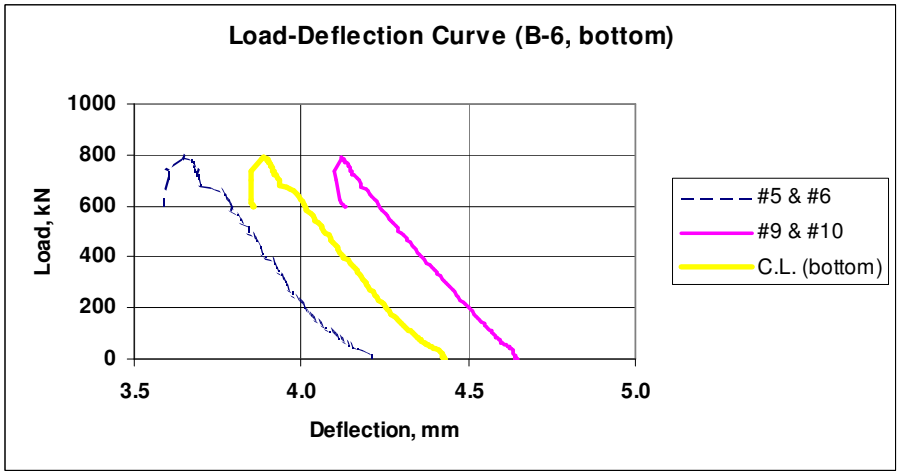

Fig. C.108 Load versus deflection curve (LDS #5 & #6, LDS #9 & #10 and bottom CL)

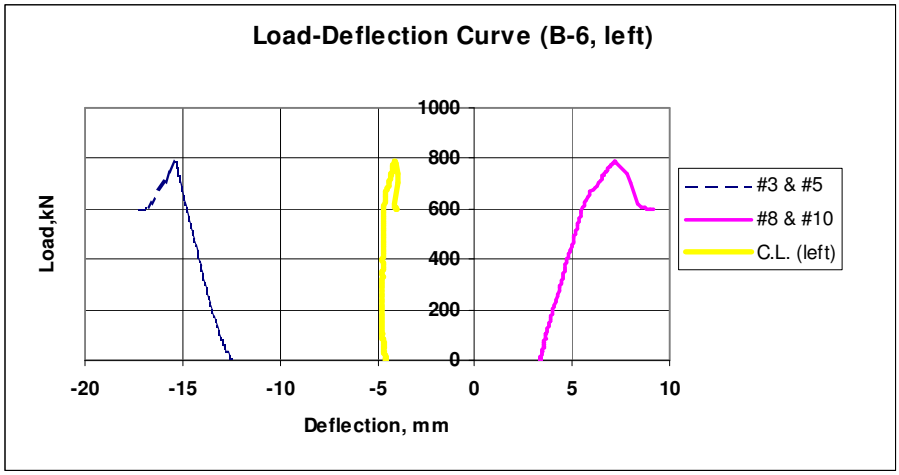

Fig. C.109 Load versus deflection curve (LDS #3 & #5, LDS #8 & #10 and left CL)

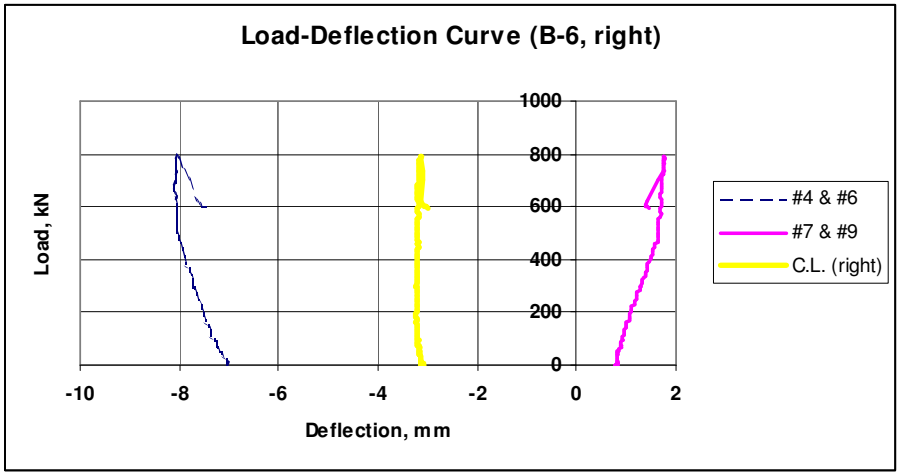

Fig. C.110 Load versus deflection curve (LDS #4 & #6, LDS #7 & #9 and right CL)

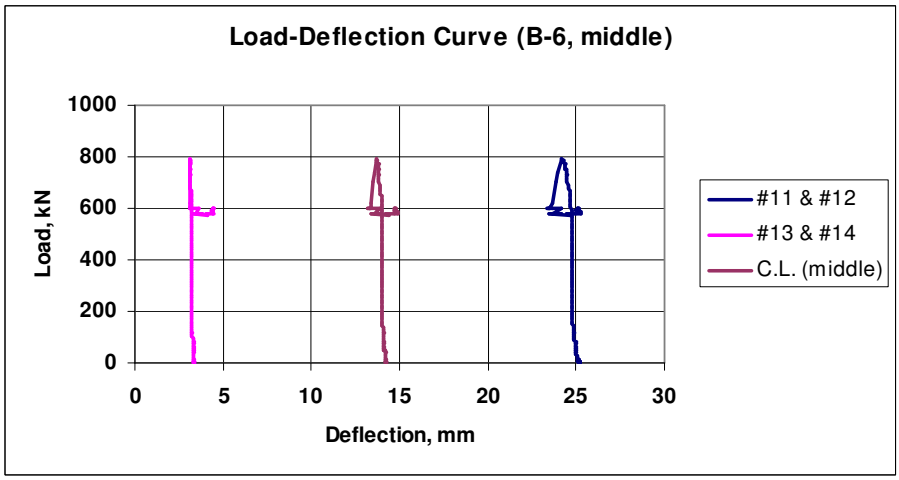

Fig. C.111 Load versus deflection curve (LDS #11 & #12, LDS #13 & #14, middle CL)

2.7 Wall ***B-7***

There is no data available for wall test specimens ***B-7*** – the load cell was broken.

2.8 Wall ***B-8***

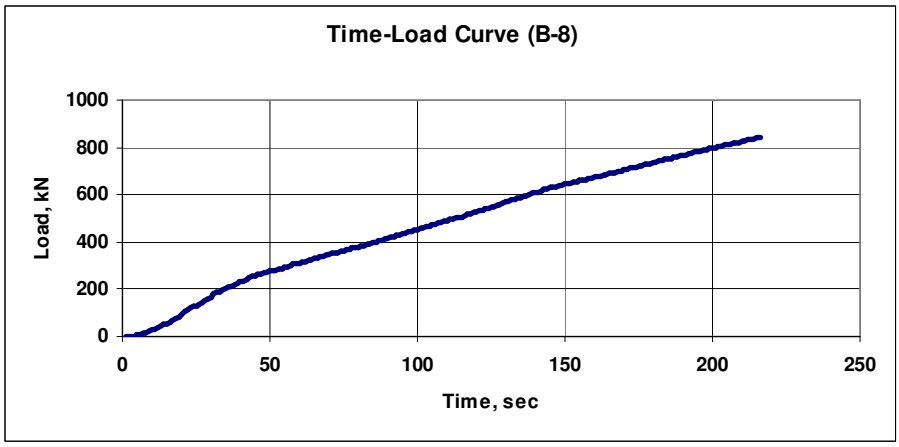

Fig. C.112 Time versus load curve

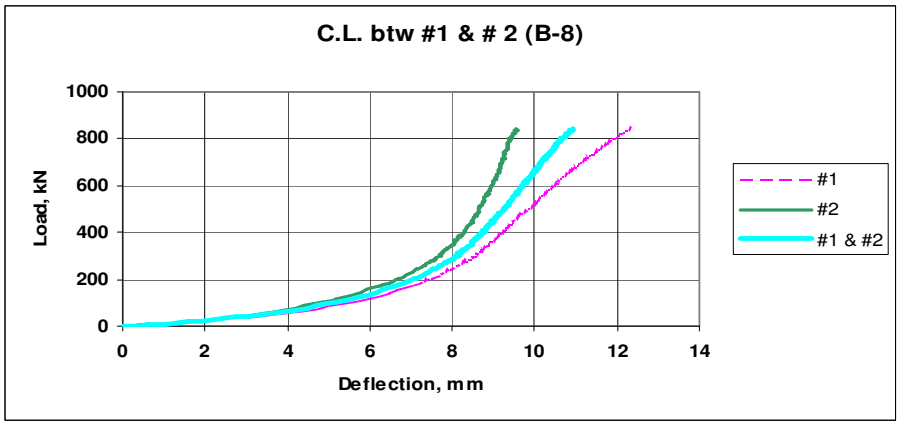

Fig. C.113 Load versus deflection curve (LDS #1, LDS #2 and CL)

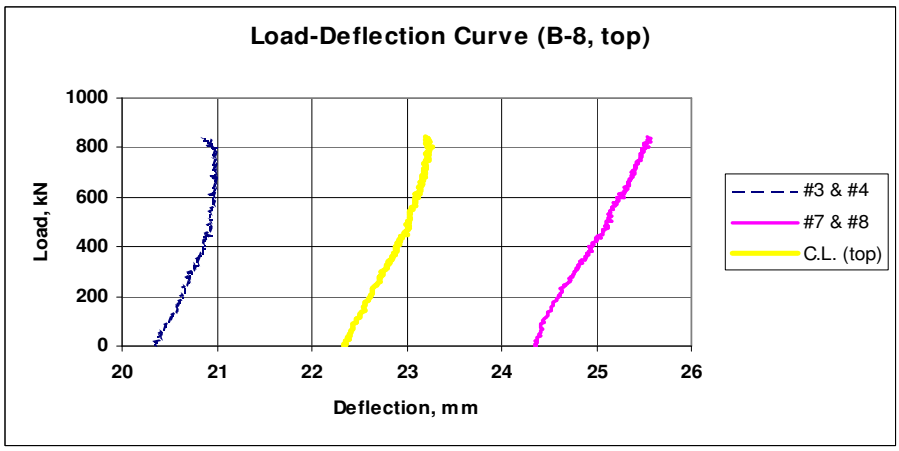

Fig. C.114 Load versus deflection curve (LDS #3 & #4, LDS #7 & #8 and top CL)

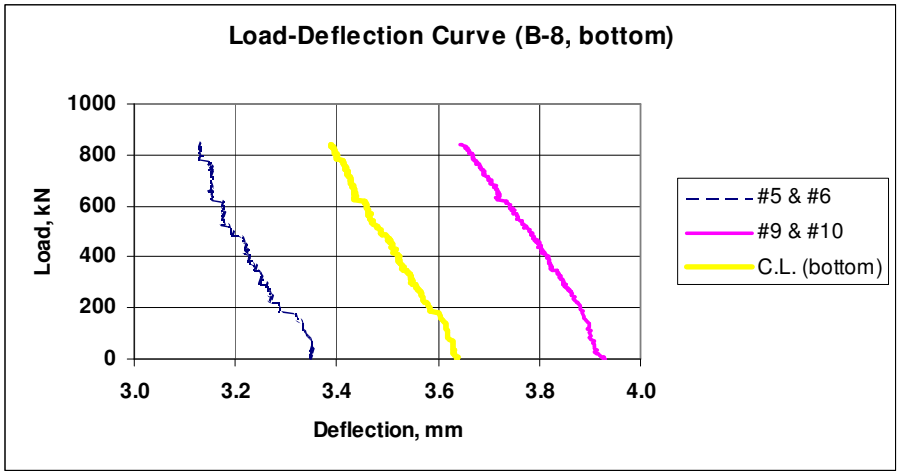

Fig. C.115 Load versus deflection curve (LDS #5 & #6, LDS #9 & #10 and bottom CL)

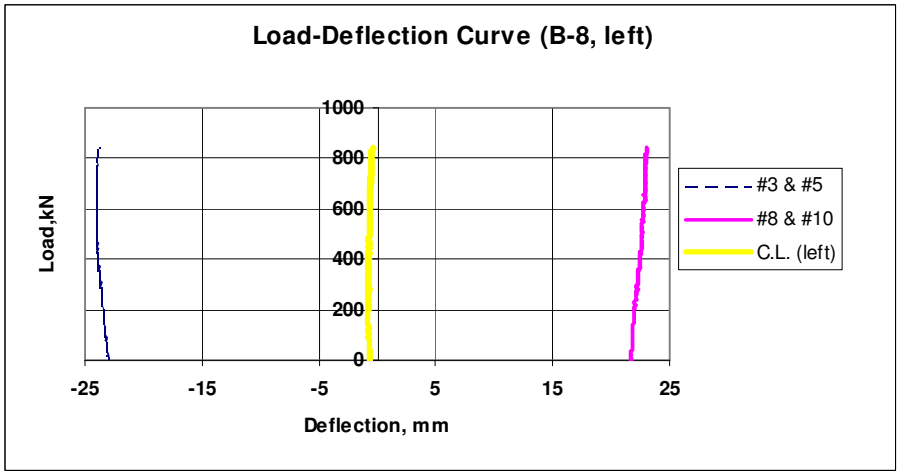

Fig. C.116 Load versus deflection curve (LDS #3 & #5, LDS #8 & #10 and left CL)

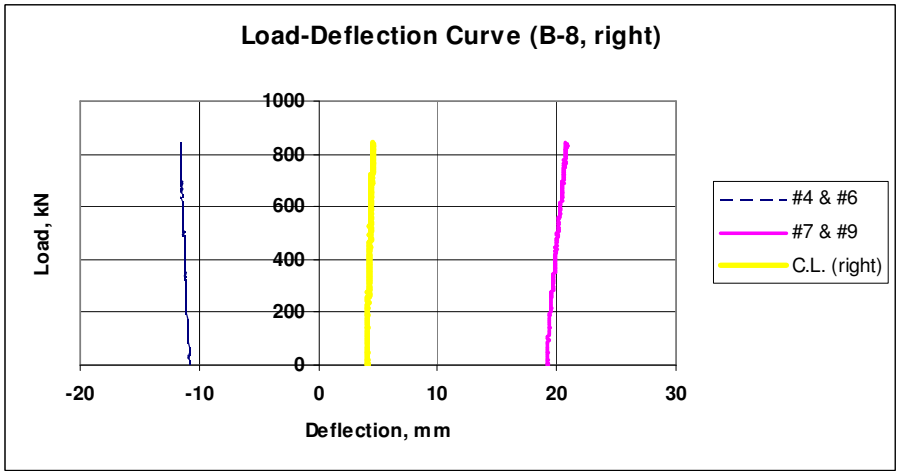

Fig. C.117 Load versus deflection curve (LDS #4 & #6, LDS #7 & #9 and right CL)

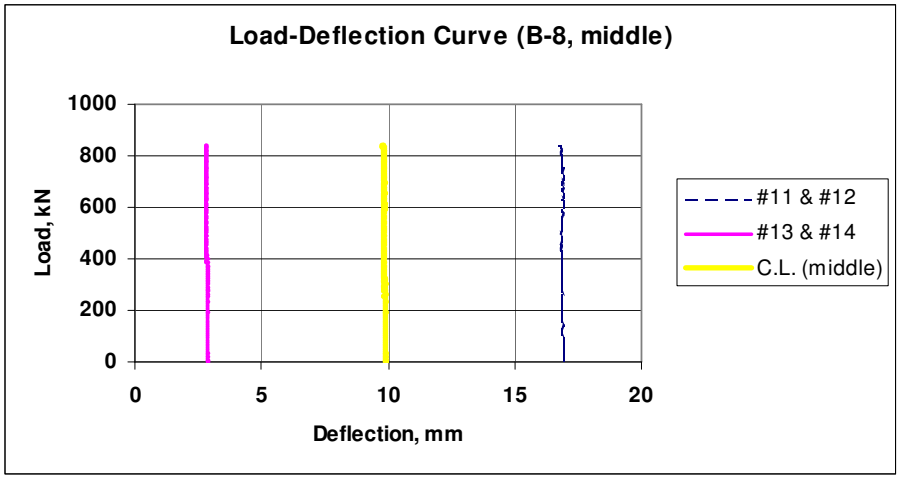

Fig. C.118 Load versus deflection curve (LDS #11 & #12, LDS #13 & #14, middle CL)

2.9 Wall ***B-9***

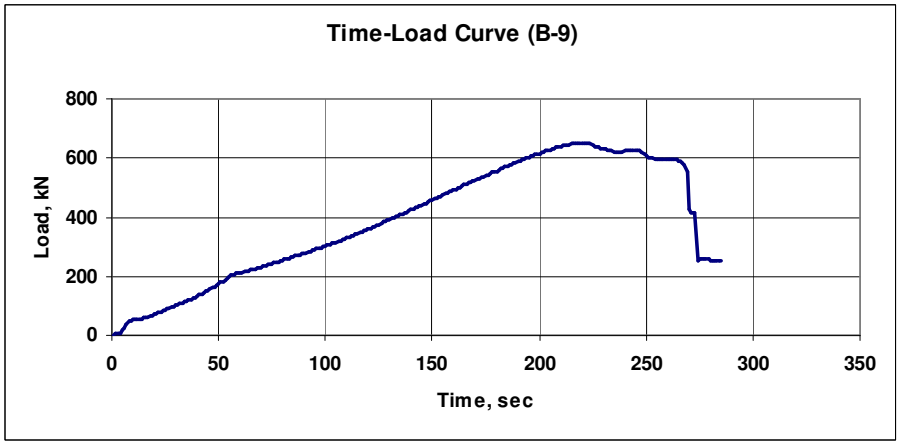

Fig. C.119 Time versus load curve

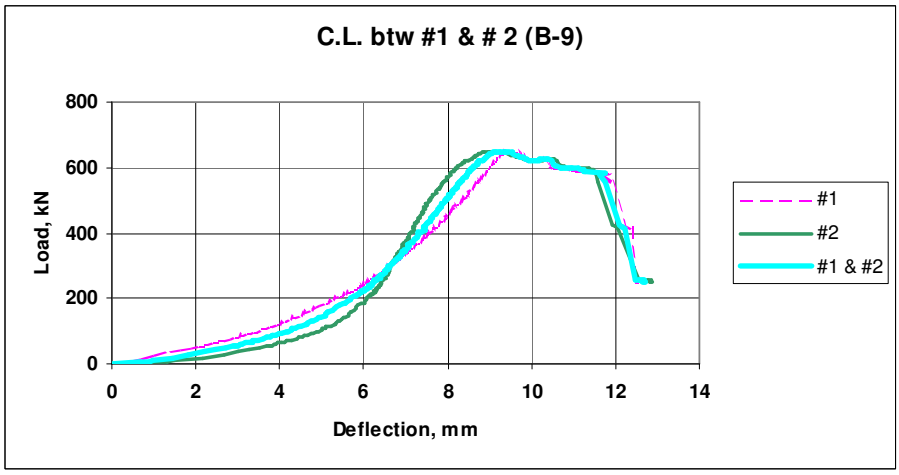

Fig. C.120 Load versus deflection curve (LDS #1, LDS #2 and CL)

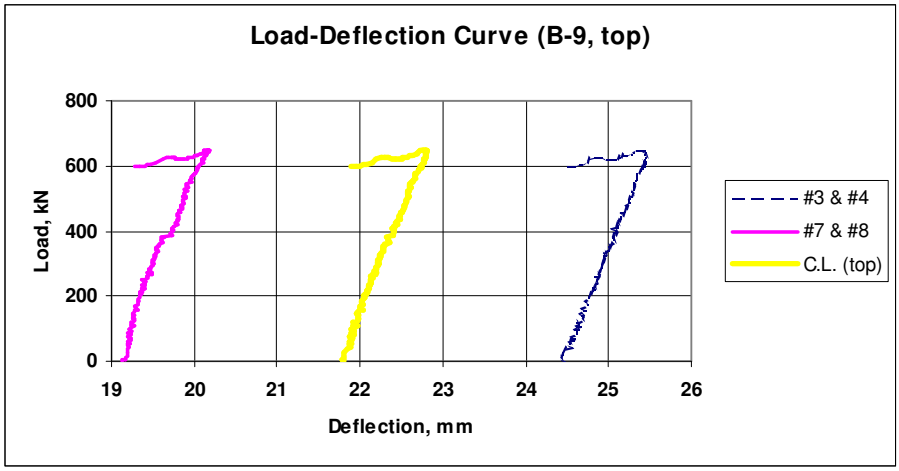

Fig. C.121 Load versus deflection curve (LDS #3 & #4, LDS #7 & #8 and top CL)

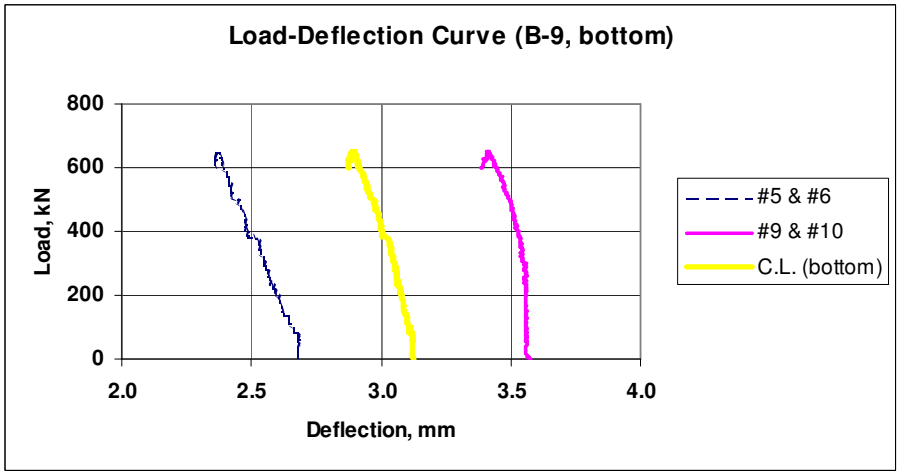

Fig. C.122 Load versus deflection curve (LDS #5 & #6, LDS #9 & #10 and bottom CL)

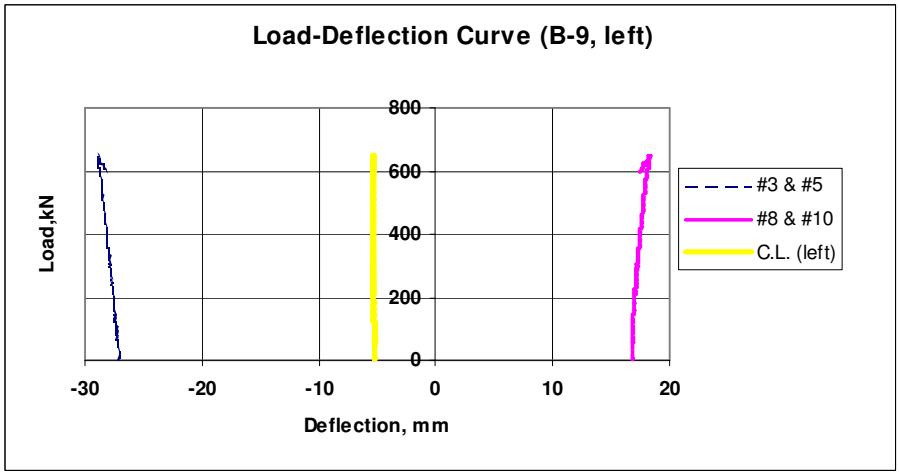

Fig. C.123 Load versus deflection curve (LDS #3 & #5, LDS #8 & #10 and left CL)

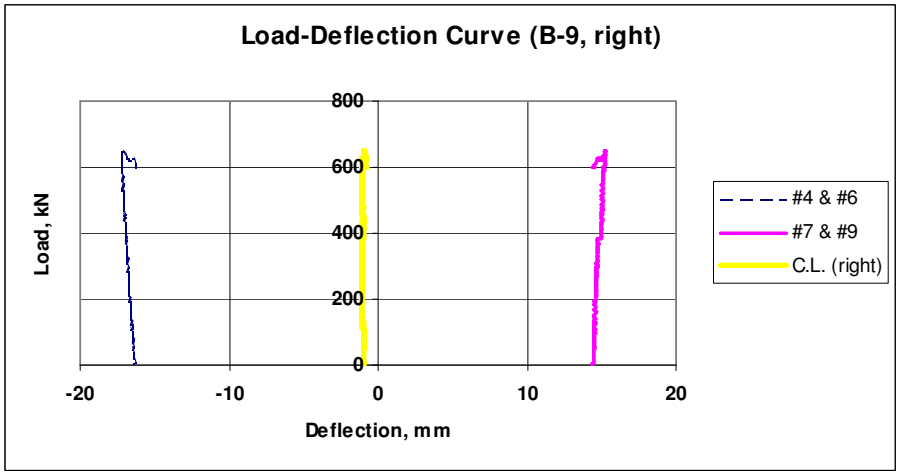

Fig. C.124 Load versus deflection curve (LDS #4 & #6, LDS #7 & #9 and right CL)

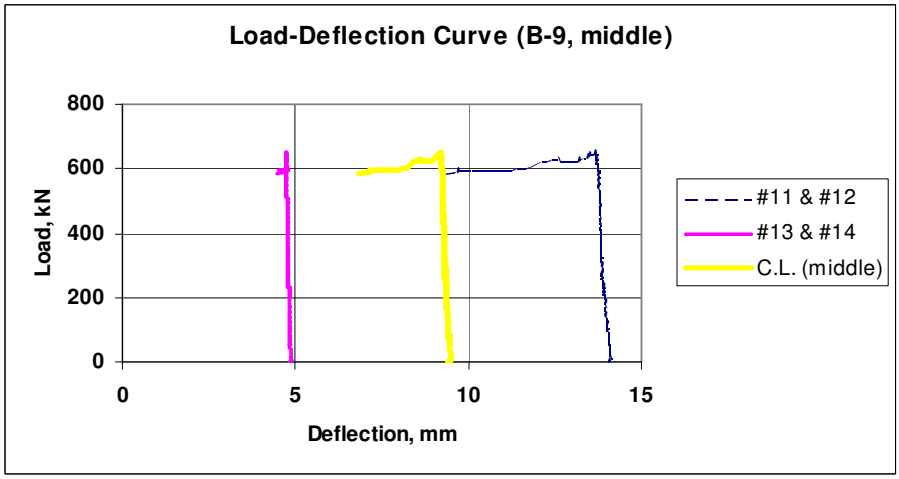

Fig. C.125 Load versus deflection curve (LDS #11 & #12, LDS #13 & #14, middle CL)

2.10 Wall ***B-10***

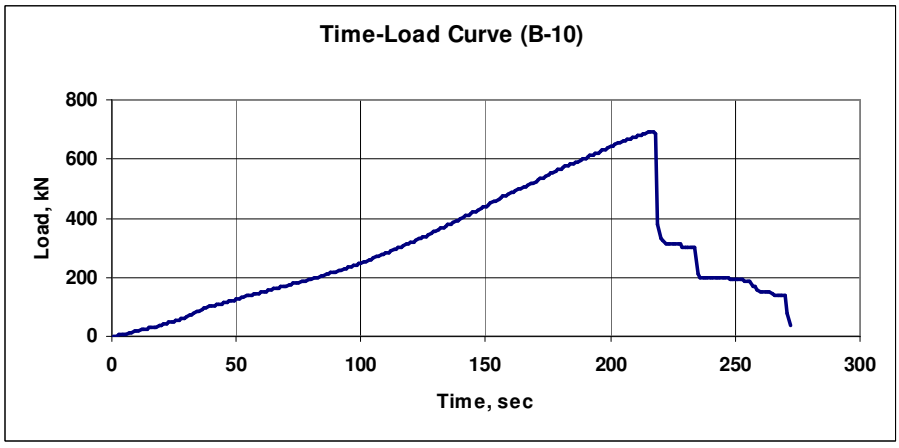

Fig. C.126 Time versus load curve

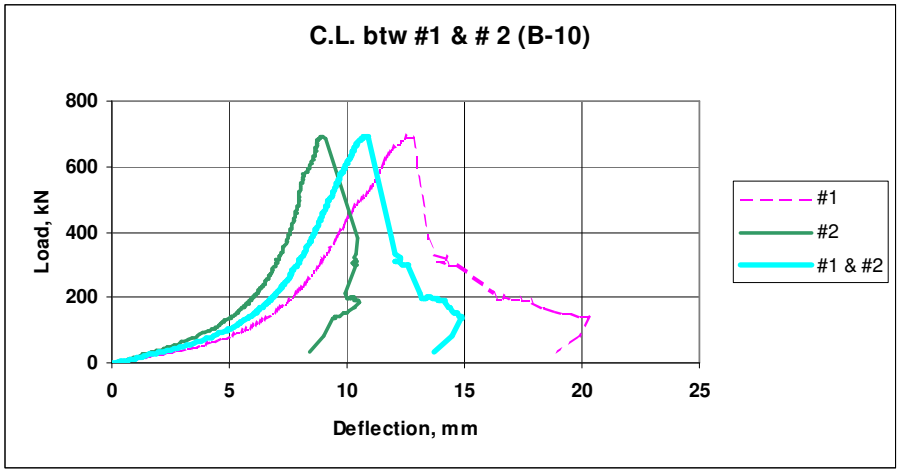

Fig. C.127 Load versus deflection curve (LDS #1, LDS #2 and CL)

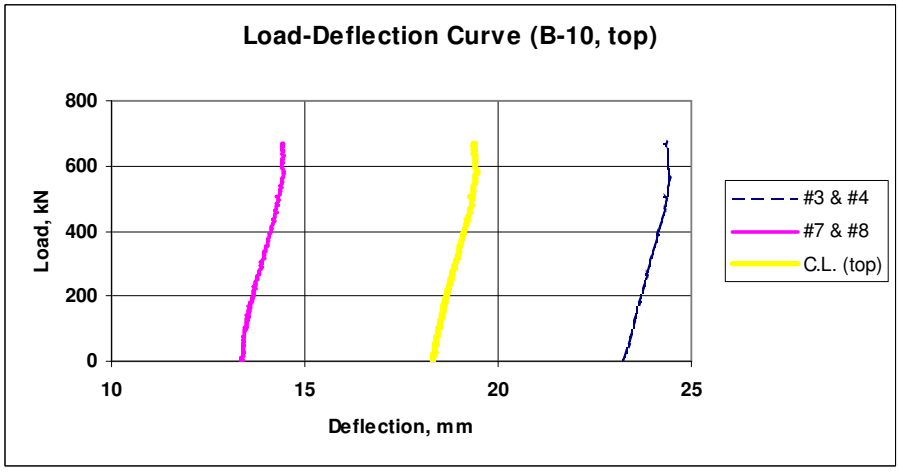

Fig. C.128 Load versus deflection curve (LDS #3 & #4, LDS #7 & #8 and top CL)

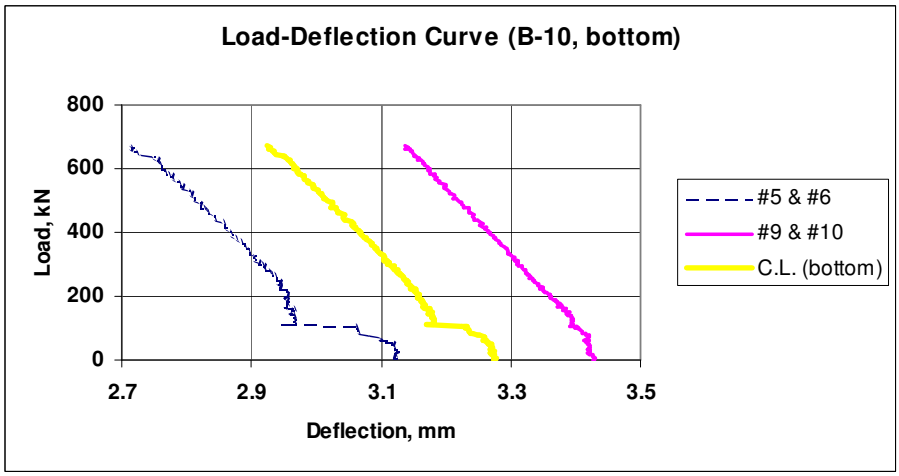

Fig. C.129 Load versus deflection curve (LDS #5 & #6, LDS #9 & #10 and bottom CL)

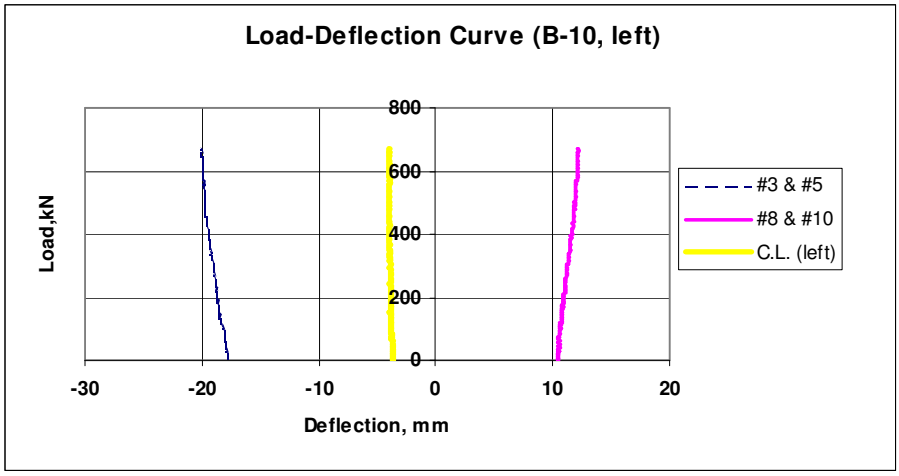

Fig. C.130 Load versus deflection curve (LDS #3 & #5, LDS #8 & #10 and left CL)

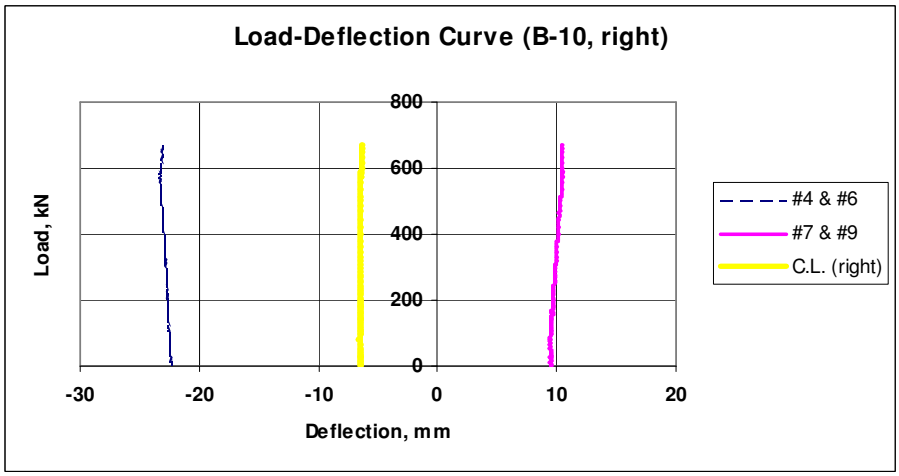

Fig. C.131 Load versus deflection curve (LDS #4 & #6, LDS #7 & #9 and right CL)

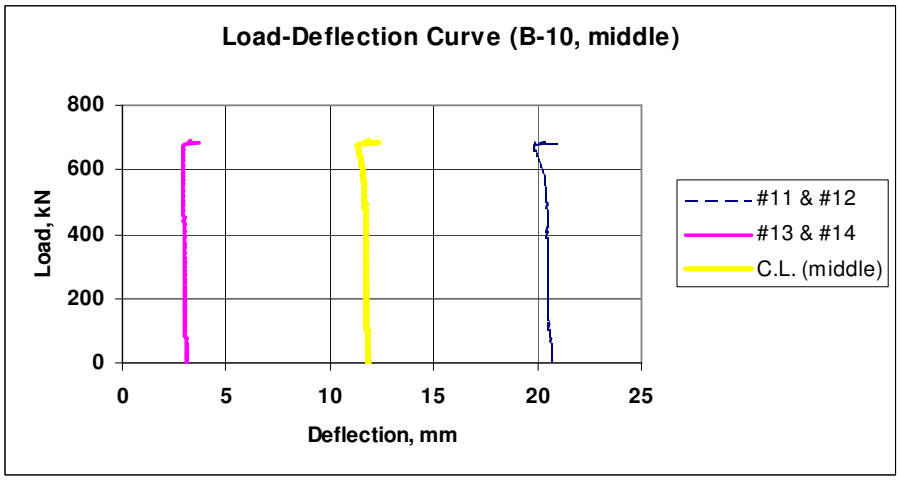

Fig. C.132 Load versus deflection curve (LDS #11 & #12, LDS #13 & #14, middle CL)

3. Test results for wall specimens type *C*

3.1 Wall *C-1*

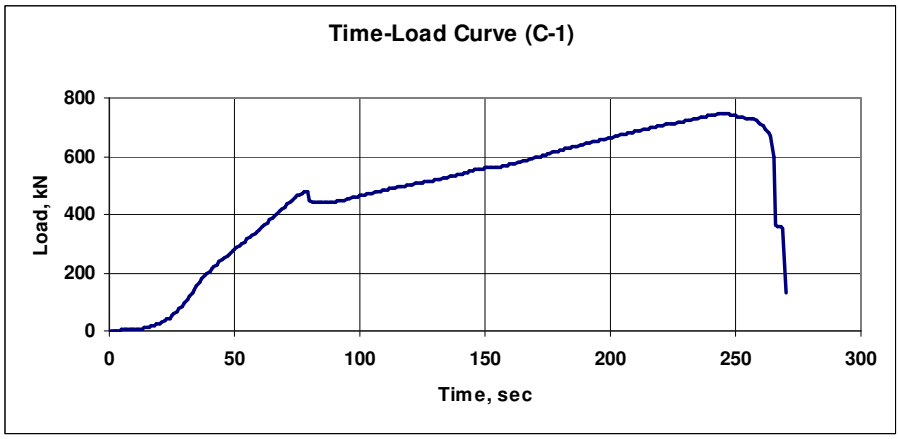

Fig. C.133 Time versus load curve

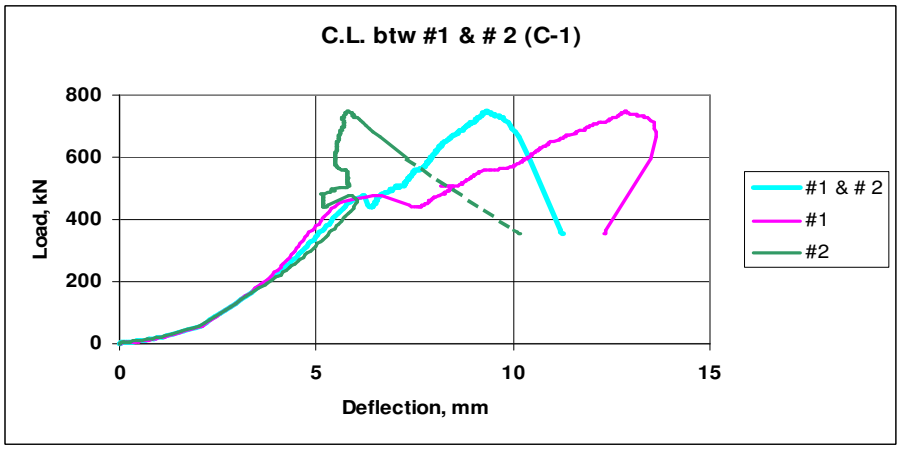

Fig. C.134 Load versus deflection curve (LDS #1, LDS #2 and CL)

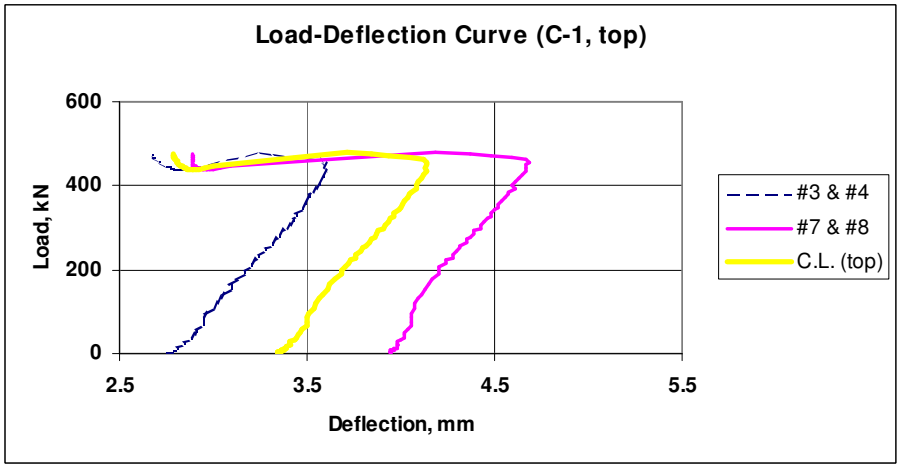

Fig. C.135 Load versus deflection curve (LDS #3 & #4, LDS #7 & #8 and top CL)

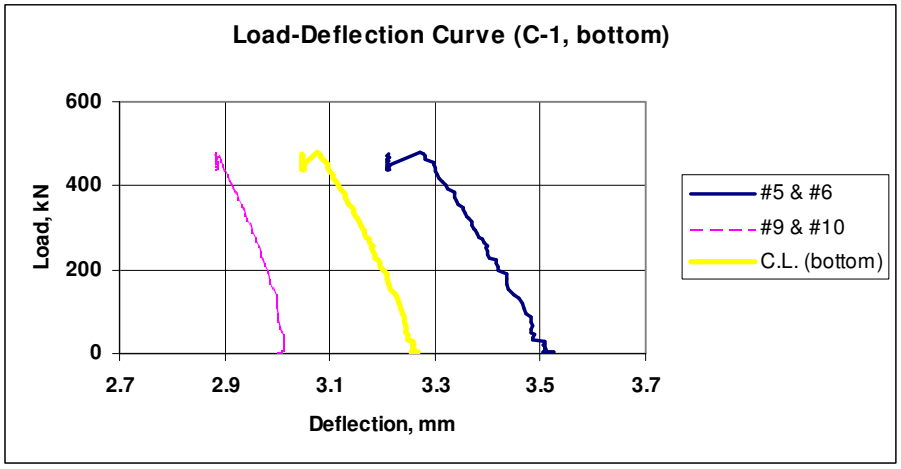

Fig. C.136 Load versus deflection curve (LDS #5 & #6, LDS #9 & #10 and bottom CL)

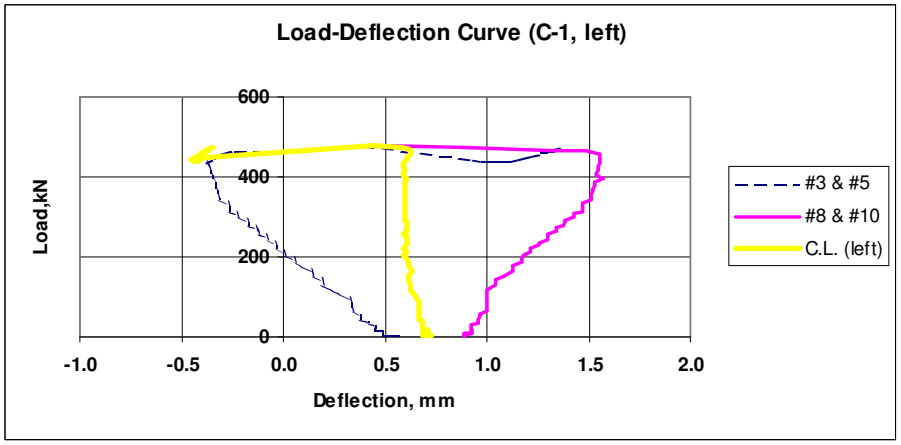

Fig. C.137 Load versus deflection curve (LDS #3 & #5, LDS #8 & #10 and left CL)

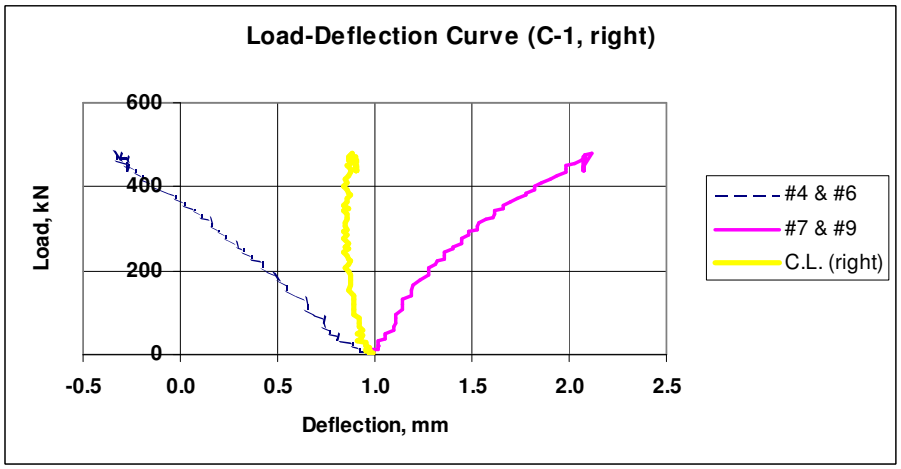

Fig. C.138 Load versus deflection curve (LDS #4 & #6, LDS #7 & #9 and right CL)

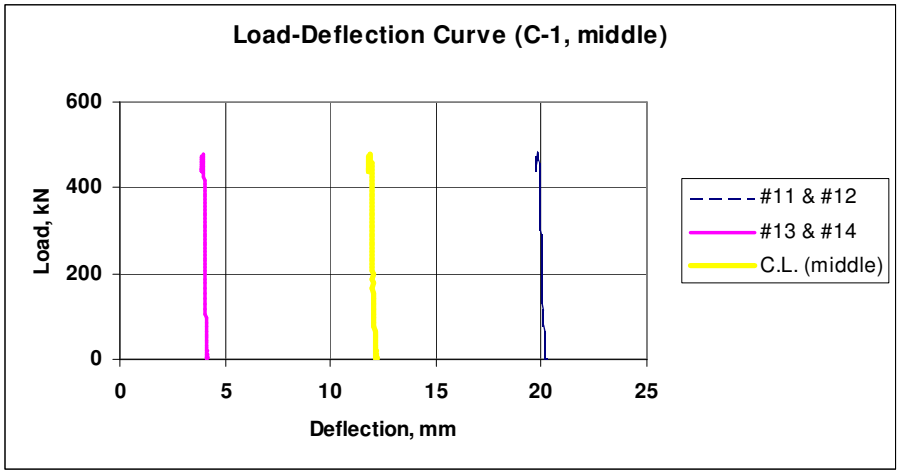

Fig. C.139 Load versus deflection curve (LDS #11 & #12, LDS #13 & #14, middle CL)

3.2 Wall ***C-2***

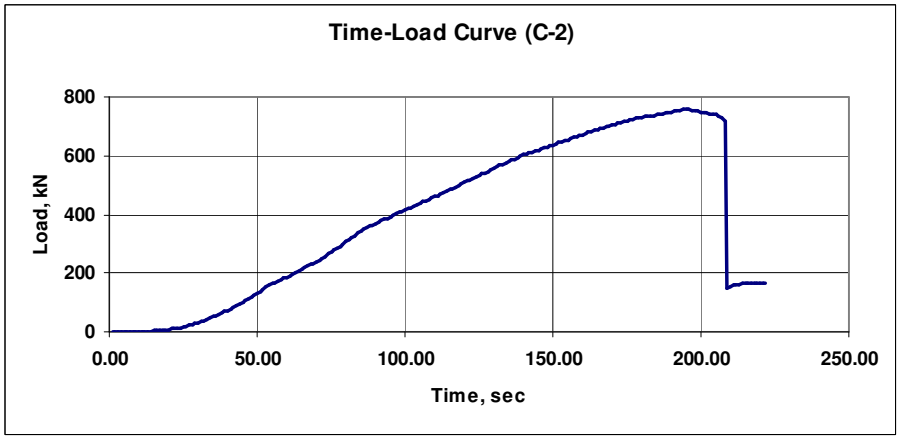

Fig. C.140 Time versus load curve

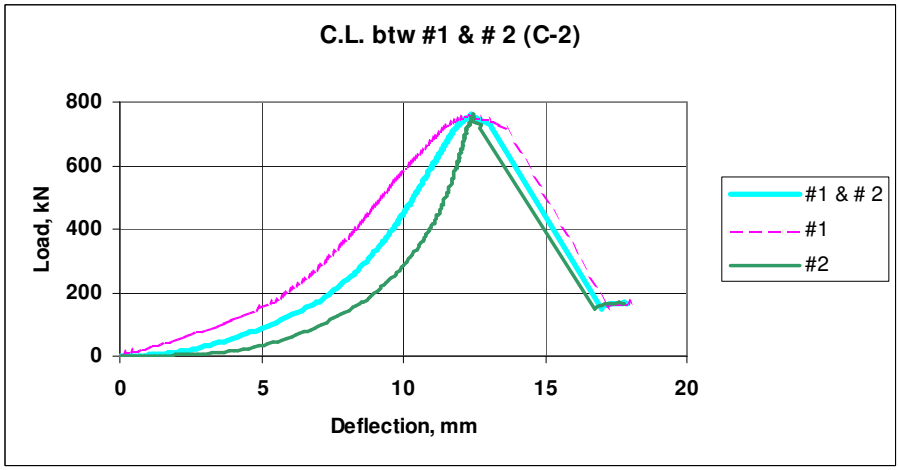

Fig. C.141 Load versus deflection curve (LDS #1, LDS #2 and CL)

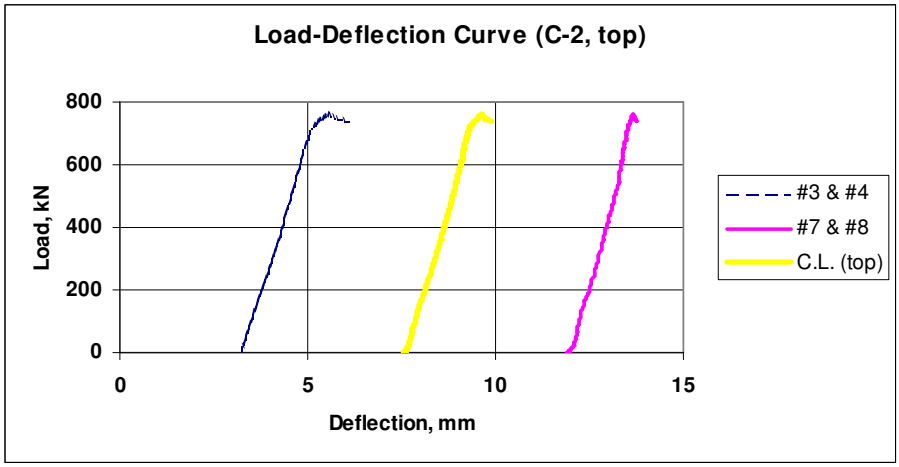

Fig. C.142 Load versus deflection curve (LDS #3 & #4, LDS #7 & #8 and top CL)

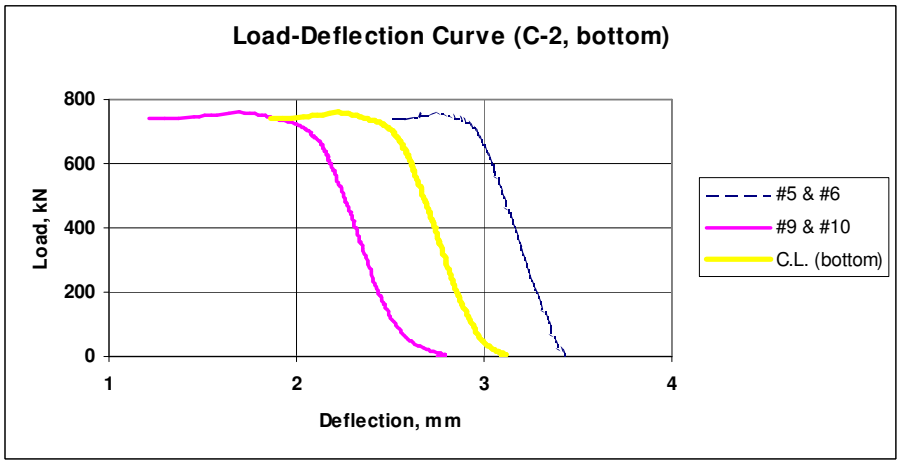

Fig. C.143 Load versus deflection curve (LDS #5 & #6, LDS #9 & #10 and bottom CL)

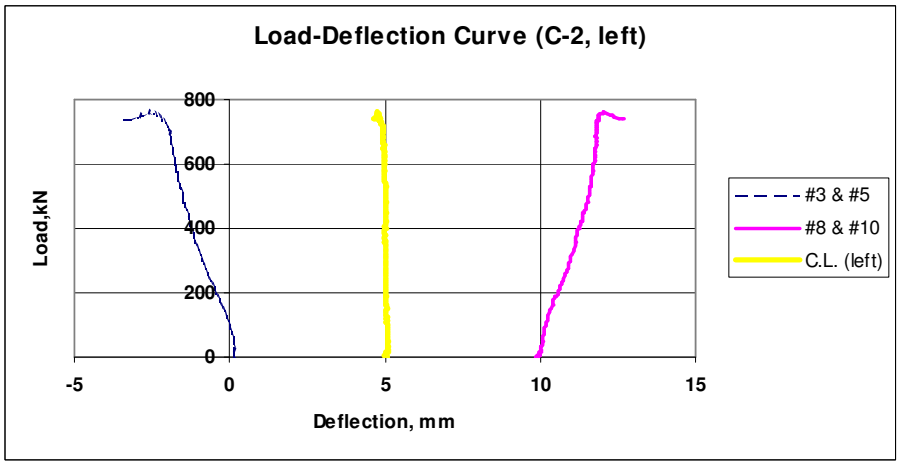

Fig. C.144 Load versus deflection curve (LDS #3 & #5, LDS #8 & #10 and left CL)

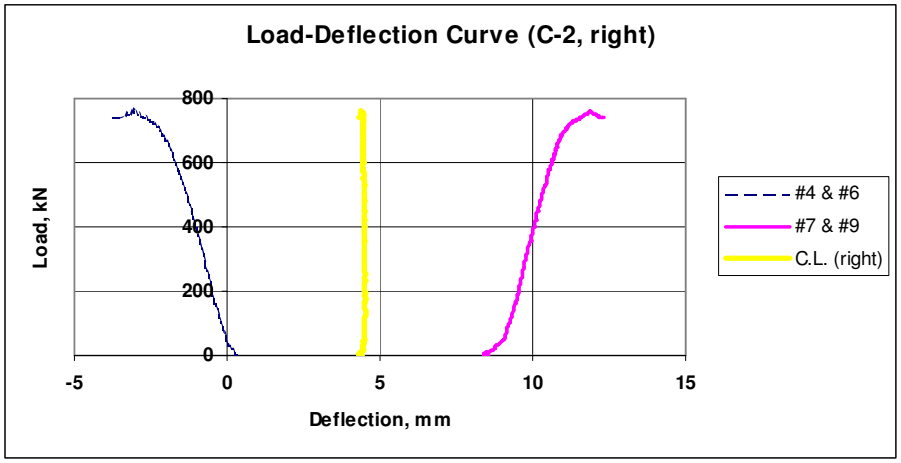

Fig. C.145 Load versus deflection curve (LDS #4 & #6, LDS #7 & #9 and right CL)

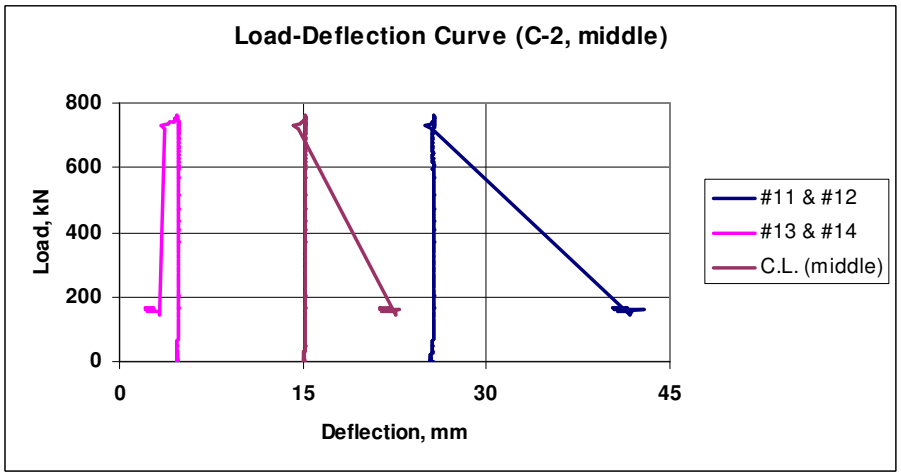

Fig. C.146 Load versus deflection curve (LDS #11 & #12, LDS #13 & #14, middle CL)

3.3 Wall ***C-3***

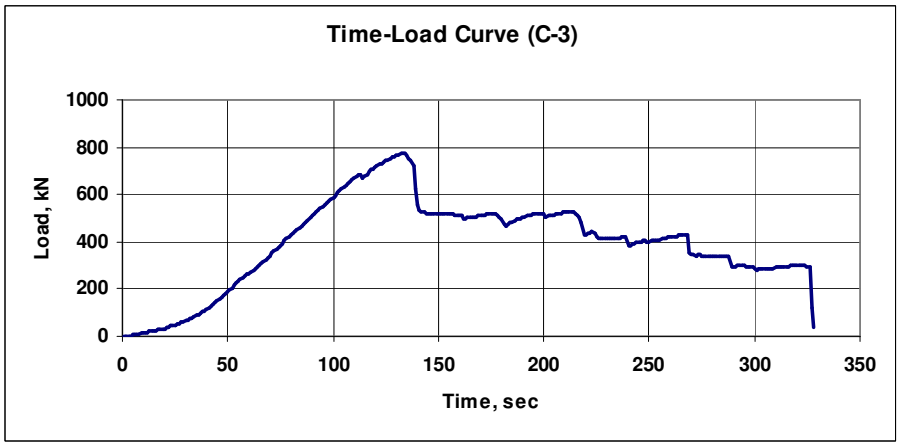

Fig. C.147 Time versus load curve

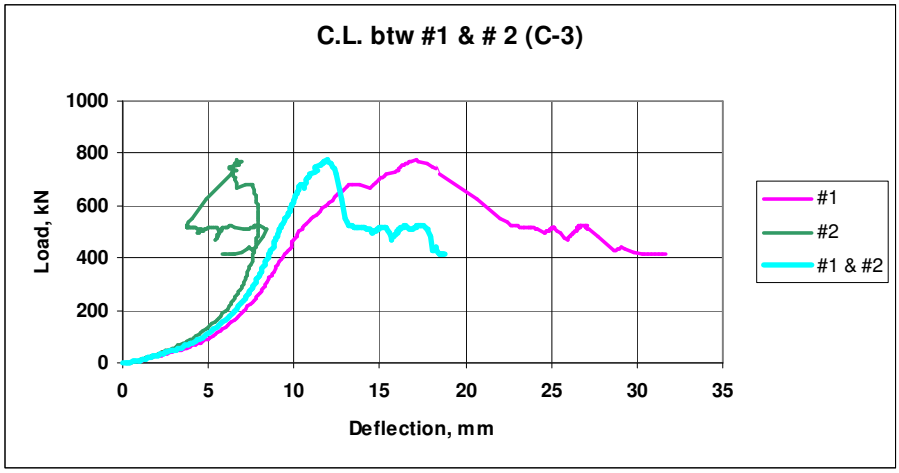

Fig. C.148 Load versus deflection curve (LDS #1, LDS #2 and CL)

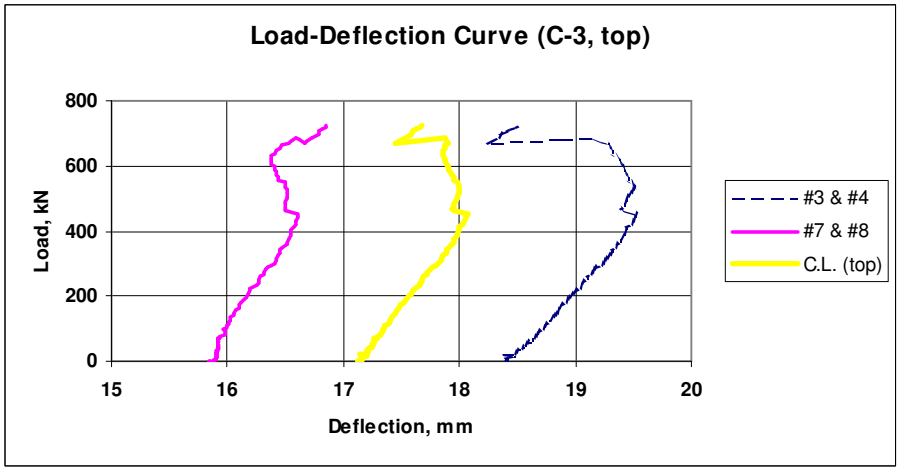

Fig. C.149 Load versus deflection curve (LDS #3 & #4, LDS #7 & #8 and top CL)

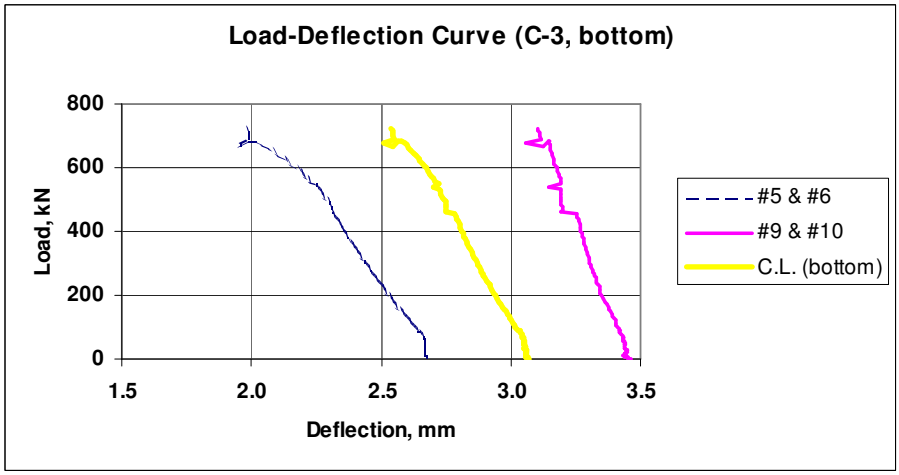

Fig. C.150 Load versus deflection curve (LDS #5 & #6, LDS #9 & #10 and bottom CL)

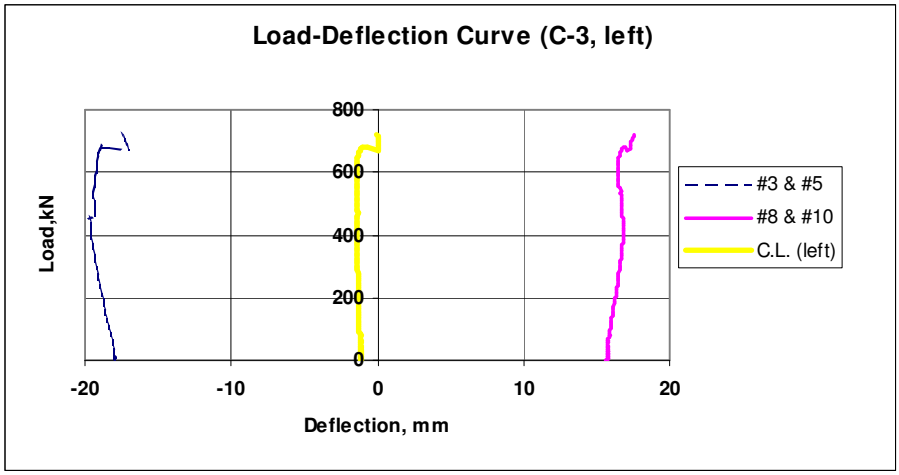

Fig. C.151 Load versus deflection curve (LDS #3 & #5, LDS #8 & #10 and left CL)

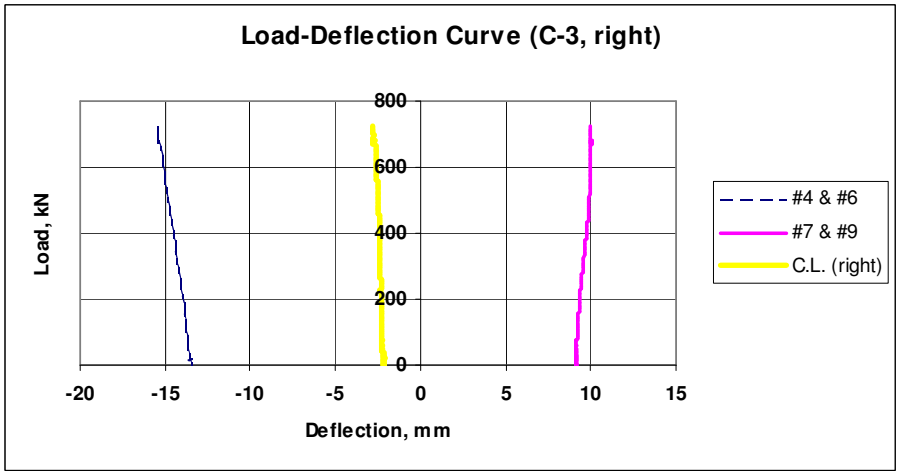

Fig. C.152 Load versus deflection curve (LDS #4 & #6, LDS #7 & #9 and right CL)

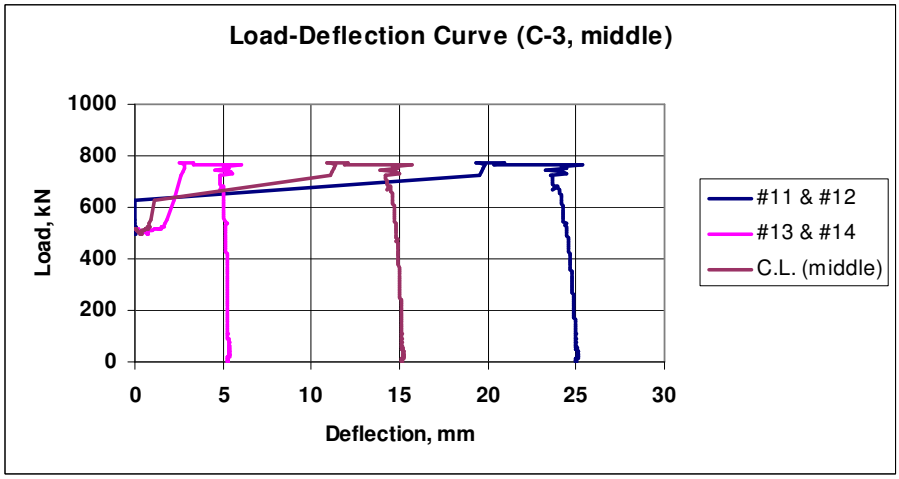

Fig. C.153 Load versus deflection curve (LDS #11 & #12, LDS #13 & #14, middle CL)

3.4 Wall ***C-4***

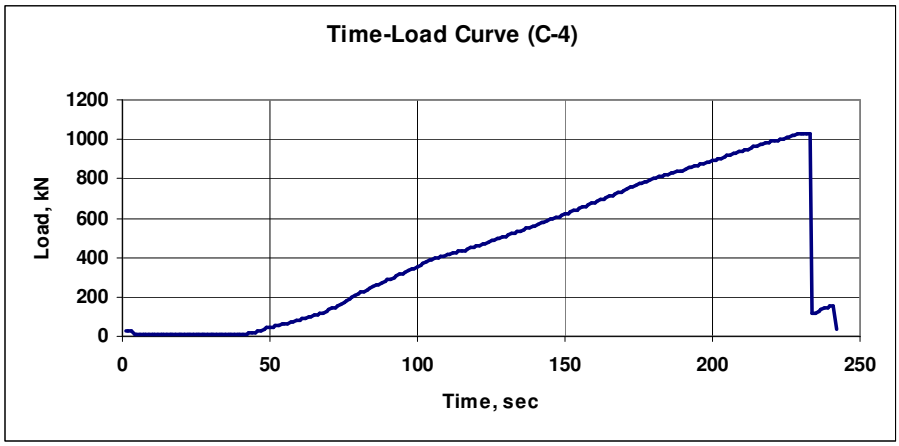

Fig. C.154 Time versus load curve

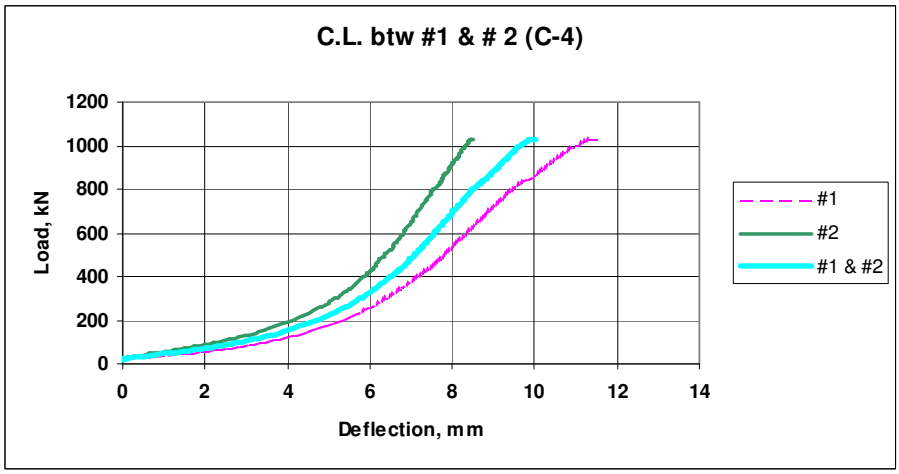

Fig. C.155 Load versus deflection curve (LDS #1, LDS #2 and CL)

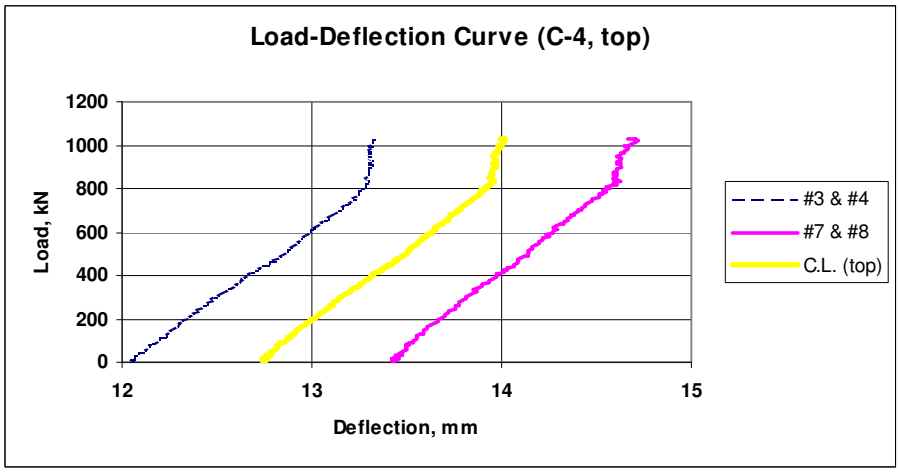

Fig. C.156 Load versus deflection curve (LDS #3 & #4, LDS #7 & #8 and top CL)

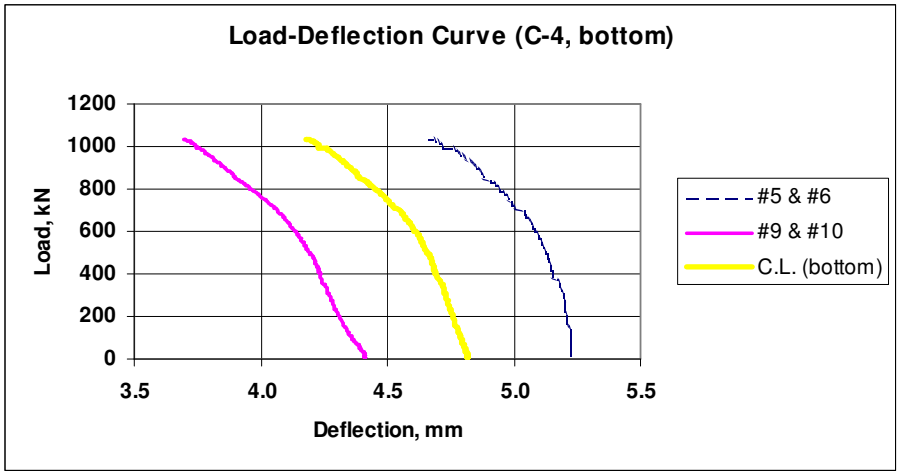

Fig. C.157 Load versus deflection curve (LDS #5 & #6, LDS #9 & #10 and bottom CL)

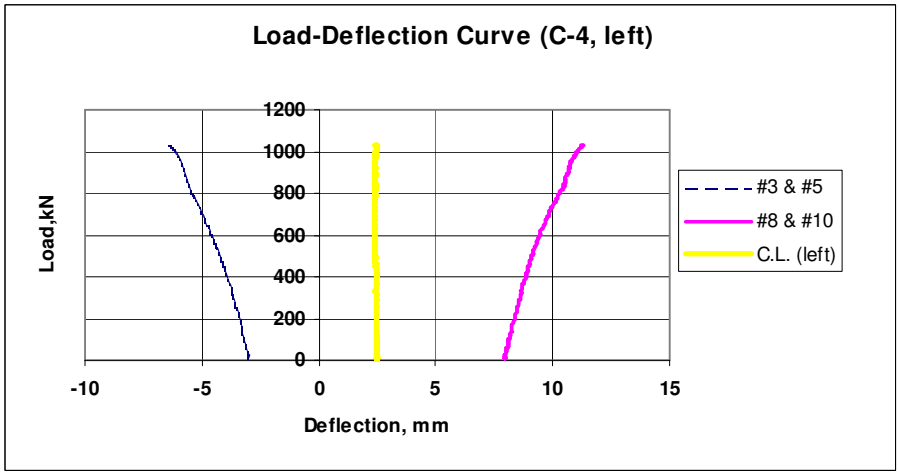

Fig. C.158 Load versus deflection curve (LDS #3 & #5, LDS #8 & #10 and left CL)

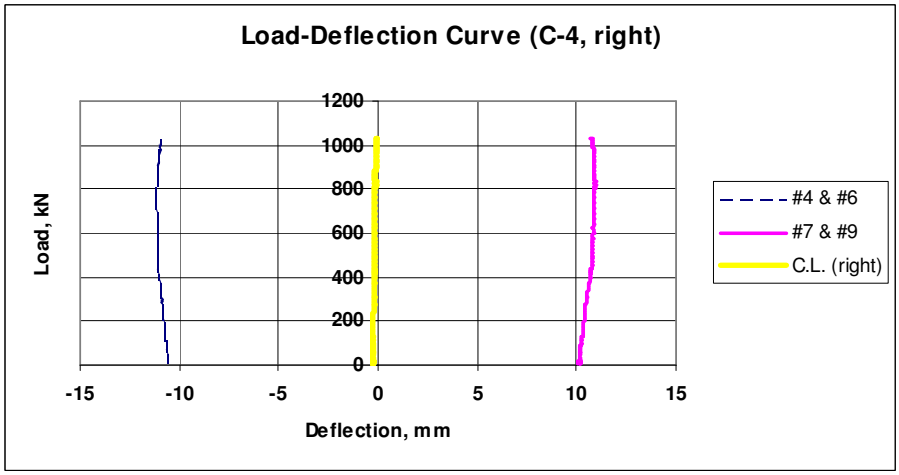

Fig. C.159 Load versus deflection curve (LDS #4 & #6, LDS #7 & #9 and right CL)

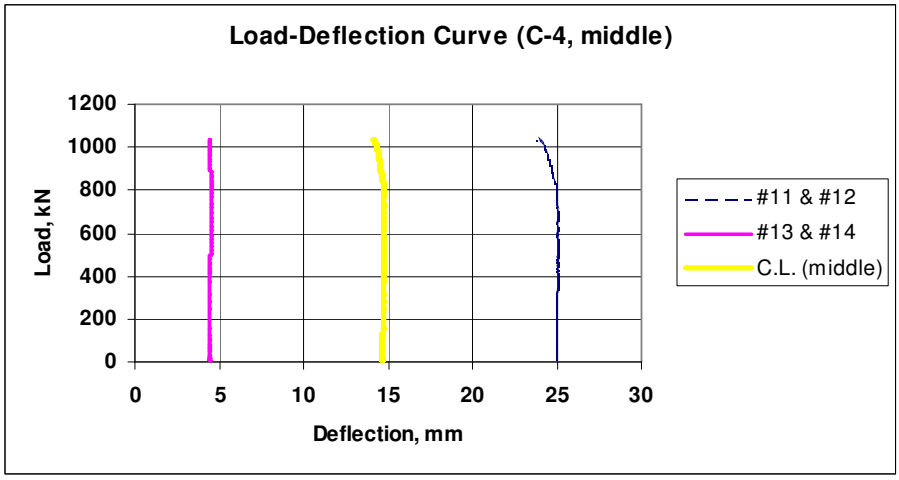

Fig. C.160 Load versus deflection curve (LDS #11 & #12, LDS #13 & #14, middle CL)

3.5 Wall ***C-5***

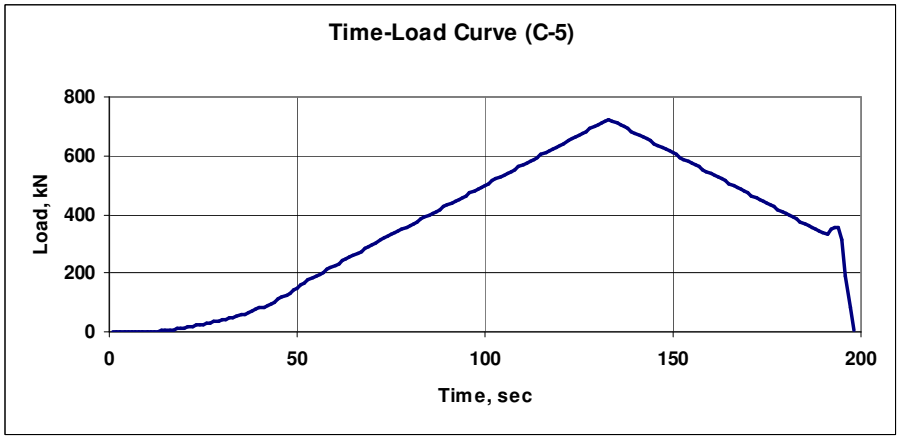

Fig. C.161 Time versus load curve

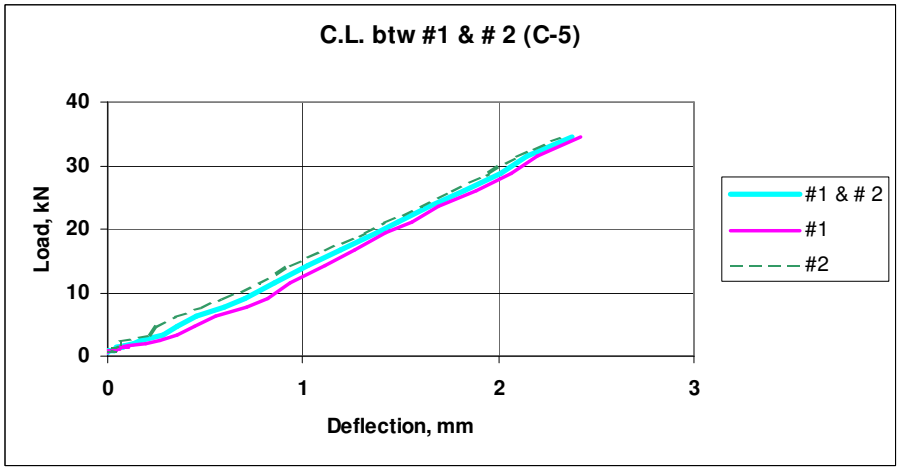

Fig. C.162 Load versus deflection curve (LDS #1, LDS #2 and CL)

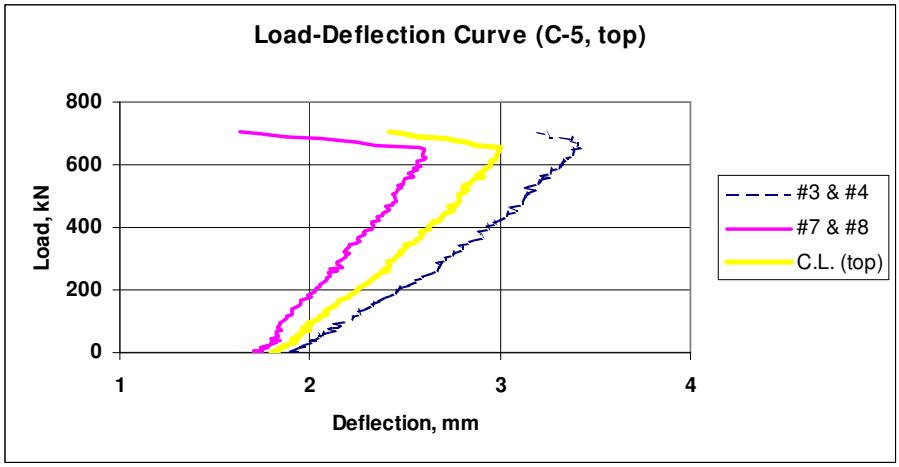

Fig. C.163 Load versus deflection curve (LDS #3 & #4, LDS #7 & #8 and top CL)

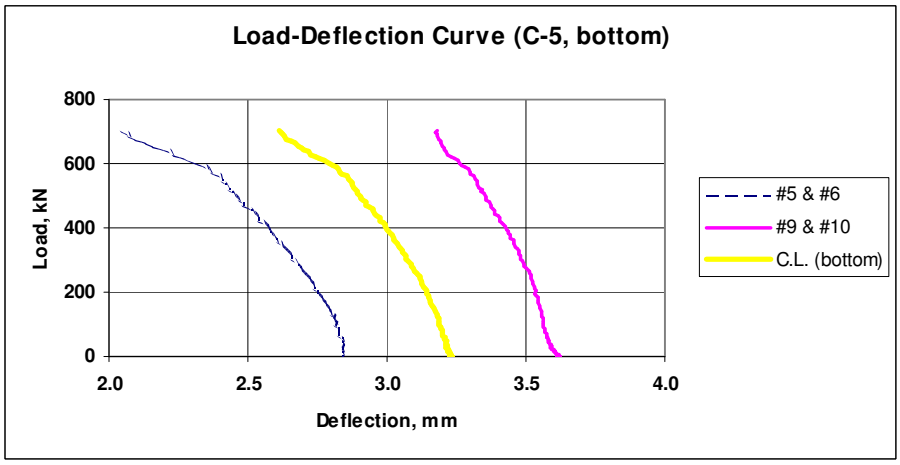

Fig. C.164 Load versus deflection curve (LDS #5 & #6, LDS #9 & #10 and bottom CL)

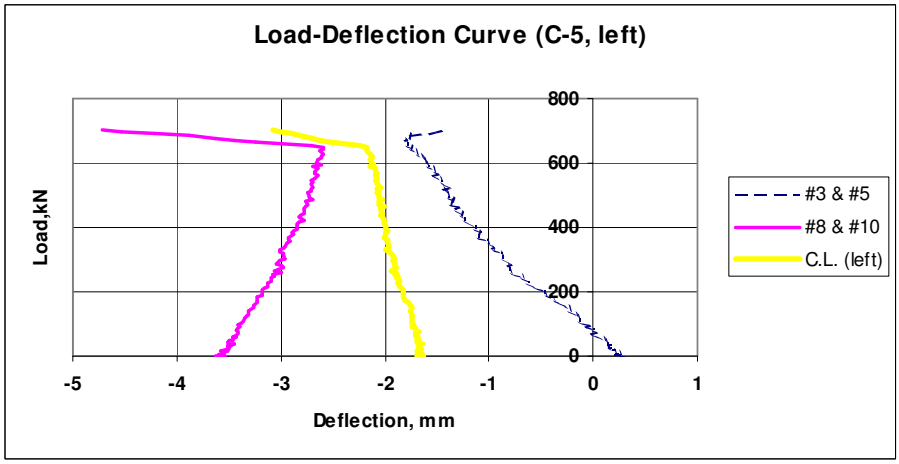

Fig. C.165 Load versus deflection curve (LDS #3 & #5, LDS #8 & #10 and left CL)

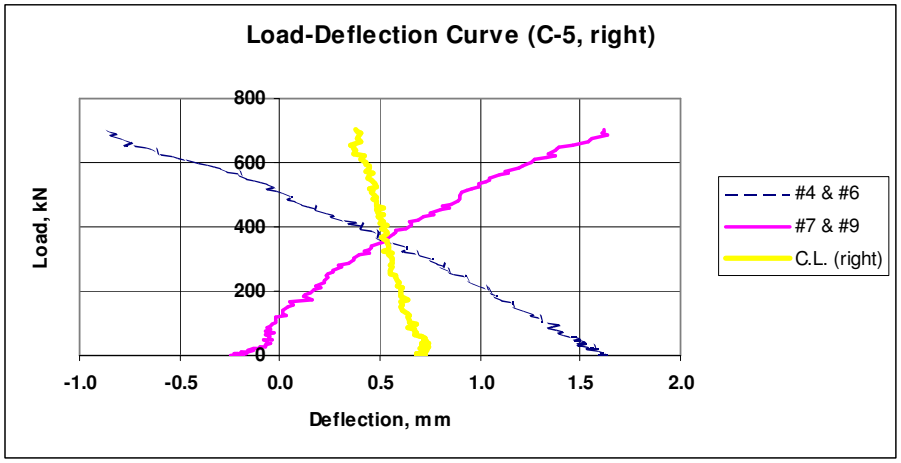

Fig. C.166 Load versus deflection curve (LDS #4 & #6, LDS #7 & #9 and right CL)

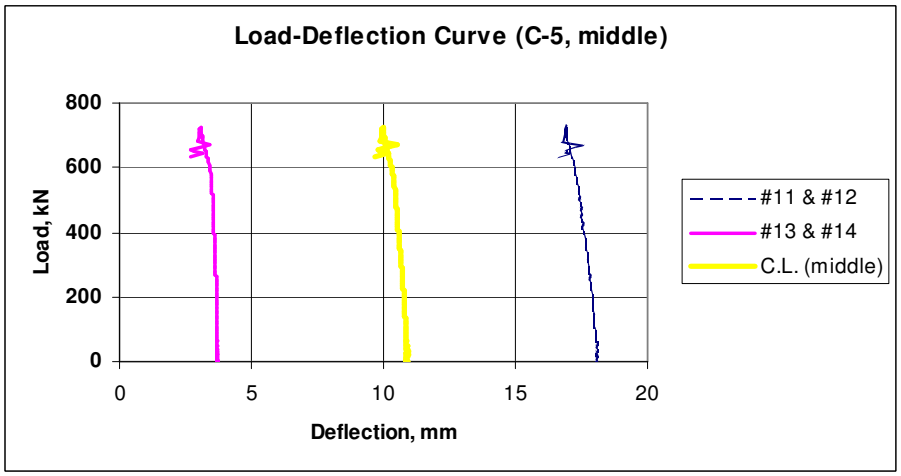

Fig. C.167 Load versus deflection curve (LDS #11 & #12, LDS #13 & #14, middle CL)

3.6 Wall ***C-6***

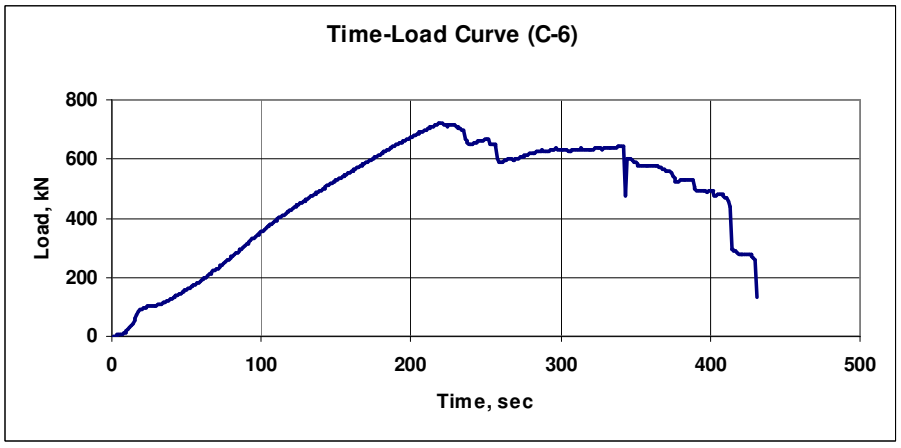

Fig. C.168 Time versus load curve

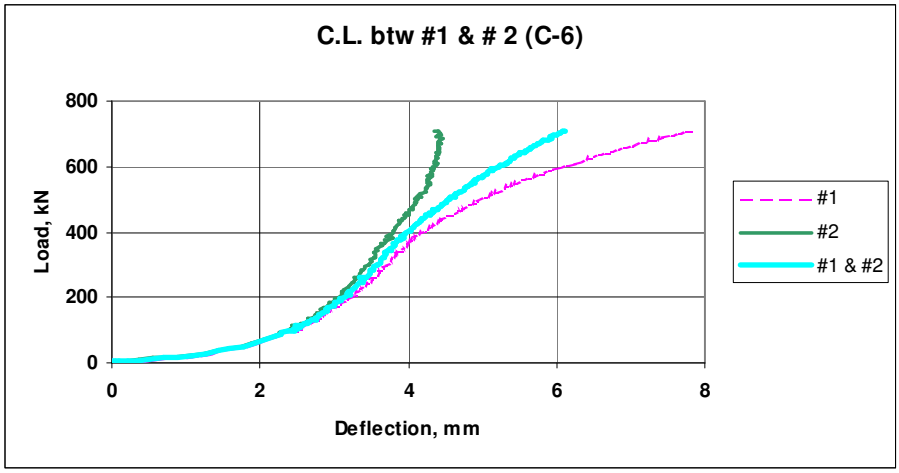

Fig. C.169 Load versus deflection curve (LDS #1, LDS #2 and CL)

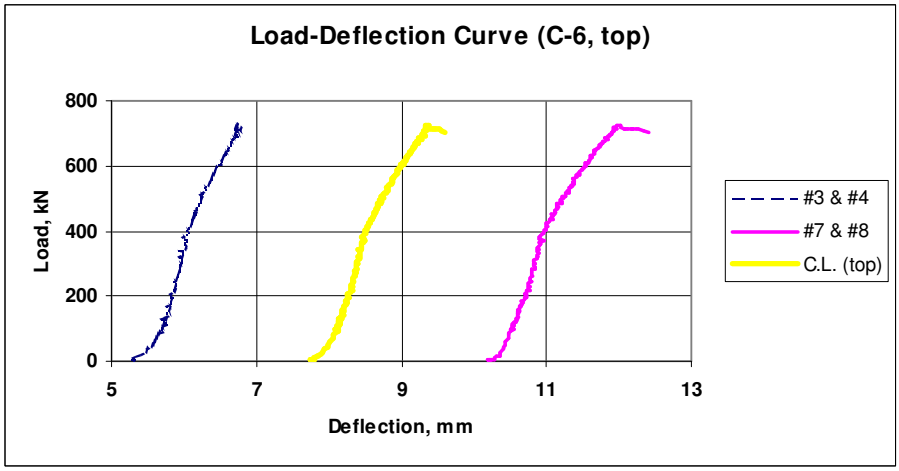

Fig. C.170 Load versus deflection curve (LDS #3 & #4, LDS #7 & #8 and top CL)

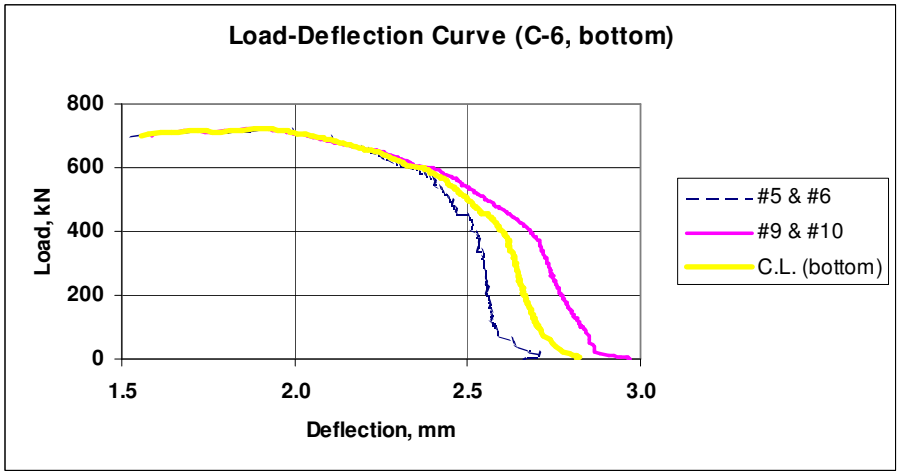

Fig. C.171 Load versus deflection curve (LDS #5 & #6, LDS #9 & #10 and bottom CL)

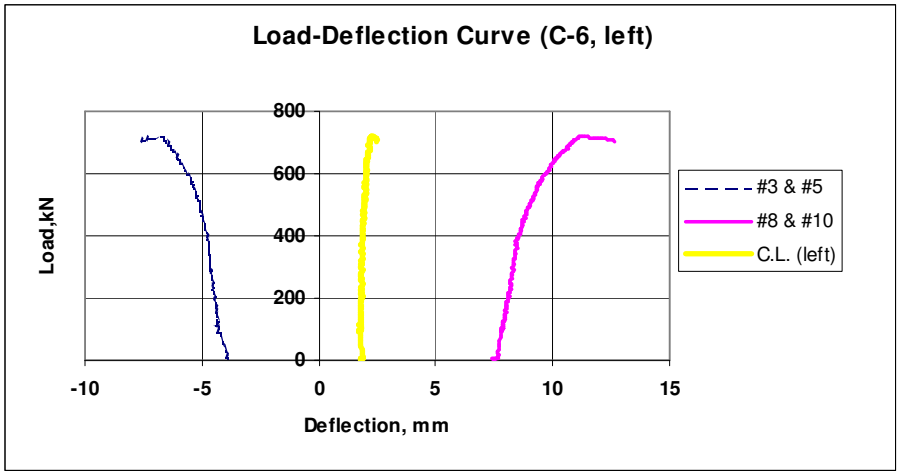

Fig. C.172 Load versus deflection curve (LDS #3 & #5, LDS #8 & #10 and left CL)

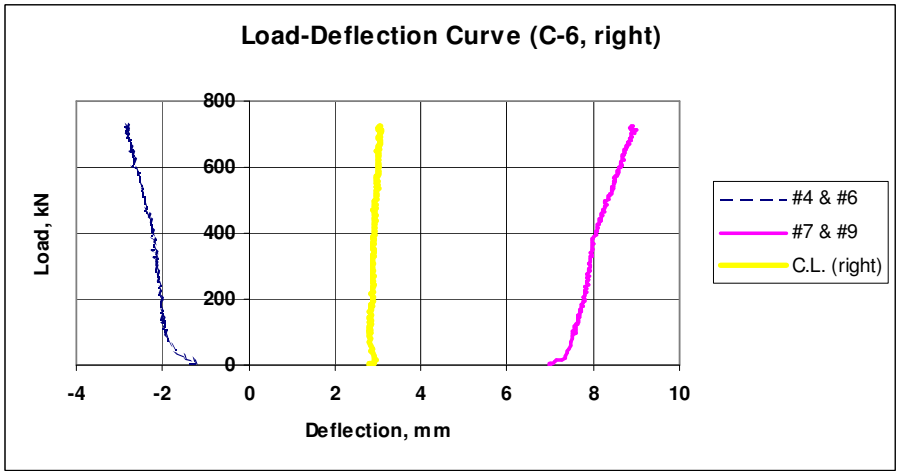

Fig. C.173 Load versus deflection curve (LDS #4 & #6, LDS #7 & #9 and right CL)

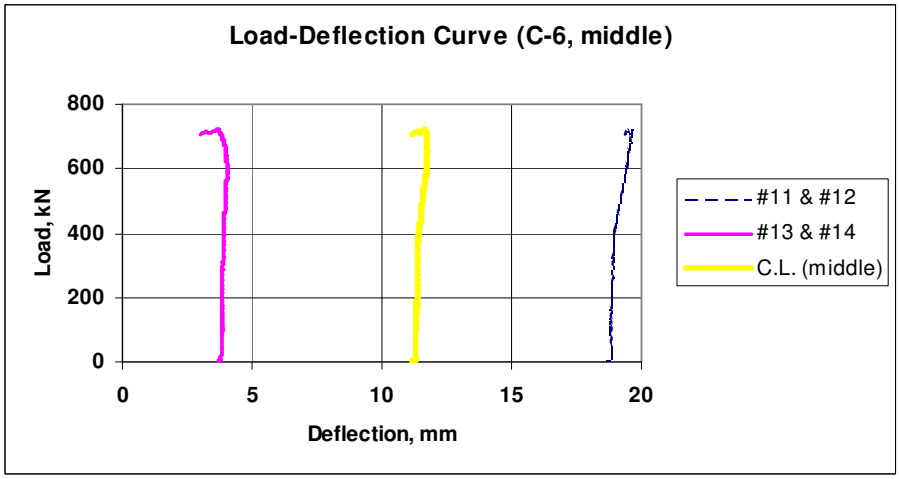

Fig. C.174 Load versus deflection curve (LDS #11 & #12, LDS #13 & #14, middle CL)

3.7 Wall ***C-7***

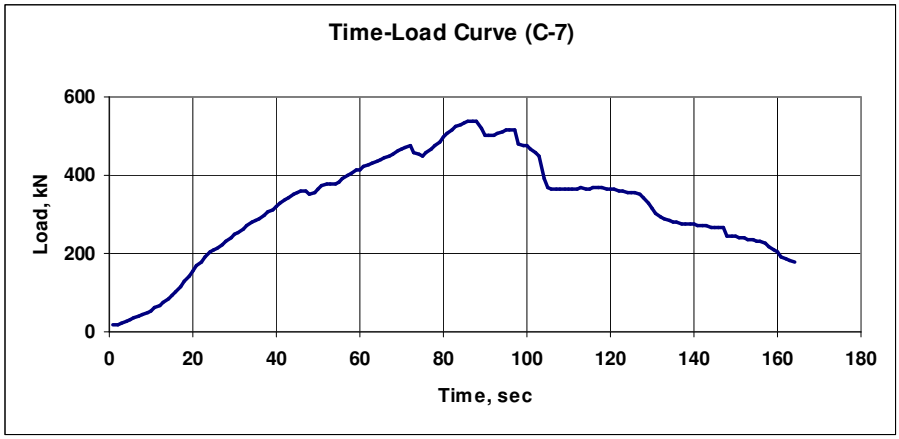

Fig. C.175 Time versus load curve

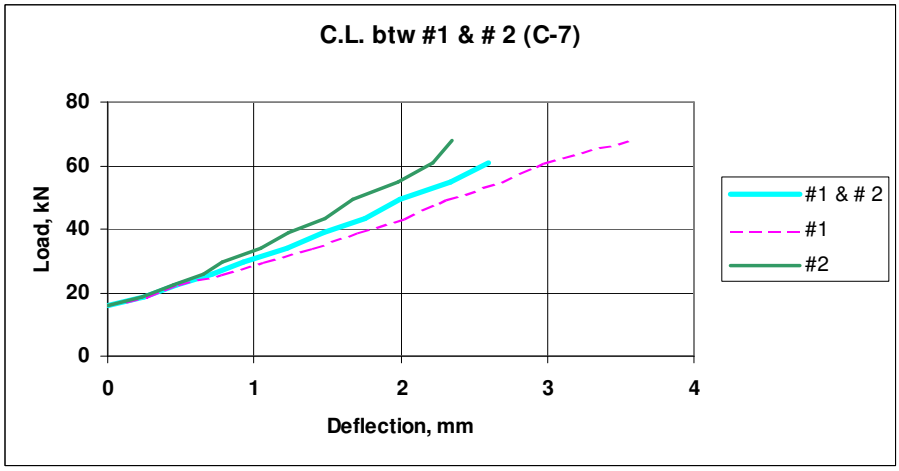

Fig. C.176 Load versus deflection curve (LDS #1, LDS #2 and CL)

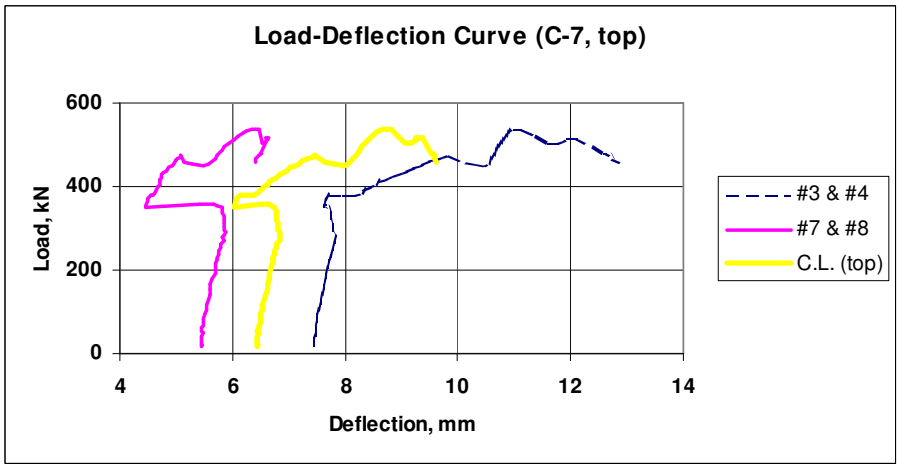

Fig. C.177 Load versus deflection curve (LDS #3 & #4, LDS #7 & #8 and top CL)

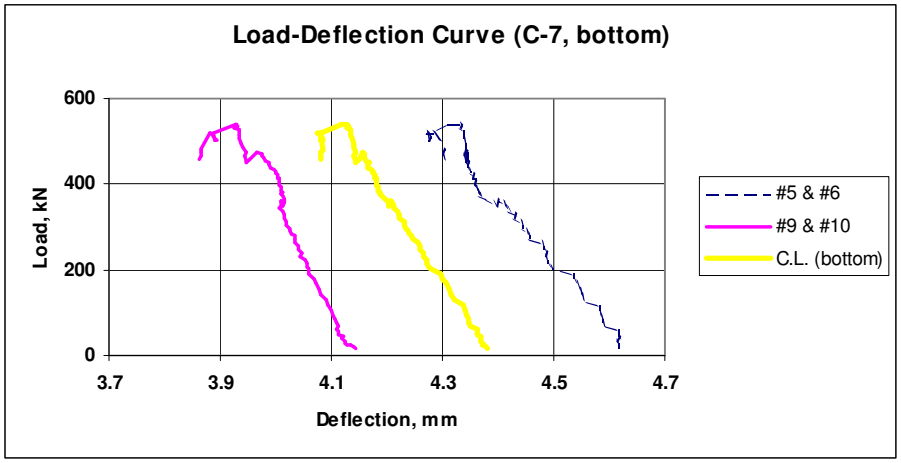

Fig. C.178 Load versus deflection curve (LDS #5 & #6, LDS #9 & #10 and bottom CL)

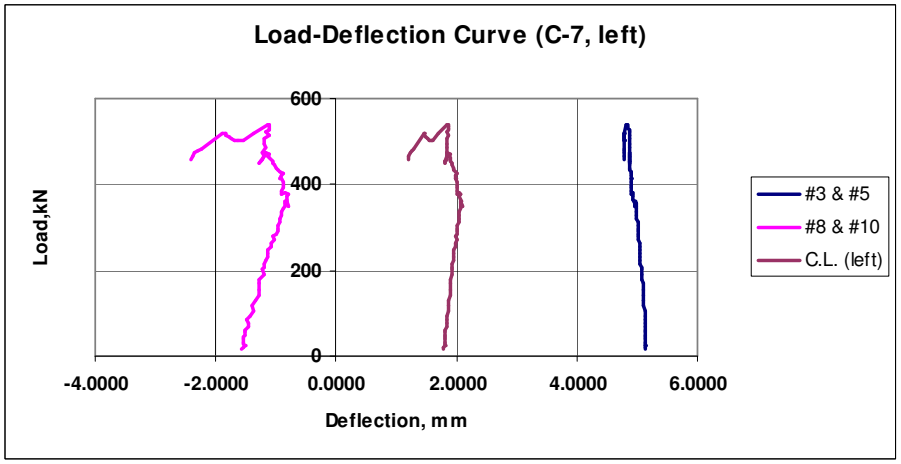

Fig. C.179 Load versus deflection curve (LDS #3 & #5, LDS #8 & #10 and left CL)

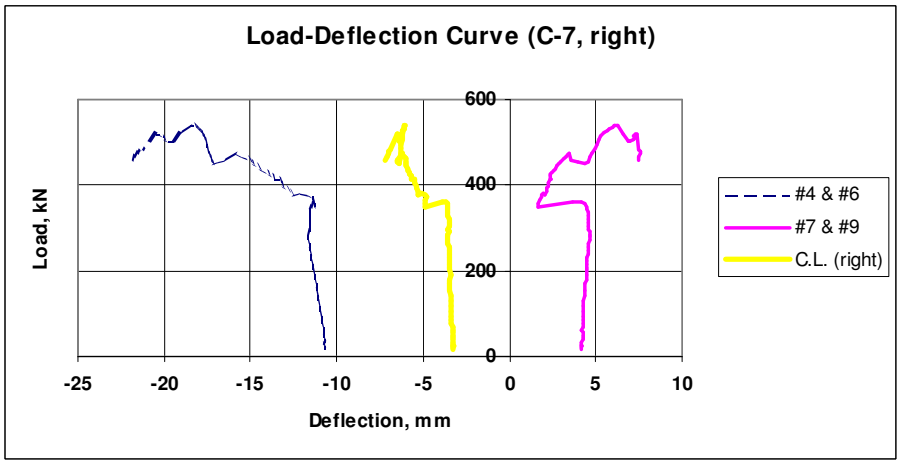

Fig. C.180 Load versus deflection curve (LDS #4 & #6, LDS #7 & #9 and right CL)

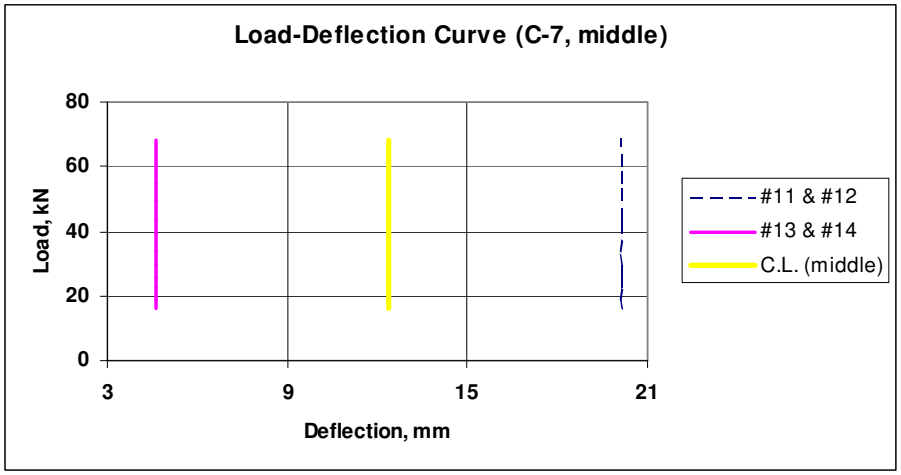

Fig. C.181 Load versus deflection curve (LDS #11 & #12, LDS #13 & #14, middle CL)

3.8 Wall ***C-8***

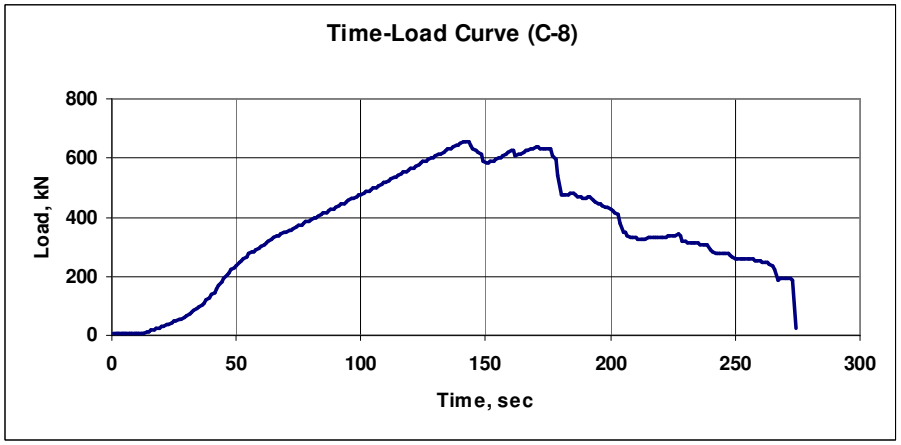

Fig. C.182 Time versus load curve

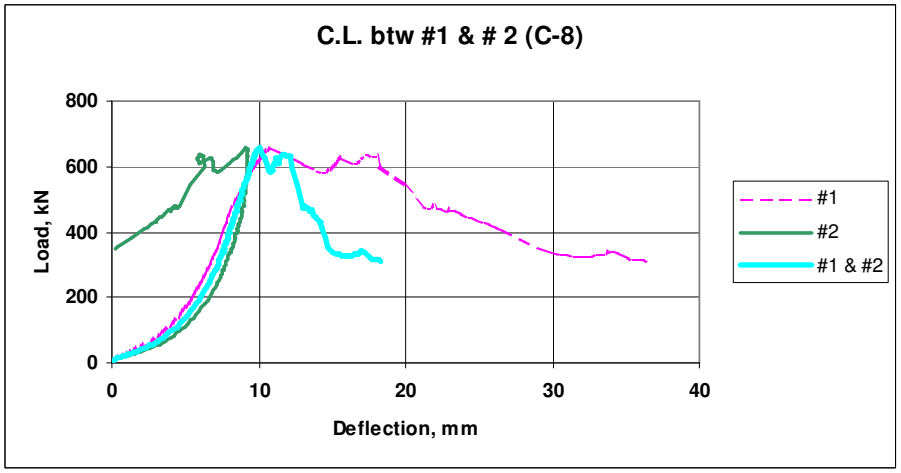

Fig. C.183 Load versus deflection curve (LDS #1, LDS #2 and CL)

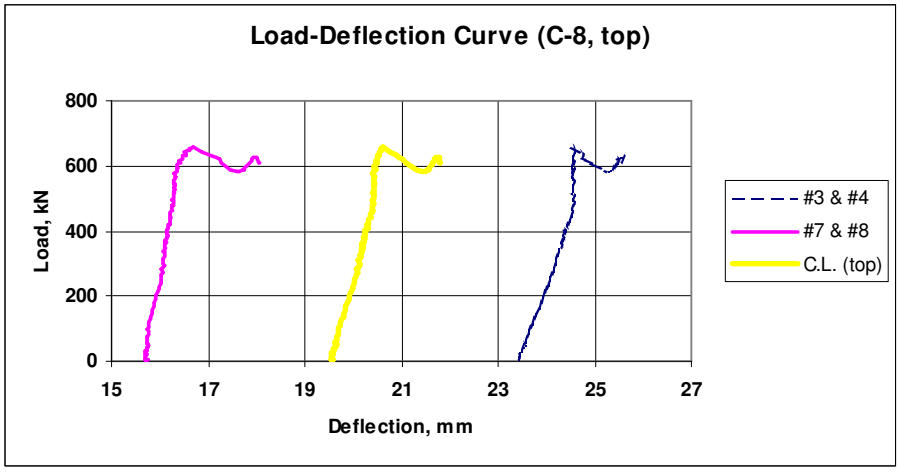

Fig. C.184 Load versus deflection curve (LDS #3 & #4, LDS #7 & #8 and top CL)

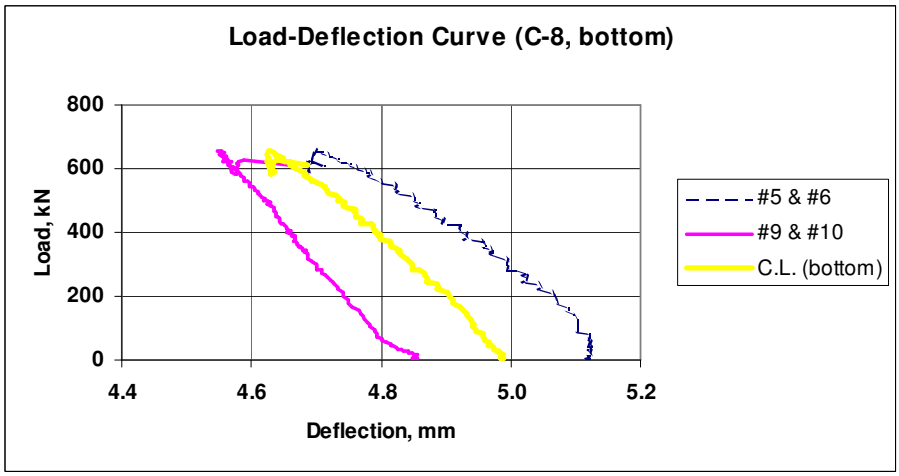

Fig. C.185 Load versus deflection curve (LDS #5 & #6, LDS #9 & #10 and bottom CL)

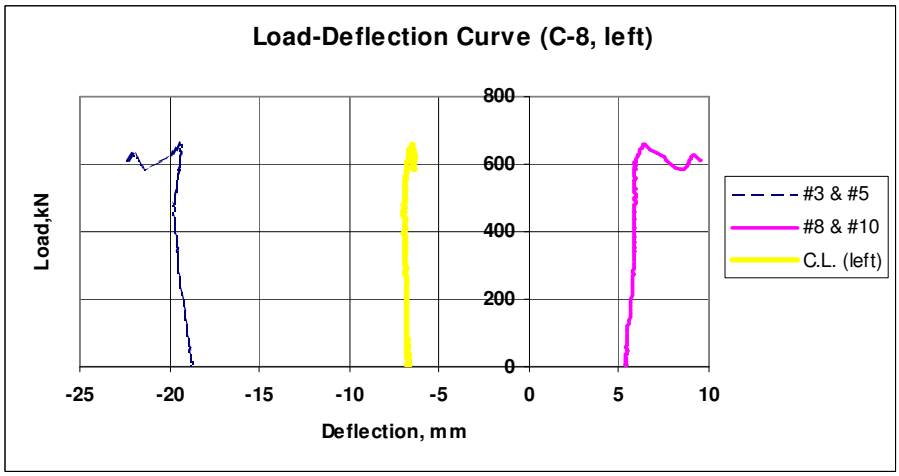

Fig. C.186 Load versus deflection curve (LDS #3 & #5, LDS #8 & #10 and left CL)

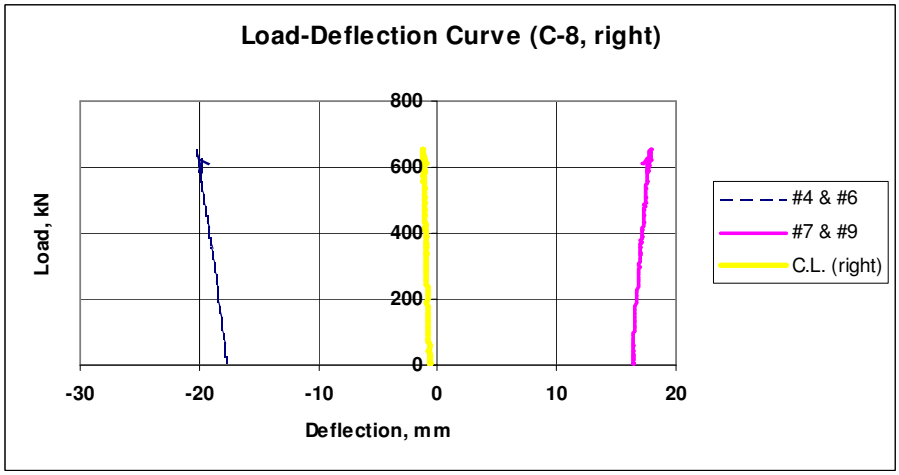

Fig. C.187 Load versus deflection curve (LDS #4 & #6, LDS #7 & #9 and right CL)

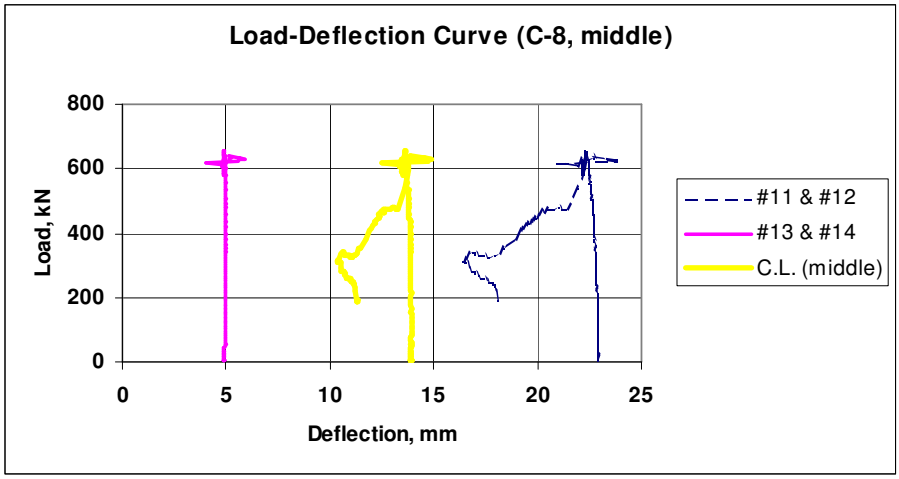

Fig. C.188 Load versus deflection curve (LDS #11 & #12, LDS #13 & #14, middle CL)

3.9 Wall ***C-9***

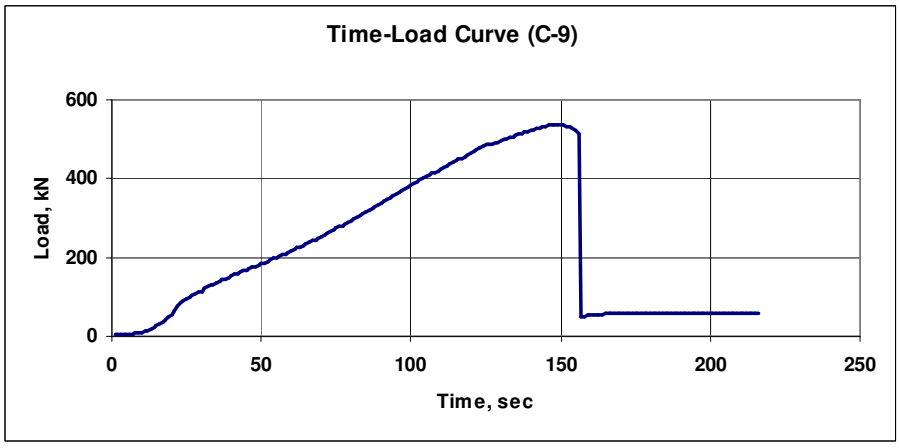

Fig. C.189 Time versus load curve

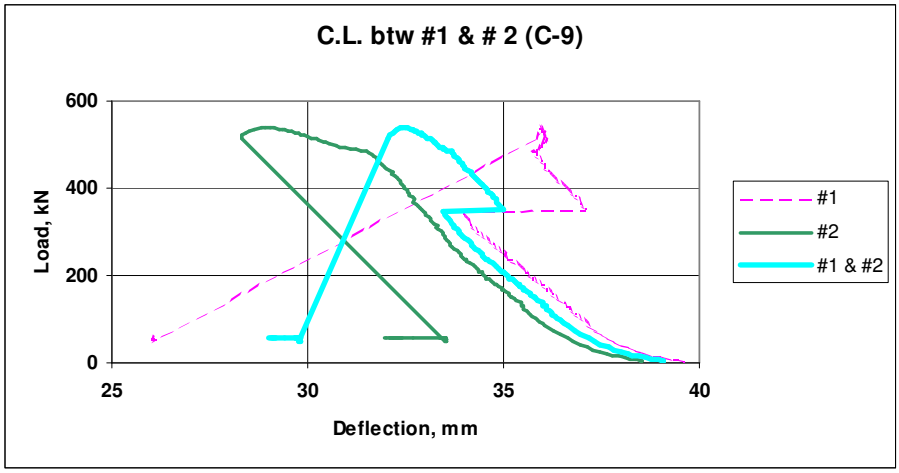

Fig. C.190 Load versus deflection curve (LDS #1, LDS #2 and CL)

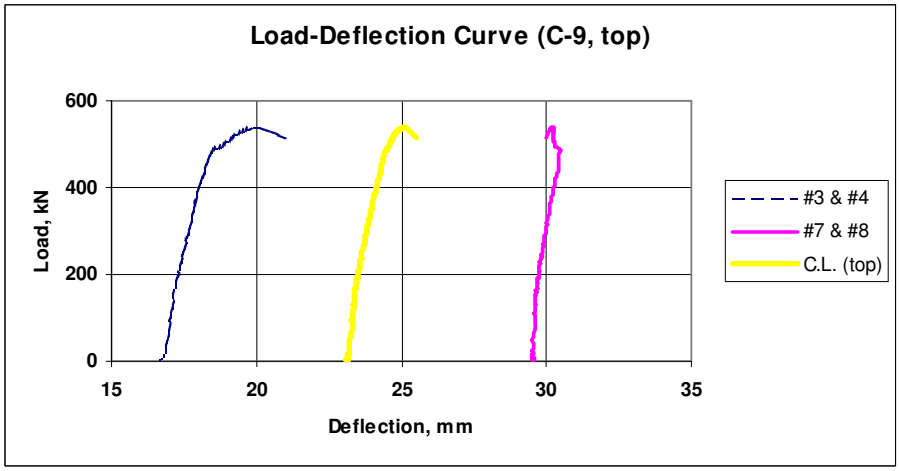

Fig. C.191 Load versus deflection curve (LDS #3 & #4, LDS #7 & #8 and top CL)

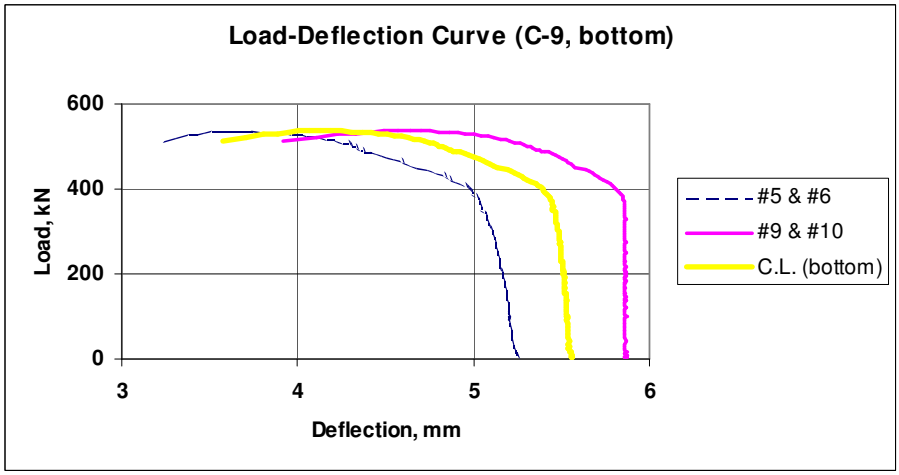

Fig. C.192 Load versus deflection curve (LDS #5 & #6, LDS #9 & #10 and bottom CL)

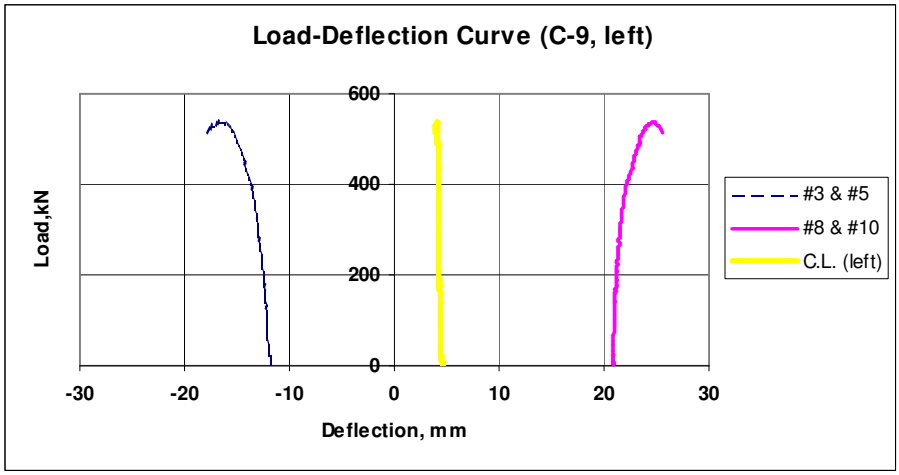

Fig. C.193 Load versus deflection curve (LDS #3 & #5, LDS #8 & #10 and left CL)

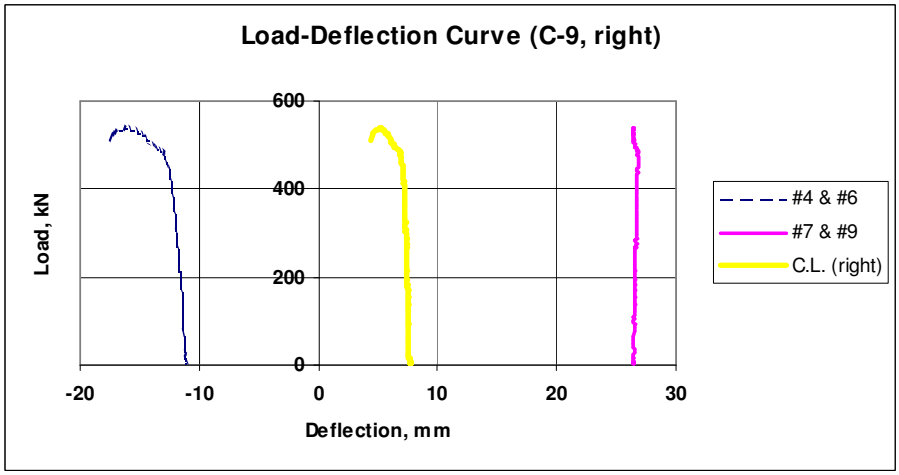

Fig. C.194 Load versus deflection curve (LDS #4 & #6, LDS #7 & #9 and right CL)

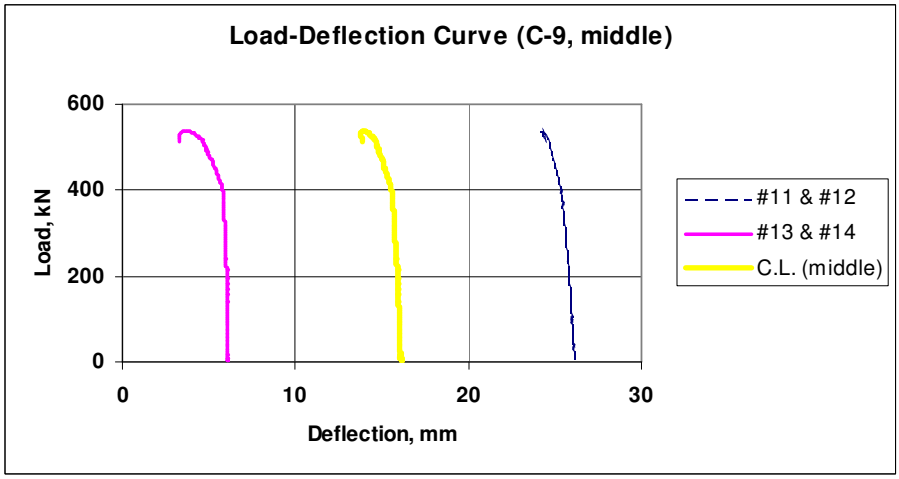

Fig. C.195 Load versus deflection curve (LDS #11 & #12, LDS #13 & #14, middle CL)

3.10 Wall *C-10*

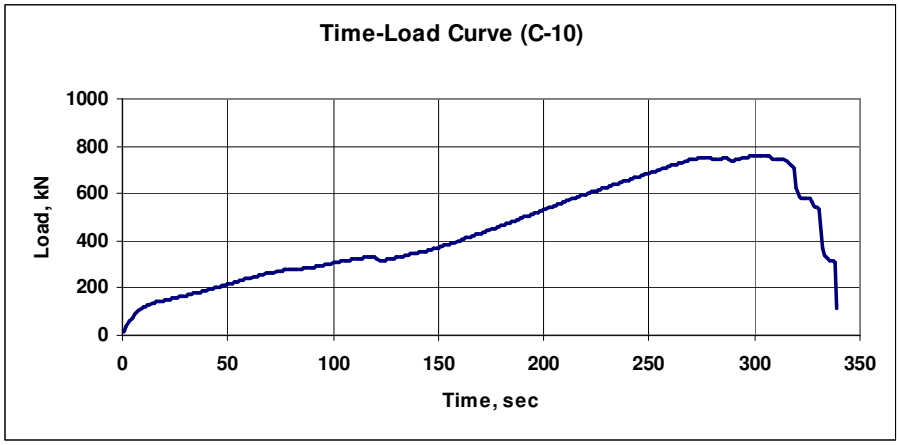

Fig. C.196 Time versus load curve

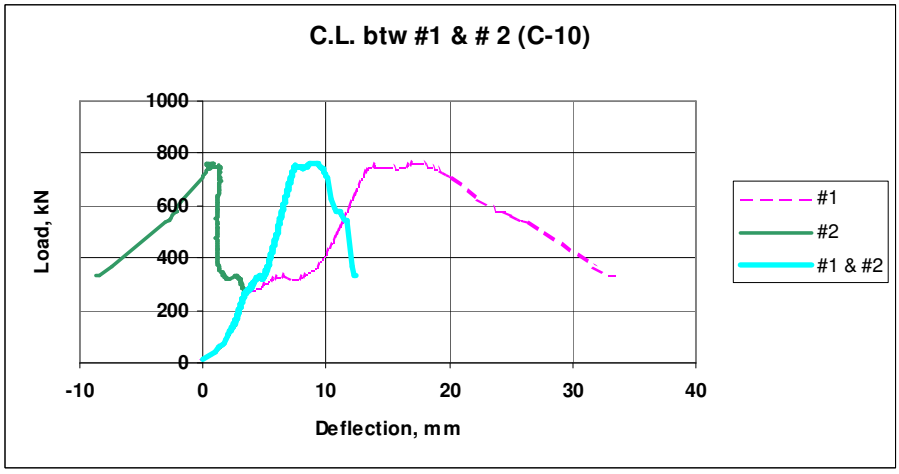

Fig. C.187 Load versus deflection curve (LDS #1, LDS #2 and CL)

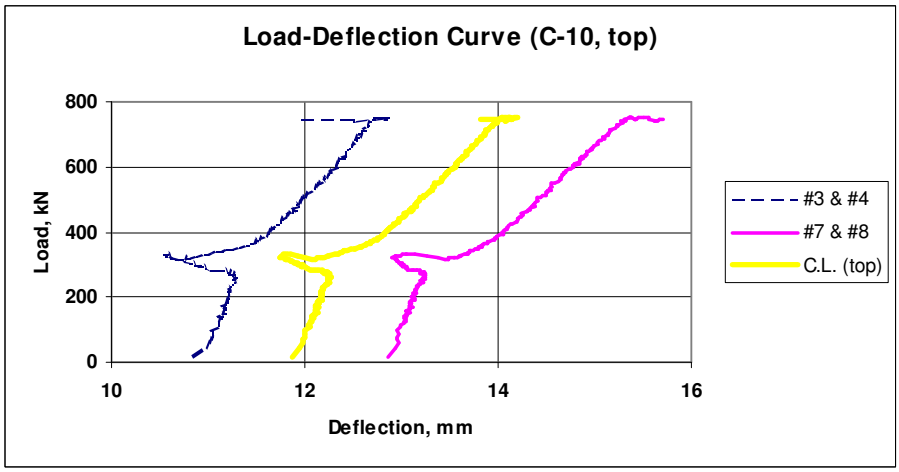

Fig. C.198 Load versus deflection curve (LDS #3 & #4, LDS #7 & #8 and top CL)

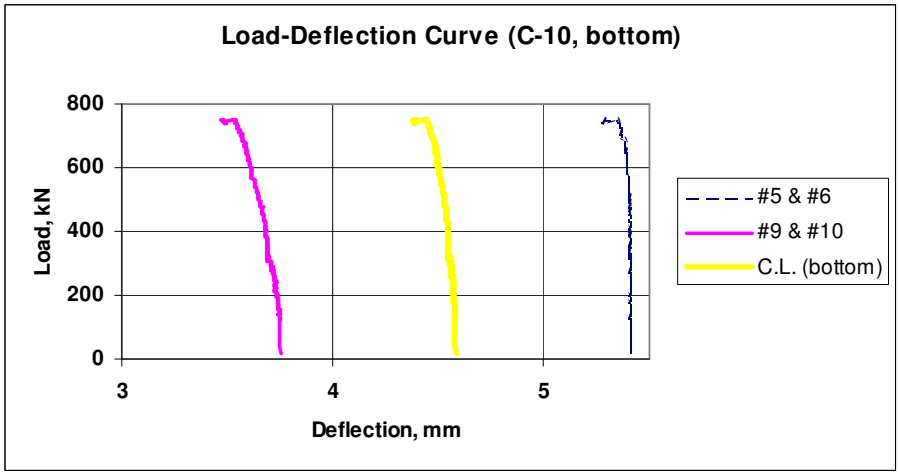

Fig. C.199 Load versus deflection curve (LDS #5 & #6, LDS #9 & #10 and bottom CL)

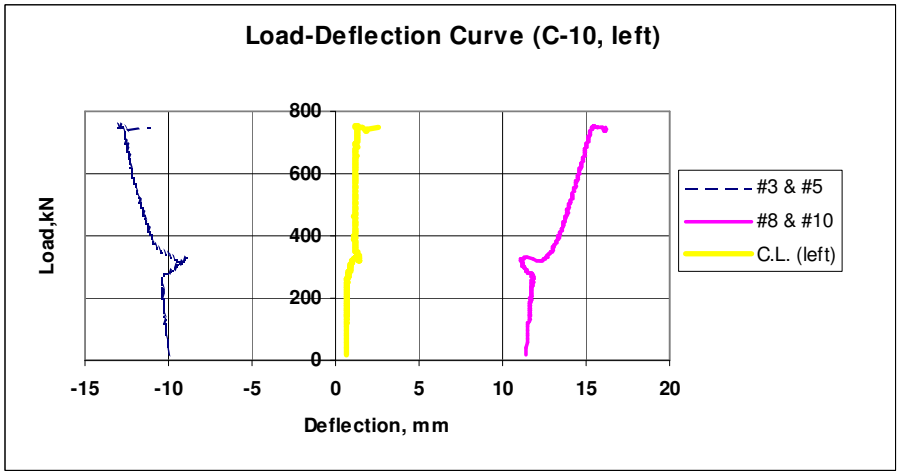

Fig. C.200 Load versus deflection curve (LDS #3 & #5, LDS #8 & #10 and left CL)

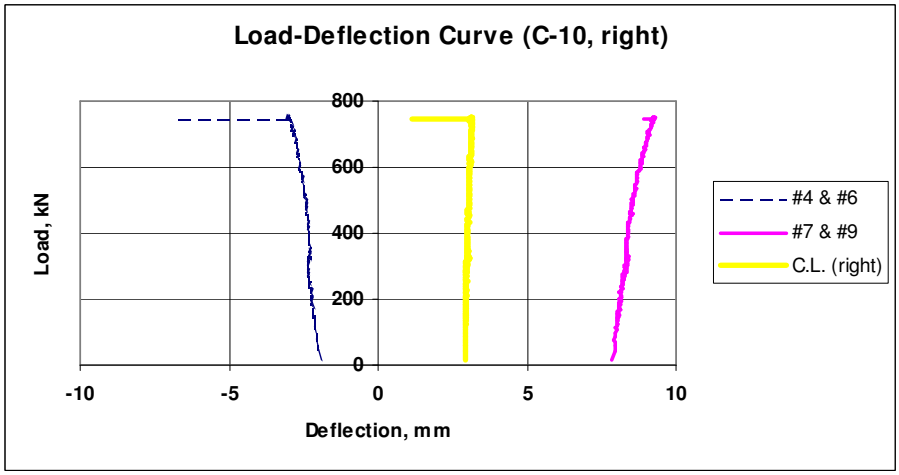

Fig. C.201 Load versus deflection curve (LDS #4 & #6, LDS #7 & #9 and right CL)

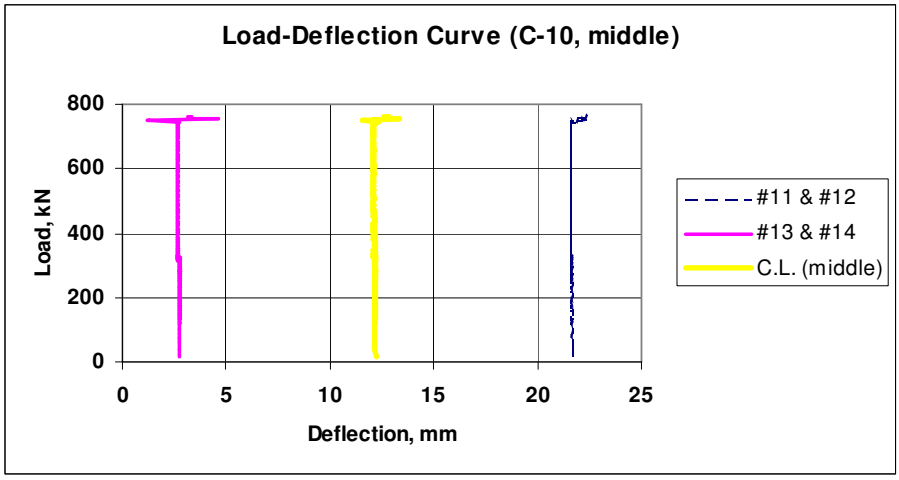

Fig. C.202 Load versus deflection curve (LDS #11 & #12, LDS #13 & #14, middle CL)

APPENDIX D

Stress – Strain Data

This appendix presents sets of important stress-strain curves.

These curves represent the raw data prior to processing. Some of the curves appear to be reversed because the way that LDS's were mounted.

1. Stress versus strain curves for wall specimens of type ***A*** are given in Fig. D.1 to D.39:

- Wall ***A-1***

Fig. D.1 Stress versus strain curve (CL between LDS #1 and LDS #2)
Fig. D.2 Stress versus strain curve (CL between LDS #3 & #5 and LDS #8 & #10)
Fig. D.3 Stress versus strain curve (CL between LDS #4 & #6, LDS #7 & #9)

- Wall ***A-2***

Fig. D.4 Stress versus strain curve (CL between LDS #1 and LDS #2)
Fig. D.5 Stress versus strain curve (CL between LDS #3 & #5 and LDS #8 & #10)
Fig. D.6 Stress versus strain curve (CL between LDS #4 & #6, LDS #7 & #9)
Fig. D.7 Stress versus strain curve (CL between LDS #11 & #12, LDS #13 & #14)

- Wall ***A-3***

Fig. D.8 Stress versus strain curve (CL between LDS #1 and LDS #2)
Fig. D.9 Stress versus strain curve (CL between LDS #3 & #5 and LDS #8 & #10)
Fig. D.10 Stress versus strain curve (CL between LDS #4 & #6, LDS #7 & #9)
Fig. D.11 Stress versus strain curve (CL between LDS #11 & #12, LDS #13 & #14)

- Wall ***A-4***

Fig. D.12 Stress versus strain curve (CL between LDS #1 and LDS #2)
Fig. D.13 Stress versus strain curve (CL between LDS #3 & #5 and LDS #8 & #10)
Fig. D.14 Stress versus strain curve (CL between LDS #4 & #6, LDS #7 & #9)
Fig. D.15 Stress versus strain curve (CL between LDS #11 & #12, LDS #13 & #14)

- Wall ***A-5***

Fig. D.16 Stress versus strain curve (CL between LDS #1 and LDS #2)

Fig. D.17 Stress versus strain curve (CL between LDS #3 & #5 and LDS #8 & #10)
Fig. D.18 Stress versus strain curve (CL between LDS #4 & #6, LDS #7 & #9)
Fig. D.19 Stress versus strain curve (CL between LDS #11 & #12, LDS #13 & #14)

- Wall ***A-6***

Fig. D.20 Stress versus strain curve (CL between LDS #1 and LDS #2)
Fig. D.21 Stress versus strain curve (CL between LDS #3 & #5 and LDS #8 & #10)
Fig. D.22 Stress versus strain curve (CL between LDS #4 & #6, LDS #7 & #9)
Fig. D.23 Stress versus strain curve (CL between LDS #11 & #12, LDS #13 & #14)

- Wall ***A-7***

Fig. D.24 Stress versus strain curve (CL between LDS #1 and LDS #2)
Fig. D.25 Stress versus strain curve (CL between LDS #3 & #5 and LDS #8 & #10)
Fig. D.26 Stress versus strain curve (CL between LDS #4 & #6, LDS #7 & #9)
Fig. D.27 Stress versus strain curve (CL between LDS #11 & #12, LDS #13 & #14)

- Wall ***A-8***

Fig. D.28 Stress versus strain curve (CL between LDS #1 and LDS #2)
Fig. D.29 Stress versus strain curve (CL between LDS #3 & #5 and LDS #8 & #10)
Fig. D.30 Stress versus strain curve (CL between LDS #4 & #6, LDS #7 & #9)
Fig. D.31 Stress versus strain curve (CL between LDS #11 & #12, LDS #13 & #14)

- Wall ***A-9***

Fig. D.32 Stress versus strain curve (CL between LDS #1 and LDS #2)
Fig. D.33 Stress versus strain curve (CL between LDS #3 & #5 and LDS #8 & #10)
Fig. D.34 Stress versus strain curve (CL between LDS #4 & #6, LDS #7 & #9)
Fig. D.35 Stress versus strain curve (CL between LDS #11 & #12, LDS #13 & #14)

- Wall ***A-10***

Fig. D.36 Stress versus strain curve (CL between LDS #1 and LDS #2)
Fig. D.37 Stress versus strain curve (CL between LDS #3 & #5 and LDS #8 & #10)
Fig. D.38 Stress versus strain curve (CL between LDS #4 & #6, LDS #7 & #9)
Fig. D.39 Stress versus strain curve (CL between LDS #11 & #12, LDS #13 & #14)

2. Stress versus strain curves for the wall specimens of type ***B*** are given in Fig. D.40 to Fig. D.75:

- Wall ***B-1***

Fig. D.40 Stress versus strain curve (CL between LDS #1 and LDS #2)
Fig. D.41 Stress versus strain curve (CL between LDS #3 & #5 and LDS #8 & #10)
Fig. D.42 Stress versus strain curve (CL between LDS #4 & #6, LDS #7 & #9)
Fig. D.43 Stress versus strain curve (CL between LDS #11 & #12, LDS #13 & #14)

- Wall ***B-2***

Fig. D.44 Stress versus strain curve (CL between LDS #1 and LDS #2)
Fig. D.45 Stress versus strain curve (CL between LDS #3 & #5 and LDS #8 & #10)
Fig. D.46 Stress versus strain curve (CL between LDS #4 & #6, LDS #7 & #9)
Fig. D.47 Stress versus strain curve (CL between LDS #11 & #12, LDS #13 & #14)

- Wall ***B-3***

Fig. D.48 Stress versus strain curve (CL between LDS #1 and LDS #2)
Fig. D.49 Stress versus strain curve (CL between LDS #3 & #5 and LDS #8 & #10)
Fig. D.50 Stress versus strain curve (CL between LDS #4 & #6, LDS #7 & #9)
Fig. D.51 Stress versus strain curve (CL between LDS #11 & #12, LDS #13 & #14)

- Wall ***B-4***

Fig. D.52 Stress versus strain curve (CL between LDS #1 and LDS #2)
Fig. D.53 Stress versus strain curve (CL between LDS #3 & #5 and LDS #8 & #10)
Fig. D.54 Stress versus strain curve (CL between LDS #4 & #6, LDS #7 & #9)
Fig. D.55 Stress versus strain curve (CL between LDS #11 & #12, LDS #13 & #14)

- Wall ***B-5***

Fig. D.56 Stress versus strain curve (CL between LDS #1 and LDS #2)
Fig. D.57 Stress versus strain curve (CL between LDS #3 & #5 and LDS #8 & #10)
Fig. D.58 Stress versus strain curve (CL between LDS #4 & #6, LDS #7 & #9)
Fig. D.59 Stress versus strain curve (CL between LDS #11 & #12, LDS #13 & #14)

- Wall ***B-6***

Fig. D.60 Stress versus strain curve (CL between LDS #1 and LDS #2)
Fig. D.61 Stress versus strain curve (CL between LDS #3 & #5 and LDS #8 & #10)
Fig. D.62 Stress versus strain curve (CL between LDS #4 & #6, LDS #7 & #9)
Fig. D.63 Stress versus strain curve (CL between LDS #11 & #12, LDS #13 & #14)

- Wall ***B-7***

There is no data available for wall test specimens ***B-7*** – the load cell was broken.

- Wall ***B-8***

Fig. D.64 Stress versus strain curve (CL between LDS #1 and LDS #2)
Fig. D.65 Stress versus strain curve (CL between LDS #3 & #5 and LDS #8 & #10)
Fig. D.66 Stress versus strain curve (CL between LDS #4 & #6, LDS #7 & #9)
Fig. D.67 Stress versus strain curve (CL between LDS #11 & #12, LDS #13 & #14)

- Wall ***B-9***

Fig. D.68 Stress versus strain curve (CL between LDS #1 and LDS #2)
Fig. D.69 Stress versus strain curve (CL between LDS #3 & #5 and LDS #8 & #10)
Fig. D.70 Stress versus strain curve (CL between LDS #4 & #6, LDS #7 & #9)
Fig. D.71 Stress versus strain curve (CL between LDS #11 & #12, LDS #13 & #14)

- Wall ***B-10***

Fig. D.72 Stress versus strain curve (CL between LDS #1 and LDS #2)
Fig. D.73 Stress versus strain curve (CL between LDS #3 & #5 and LDS #8 & #10)
Fig. D.74 Stress versus strain curve (CL between LDS #4 & #6, LDS #7 & #9)
Fig. D.75 Stress versus strain curve (CL between LDS #11 & #12, LDS #13 & #14)

3. Stress versus strain curves for the wall specimens of type ***C*** are given in Fig. D.76 to Fig. D.115:

- Wall ***C-1***

Fig. D.76 Stress versus strain curve (CL between LDS #1 and LDS #2)
Fig. D.77 Stress versus strain curve (CL between LDS #3 & #5 and LDS #8 & #10)
Fig. D.78 Stress versus strain curve (CL between LDS #4 & #6, LDS #7 & #9)
Fig. D.79 Stress versus strain curve (CL between LDS #11 & #12, LDS #13 & #14)

- Wall ***C-2***

Fig. D.80 Stress versus strain curve (CL between LDS #1 and LDS #2)
Fig. D.81 Stress versus strain curve (CL between LDS #3 & #5 and LDS #8 & #10)
Fig. D.82 Stress versus strain curve (CL between LDS #4 & #6, LDS #7 & #9)
Fig. D.83 Stress versus strain curve (CL between LDS #11 & #12, LDS #13 & #14)

- Wall ***C-3***

Fig. D.84 Stress versus strain curve (CL between LDS #1 and LDS #2)
Fig. D.85 Stress versus strain curve (CL between LDS #3 & #5 and LDS #8 & #10)
Fig. D.86 Stress versus strain curve (CL between LDS #4 & #6, LDS #7 & #9)
Fig. D.87 Stress versus strain curve (CL between LDS #11 & #12, LDS #13 & #14)

- Wall ***C-4***

Fig. D.88 Stress versus strain curve (CL between LDS #1 and LDS #2)
Fig. D.89 Stress versus strain curve (CL between LDS #3 & #5 and LDS #8 & #10)
Fig. D.90 Stress versus strain curve (CL between LDS #4 & #6, LDS #7 & #9)
Fig. D.91 Stress versus strain curve (CL between LDS #11 & #12, LDS #13 & #14)

- Wall ***C-5***

Fig. D.92 Stress versus strain curve (CL between LDS #1 and LDS #2)
Fig. D.93 Stress versus strain curve (CL between LDS #3 & #5 and LDS #8 & #10)
Fig. D.94 Stress versus strain curve (CL between LDS #4 & #6, LDS #7 & #9)
Fig. D.95 Stress versus strain curve (CL between LDS #11 & #12, LDS #13 & #14)

- Wall ***C-6***

Fig. D.96 Stress versus strain curve (CL between LDS #1 and LDS #2)
Fig. D.97 Stress versus strain curve (CL between LDS #3 & #5 and LDS #8 & #10)
Fig. D.98 Stress versus strain curve (CL between LDS #4 & #6, LDS #7 & #9)
Fig. D.99 Stress versus strain curve (CL between LDS #11 & #12, LDS #13 & #14)

- Wall ***C-7***

- Wall ***C-8***

- Wall ***C-9***

- Wall ***C-10***

1. Wall specimens type *A*

1.1 Wall *A-1*

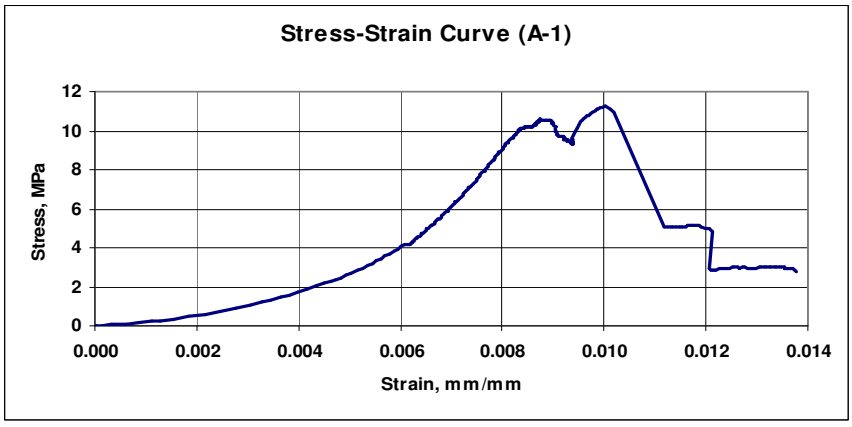

Fig. D.1 Stress versus Strain curve (CL between LDS #1 and LDS #2)

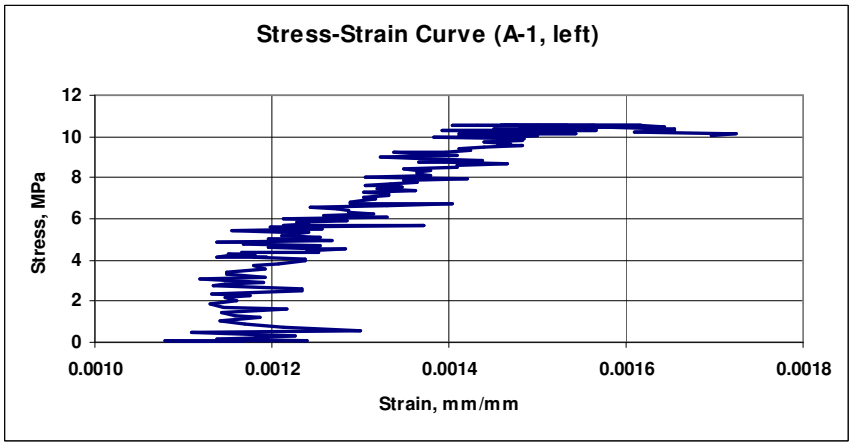

Fig. D.2 Stress versus Strain curve (CL between LDS #3&5 and LDS #8&10)

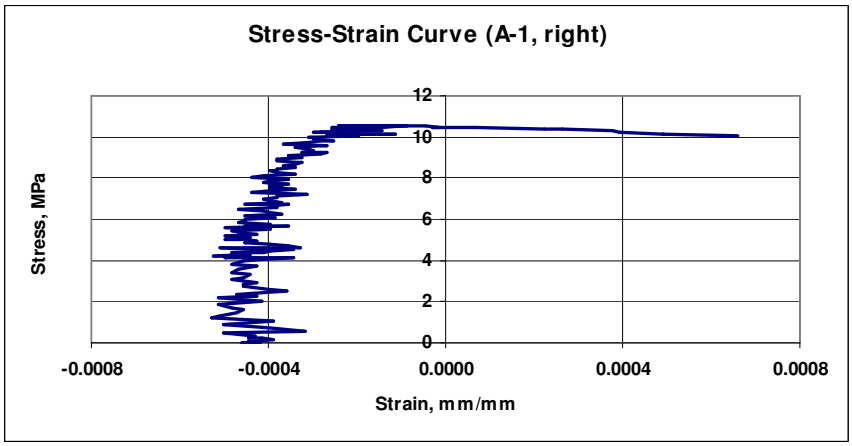

Fig. D.3 Stress versus Strain curve (CL between LDS #4&6 and LDS #7&9)

1.2 Wall ***A-2***

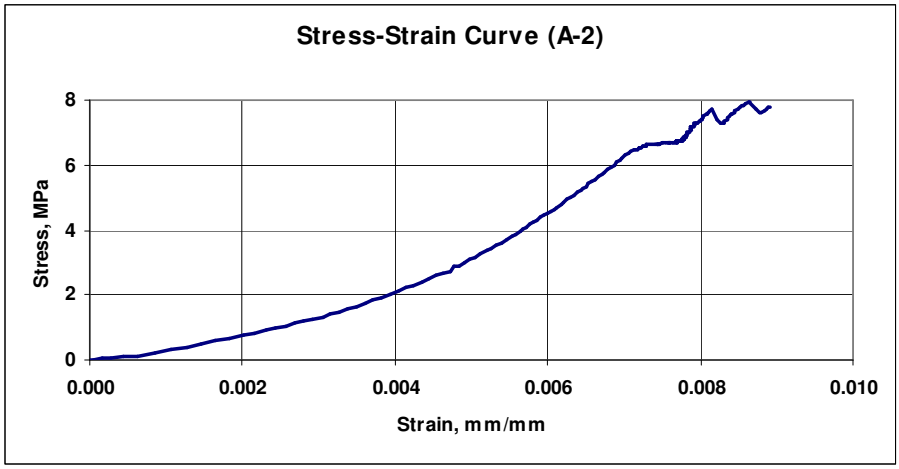

Fig. D.4 Stress versus Strain curve (CL between LDS #1 and LDS #2)

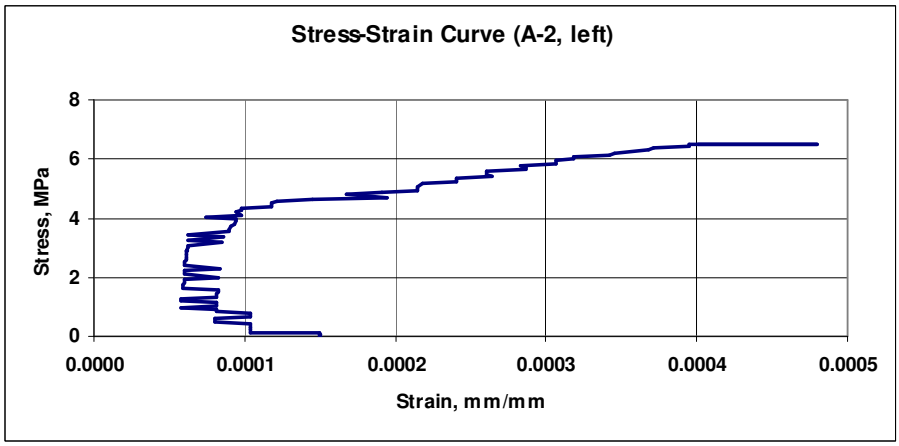

Fig. D.5 Stress versus Strain curve (CL between LDS #3&5 and LDS #8&10)

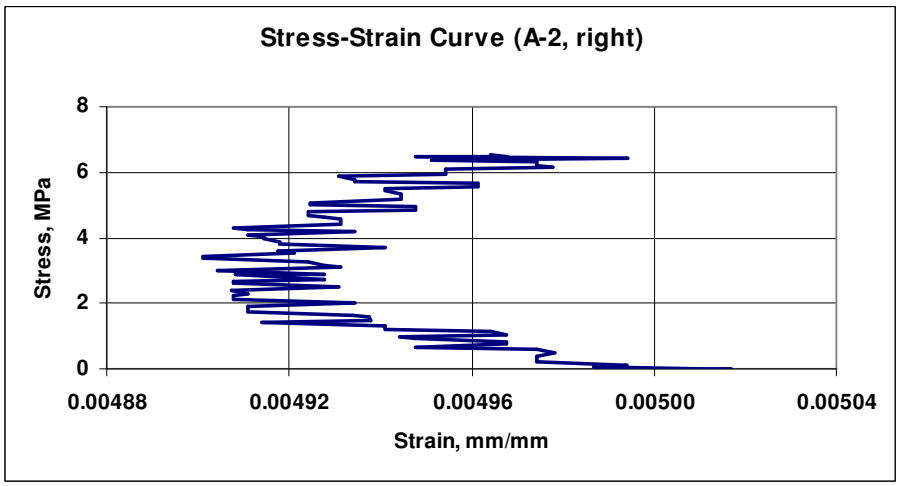

Fig. D.6 Stress versus Strain curve (CL between LDS #4&6 and LDS #7&9)

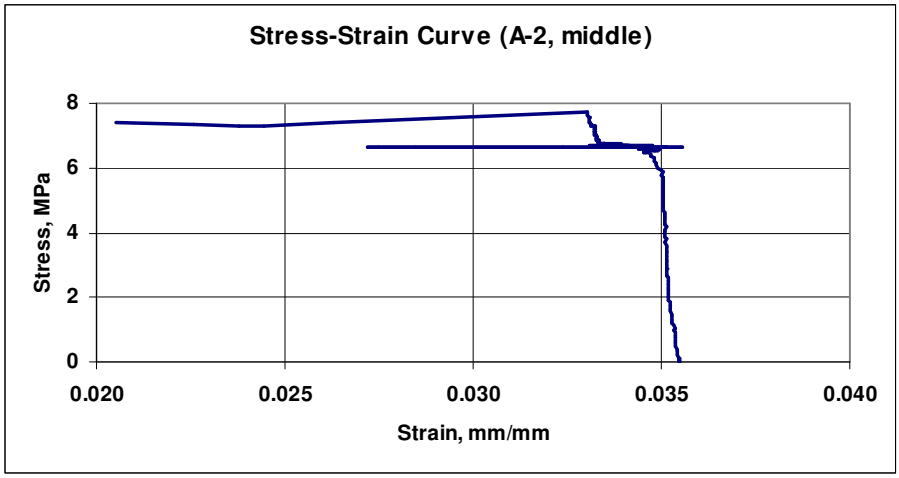

Fig. D.7 Stress versus Strain curve (CL between LDS #11&12 and LDS #13&14)

1.3 Wall ***A-3***

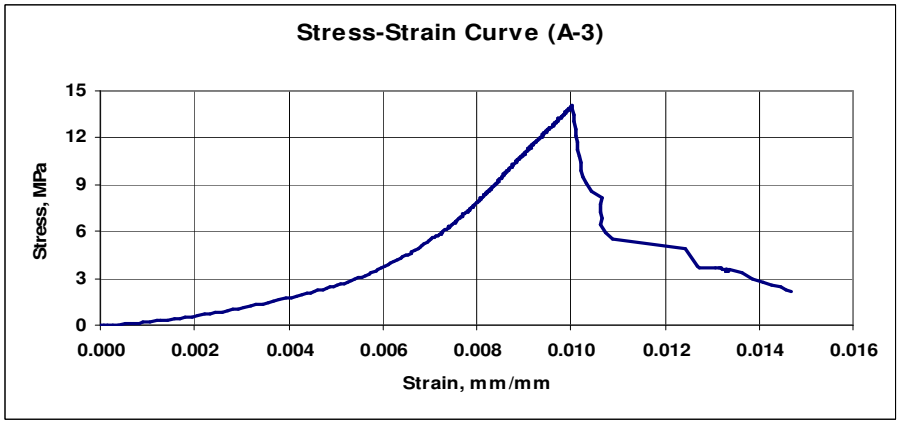

Fig. D.8 Stress versus Strain curve (CL between LDS #1 and LDS #2)

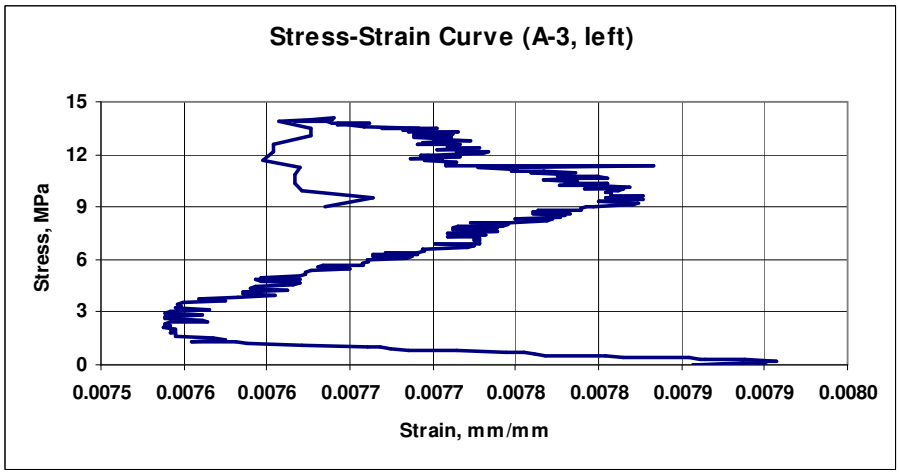

Fig. D.9 Stress versus Strain curve (CL between LDS #3&5 and LDS #8&10)

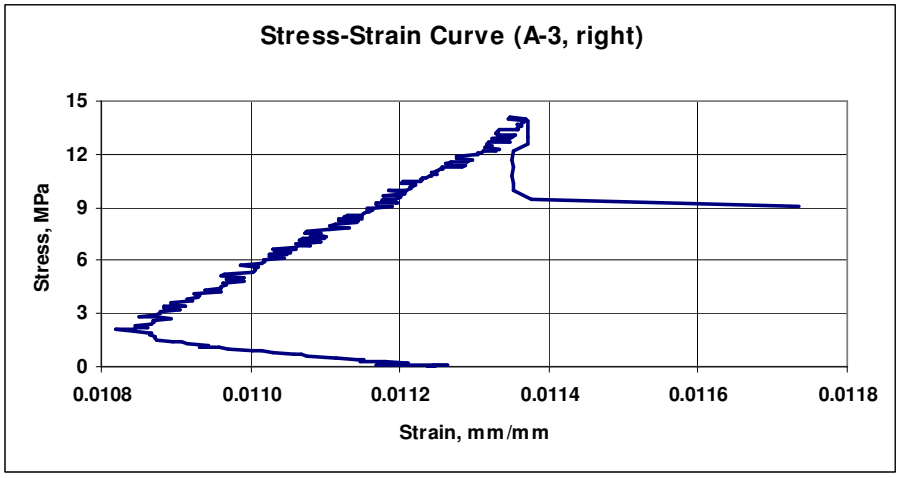

Fig. D.10 Stress versus Strain curve (CL between LDS #4&6 and LDS #7&9)

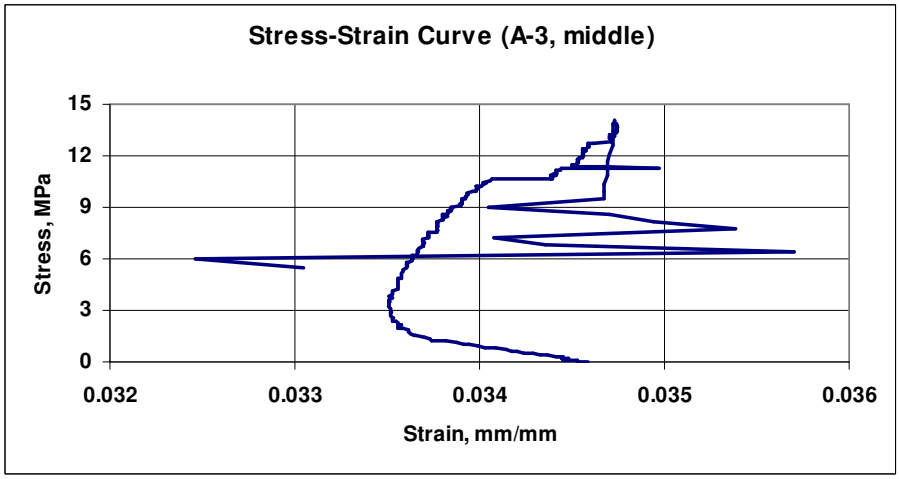

Fig. D.11 Stress versus Strain curve (CL between LDS #11&12 and LDS #13&14)

1.4 Wall ***A-4***

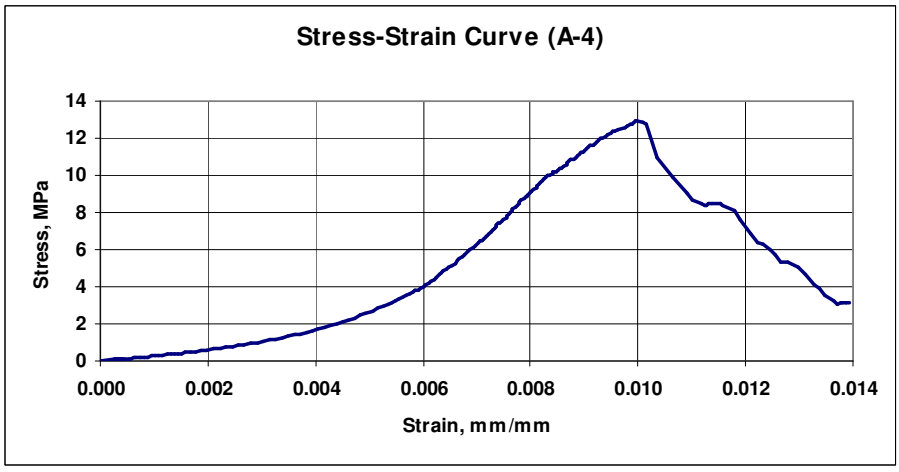

Fig. D.12 Stress versus Strain curve (CL between LDS #1 and LDS #2)

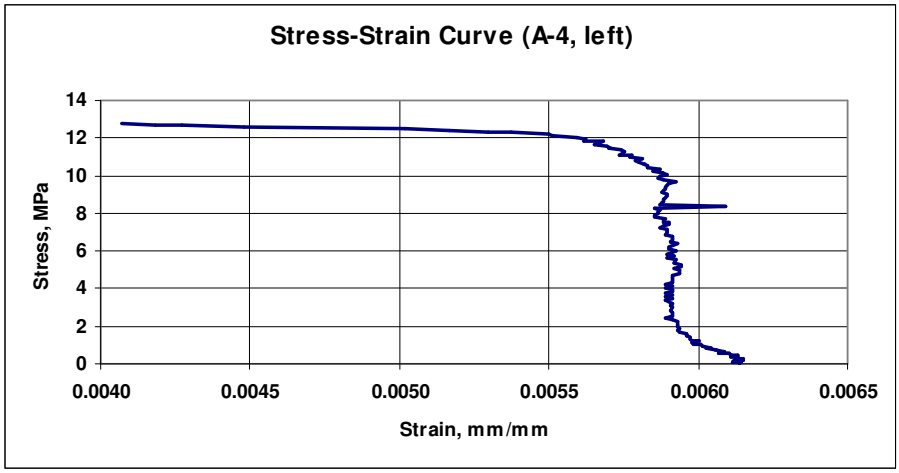

Fig. D.13 Stress versus Strain curve (CL between LDS #3&5 and LDS #8&10)

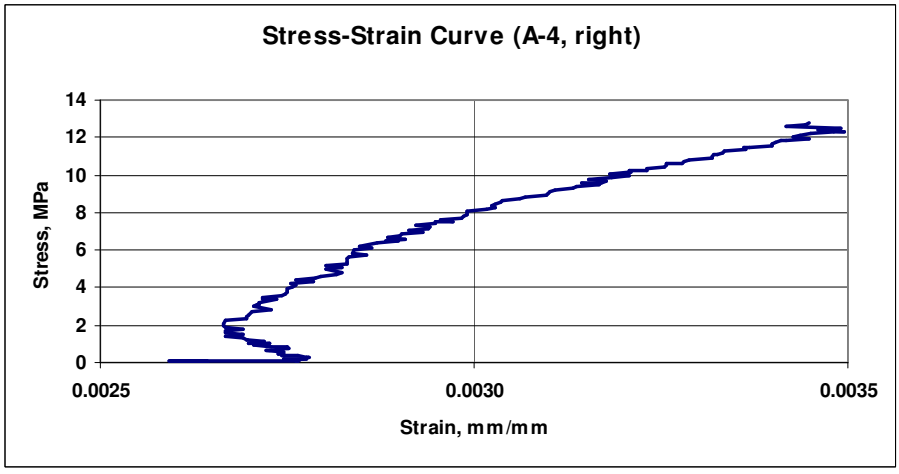

Fig. D.14 Stress versus Strain curve (CL between LDS #4&6 and LDS #7&9)

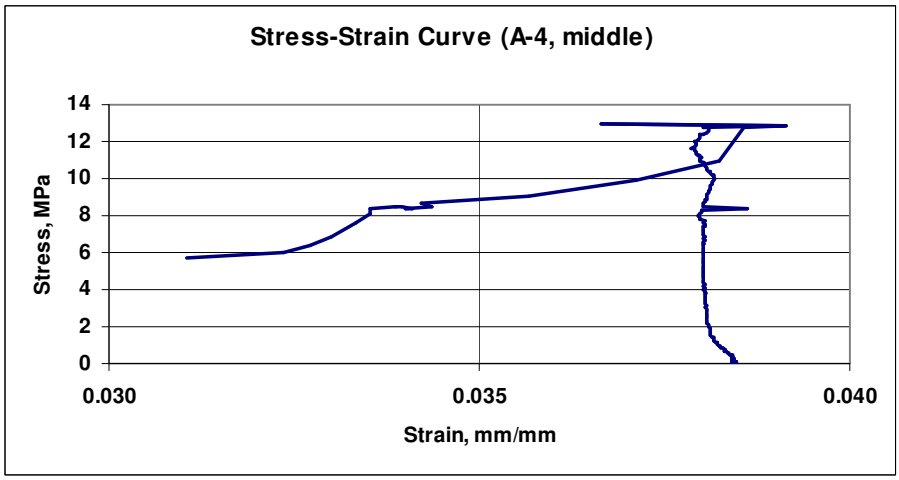

Fig. D.15 Stress versus Strain curve (CL between LDS #11&12 and LDS #13&14)

1.5 Wall ***A-5***

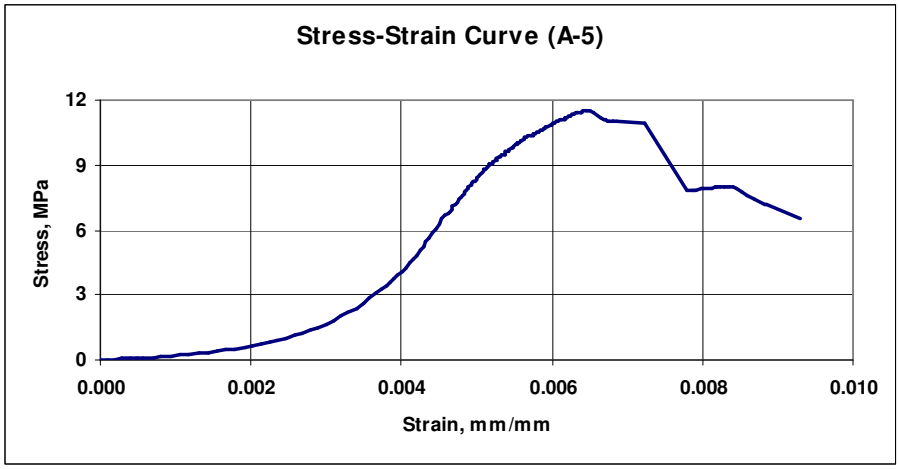

Fig. D.16 Stress versus Strain curve (CL between LDS #1 and LDS #2)

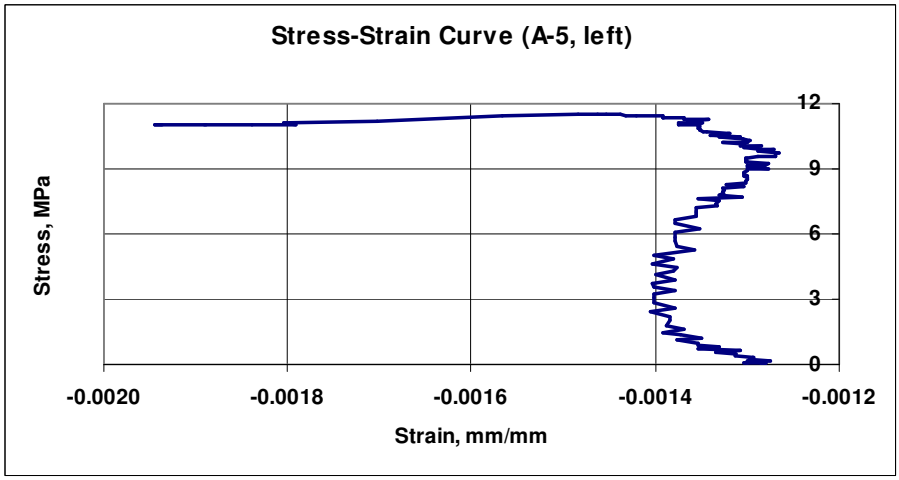

Fig. D.17 Stress versus Strain curve (CL between LDS #3&5 and LDS #8&10)

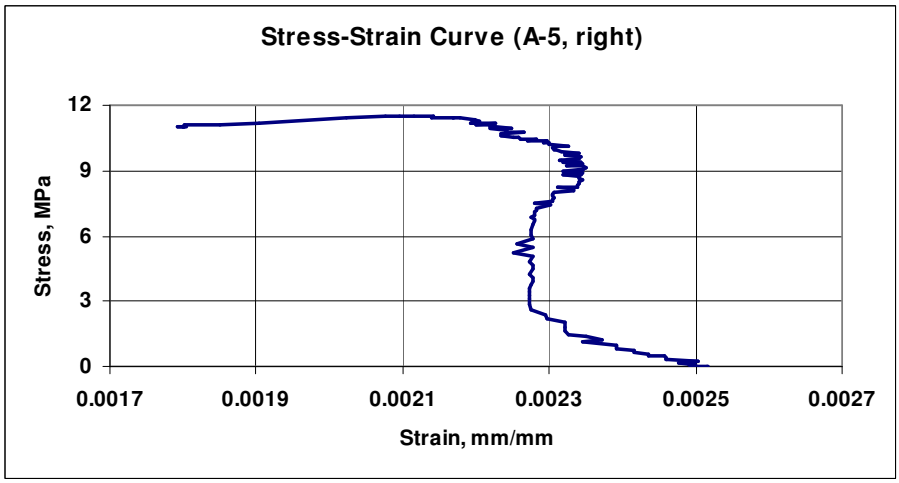

Fig. D.18 Stress versus Strain curve (CL between LDS #4&6 and LDS #7&9)

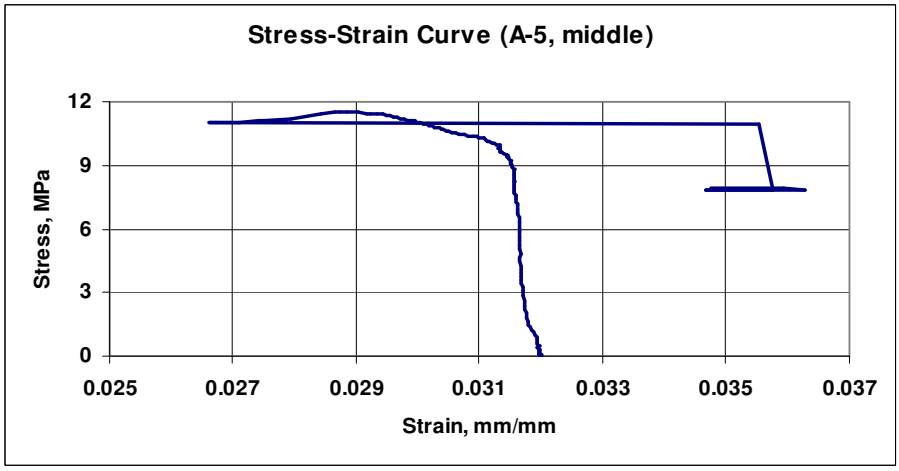

Fig. D.19 Stress versus Strain curve (CL between LDS #11&12 and LDS #13&14)

1.6 Wall ***A-6***

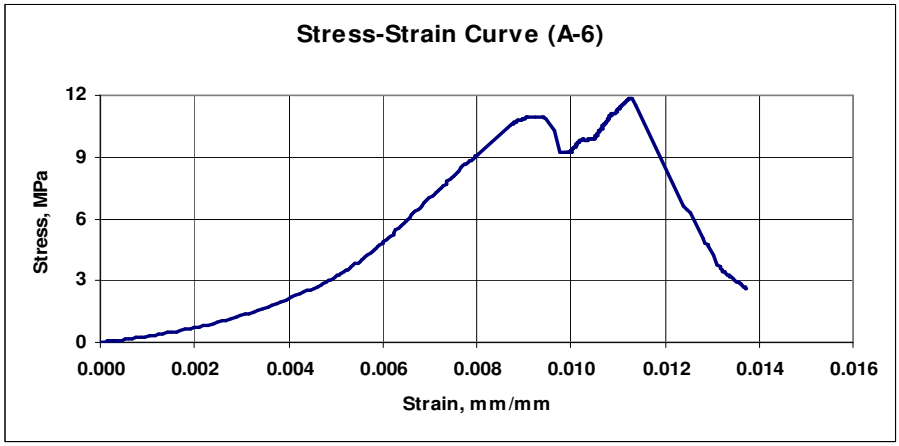

Fig. D.20 Stress versus Strain curve (CL between LDS #1 and LDS #2)

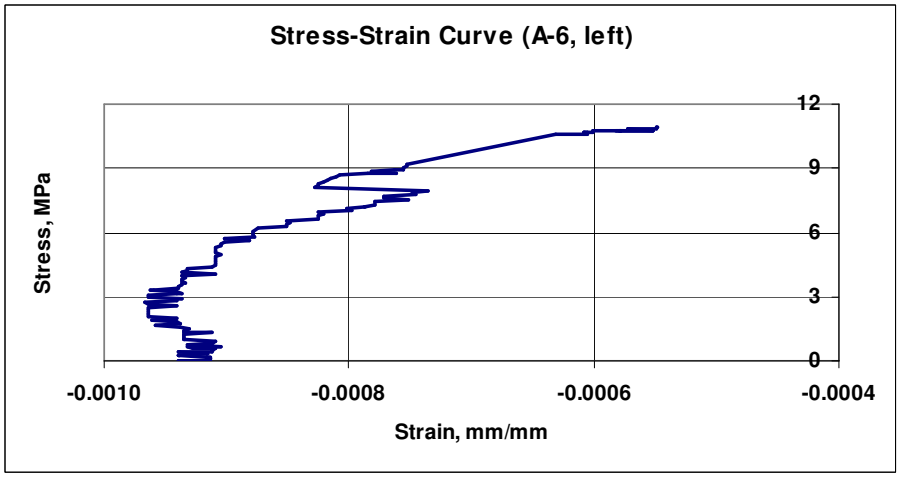

Fig. D.21 Stress versus Strain curve (CL between LDS #3&5 and LDS #8&10)

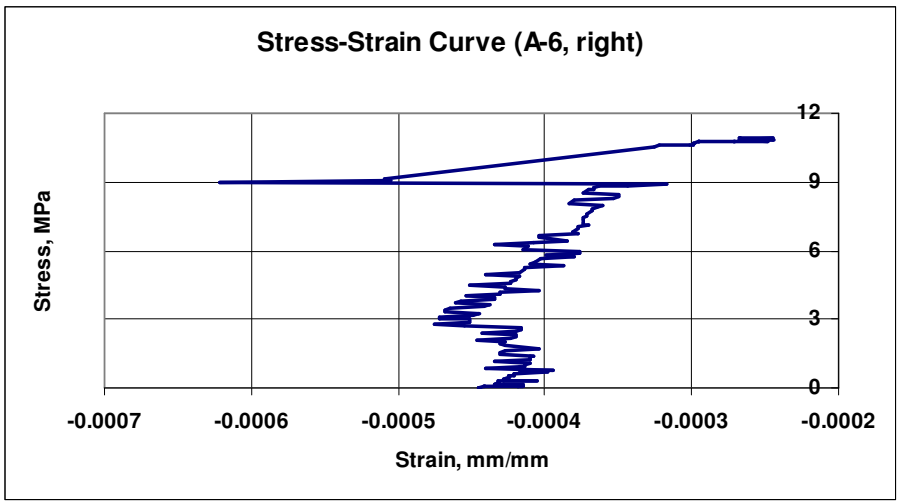

Fig. D.22 Stress versus Strain curve (CL between LDS #4&6 and LDS #7&9)

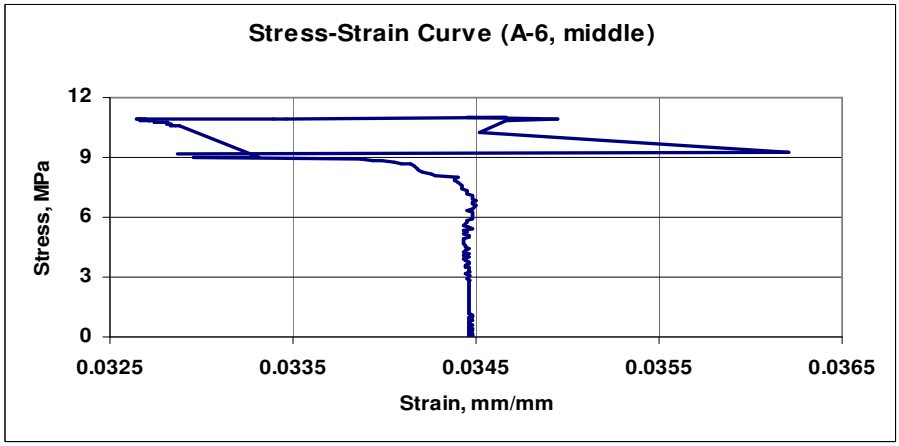

Fig. D.23 Stress versus Strain curve (CL between LDS #11&12 and LDS #13&14)

1.7 Wall ***A-7***

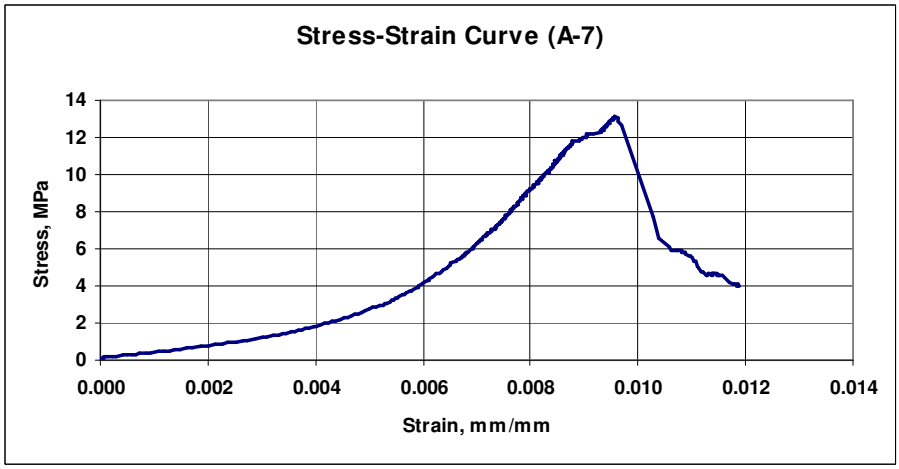

Fig. D.24 Stress versus Strain curve (CL between LDS #1 and LDS #2)

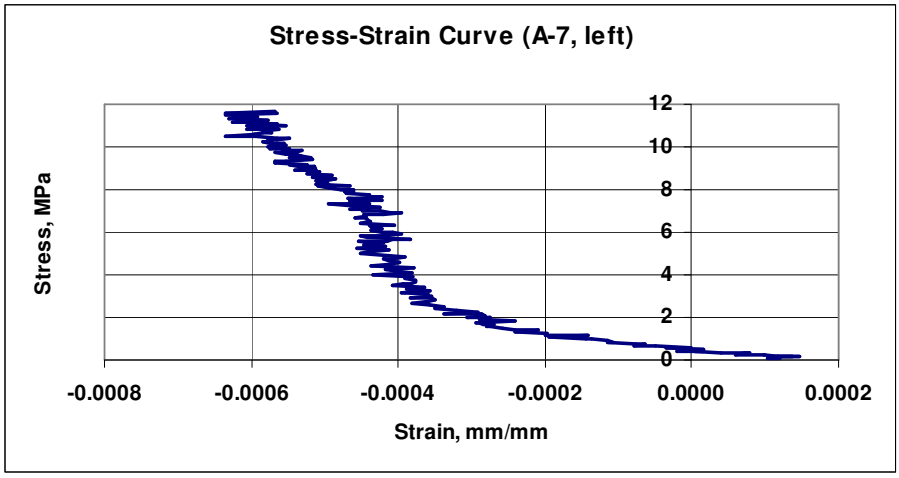

Fig. D.25 Stress versus Strain curve (CL between LDS #3&5 and LDS #8&10)

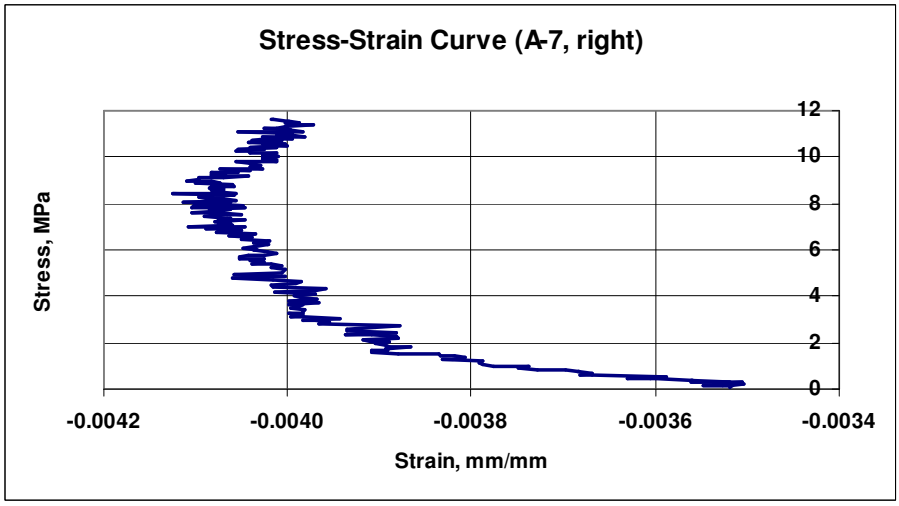

Fig. D.26 Stress versus Strain curve (CL between LDS #4&6 and LDS #7&9)

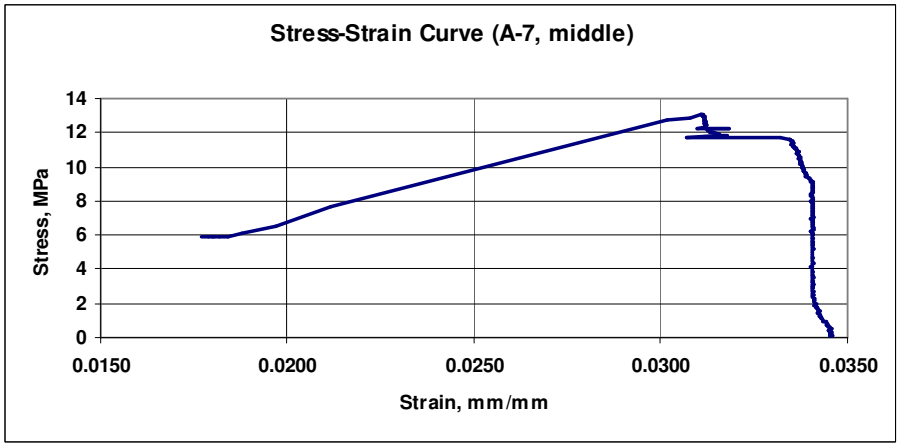

Fig. D.27 Stress versus Strain curve (CL between LDS #11&12 and LDS #13&14)

1.8 Wall ***A-8***

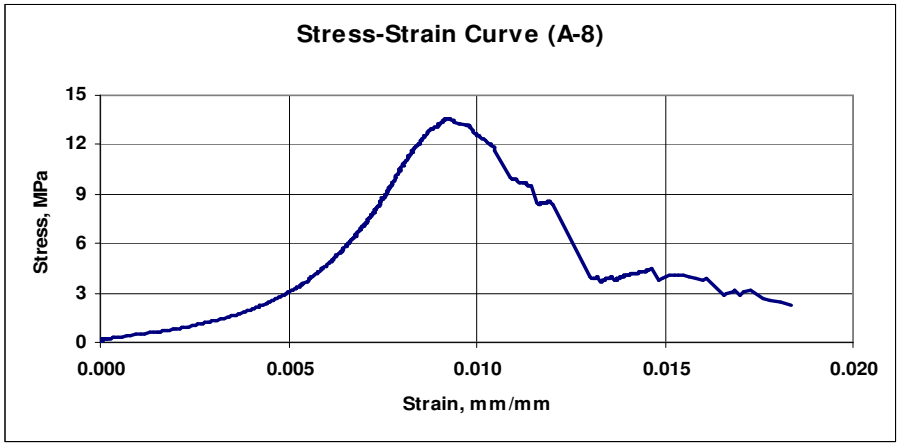

Fig. D.28 Stress versus Strain curve (CL between LDS #1 and LDS #2)

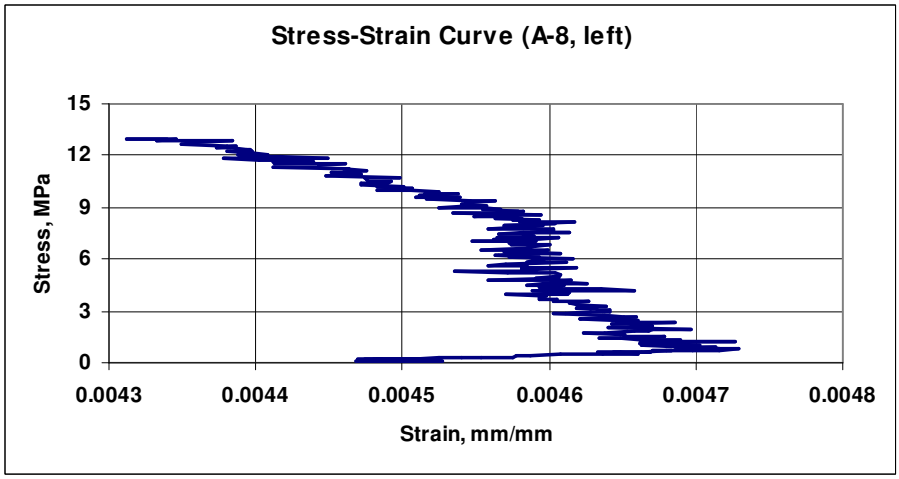

Fig. D.29 Stress versus Strain curve (CL between LDS #3&5 and LDS #8&10)

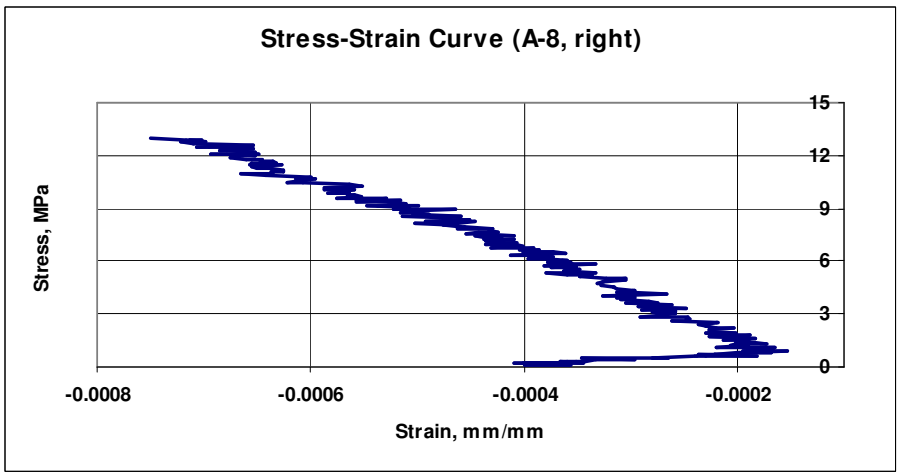

Fig. D.30 Stress versus Strain curve (CL between LDS #4&6 and LDS #7&9)

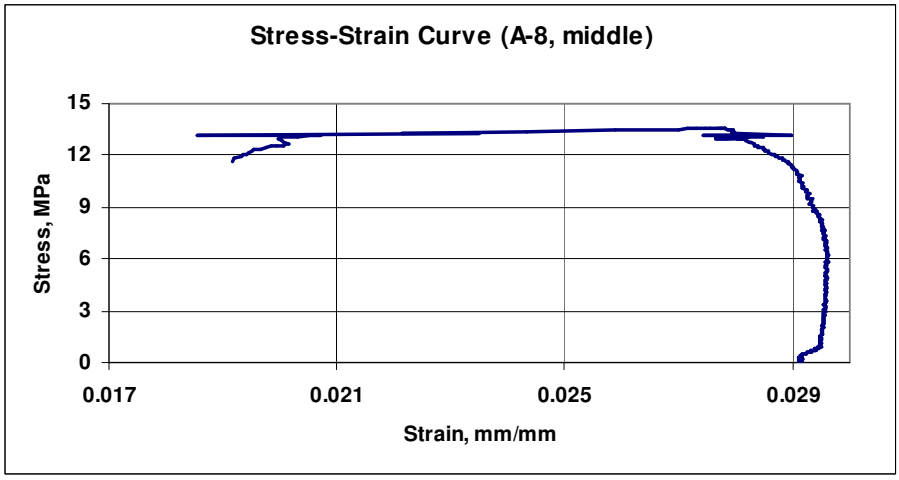

Fig. D.31 Stress versus Strain curve (CL between LDS #11&12 and LDS #13&14)

1.9 Wall ***A-9***

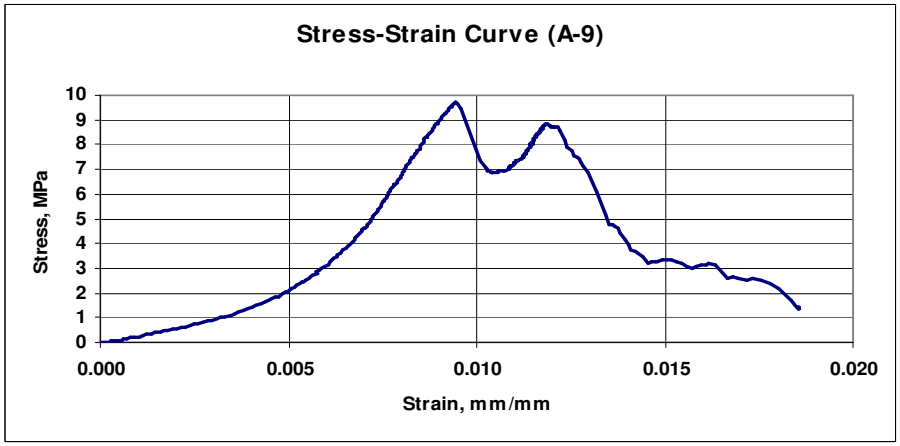

Fig. D.32 Stress versus Strain curve (CL between LDS #1 and LDS #2)

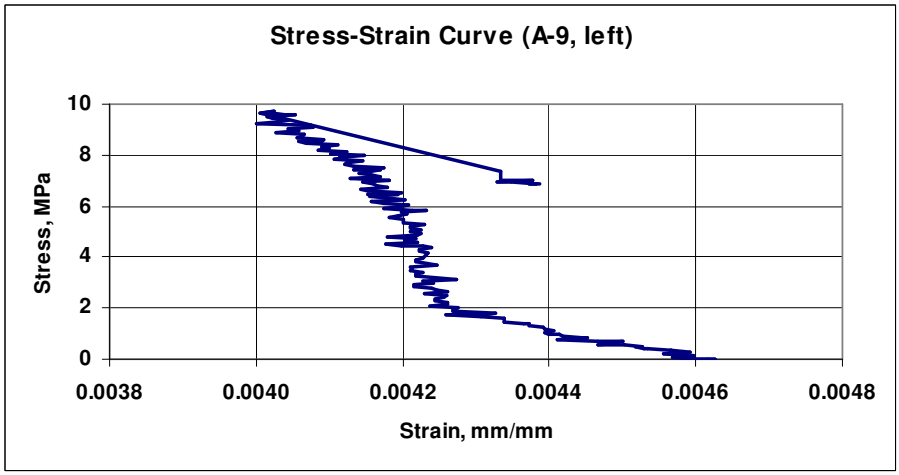

Fig. D.33 Stress versus Strain curve (CL between LDS #3&5 and LDS #8&10)

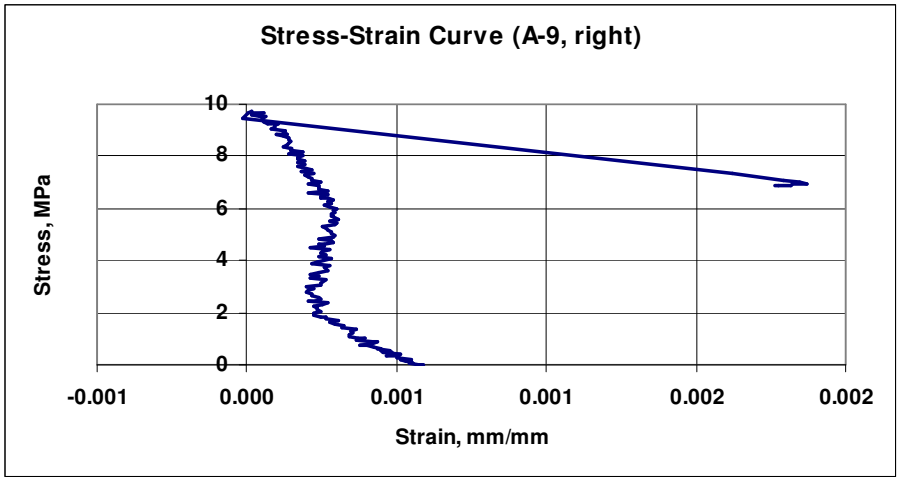

Fig. D.34 Stress versus Strain curve (CL between LDS #4&6 and LDS #7&9)

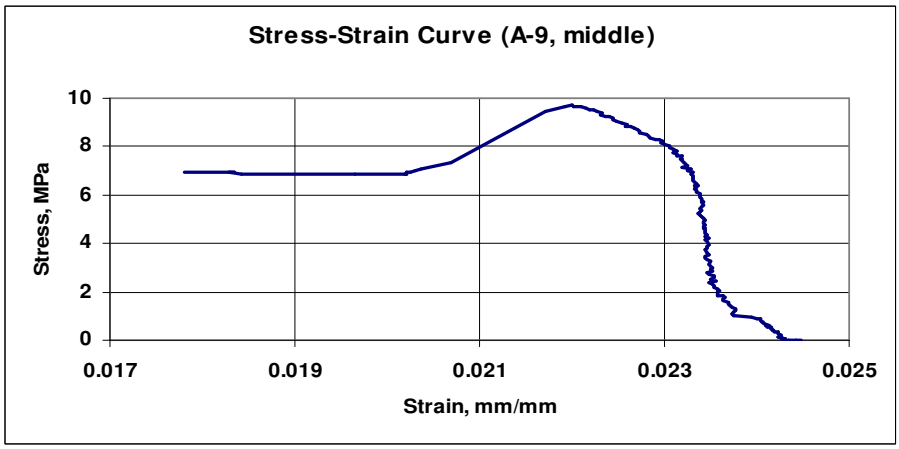

Fig. D.35 Stress versus Strain curve (CL between LDS #11&12 and LDS #13&14)

1.10 Wall ***A-10***

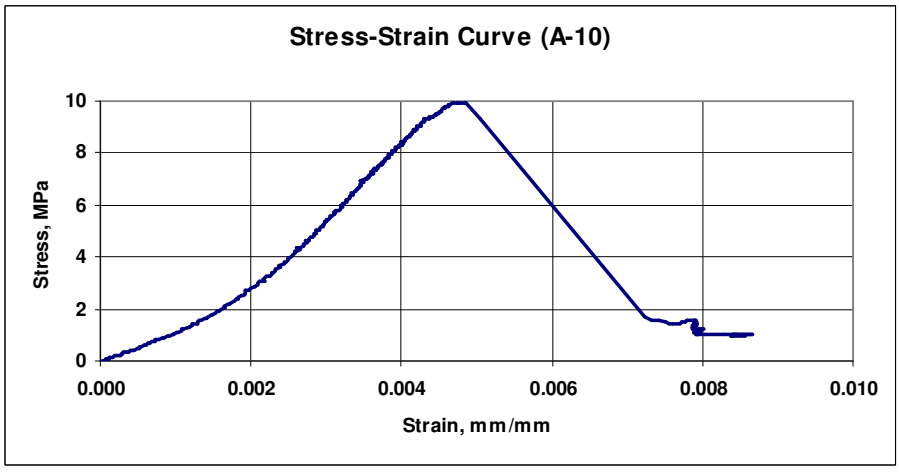

Fig. D.36 Stress versus Strain curve (CL between LDS #1 and LDS #2)

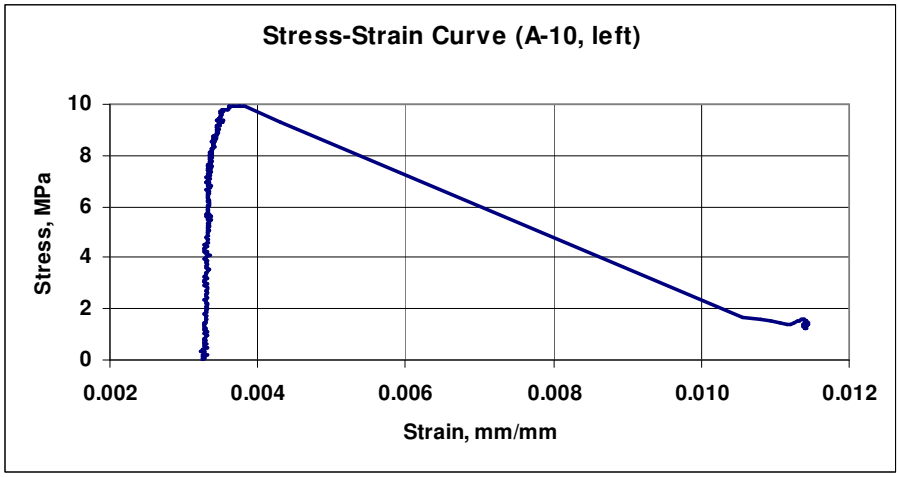

Fig. D.37 Stress versus Strain curve (CL between LDS #3&5 and LDS #8&10)

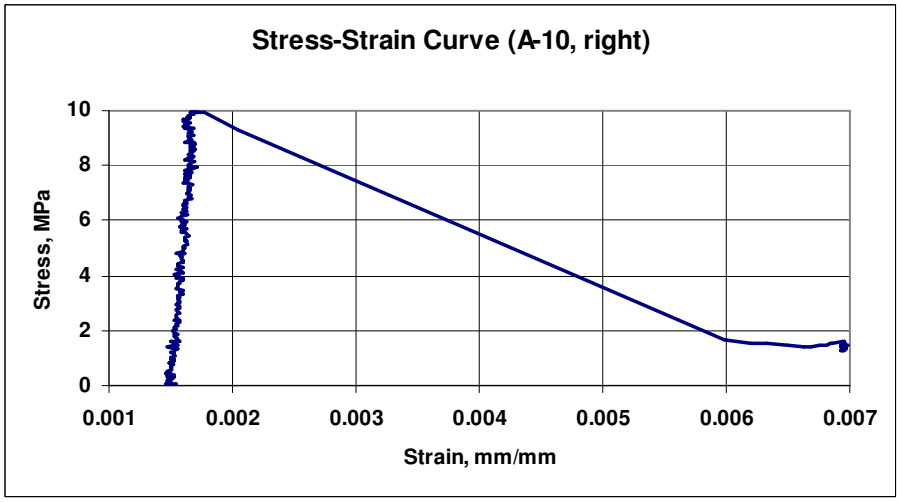

Fig. D.38 Stress versus Strain curve (CL between LDS #4&6 and LDS #7&9)

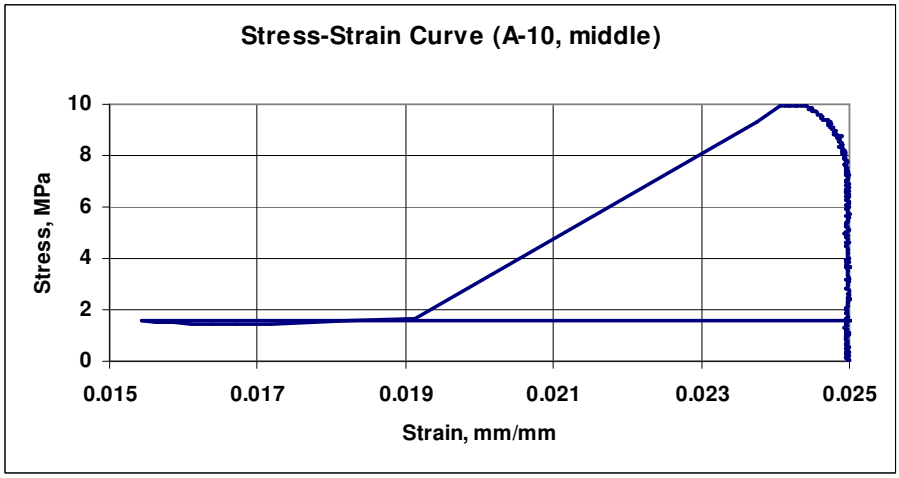

Fig. D.39 Stress versus Strain curve (CL between LDS #11&12 and LDS #13&14)

2. Wall specimens type *B*

2.1 Wall *B-1*

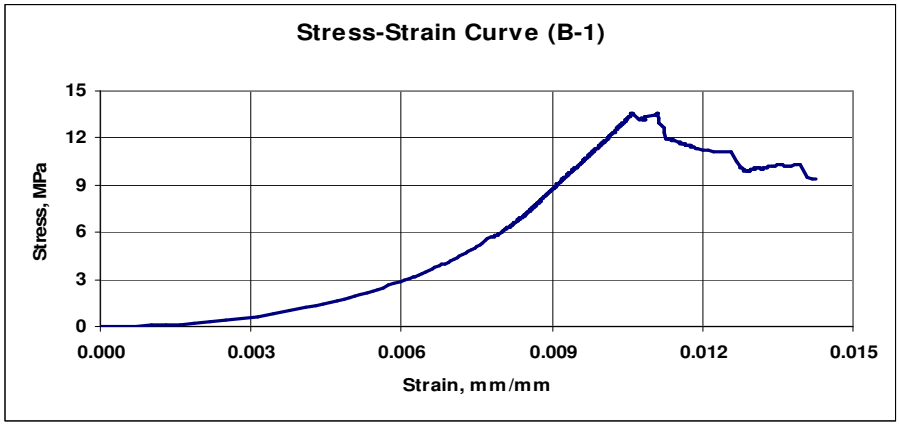

Fig. D.40 Stress versus Strain curve (CL between LDS #1 and LDS #2)

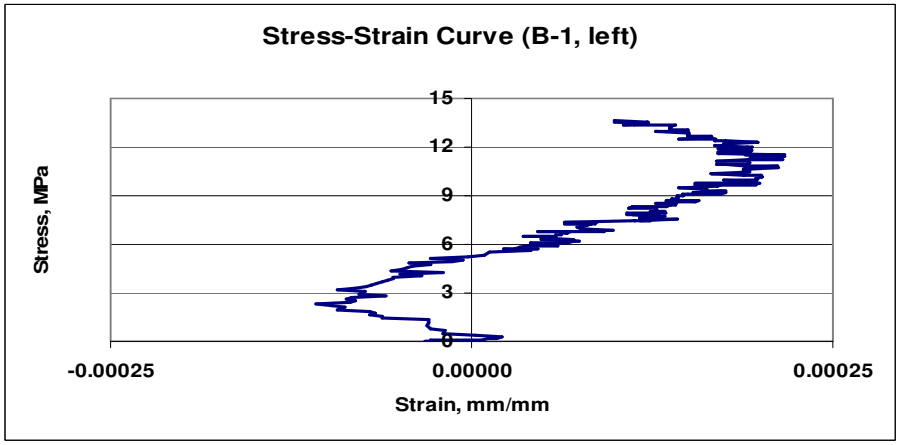

Fig. D.41 Stress versus Strain curve (CL between LDS #3&5 and LDS #8&10)

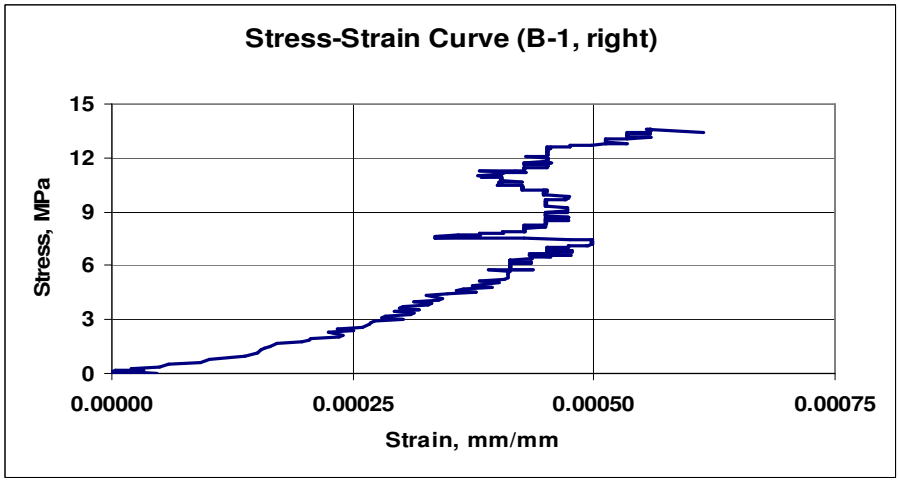

Fig. D.42 Stress versus Strain curve (CL between LDS #4&6 and LDS #7&9)

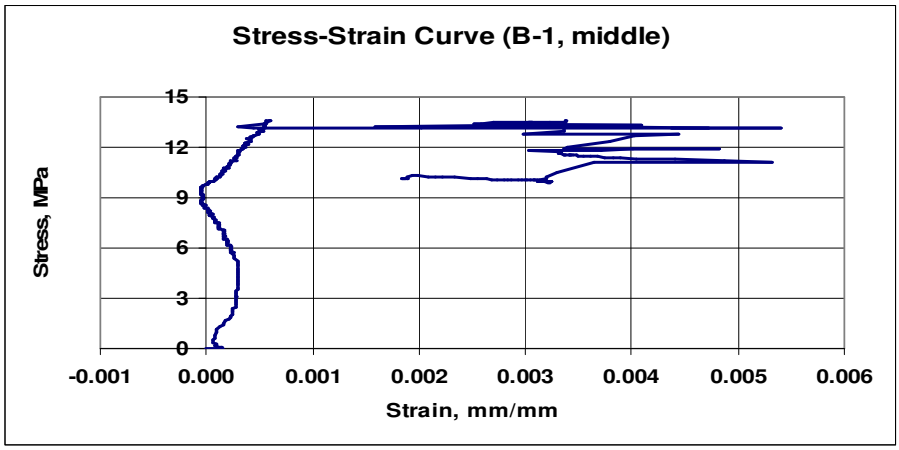

Fig. D.43 Stress versus Strain curve (CL between LDS #11&12 and LDS #13&14)

2.2 Wall ***B-2***

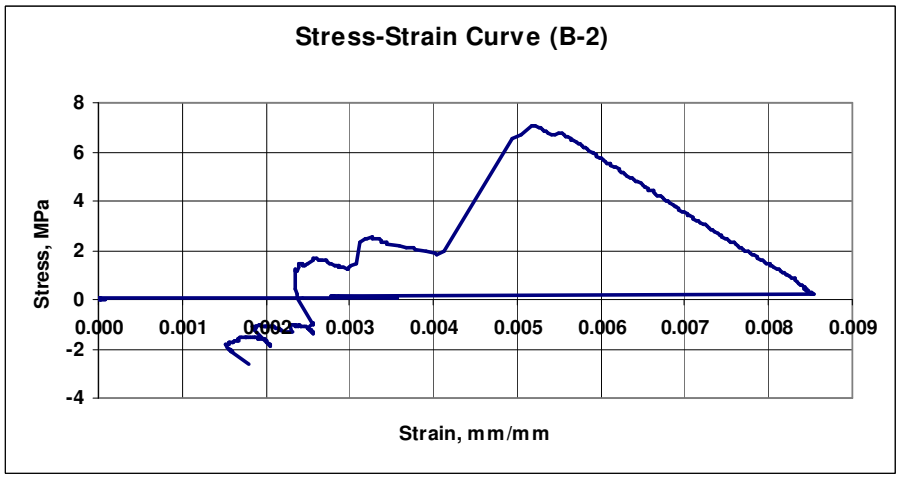

Fig. D.44 Stress versus Strain curve (CL between LDS #1 and LDS #2)

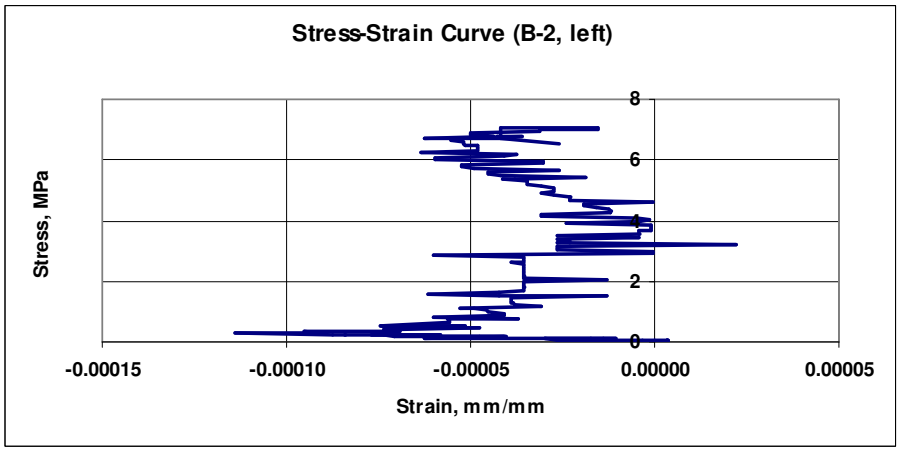

Fig. D.45 Stress versus Strain curve (CL between LDS #3&5 and LDS #8&10)

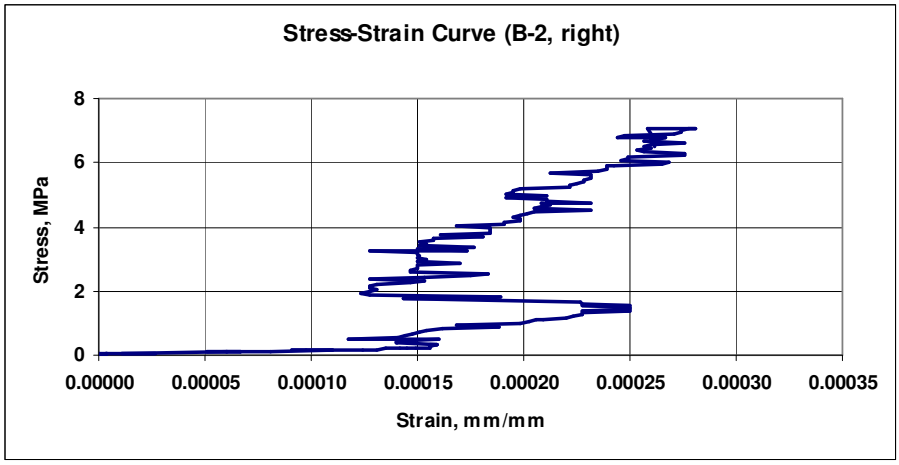

Fig. D.46 Stress versus Strain curve (CL between LDS #4&6 and LDS #7&9)

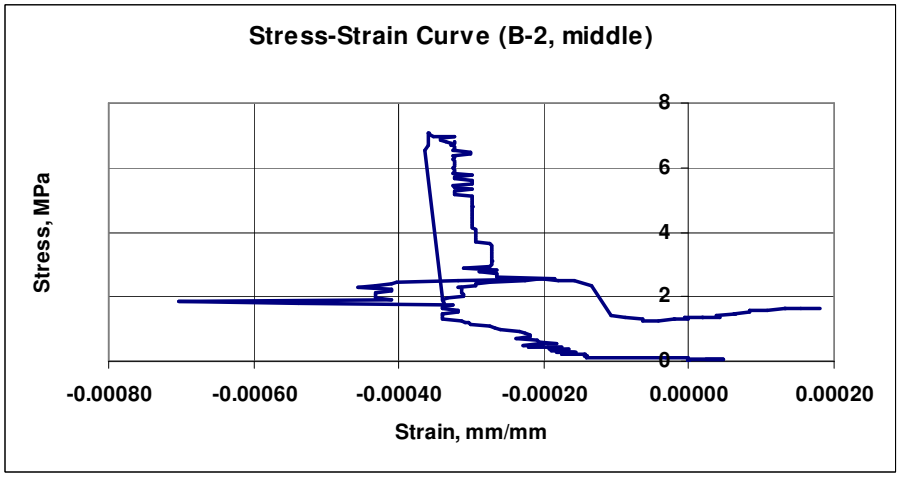

Fig. D.47 Stress versus Strain curve (CL between LDS #11&12 and LDS #13&14)

2.3 Wall ***B-3***

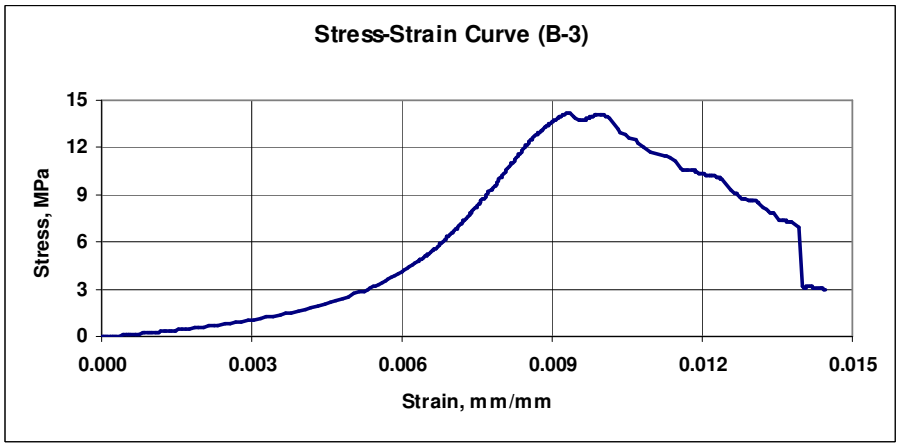

Fig. D.48 Stress versus Strain curve (CL between LDS #1 and LDS #2)

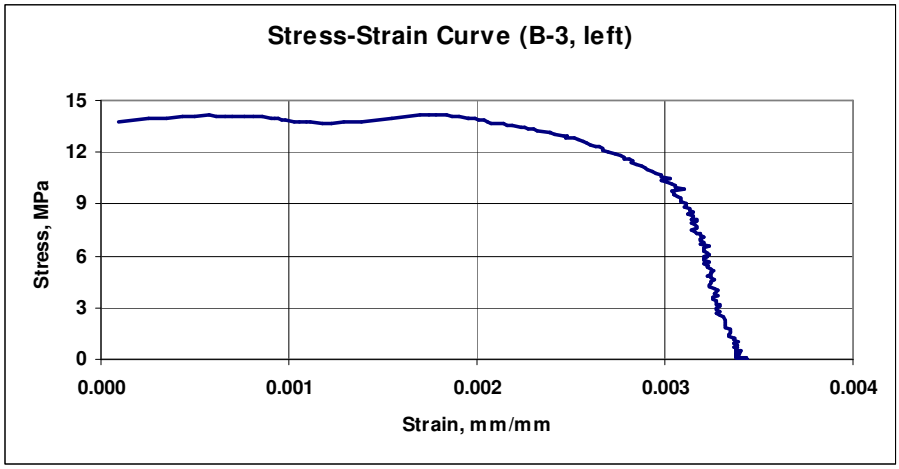

Fig. D.49 Stress versus Strain curve (CL between LDS #3&5 and LDS #8&10)

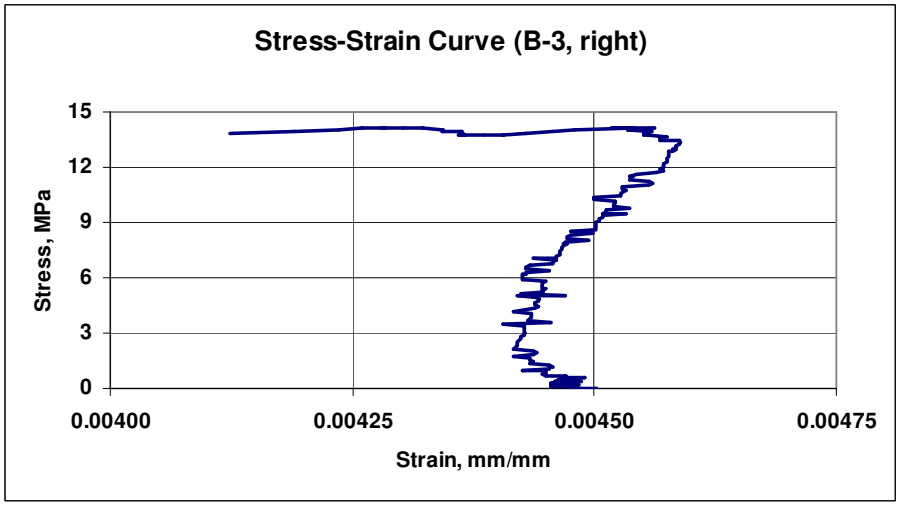

Fig. D.50 Stress versus Strain curve (CL between LDS #4&6 and LDS #7&9)

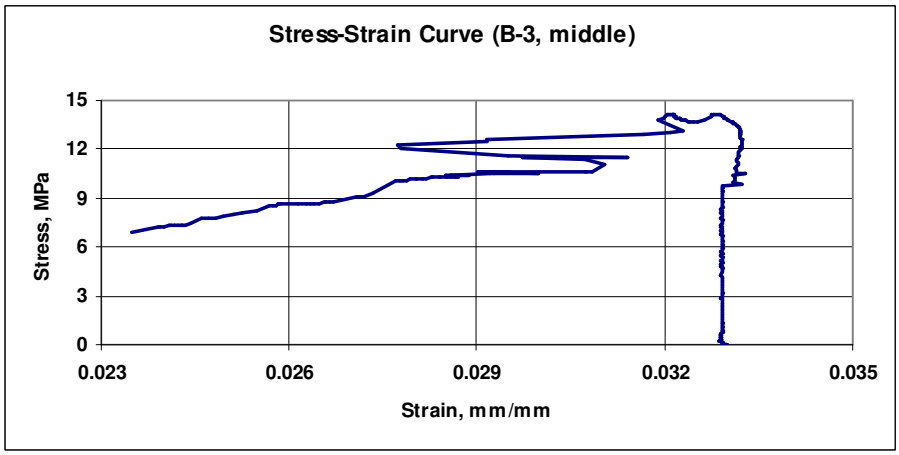

Fig. D.51 Stress versus Strain curve (CL between LDS #11&12 and LDS #13&14)

2.4 Wall ***B-4***

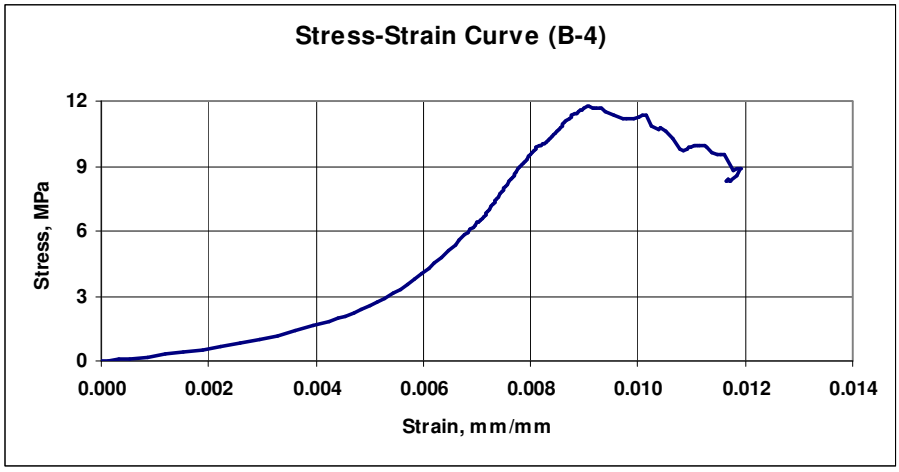

Fig. D.52 Stress versus Strain curve (CL between LDS #1 and LDS #2)

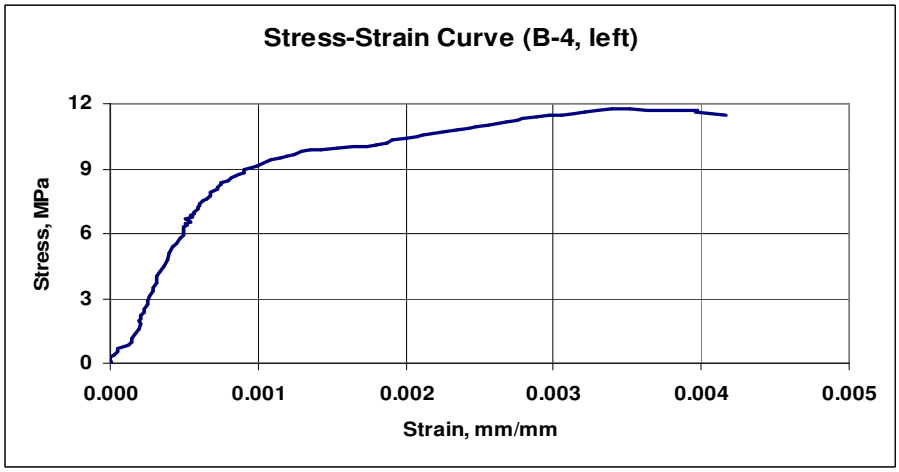

Fig. D.53 Stress versus Strain curve (CL between LDS #3&5 and LDS #8&10)

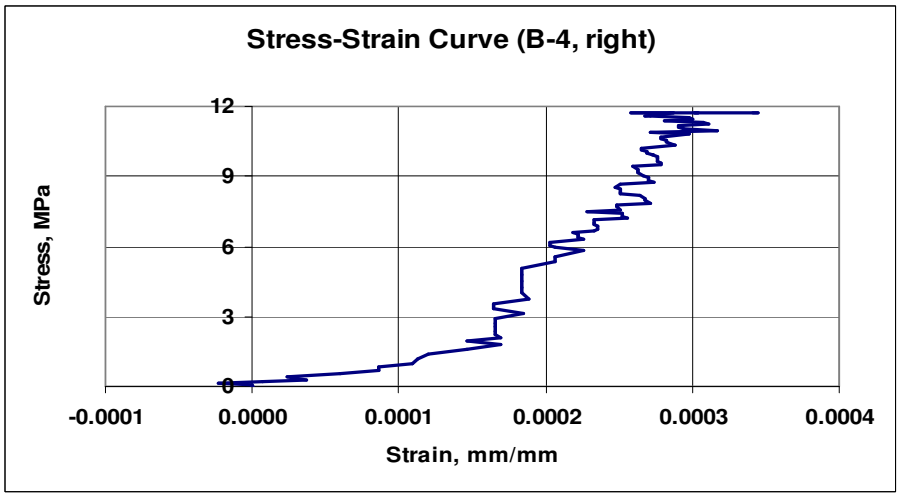

Fig. D.54 Stress versus Strain curve (CL between LDS #4&6 and LDS #7&9)

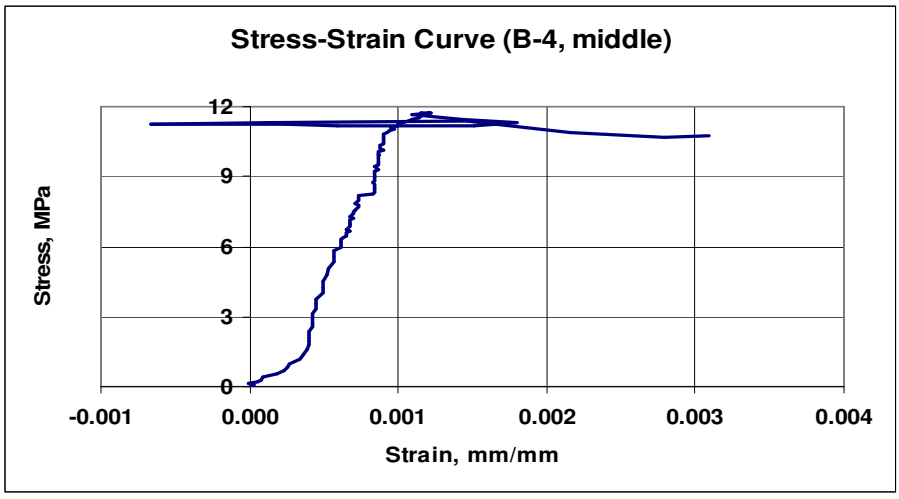

Fig. D.55 Stress versus Strain curve (CL between LDS #11&12 and LDS #13&14)

2.5 Wall ***B-5***

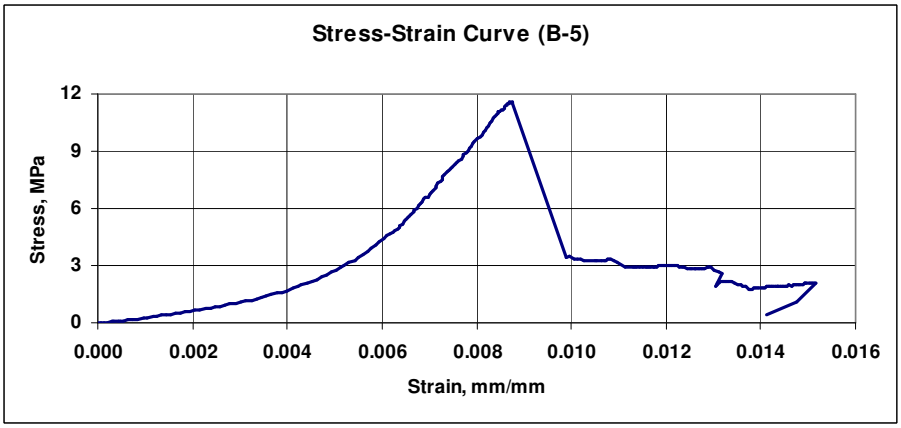

Fig. D.56 Stress versus Strain curve (CL between LDS #1 and LDS #2)

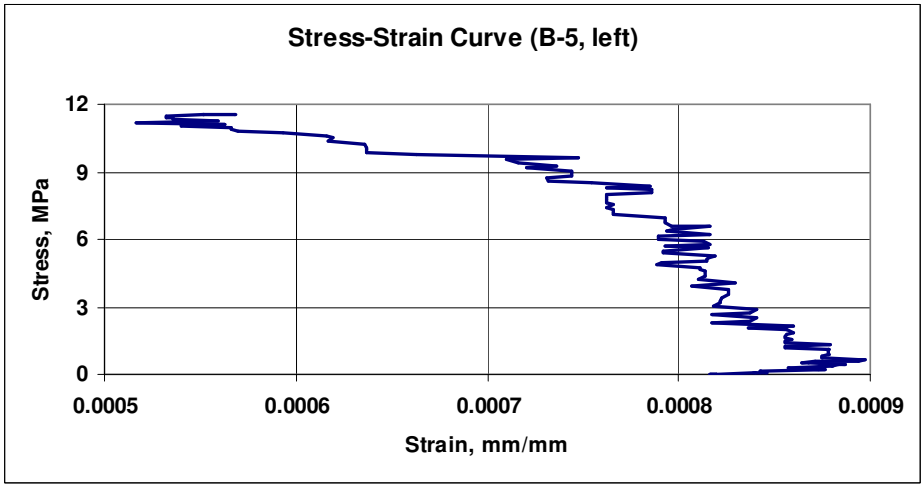

Fig. D.57 Stress versus Strain curve (CL between LDS #3&5 and LDS #8&10)

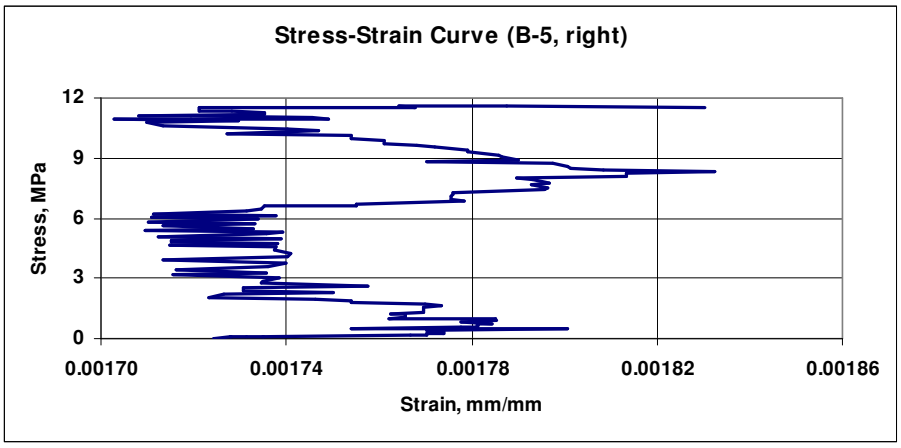

Fig. D.58 Stress versus Strain curve (CL between LDS #4&6 and LDS #7&9)

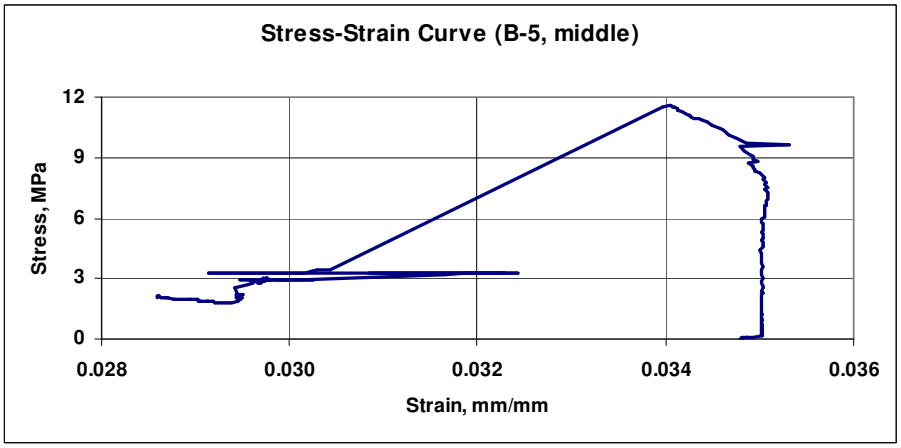

Fig. D.59 Stress versus Strain curve (CL between LDS #11&12 and LDS #13&14)

2.6 Wall ***B-6***

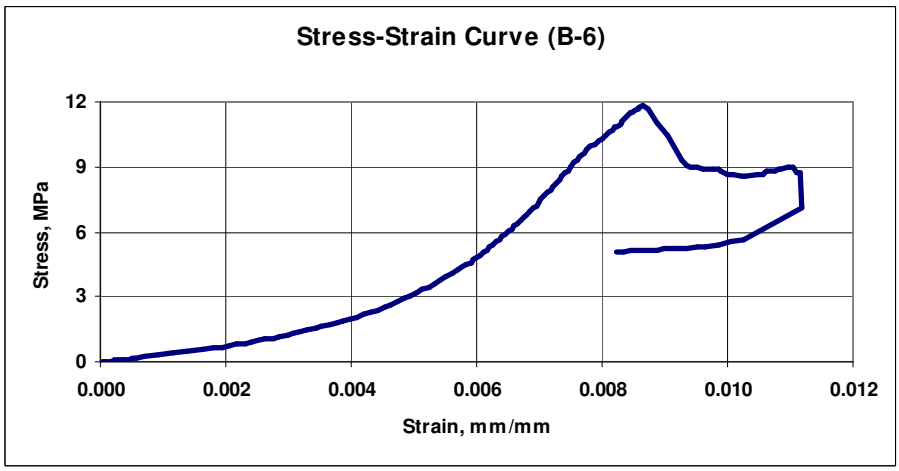

Fig. D.60 Stress versus Strain curve (CL between LDS #1 and LDS #2)

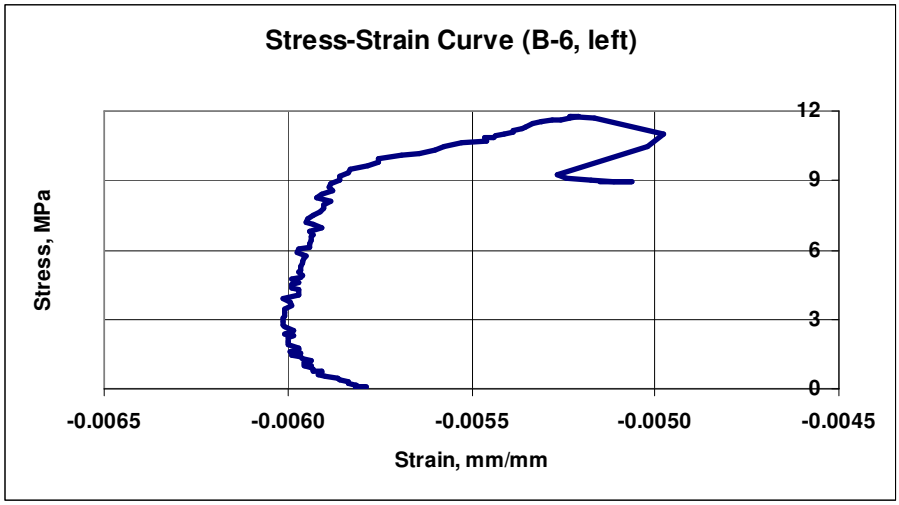

Fig. D.61 Stress versus Strain curve (CL between LDS #3&5 and LDS #8&10)

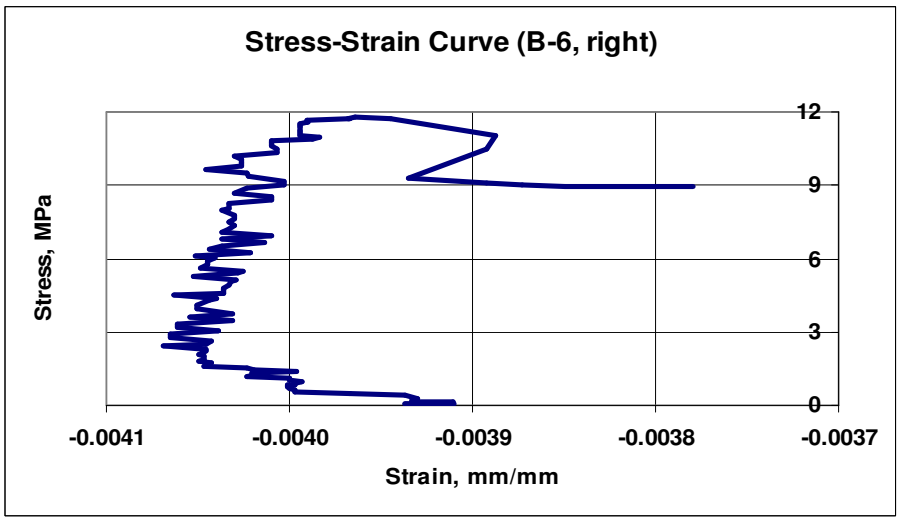

Fig. D.62 Stress versus Strain curve (CL between LDS #4&6 and LDS #7&9)

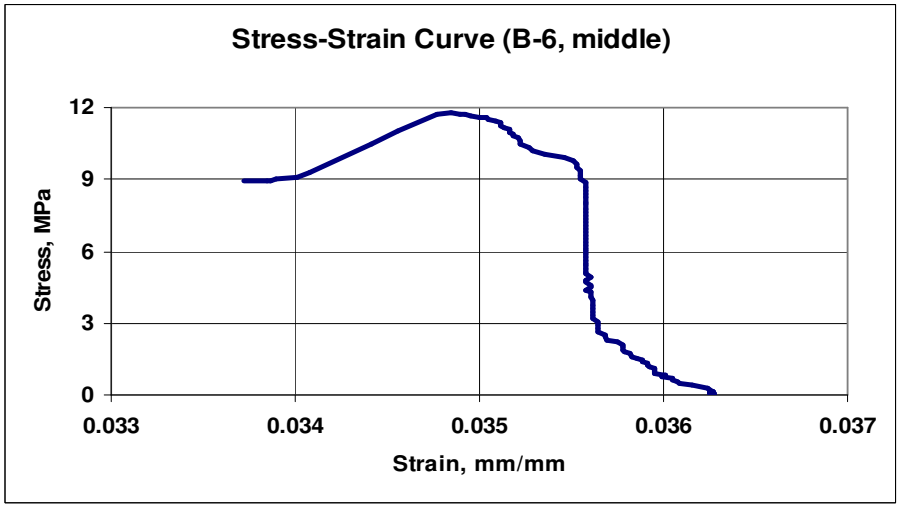

Fig. D.63 Stress versus Strain curve (CL between LDS #11&12 and LDS #13&14)

2.7 Wall ***B-7***

There is no data available for wall test specimens ***B-7*** – the load cell was broken.

2.8 Wall ***B-8***

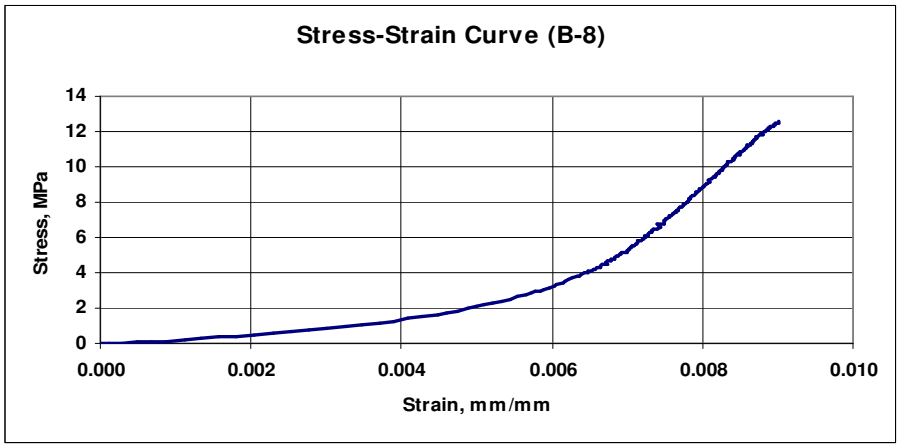

Fig. D.64 Stress versus Strain curve (CL between LDS #1 and LDS #2)

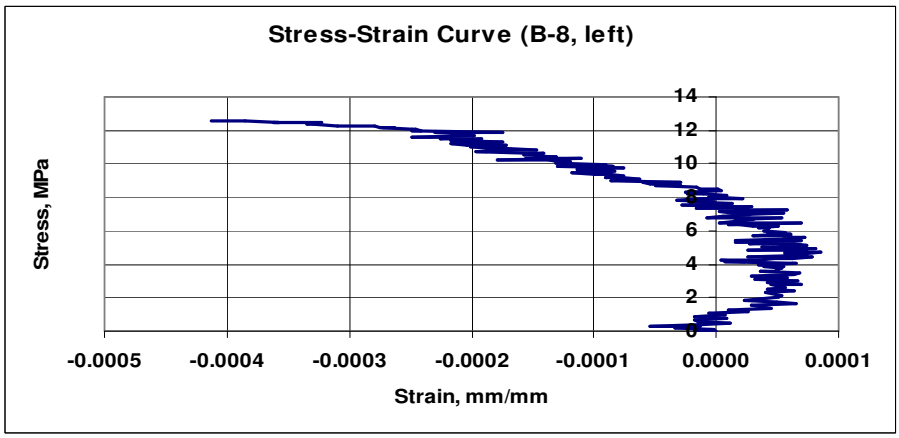

Fig. D.65 Stress versus Strain curve (CL between LDS #3&5 and LDS #8&10)

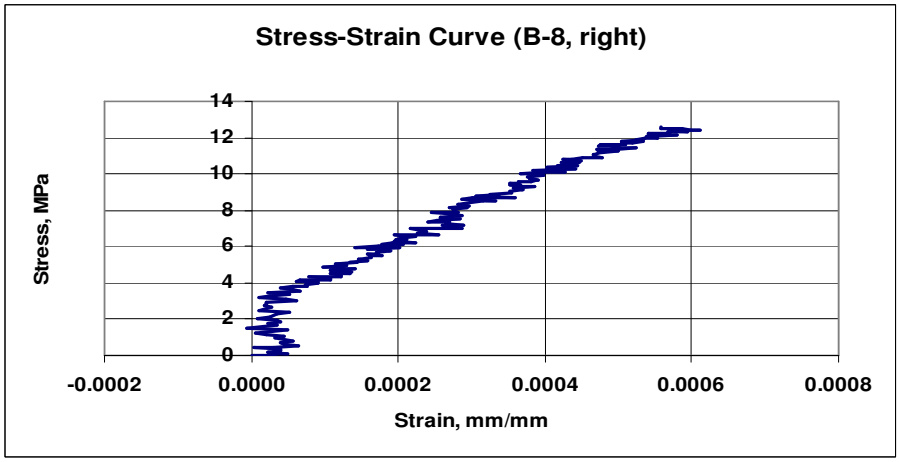

Fig. D.66 Stress versus Strain curve (CL between LDS #4&6 and LDS #7&9)

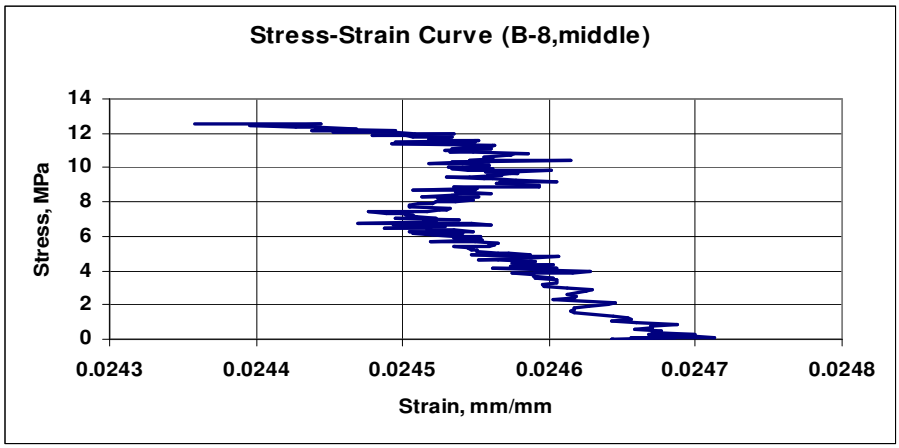

Fig. D.67 Stress versus Strain curve (CL between LDS #11&12 and LDS #13&14)

2.9 Wall ***B-9***

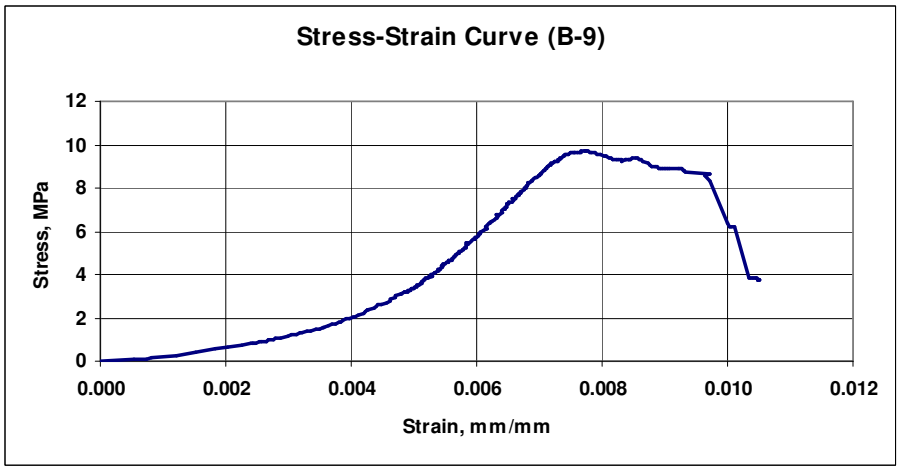

Fig. D.68 Stress versus Strain curve (CL between LDS #1 and LDS #2)

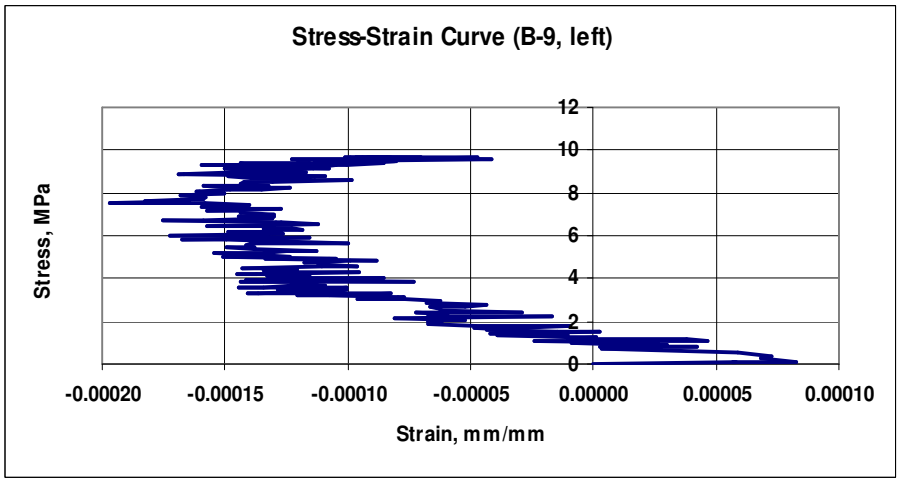

Fig. D.69 Stress versus Strain curve (CL between LDS #3&5 and LDS #8&10)

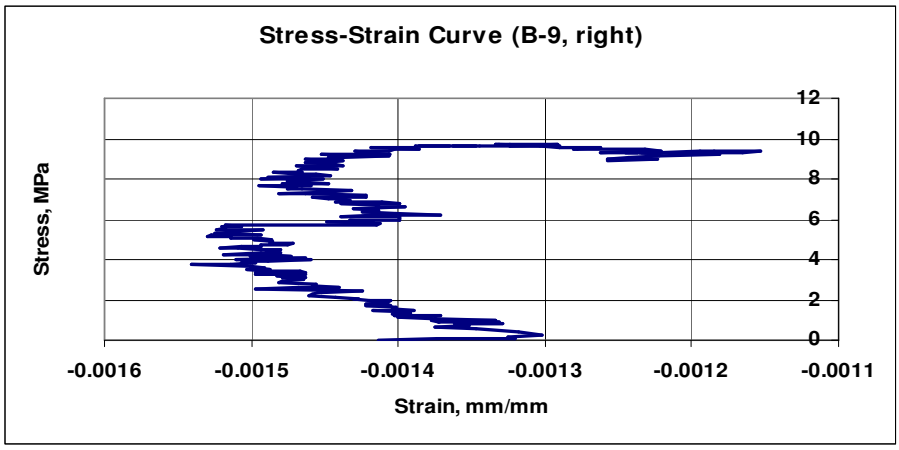

Fig. D.70 Stress versus Strain curve (CL between LDS #4&6 and LDS #7&9)

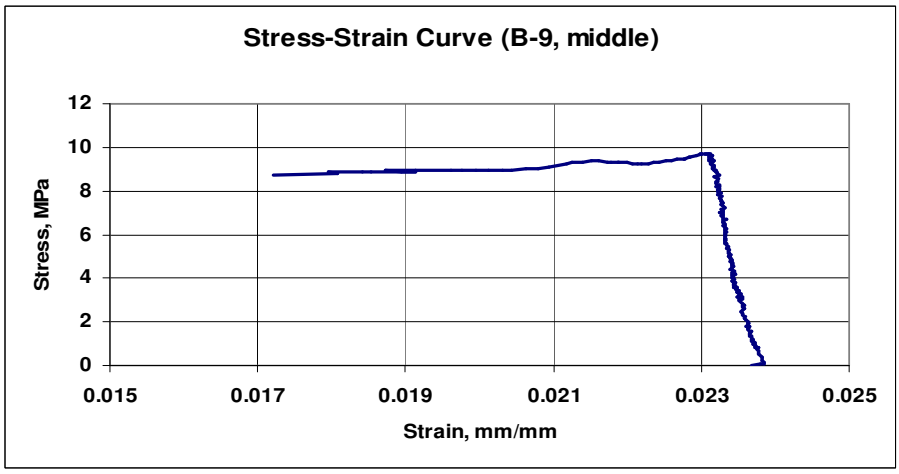

Fig. D.71 Stress versus Strain curve (CL between LDS #11&12 and LDS #13&14)

2.10 Wall ***B-10***

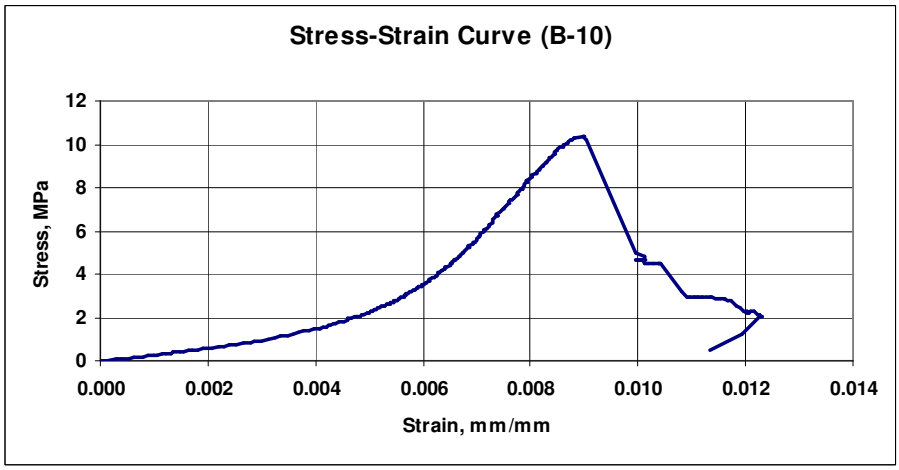

Fig. D.72 Stress versus Strain curve (CL between LDS #1 and LDS #2)

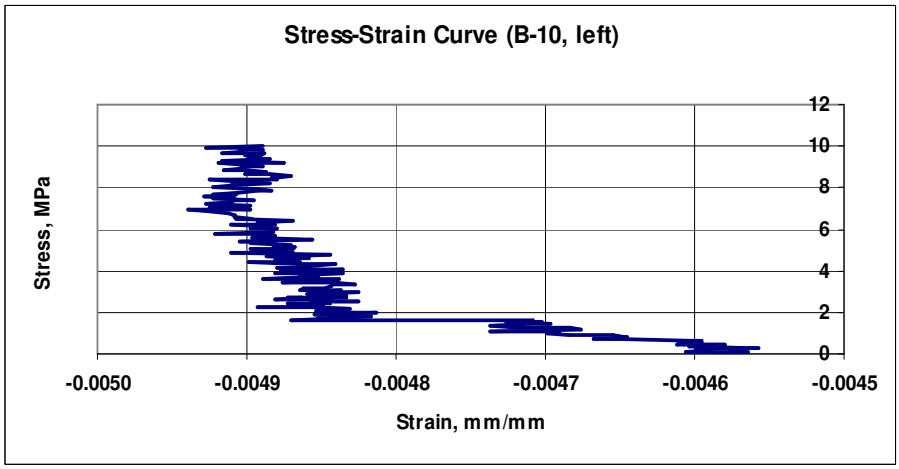

Fig. D.73 Stress versus Strain curve (CL between LDS #3&5 and LDS #8&10)

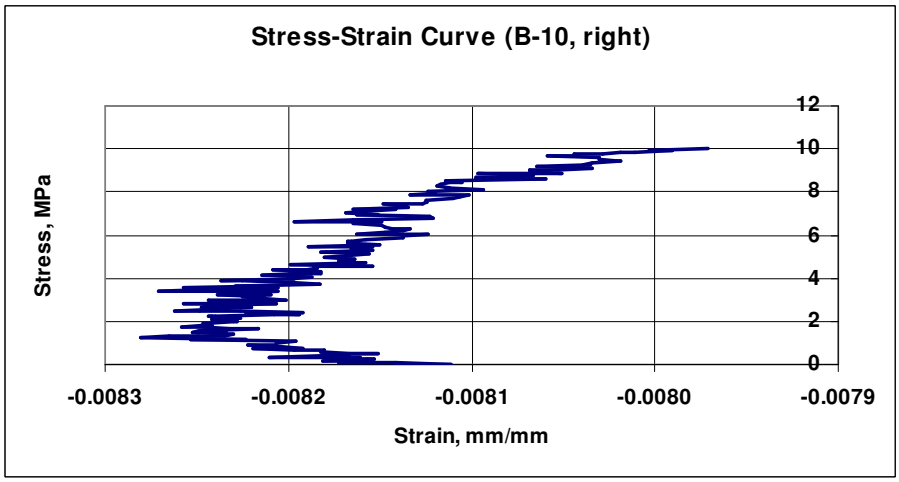

Fig. D.74 Stress versus Strain curve (CL between LDS #4&6 and LDS #7&9)

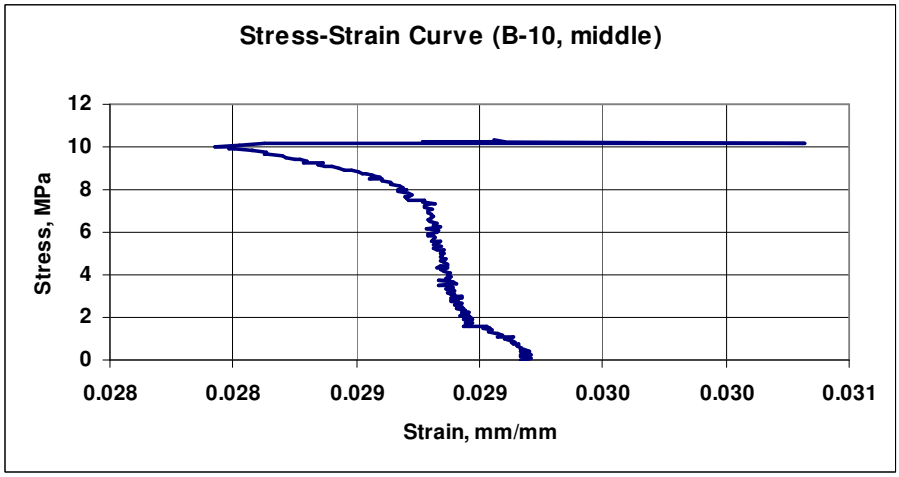

Fig. D.75 Stress versus Strain curve (CL between LDS #11&12 and LDS #13&14)

3. Wall specimens type *C*

3.1 Wall *C-1*

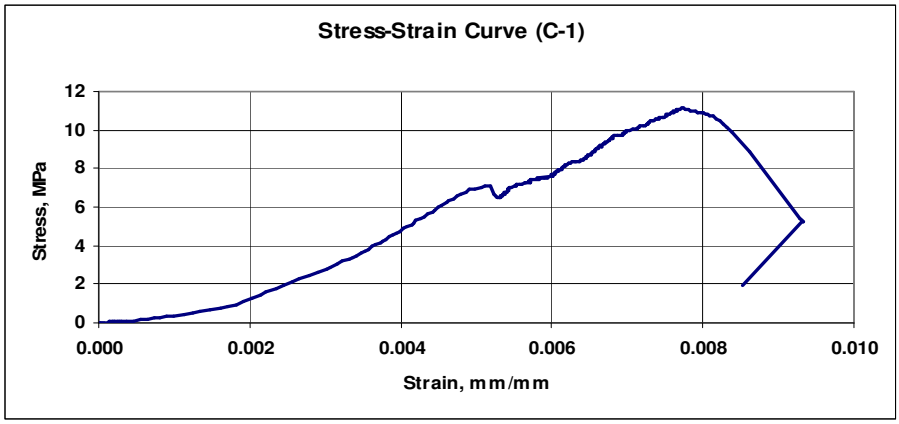

Fig. D.76 Stress versus Strain curve (CL between LDS #1 and LDS #2)

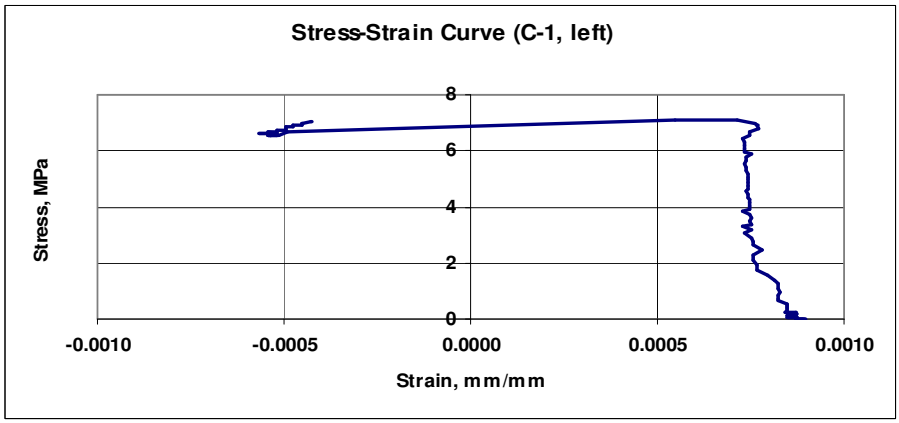

Fig. D.77 Stress versus Strain curve (CL between LDS #3&5 and LDS #8&10)

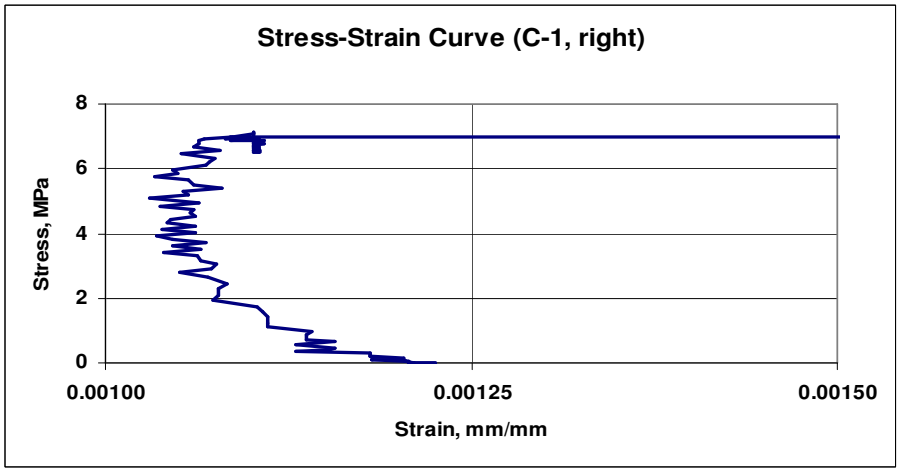

Fig. D.78 Stress versus Strain curve (CL between LDS #4&6 and LDS #7&9)

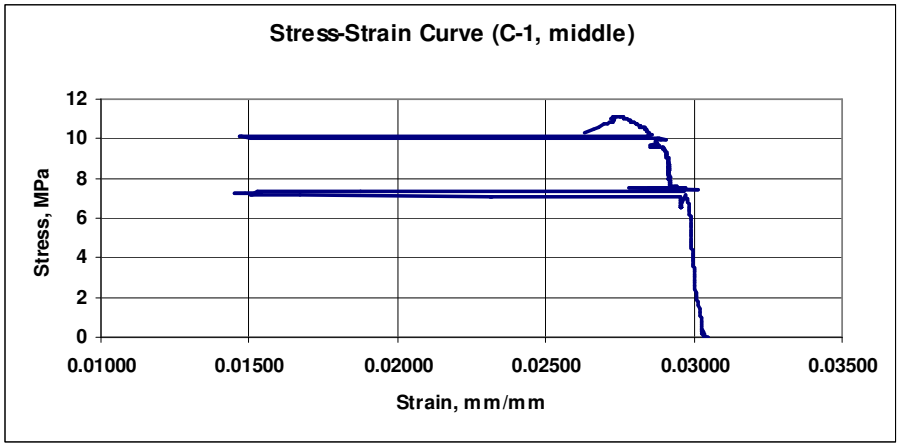

Fig. D.79 Stress versus Strain curve (CL between LDS #11&12 and LDS #13&14)

3.2 Wall ***C-2***

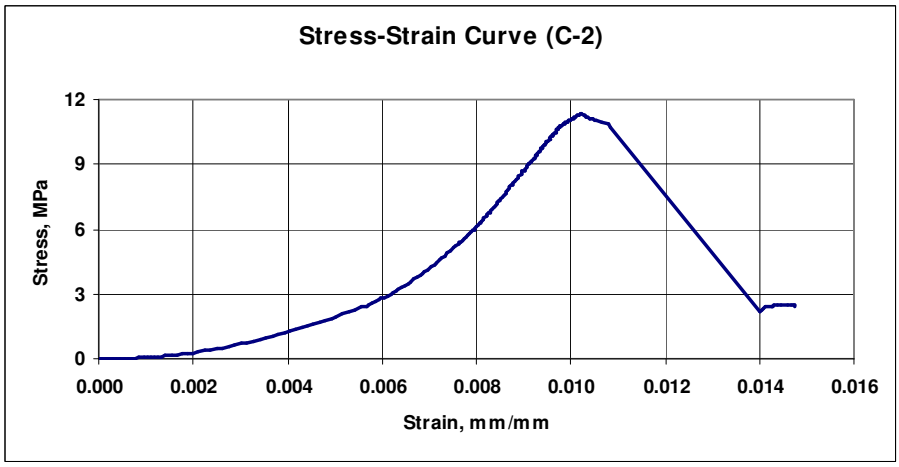

Fig. D.80 Stress versus Strain curve (CL between LDS #1 and LDS #2)

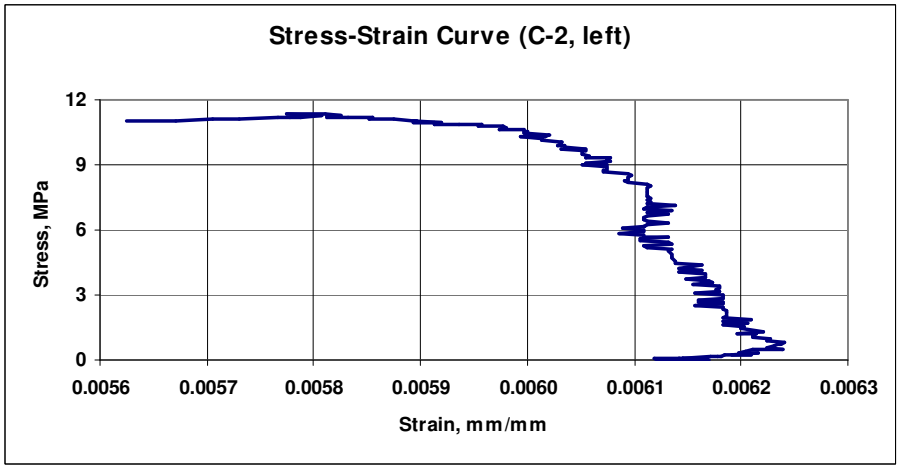

Fig. D.81 Stress versus Strain curve (CL between LDS #3&5 and LDS #8&10)

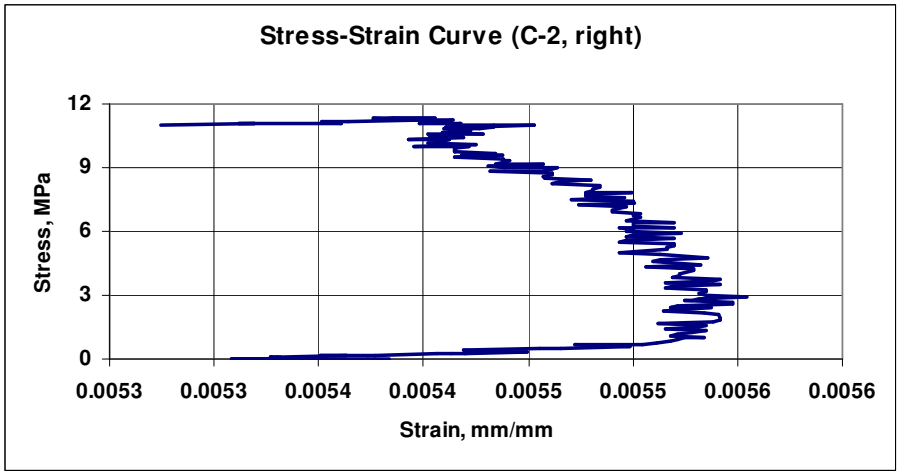

Fig. D.82 Stress versus Strain curve (CL between LDS #4&6 and LDS #7&9)

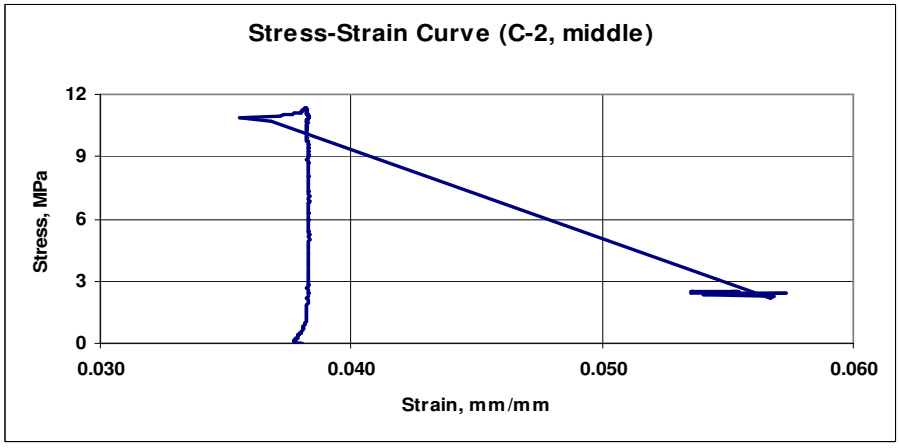

Fig. D.83 Stress versus Strain curve (CL between LDS #11&12 and LDS #13&14)

3.3 Wall ***C-3***

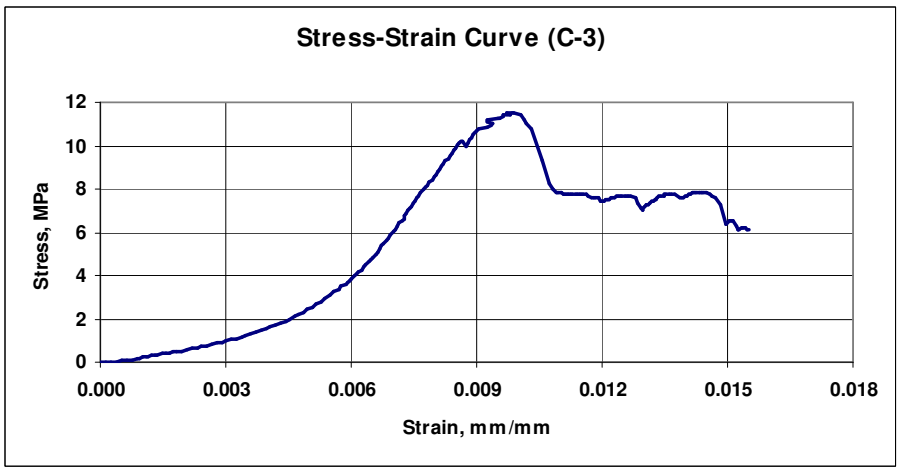

Fig. D.84 Stress versus Strain curve (CL between LDS #1 and LDS #2)

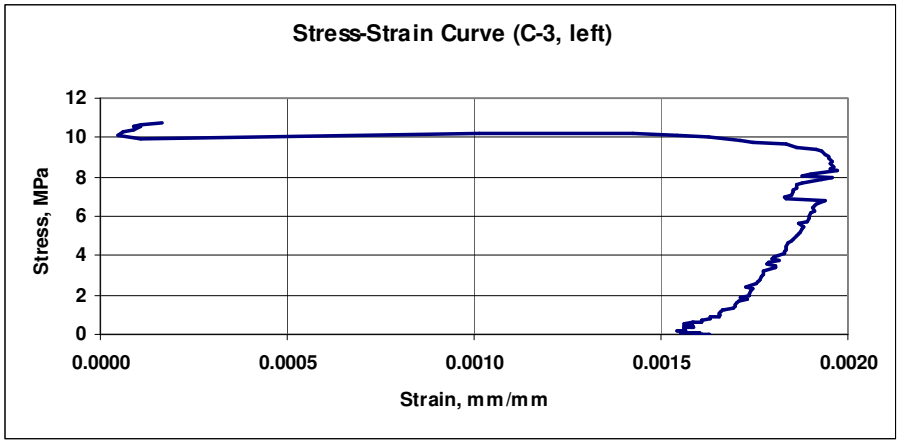

Fig. D.85 Stress versus Strain curve (CL between LDS #3&5 and LDS #8&10)

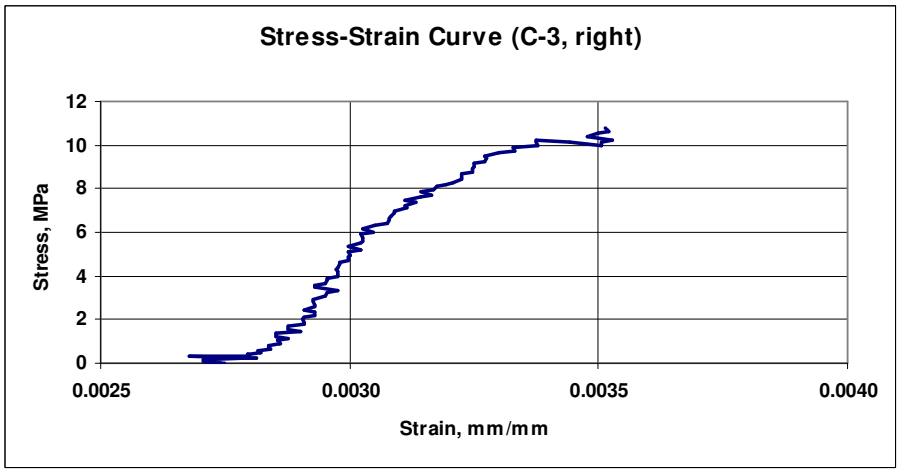

Fig. D.86 Stress versus Strain curve (CL between LDS #4&6 and LDS #7&9)

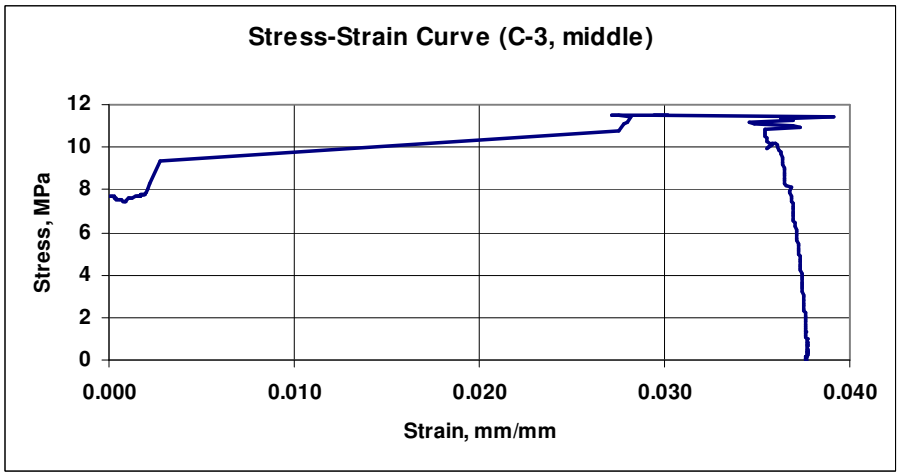

Fig. D.87 Stress versus Strain curve (CL between LDS #11&12 and LDS #13&14)

3.4 Wall ***C-4***

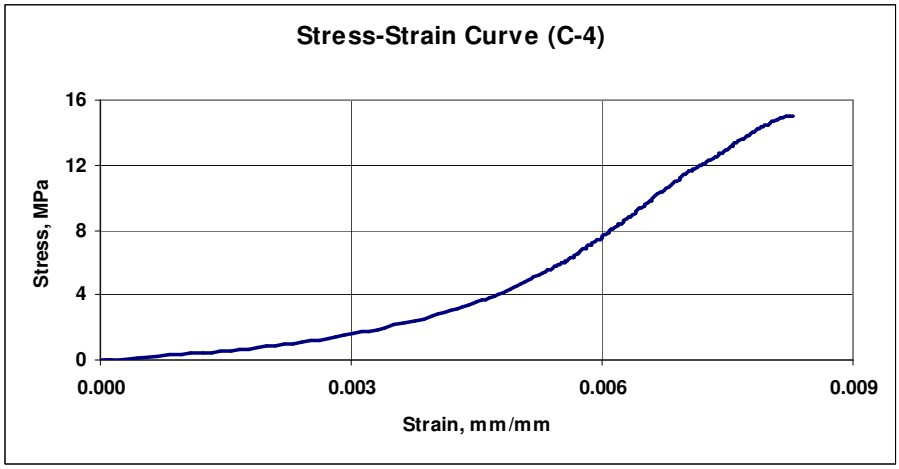

Fig. D.88 Stress versus Strain curve (CL between LDS #1 and LDS #2)

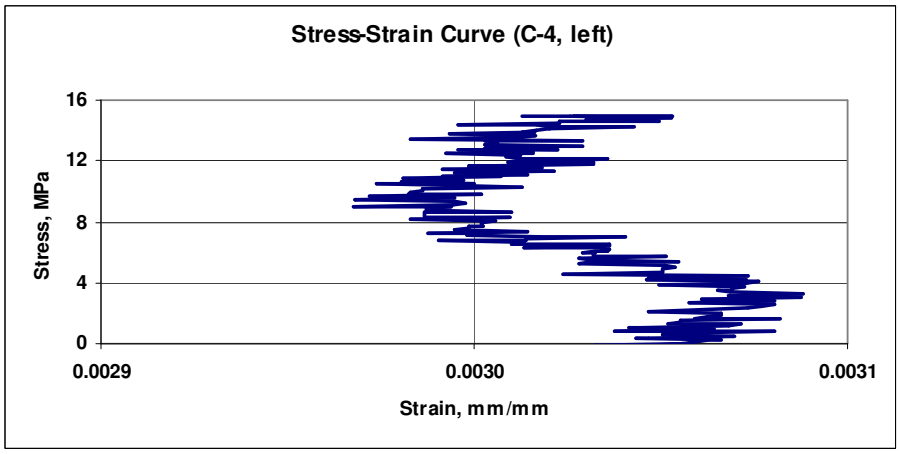

Fig. D.89 Stress versus Strain curve (CL between LDS #3&5 and LDS #8&10)

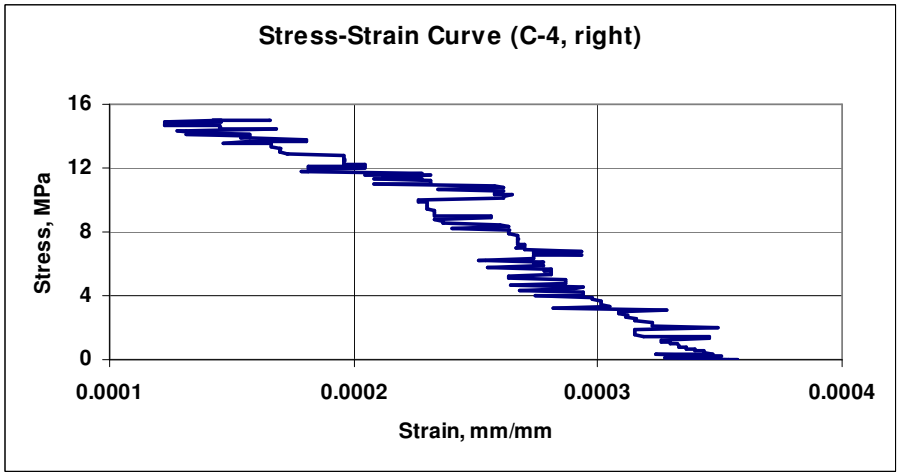

Fig. D.90 Stress versus Strain curve (CL between LDS #4&6 and LDS #7&9)

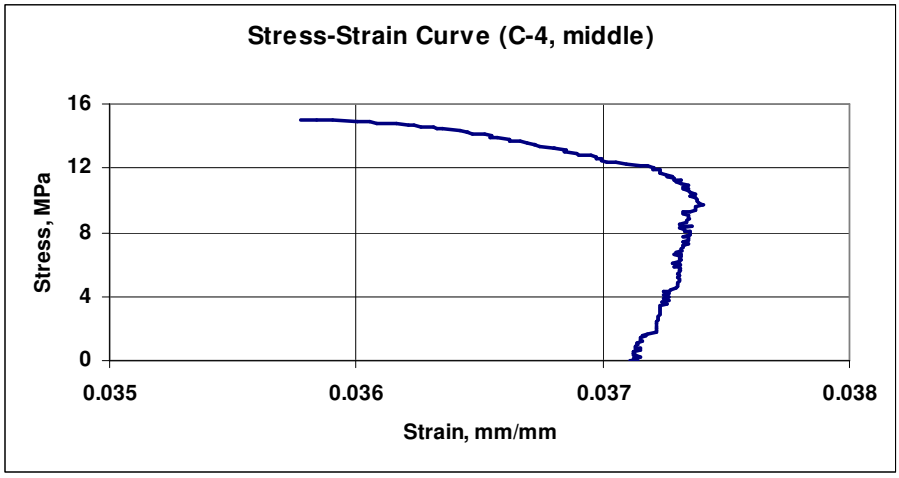

Fig. D.91 Stress versus Strain curve (CL between LDS #11&12 and LDS #13&14)

3.5 Wall ***C-5***

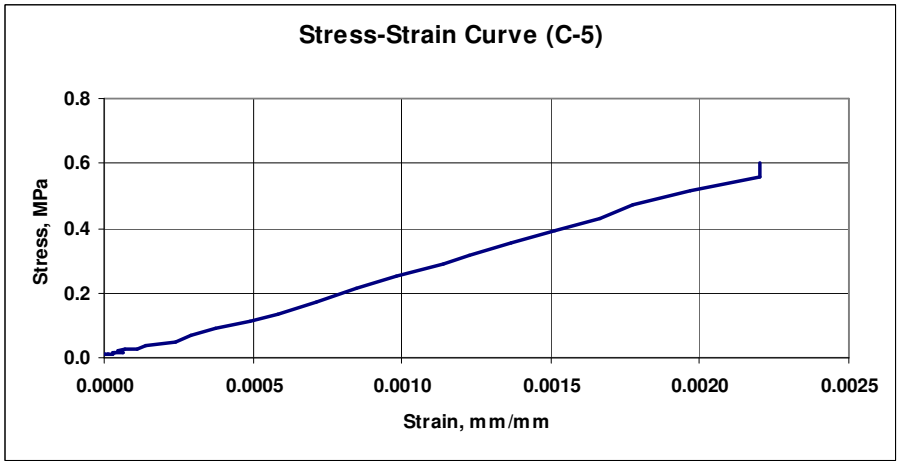

Fig. D.92 Stress versus Strain curve (CL between LDS #1 and LDS #2)

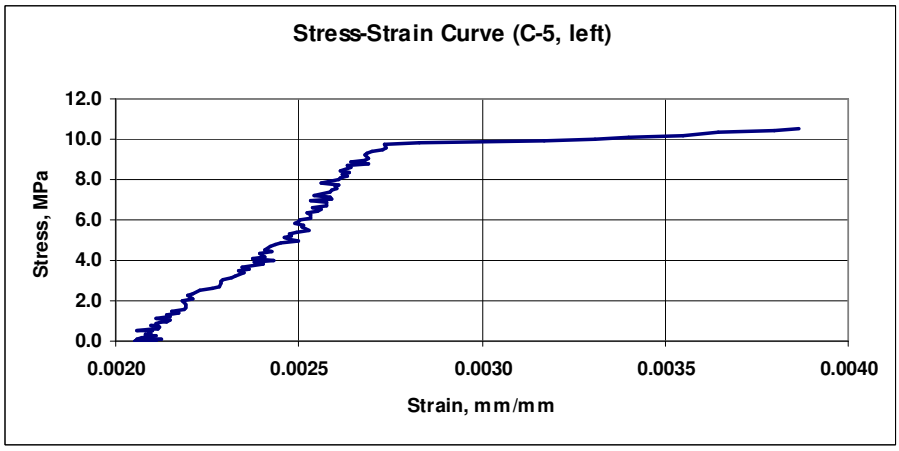

Fig. D.93 Stress versus Strain curve (CL between LDS #3&5 and LDS #8&10)

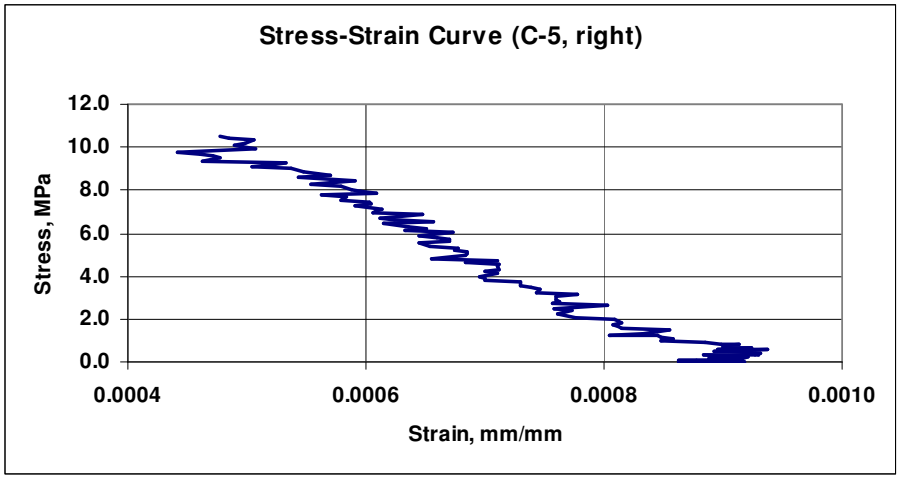

Fig. D.94 Stress versus Strain curve (CL between LDS #4&6 and LDS #7&9)

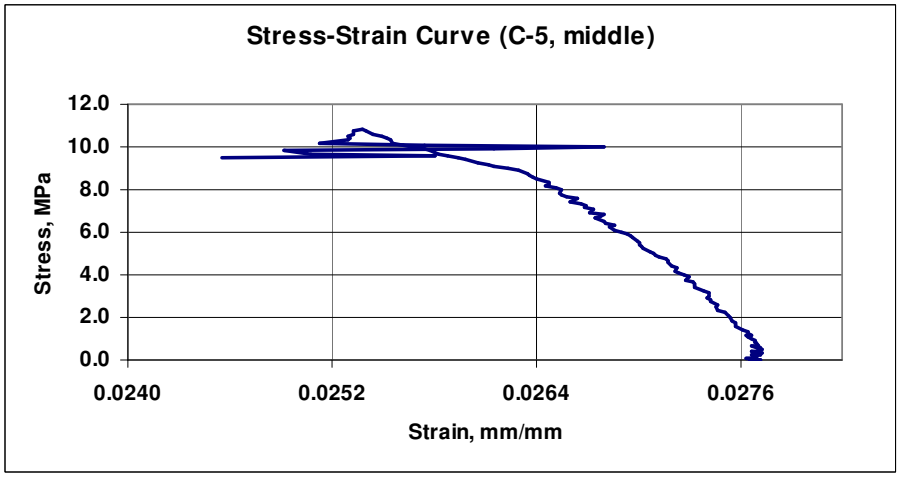

Fig. D.95 Stress versus Strain curve (CL between LDS #11&12 and LDS #13&14)

3.6 Wall ***C-6***

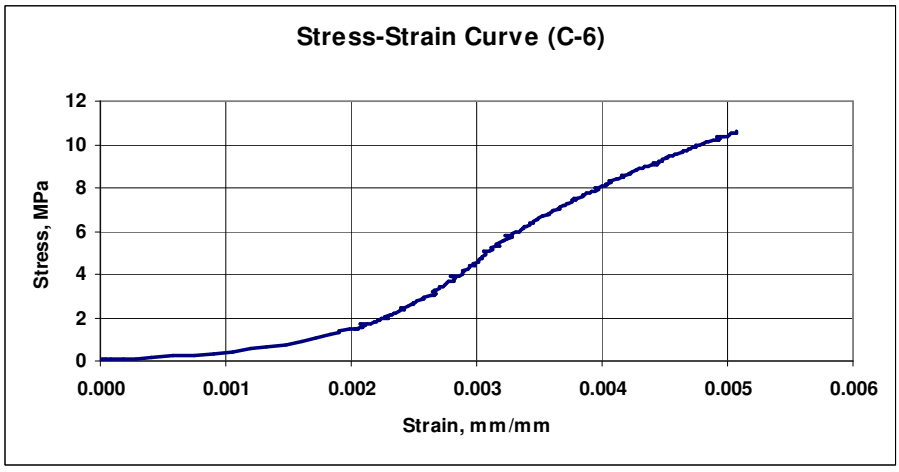

Fig. D.96 Stress versus Strain curve (CL between LDS #1 and LDS #2)

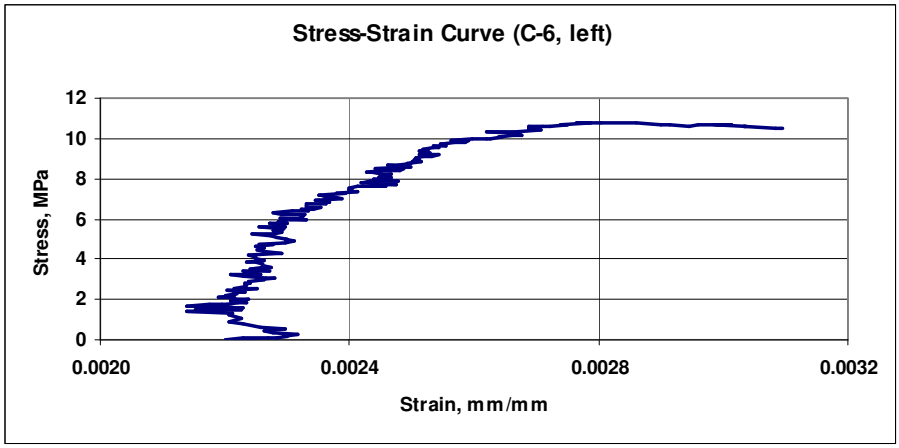

Fig. D.97 Stress versus Strain curve (CL between LDS #3&5 and LDS #8&10)

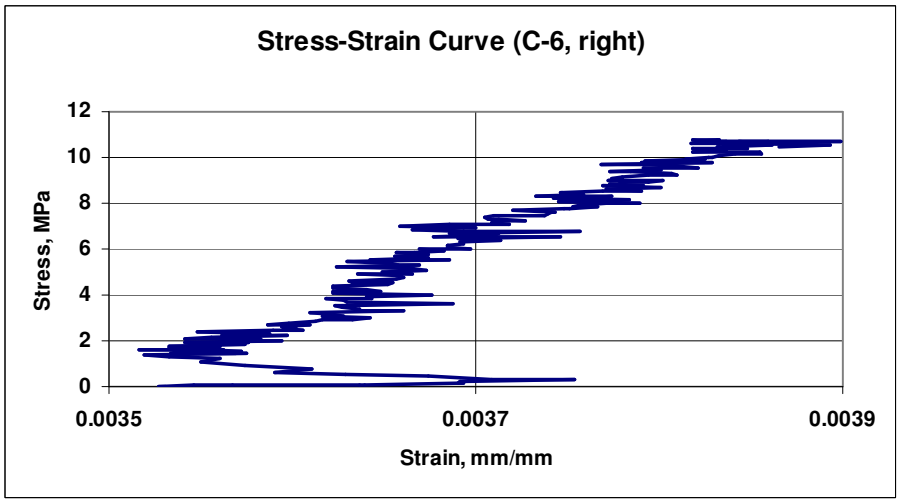

Fig. D.98 Stress versus Strain curve (CL between LDS #4&6 and LDS #7&9)

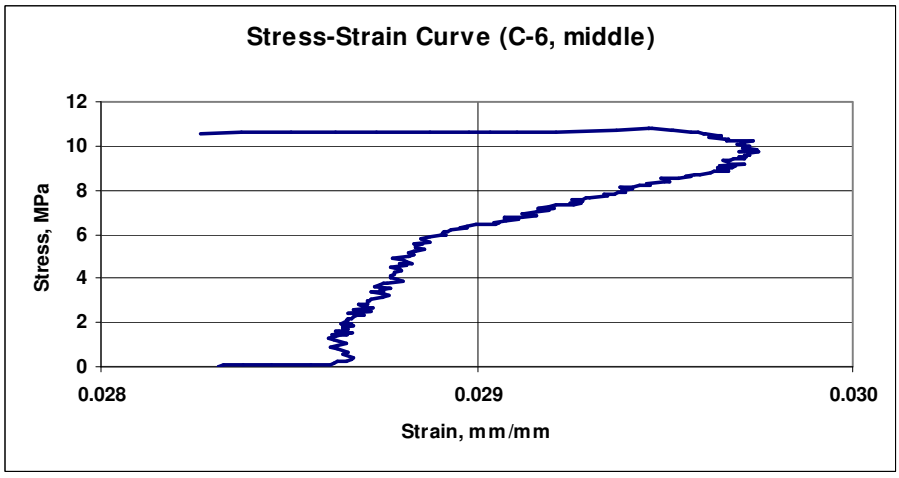

Fig. D.99 Stress versus Strain curve (CL between LDS #11&12 and LDS #13&14)

3.7 Wall ***C-7***

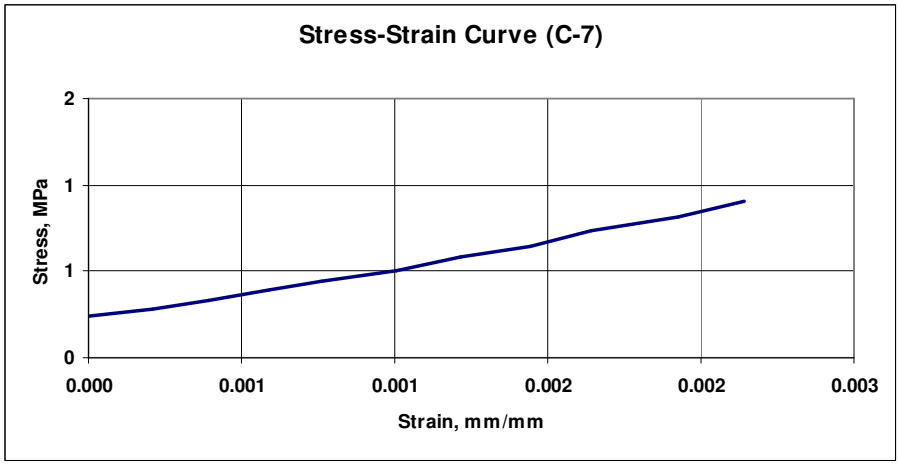

Fig. D.100 Stress versus Strain curve (CL between LDS #1 and LDS #2)

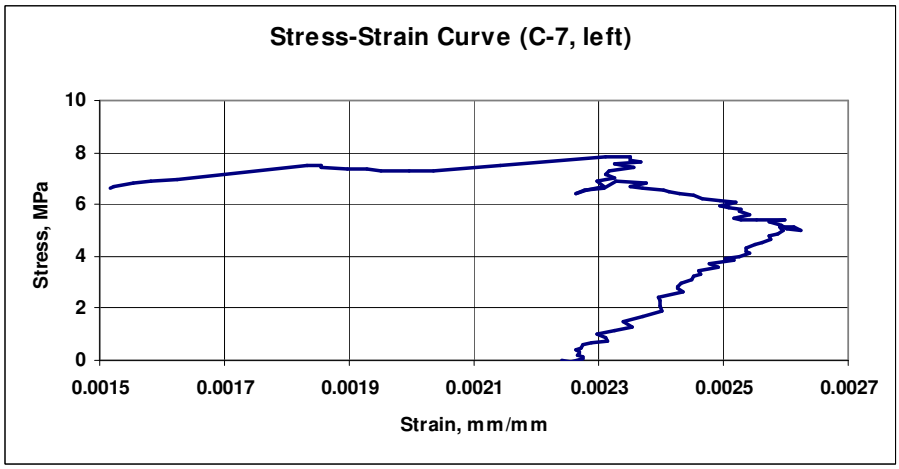

Fig. D.101 Stress versus Strain curve (CL between LDS #3&5 and LDS #8&10)

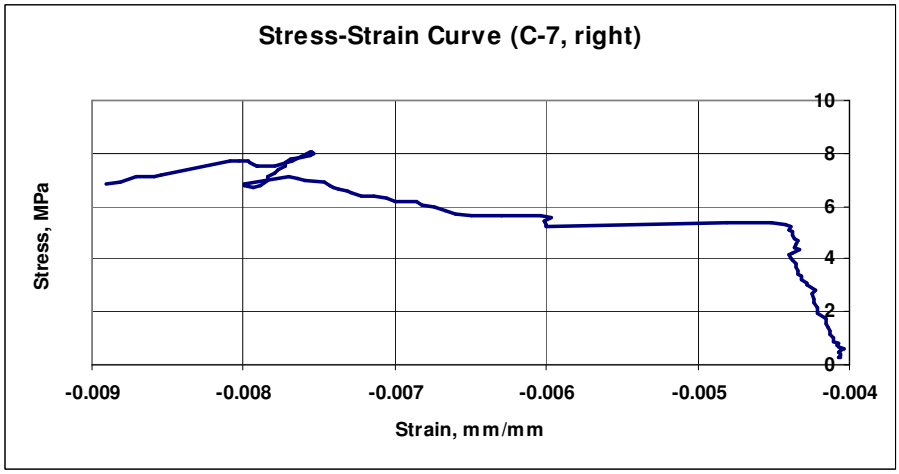

Fig. D.102 Stress versus Strain curve (CL between LDS #4&6 and LDS #7&9)

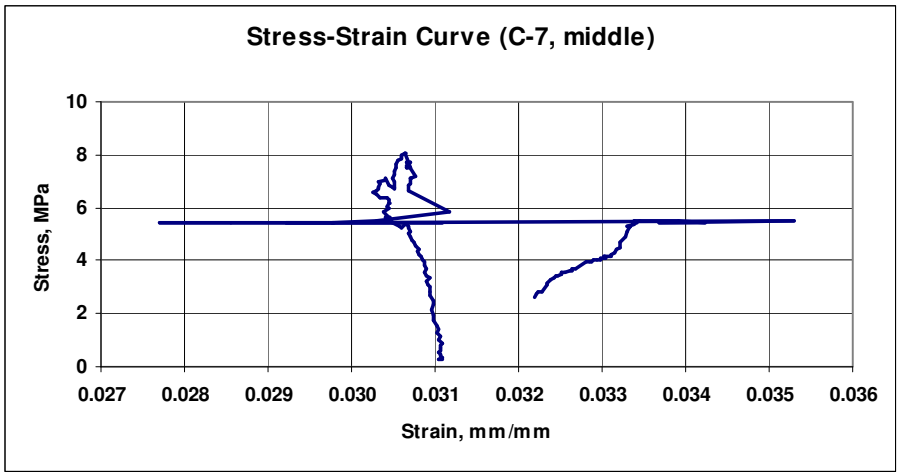

Fig. D.103 Stress versus Strain curve (CL between LDS #11&12 and LDS #13&14)

3.8 Wall ***C-8***

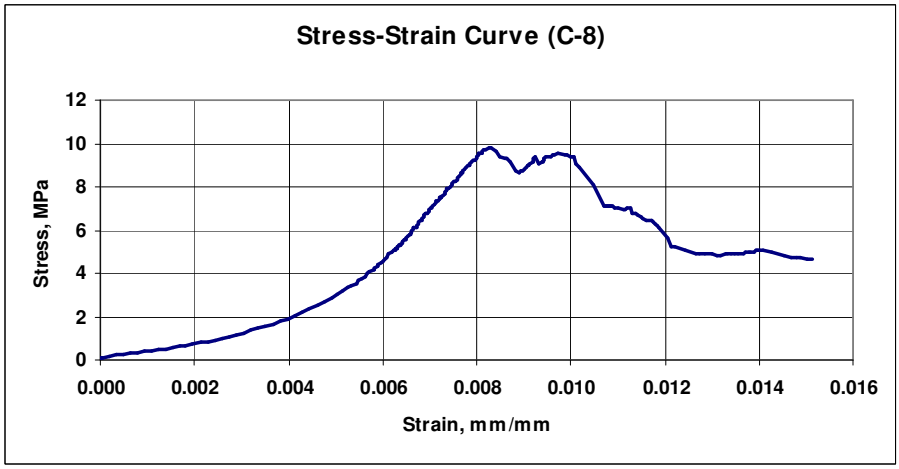

Fig. D.104 Stress versus Strain curve (CL between LDS #1 and LDS #2)

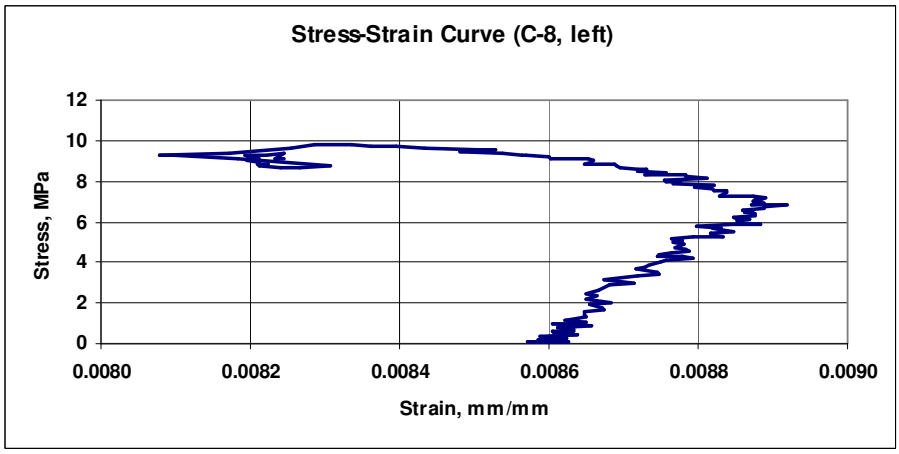

Fig. D.105 Stress versus Strain curve (CL between LDS #3&5 and LDS #8&10)

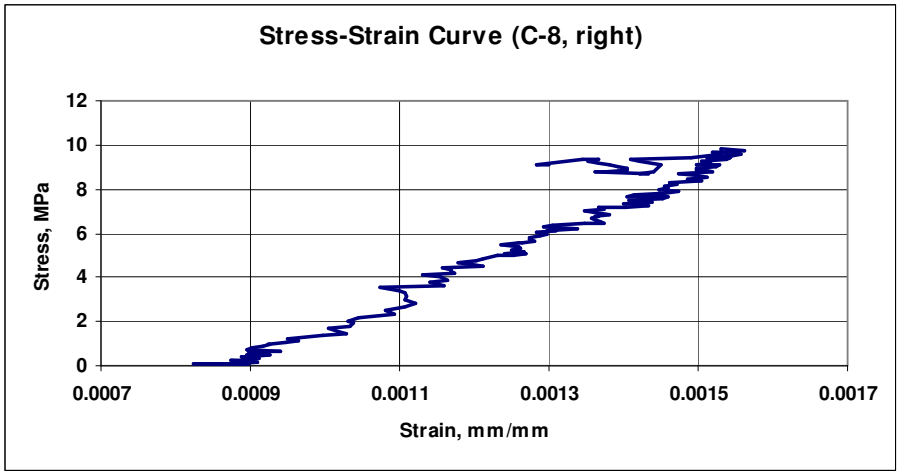

Fig. D.106 Stress versus Strain curve (CL between LDS #4&6 and LDS #7&9)

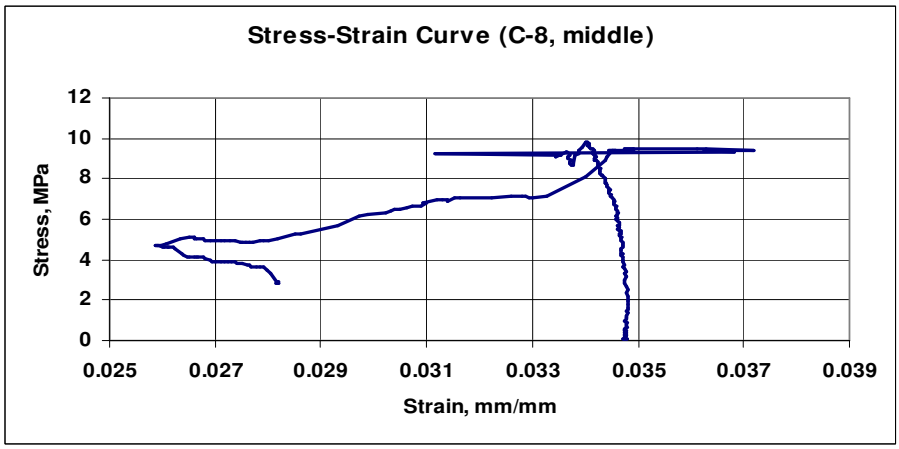

Fig. D.107 Stress versus Strain curve (CL between LDS #11&12 and LDS #13&14)

3.9 Wall ***C-9***

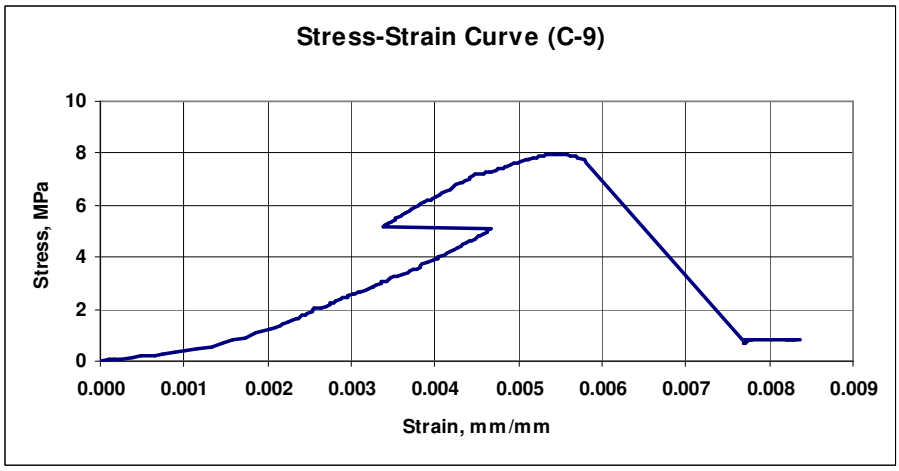

Fig. D.108 Stress versus Strain curve (CL between LDS #1 and LDS #2)

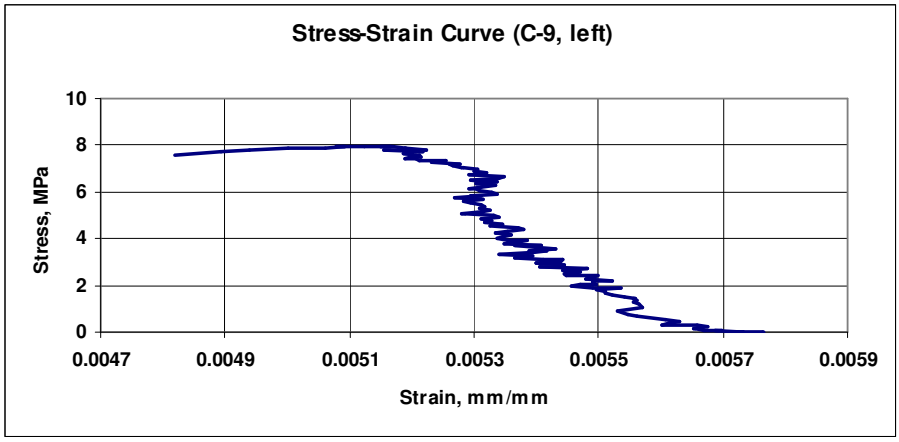

Fig. D.109 Stress versus Strain curve (CL between LDS #3&5 and LDS #8&10)

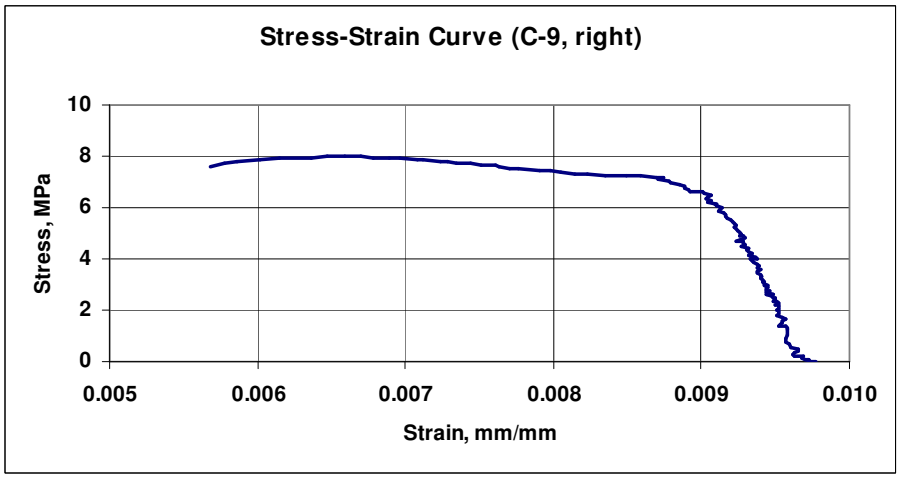

Fig. D.110 Stress versus Strain curve (CL between LDS #4&6 and LDS #7&9)

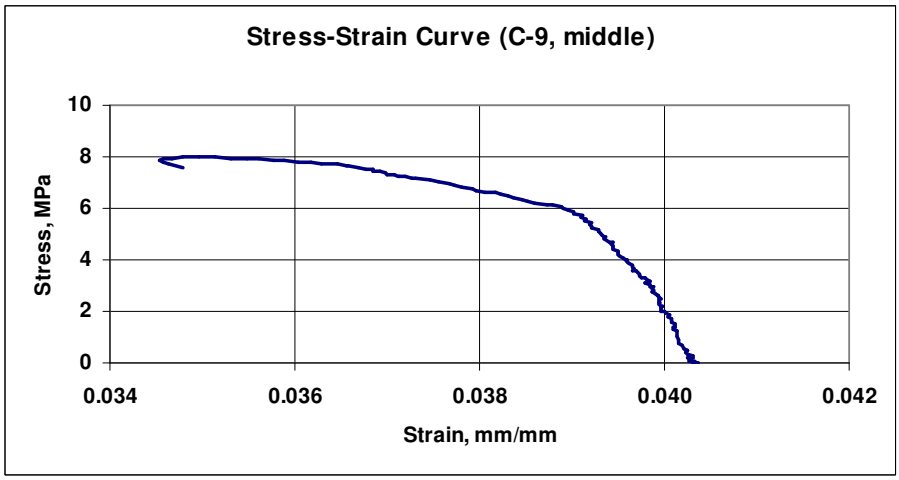

Fig. D.111 Stress versus Strain curve (CL between LDS #11&12 and LDS #13&14)

3.10 Wall *C-10*

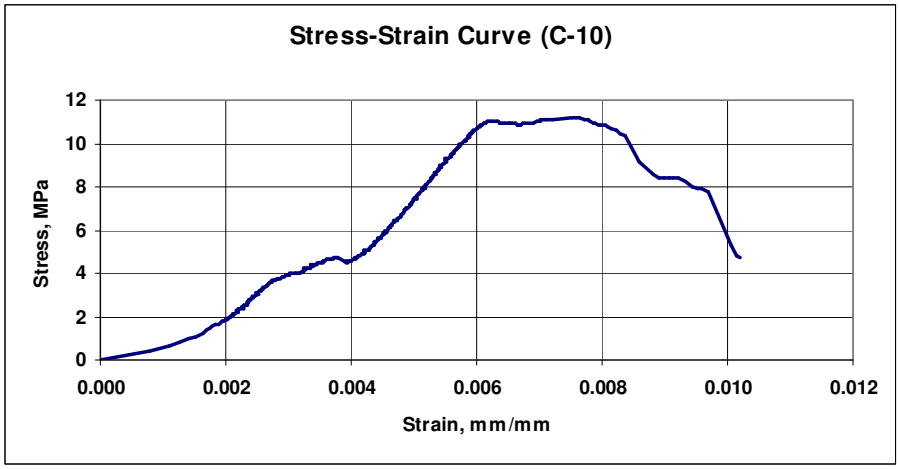

Fig. D.112 Stress versus Strain curve (CL between LDS #1 and LDS #2)

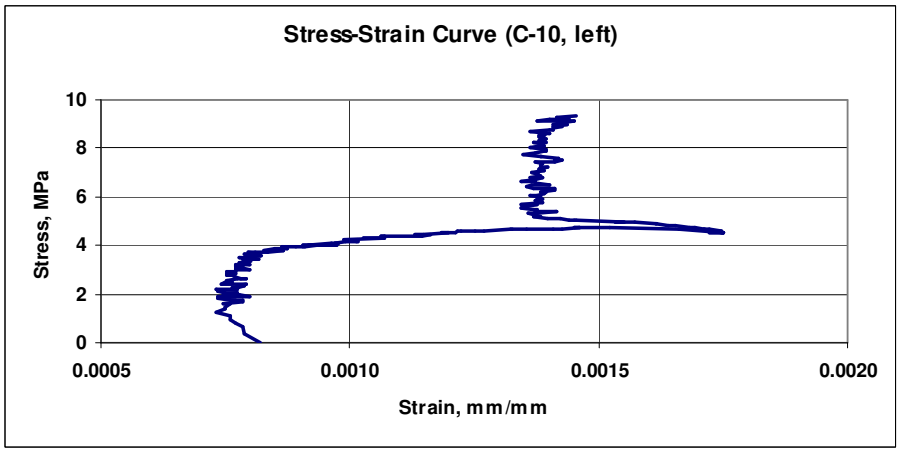

Fig. D.113 Stress versus Strain curve (CL between LDS #3&5 and LDS #8&10)

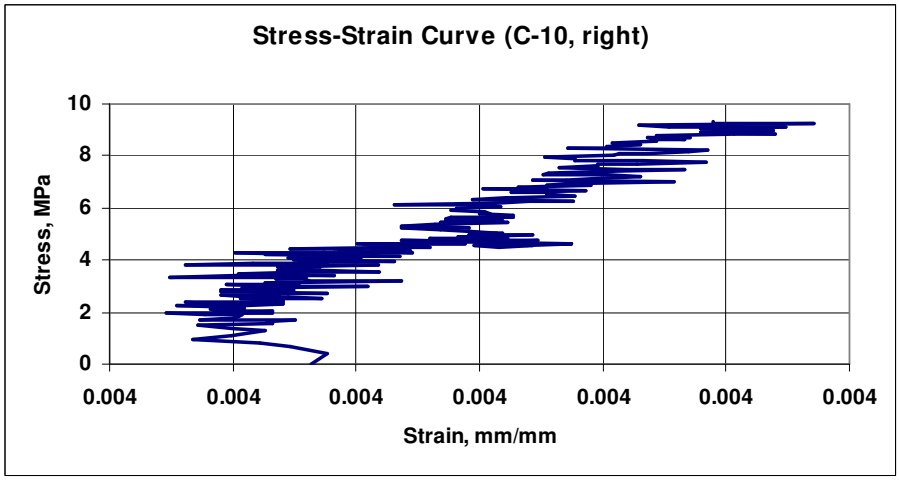

Fig. D.114 Stress versus Strain curve (CL between LDS #4&6 and LDS #7&9)

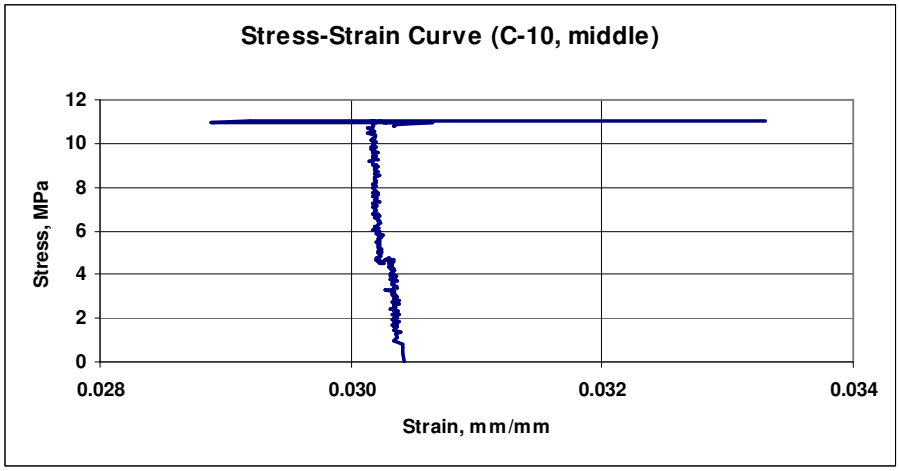

Fig. D.115 Stress versus Strain curve (CL between LDS #11&12 and LDS #13&14).

APPENDIX E

Summary of test results for component materials

This appendix presents the testing data of component materials:

1. Mortar specimens

2. Grout Specimens

3. Prisms

1. Test results for mortar specimens

Table E.1 Summation of test results for set #1 of mortar cylinders

Test on October 26, 2001				
Cylinder No.	Max Load kN	Max Displacement mm	Max Stress MPa	Max Strain mm/mm
Article III. M-1	27.50	0.114	5.991	0.0018
M-2	46.50	0.161	10.207	0.0025
M-3	46.80	0.191	10.244	0.0030
M-4	46.70	0.152	10.273	0.0024
M-5	55.50	0.267	12.176	0.0042
Average	**44.6**	**0.177**	**9.778**	**0.0028**

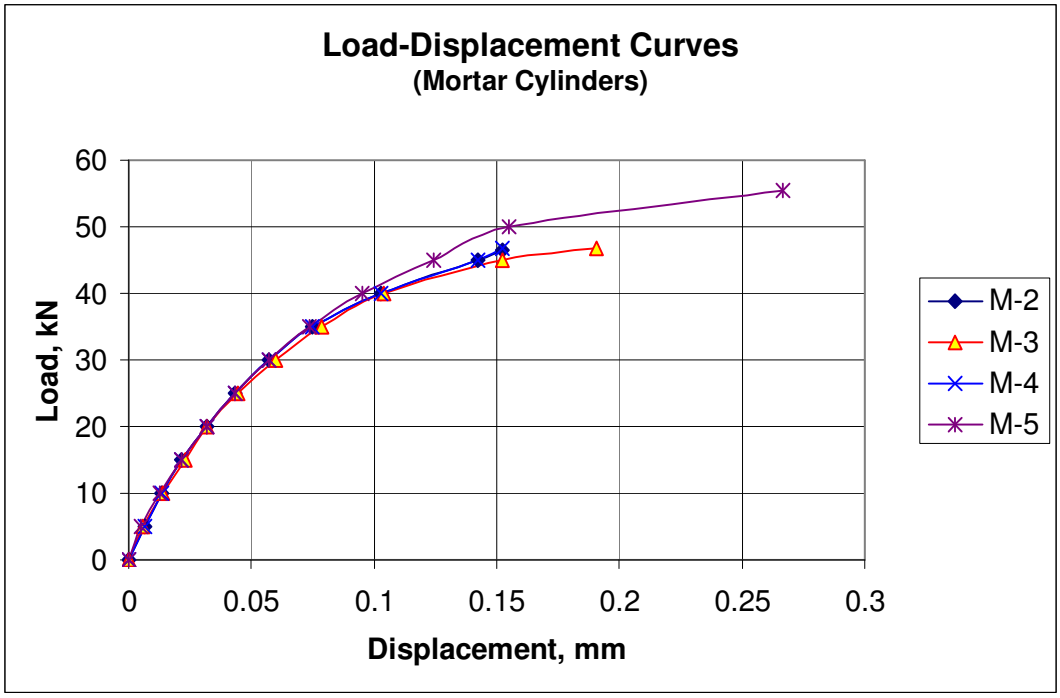

Fig. E.1 Load versus deflection curves for set #1 of mortar cylinders

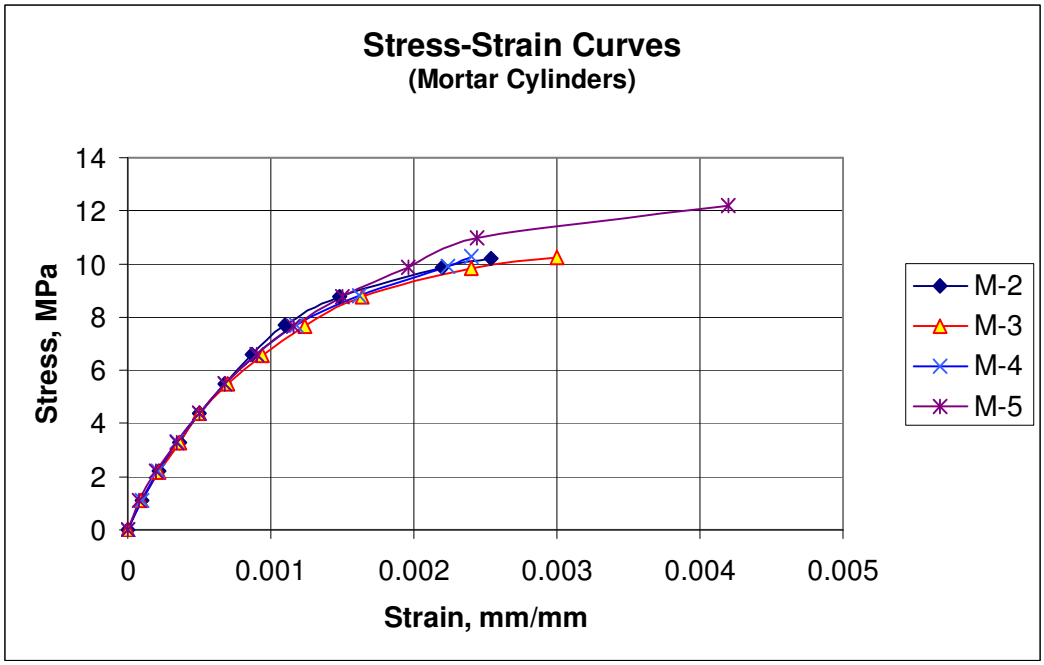

Fig. E.2 Stress versus strain curves for set #1 of mortar cylinders

Table E.2 Summation of test results for set #2 of mortar cylinders

Test on August 27, 2002				
Cylinder No.	**Max Load kN**	**Max Displacement mm**	**Max Stress MPa**	**Max Strain mm/mm**
M-6	72	0.127	12.751	0.0020
M-7	74	0.163	16.227	0.0026
M-8	72.5	0.179	15.906	0.0028
M-9	64	0.138	14.038	0.0022
M-10	72.5	0.183	15.935	0.0029
Average	**71**	**0.158**	**14.971**	**0.0025**

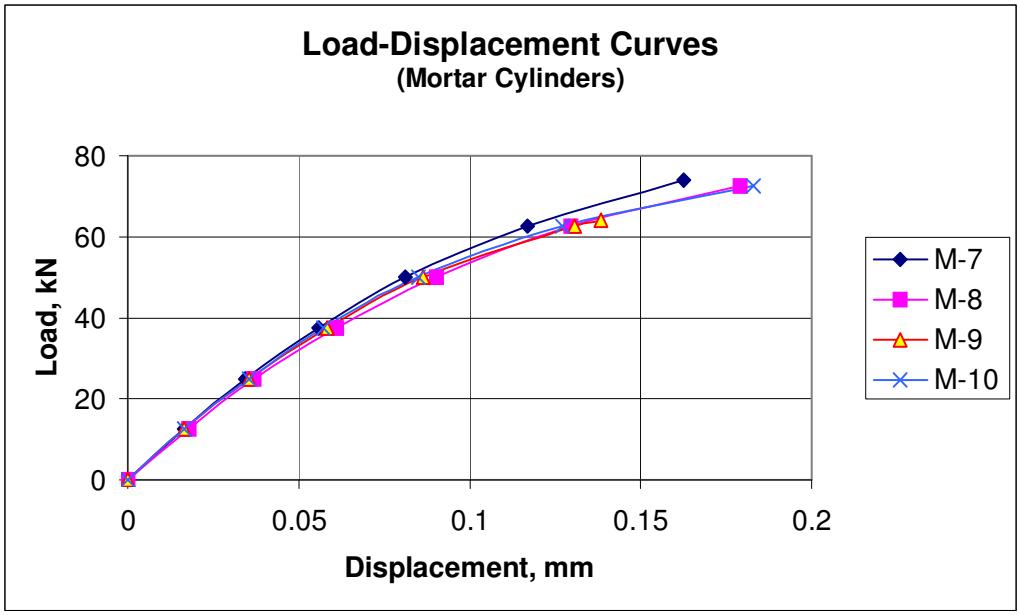

Fig. E.3 Load versus deflection curve for set #2 of mortar cylinders

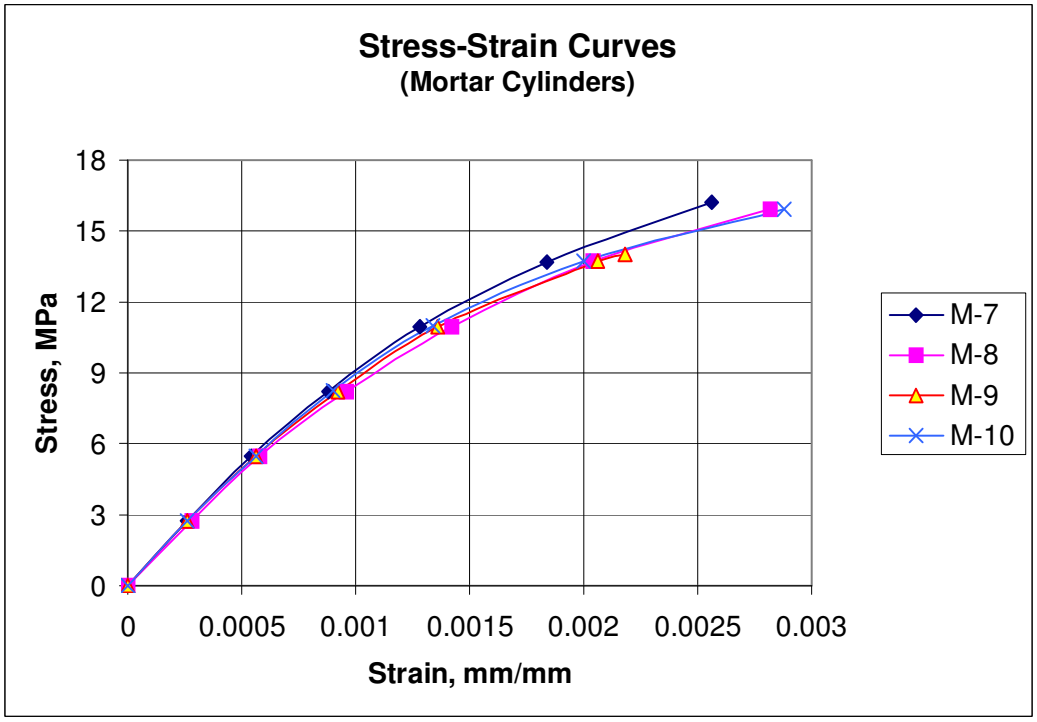

Fig. E.4 Stress versus strain curves for set #2 of mortar cylinders

2. Test results for grout specimens

Table E.3 Summation of test results for set #1 of grout cubes

Grout cubes					
Oct. 26/01					
	a	b	Article IV. rea mm2	Article V. oad kN	Stress MPa
GC-1	102.30	102.50	10485.75	248.00	23.65
GC-2	98.90	99.20	9810.88	198.00	20.18
GC-3	99.20	98.50	9771.20	195.00	19.96
GC-4	101.30	101.30	10261.69	205.00	19.98
GC-5	102.20	102.10	10434.62	185.00	17.73
Average		**Load = 206.20 kN**		**Stress = 20.30 MPa**	

Table E.4 Summation of test results for set #2 of grout cubes

Grout cubes					
Aug.15/02					
Cube	a	b	Area mm2	Load kN	Stress MPa
GC-6	103.30	103.50	10691.55	187.50	17.54
GC-7	102.90	102.20	10516.38	250.00	23.77
GC-8	101.20	101.50	10271.80	240.00	23.36
GC-9	98.30	99.30	9761.19	195.50	20.03
GC-10	102.20	102.90	10516.38	210.00	19.97
Average		**Load = 216.60 kN**		**Stress = 20.93 MPa**	

Table E.5 Summation of test results for set #1 of grout cylinders

Test on October 26, 2001				
Cylinder No.	**Max Load kN**	**Max Displacement mm**	**Max Stress MPa**	**Max Strain mm/mm**
G-1	80.00	0.0749	17.6814	0.00118
G-2	56.00	0.0572	12.2476	0.00090
G-3	81.00	0.1041	17.6688	0.00164
G-4	90.00	0.0940	19.6836	0.00148
G-5	81.00	0.1016	17.8553	0.00160
Average	**77.6**	**0.0864**	**17.0273**	**0.00136**

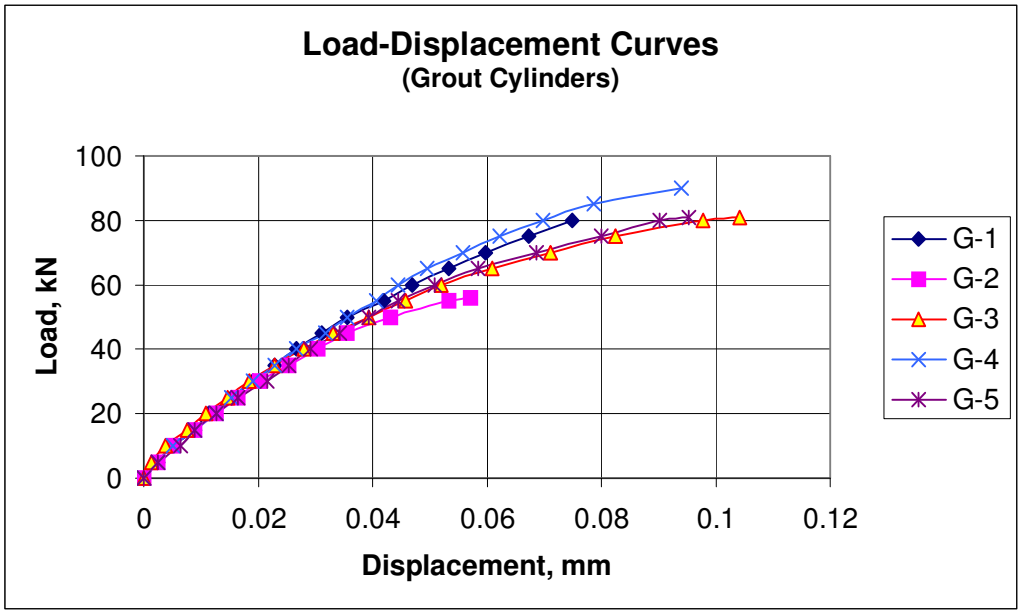

Fig. E.5 Load versus displacement curves for set #1 of grout cylinders

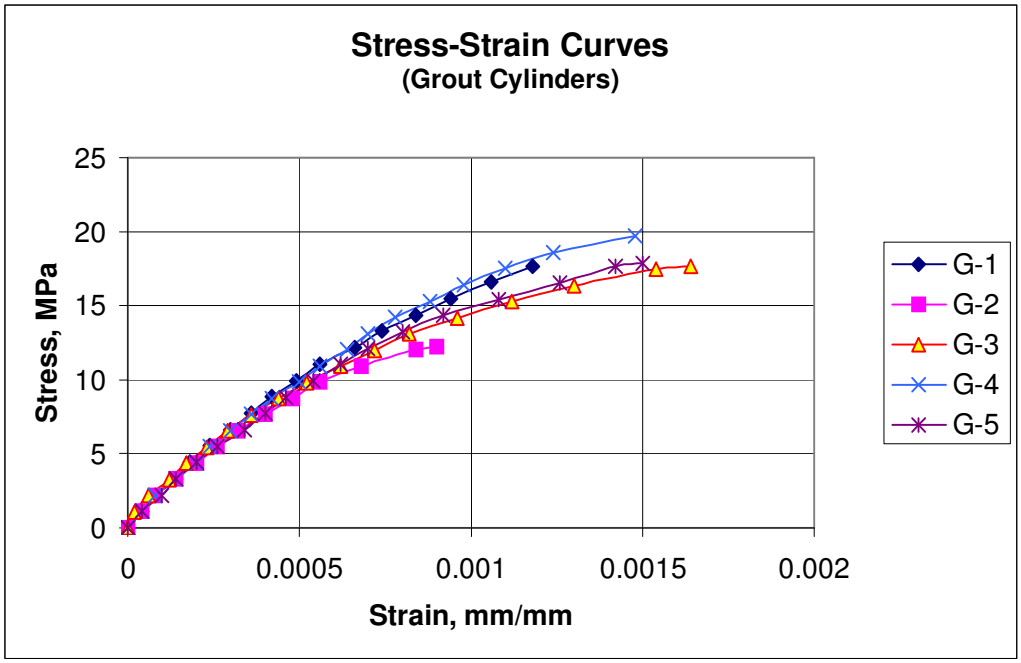

Fig. E.6 Stress versus strain curves for set #1 of grout cylinders

Table E.6 Summation of test results for set #2 of grout cylinders

Test on August 15, 2002				
Cylinder No.	**Max Load kN**	**Max Displacement mm**	**Max Stress MPa**	**Max Strain mm/mm**
G-6	75	0.0762	16.4245	0.00120
G-7	84.25	0.0533	18.4502	0.00084
G-8	71.75	0.0584	15.7872	0.00092
G-9	76.25	0.0597	16.7641	0.00094
G-10	84	0.0622	18.5655	0.00098
Average	**78.25**	**0.0620**	**17.1983**	**0.00098**

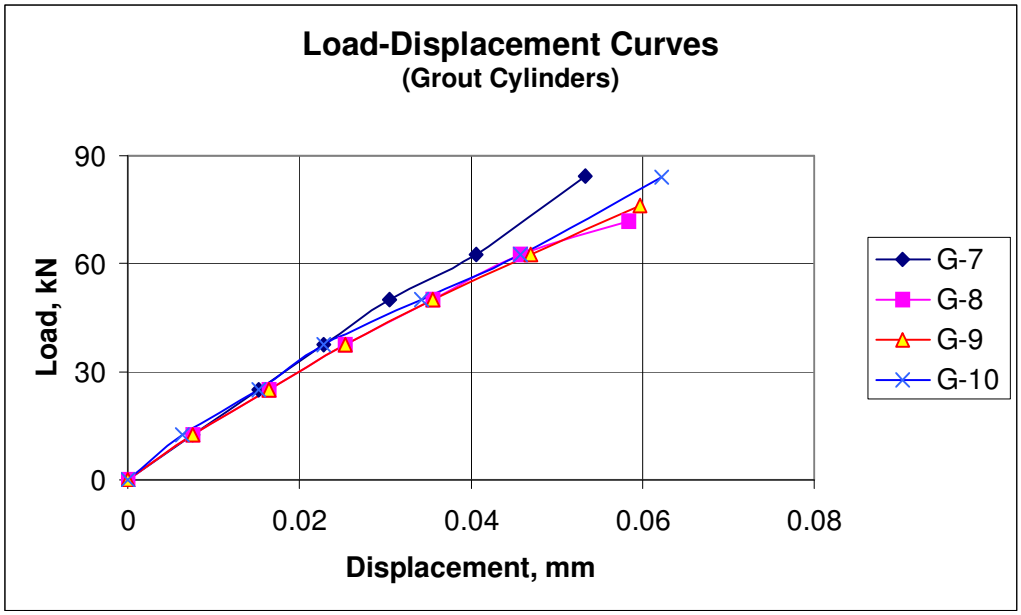

Fig. E.7 Load versus displacement curves for set #2 of grout cylinders

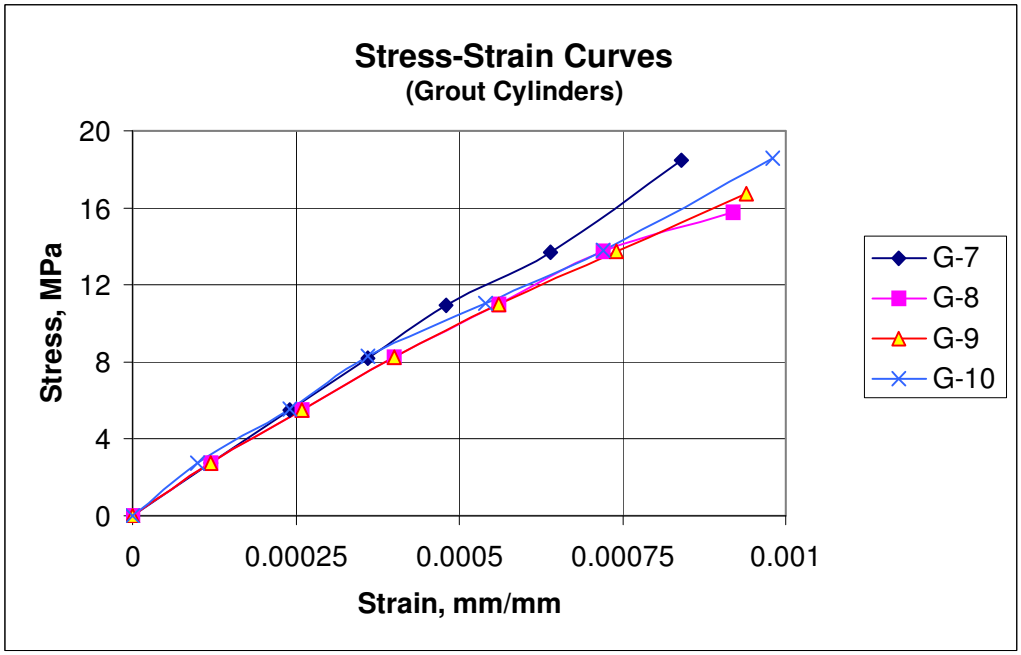

Fig. E.8 Stress versus strain curves for set #2 of grout cylinders

3. Test results for prisms

Table E.7 Summation of test results for set #1 of concrete prisms

Set #1 Test on February 27, 2002			
Prism No.	**Failure Load kN**	**Failure Stress MPa**	**Modulus of Elasticity MPa**
P-1	267.82	9.11	2506.80
P-2	295.03	10.03	3073.81
P-3	308.82	10.50	0ut of range
P-4	237.70	8.08	3536.99
P-5	259.47	8.82	2837.36
Average	**273.77**	**9.31**	**2988.74**
STDEV	28.382	0.965	433.20
COVAR	10.367%	10.367%	14.49%

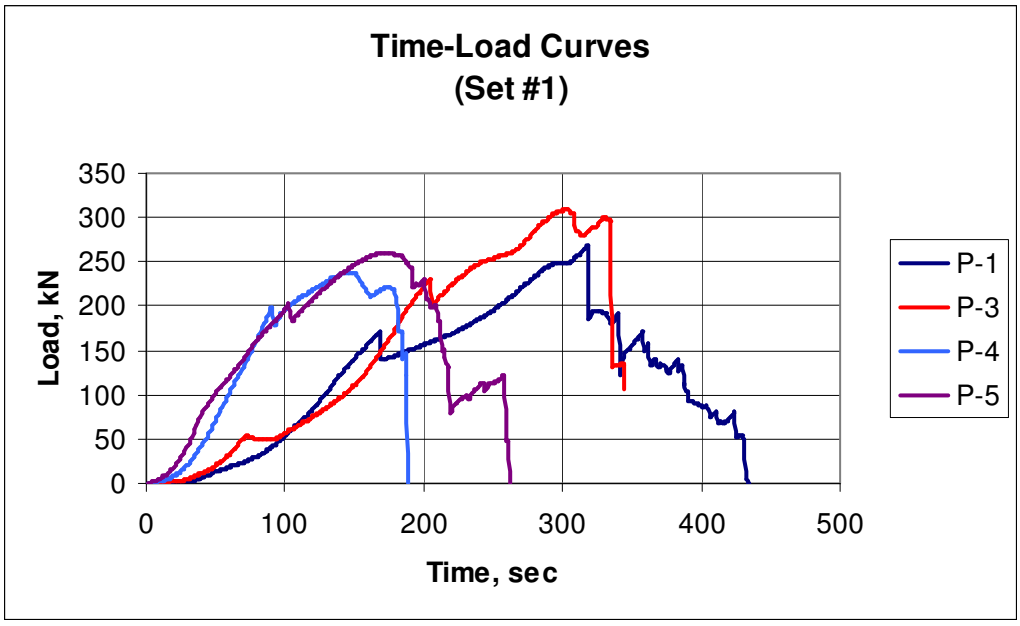

Fig. E.9 Time versus load curves for set #1 of concrete prisms

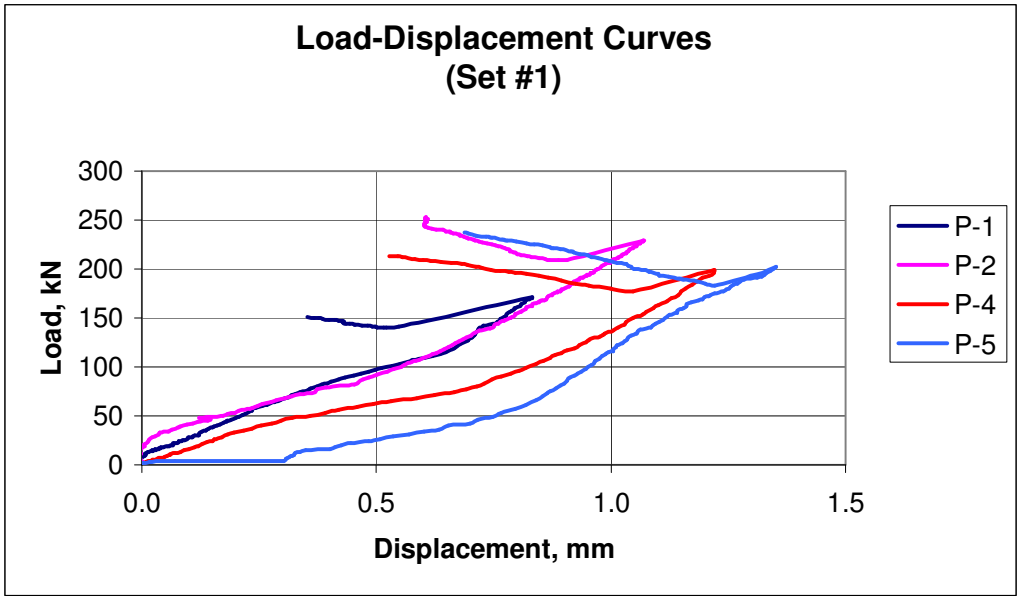

Fig. E.10 Load versus displacement curves for set #1 of concrete prisms

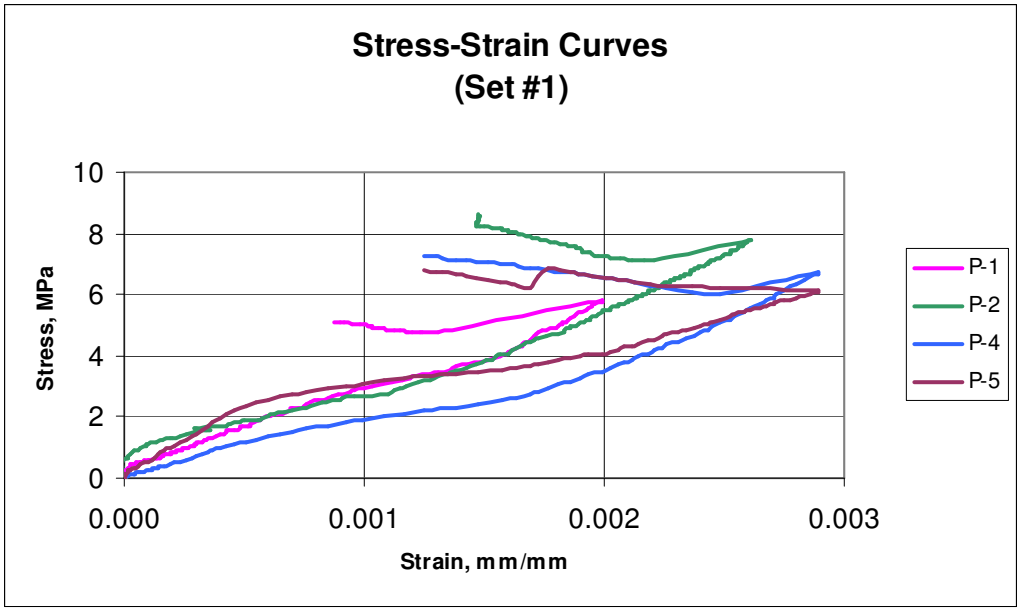

Fig. E.11 Stress versus strain curves for set #1 of concrete prisms

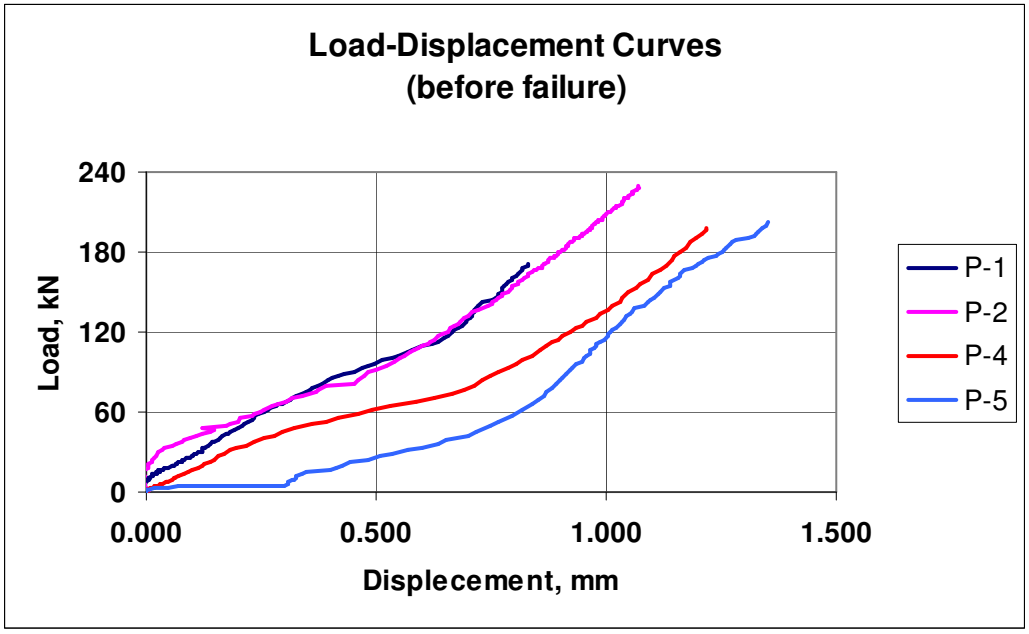

Fig. E.12 Load versus displacement curves (before failure) for set #1 of concrete prisms

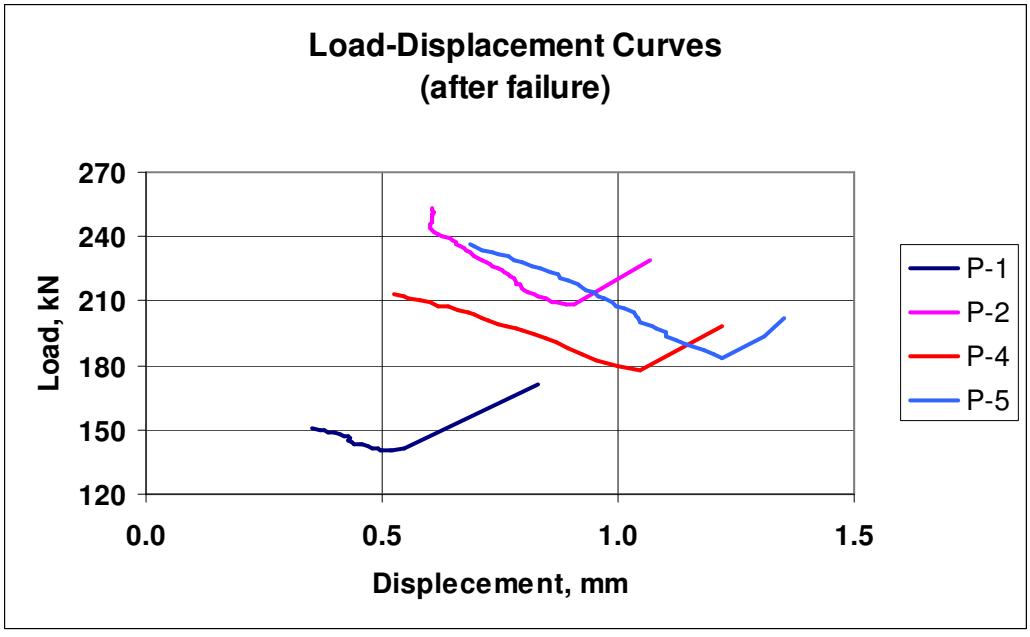

Fig. E.13 Load versus displacement curves (after failure) for set #1 of concrete prisms

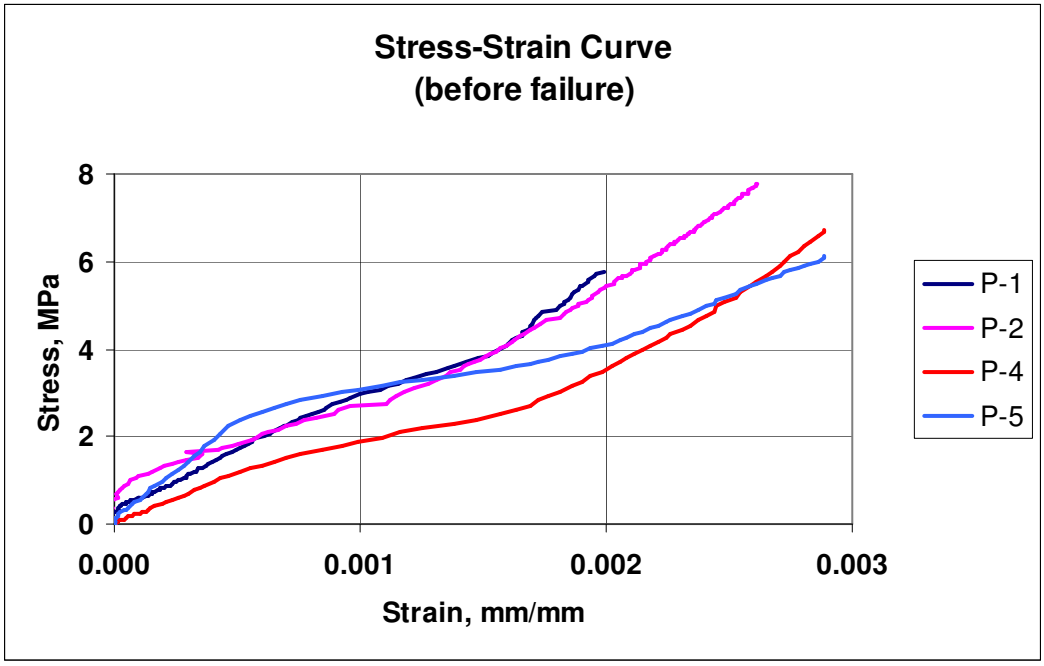

Fig. E.14 Stress versus strain curves (before failure) for set #1 of concrete prisms

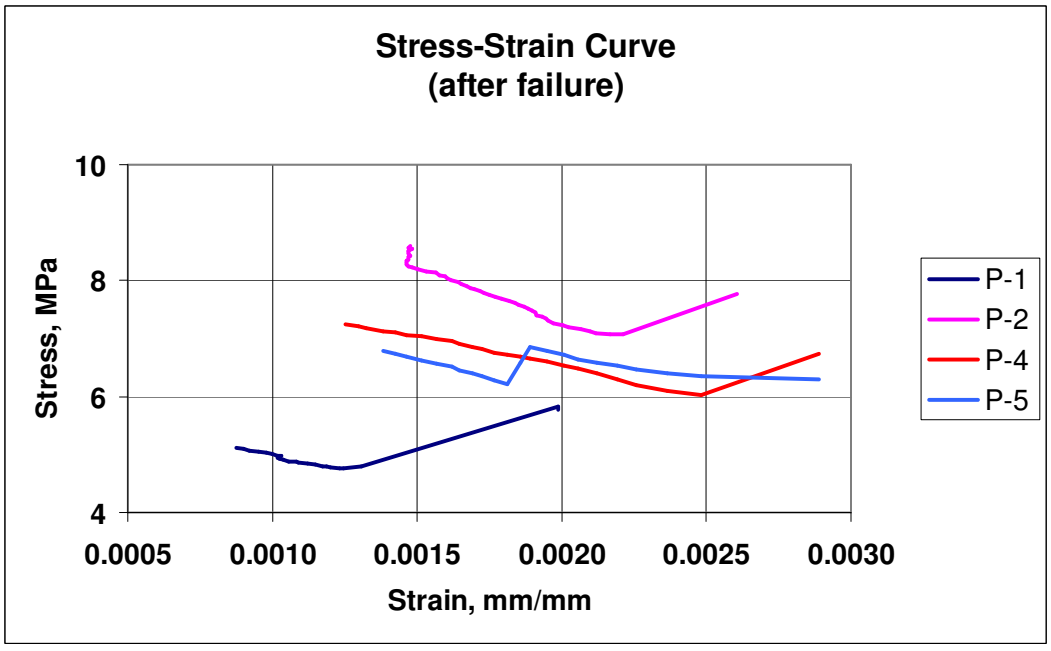

Fig. E.15 Stress versus strain curves (after failure) for set #1 of concrete prisms

Table E.8 Summation of test results for set #2 of concrete prisms

Article VI. **Set #2** Test on August 21, 2002		
Prism No.	**Failure Load kN**	**Failure Stress MPa**
P-6	321.55	10.93
P-8	339.61	11.55
Average	**330.58**	**11.24**
STDEV	12.774	0.434
COVAR	3.864%	3.864%

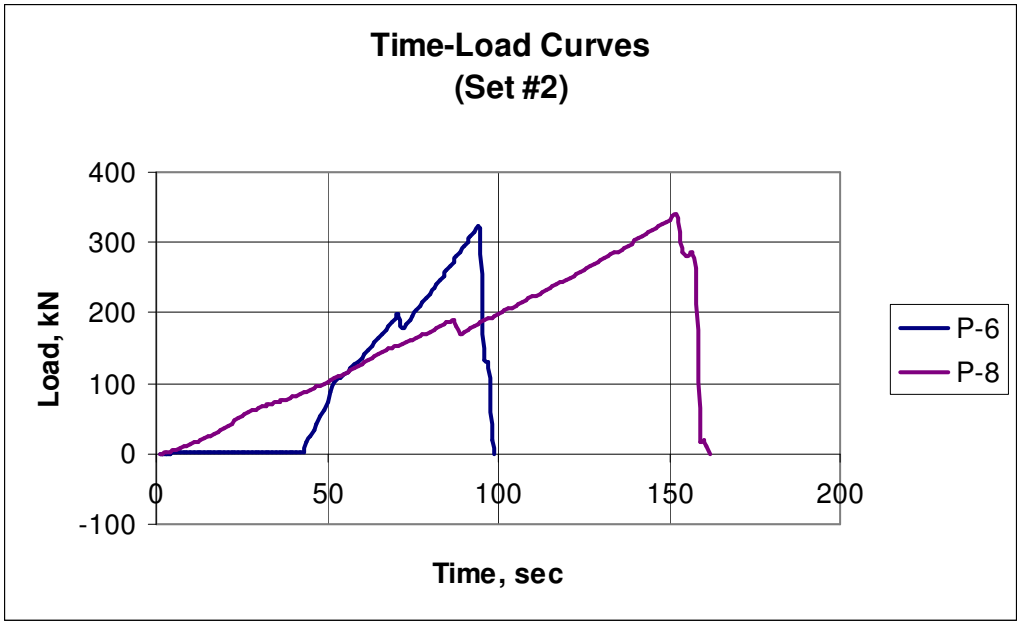

Fig. E.16 Time versus load curves for set #2 of concrete prism

APPENDIX F

Photos

This appendix presents the data of photos for the test specimens of types A, B and C and Test Prisms.

Test Specimens type ***A***

Photo F-1 Wall A-1 January 31/02, First crack appearance
Photo F-2 Wall A-1 Crack widening and spalling
Photo F-3 Wall A-1 Crack widening and spalling
Photo F-4 Wall A-1 Crack widening and bending
Photo F-5 Wall A-1 Prefailure
Photo F-6 Wall A-1 Failure
Photo F-7 Wall A-1 Failed Specimen
Photo F-8 Wall A-3 March 06/02, First crack
Photo F-9 Wall A-3 Shell spalling
Photo F-10 Wall A-3 Crack widening, LDSs taking away
Photo F-11 Wall A-4 March 11/02, First crack
Photo F-12 Wall A-4 Crack widening and spalling
Photo F-13 Wall A-4 Prefailure
Photo F-14 Wall A-5 March 12/02, First crack
Photo F-15 Wall A-5 Crack widening and spalling
Photo F-16 Wall A-5 Core column after testing (poor quality of bottom core)
Photo F-17 Wall A-7 August 16/02, Cracking and spalling
Photo F-18 Wall A-7 Crack widening
Photo F-19 Wall A-8 August 19/02, First crack
Photo F-20 Wall A-8 Crack widening and spalling
Photo F-21 Wall A-8 Prefailure
Photo F-22 Wall A-9 August 19/02, First crack
Photo F-23 Wall A-9 Spalling
Photo F-24 Wall A-9 Crack widening and spalling
Photo F-25 Wall A-10 August 19/02, First crack
Photo F-26 Wall A-10 Spalling

Test Specimens type ***B***

Photo F-27 Wall B-1 Feb. 28/02, First crack appearance
Photo F-28 Wall B-1 Prefailure
Photo F-29 Wall B-2 March 04/02, First crack
Photo F-30 Wall B-2 Crack widening
Photo F-31 Wall B-8 August 20/02, First crack
Photo F-32 Wall B-8 Crack widening
Photo F-33 Wall B-8 Prefailure
Photo F-34 Wall B-9 August 20/02, First crack
Photo F-35 Wall B-9 Wall splitting
Photo F-36 Wall B-9 Prefailure
Photo F-37 Wall B-9 Column after testing
Photo F-38 Wall B-10 August 20/02, First crack
Photo F-39 Wall B-10 Crack widening
Photo F-40 Wall B-10 Wall splitting

Test Specimens type ***C***

Photo F-41 Wall C-1 March 05/02, Crack widening and splitting
Photo F-42 Wall C-1 Grouted reinforced confined column after testing
Photo F-43 Wall C-2 March 06/02, First crack
Photo F-44 Wall C-2 Crack widening and bending
Photo F-45 Wall C-2 Failure
Photo F-46 Wall C-2 Grouted core after testing
Photo F-47 Wall C-5 August 14/02, First crack
Photo F-48 Wall C-5 Crack widening
Photo F-49 Wall C-5 Column after testing
Photo F-50 Wall C-6 August 14/02, Side cracking
Photo F-51 Wall C-6 Side splitting
Photo F-52 Wall C-6 Column after testing
Photo F-53 Wall C-7 August 15/02, Wide crack
Photo F-54 Wall C-7 Column after testing
Photo F-55 Wall C-8 August 14/02, Cracking and spalling
Photo F-56 Wall C-8 Cracking and spalling
Photo F-57 Wall C-9 August 16/02, First crack
Photo F-58 Wall C-9 Bending and spalling
Photo F-59 Wall C-9 Prefailure
Photo F-60 Wall C-9 Column after testing
Photo F-61 Wall C-10 August 16/02, First crack
Photo F-62 Wall C-10 Crack widening and spalling
Photo F-63 Wall C-10 Prefailure

Test Prisms

Test Specimens type *A*

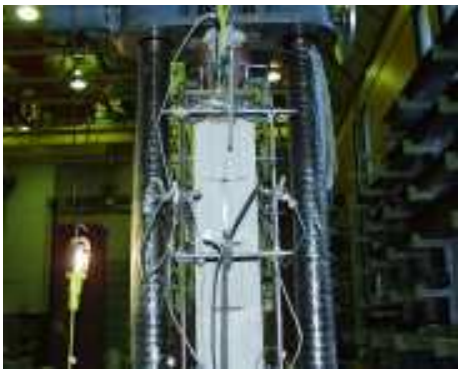

Photo F-1 Wall A-1 January 31/02, First crack appearance

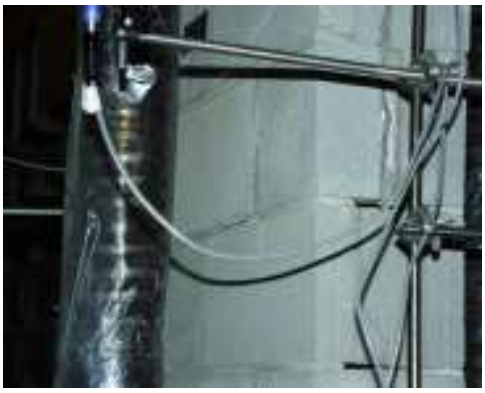

Photo F-2 Wall A-1 Crack widening and spalling

Photo F-3 Wall A-1 Crack widening and spalling

Photo F-4 Wall A-1 Crack widening and bending

Photo F-5 Wall A-1 Prefailure

Photo F-6 Wall A-1 Failure

Photo F-7 Wall A-1 Failed specimen

Photo F-8 Wall A-3 March 6/02, First crack

Photo F-9 Wall A-3 Shell spalling

Photo F-10 Wall A-3 Crack widening; LDSs taking away

Photo F-11 Wall A-4 March 11/02, First crack

Photo F-12 Wall A-4 Crack widening and spalling

Photo F-13 Wall A-4 Prefailure

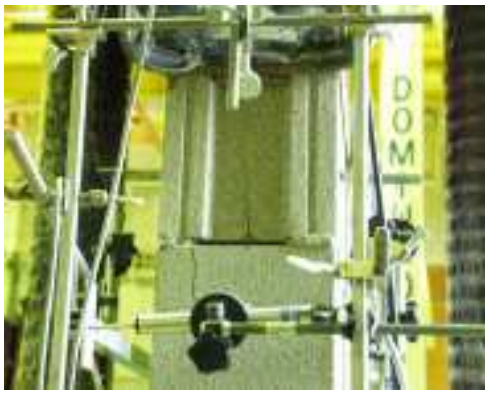

Photo F-14 Wall A-5 March 12/02, First cracks

Photo F-15 Wall A-5 Crack widening and spalling

Photo F-16 Wall A-5 Core column after testing (poor quality of bottom core)

Photo F-17 Wall A-7 August 16/02, Cracking and spalling

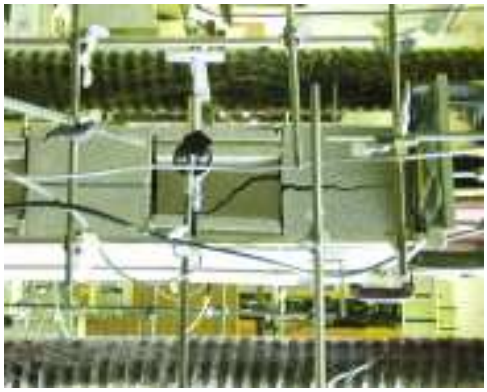

Photo F-18 Wall A-7 Crack widening

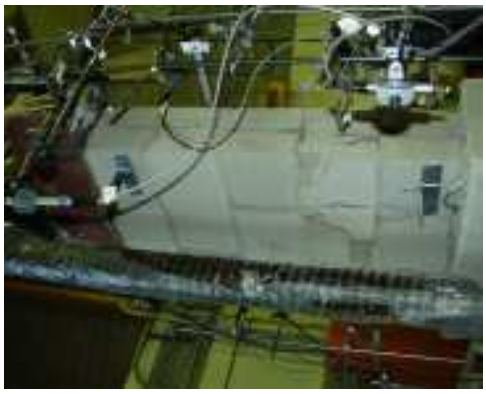

Photo F-19 Wall A-8 August 19/02, First crack

Photo F-20 Wall A-8 Crack widening and spalling

Photo F-21 Wall A-8 Prefailure

Photo F-22 Wall A-9 August 19/02, First crack

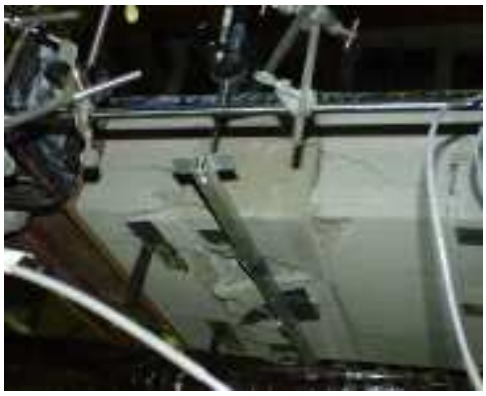

Photo F-23 Wall A-9 Spalling

Photo F-24 Wall A-9 Crack widening and spalling

Photo F-25 Wall A-10 August 19/02, First crack

Photo F-26 Wall A-10 Spalling

Test Specimens type *B*

Photo F-27 Wall B-1 February 28/02, First crack

Photo F-28 Wall B-1 Prefailure

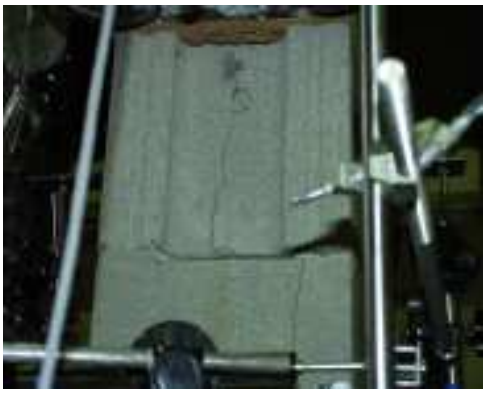

Photo F-29 Wall B-2 March 04/02, First cracks

Photo F-30 Wall B-2 Crack widening

Photo F-31 Wall B-8 August 20/02, First crack

Photo F-32 Wall B-8 Crack widening

Photo F-33 Wall B-8 Prefailure

Photo F-34 Wall B-9 August 20/02, First crack

Photo F-35 Wall B-9 Wall splitting

Photo F-36 Wall B-9 Prefailure

Photo F-37 Wall B-9 Column after testing

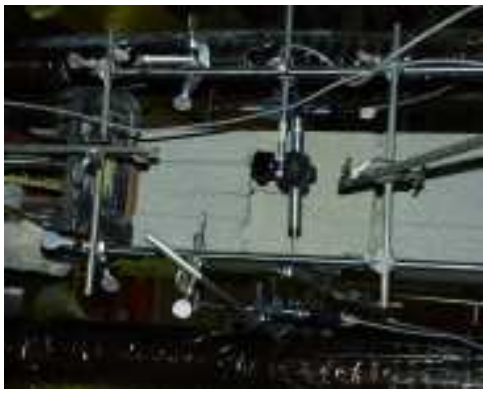

Photo F-38 Wall B-10 August 20/02, First crack

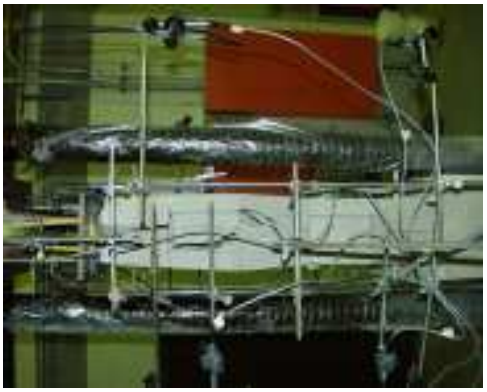

Photo F-39 Wall B-10 Crack widening

Photo F-40 Wall B-10 Wall splitting

Test Specimens type *C*

Photo F-41 Wall C-1 March 5/02, Crack widening and splitting

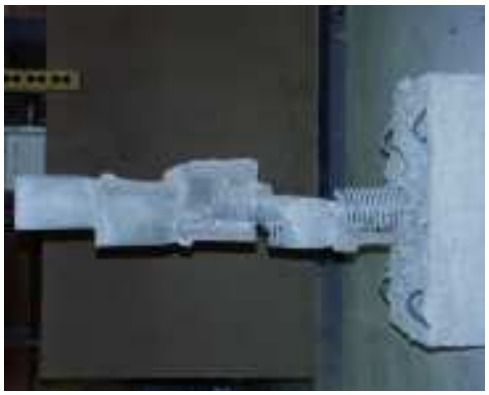

Photo F-42 Wall C-1 Grouted reinforced confined column after testing

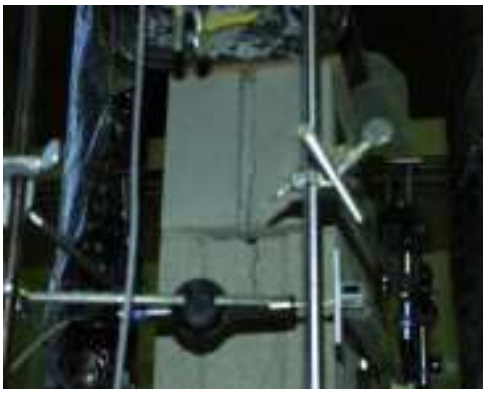

Photo F-43 Wall C-2 March 6/02, First crack

Photo F-44 Wall C-2 Crack widening and bending

Photo F-45 Wall C-2 Failure

Photo F-46 Wall C-2 Grouted core after testing

Photo F-47 Wall C-5 August 14/02, First crack

Photo F-48 Wall C-5 Crack widening

Photo F-49 Wall C-5 Column after testing

Photo F-50 Wall C-6 August 14/02, Side cracking

Photo F-51 Wall C-6 Side splitting

Photo F-52 Wall C-6 Column after testing

Photo F-53 Wall C-7 Wide crack

Photo F-54 Wall C-7 Column after testing

Photo F-55 Wall C-8 August 14/02, Cracking and spalling

Photo F-56 Wall C-8 Cracking and spalling

Photo F-57 Wall C-9 August 16/02, First crack

Photo F-58 Wall C-9 Bending and spalling

Photo F-59 Wall C-9 Prefailure

Photo F-60 Wall C-9 Column after testing

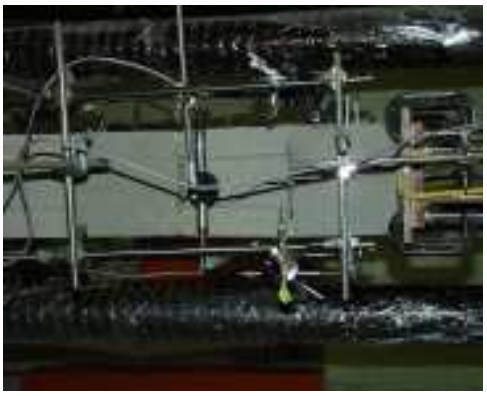

Photo F-61 Wall C-10 August 16/02, First crack

Photo F-62 Wall C-10 Crack widening and spalling

Photo F-63 Wall C-10 Prefailure

Test Prisms

Photo F-64 Prism P-6 First crack

Photo F-65 Prism P-6 Splitting and spalling

Photo F-66 Prism P-6 Side splitting

Photo F-67 Prism P-7 First crack

Photo F-68 Prism P-7 Failure

Photo F-69 Prism P-8 Side crack

Photo F-71 Prism P-8 Crack widening

Photo F-72 Prism P-8 Failure.

APPENDIX G

Calibration of instruments

This appendix presents the data of calibration for one load cell (LC) and fourteen linear-displacement sensors (LDS).

1. Load cell calibration data presented in Table G.1

2. Calibration data for Linear Displacement Sensors presented in Tables from G.2 to G.15:

Table G.2 Calibration data for LDS 1114
Table G.3 Calibration data for LDS 1115
Table G.4 Calibration data for LDS 1116
Table G.5 Calibration data for LDS 1117
Table G.6 Calibration data for LDS 1118
Table G.7 Calibration data for LDS 1119
Table G.8 Calibration data for LDS 1140
Table G.9 Calibration data for LDS 1141
Table G.10 Calibration data for LDS 1180
Table G.11 Calibration data for LDS 1181
Table G.12 Calibration data for LDS 0549
Table G.13 Calibration data for LDS 0585
Table G.14 Calibration data for LDS 12834
Table G.15 Calibration data for LDS 13553

1. Load Cell Calibration Data

To collect the load data an Artech load cell (Model No.1100/200-K, Serial No.84816; Output: 3001/200 mV/V; Weight: 3976 g) was used for axial compression tests during the experimental study.

At the start of tests the load cell was calibrated in the Structural Laboratory using a compression machine and a specially written computer program. The correlation factor was incorporated in the system and no correction of test data with respect to calibration was performed. The calibration data for load cell is presented in Table G.1.

Table G.1 Calibration data for Load Cell

Load Cell Model No.41/B92-01							
Load, kN	**Up**	**Down**	**(a)**	**(b) up**	**(d) down**	**(b) - (a)**	**(d) - (a)**
10.0	10.3825	10.6762	10.0	12.4885	12.2349	2.4885	2.2349
20.0	22.8710	22.9111	10.0	12.4851	12.4885	2.4851	2.4885
30.0	35.3561	35.3996	10.0	12.4914	12.4917	2.4914	2.4917
40.0	47.8475	47.8913	10.0	2.4926	2.4488	-7.5074	-7.5512
50.0	50.3401	50.3401	**Average:**			-0.0106	-0.0840
			Correlation factor:			**1.0473**	

2. Calibration data for Linear Displacement Sensors

Fourteen linear displacement sensors were used to collect the displacement data in axial compression of test specimens. Prior to testing all linear displacement sensors were calibrated in Structural Laboratory using micrometer and specially written computer program in Excel. The correlation factors were incorporated in the computer system and no correction of test data with respect to calibration of linear displacement sensors was performed. The calibration data is presented in Tables from G.2 to G.15.

Table G.2 Calibration data for LDS 1114

#1. LDS MG 1114 Model HS 50							
Micrometer	**LDS (up)**	**LDS (down)**	**(a)**	**(b) up**	**(d) down**	**(b) - (a)**	**(d) - (a)**
0	7.5274	7.5278	5	4.9966	5.0010	-0.0035	0.0010
5	12.5239	12.5288	5	5.0161	4.9731	0.0161	-0.0270
10	17.5400	17.5018	5	5.0051	5.0206	0.0051	0.0206
15	22.5450	22.5224	5	4.9800	4.9822	-0.0200	-0.0178
20	27.5250	27.5046	5	4.9955	5.0160	-0.0045	0.0160
25	32.5205	32.5205	**Average:**			-0.0014	-0.0015
			Correlation factor:			**1.0014**	

Table G.3 Calibration data for LDS 1115

#2. LDS MG 1115 Model HS 50							
Micrometer	**LDS (up)**	**LDS (down)**	**(a)**	**(b) up**	**(d) down**	**(b) - (a)**	**(d) - (a)**
0	9.2251	9.5275	5	4.9997	4.6889	-0.0003	-0.3111
5	14.2248	14.2164	5	4.9917	4.9689	-0.0084	-0.0311
10	19.2164	19.1853	5	5.0080	5.0132	0.0080	0.0132
15	24.2244	24.1985	5	4.9988	5.0132	-0.0013	0.0132
20	29.2231	29.2117	5	4.9879	4.9994	-0.0121	-0.0007
25	34.2110	34.2110	**Average:**			-0.0028	-0.0633
			Correlation factor:			**1.0331**	

Table G.4 Calibration data for LDS 1116

#3. LDS MG 1116 Model HS 50							
Micrometer	**LDS (up)**	**LDS (down)**	**(a)**	**(b) up**	**(d) down**	**(b) - (a)**	**(d) - (a)**
0	8.7986	8.7668	5	4.9870	4.9539	-0.0130	-0.0461
5	13.7856	13.7207	5	4.9664	4.9651	-0.0336	-0.0349
10	18.7520	18.6858	5	4.9651	4.9660	-0.0349	-0.0340
15	23.7171	23.6518	5	4.9438	4.9764	-0.0562	-0.0236
20	28.6609	28.6282	5	4.9438	4.9765	-0.0562	-0.0235
25	33.6047	33.6047	**Average:**			-0.0388	-0.0324
			Correlation factor:			**1.0356**	

Table G.5 Calibration data for LDS 1117

#4. LDS MG 1117 Model HS 50							
Micrometer	**LDS (up)**	**LDS (down)**	**(a)**	**(b) up**	**(d) down**	**(b) - (a)**	**(d) - (a)**
0	7.6793	7.6571	5	4.9938	4.9503	-0.0062	-0.0497
5	12.6731	12.6074	5	4.9277	4.9263	-0.0723	-0.0737
10	17.6008	17.5337	5	4.9405	4.9508	-0.0595	-0.0492
15	22.5413	22.4845	5	4.9578	4.9911	-0.0422	-0.0089
20	27.4991	27.4756	5	4.9064	4.9299	-0.0936	-0.0701
25	32.4055	32.4055	**Average:**			-0.0548	-0.0503
			Correlation factor:			**1.0525**	

Table G.6 Calibration data for LDS 1118

#5. LDS MG 1118 Model HS 50							
Micrometer	**LDS (up)**	**LDS (down)**	**(a)**	**(b) up**	**(d) down**	**(b) - (a)**	**(d) - (a)**
0	11.4371	11.4371	5	5.0373	5.0359	0.0373	0.0359
5	16.4744	16.4730	5	5.0345	4.9912	0.0345	-0.0088
10	21.5089	21.4642	5	5.0333	5.0359	0.0333	0.0359
15	26.5422	26.5001	5	5.0162	5.0359	0.0162	0.0359
20	31.5584	31.5360	5	5.0086	5.0310	0.0086	0.0310
25	36.5670	36.5670	**Average:**			0.0260	0.0260
			Correlation factor:			**0.9740**	

Table G.7 Calibration data for LDS 1119

#6. LDS MG 1119 Model HS 50							
Micrometer	**LDS (up)**	**LDS (down)**	**(a)**	**(b) up**	**(d) down**	**(b) - (a)**	**(d) - (a)**
0	5.5117	5.4904	5	5.0000	4.9697	0.0000	-0.0303
5	10.5117	10.4601	5	5.0048	4.9752	0.0048	-0.0248
10	15.5165	15.4353	5	4.9535	4.9727	-0.0465	-0.0273
15	20.4700	20.4080	5	4.9644	4.9995	-0.0356	-0.0005
20	25.4344	25.4075	5	4.9827	5.0096	-0.0173	0.0096
25	30.4171	30.4171	**Average:**			-0.0189	-0.0147
			Correlation factor:			**1.0168**	

Table G.8 Calibration data for LDS 1140

#7. LDS MG 1140 Model HS 50							
Micrometer	**LDS (up)**	**LDS (down)**	**(a)**	**(b) up**	**(d) down**	**(b) - (a)**	**(d) - (a)**
0	7.6178	7.6178	5	4.9557	4.9630	-0.0443	-0.0370
5	12.5735	12.5808	5	4.9976	4.9567	-0.0024	-0.0433
10	17.5711	17.5375	5	4.9767	4.9872	-0.0233	-0.0128
15	22.5478	22.5247	5	4.9439	4.9465	-0.0561	-0.0535
20	27.4917	27.4712	5	4.9824	5.0029	-0.0176	0.0029
25	32.4741	32.4741	**Average:**			-0.0287	-0.0287
			Correlation factor:			**1.0287**	

Table G.9 Calibration data for LDS 1141

#8. LDS MG 1141 Model HS 50							
Micrometer	**LDS (up)**	**LDS (down)**	**(a)**	**(b) up**	**(d) down**	**(b) - (a)**	**(d) - (a)**
0	7.0131	7.6178	5	4.9620	4.3419	-0.0380	-0.6581
5	11.9751	11.9597	5	4.9488	4.9466	-0.0512	-0.0534
10	16.9239	16.9063	5	4.9826	4.9905	-0.0174	-0.0095
15	21.9065	21.8968	5	4.9813	4.9905	-0.0187	-0.0095
20	26.8878	26.8873	5	4.9672	4.9677	-0.0328	-0.0323
25	31.8550	31.8550	**Average:**			-0.0316	-0.1526
			Correlation factor:			**1.0921**	

Table G.10 Calibration data for LDS 1180

#9. LDS MG 1180 Model HS 10							
Micrometer	**LDS (up)**	**LDS (down)**	**(a)**	**(b) up**	**(d) down**	**(b) - (a)**	**(d) - (a)**
0.0	0.3443	0.3408	2.5	2.4822	2.4792	-0.0178	-0.0208
2.5	2.8265	2.8200	2.5	2.4822	2.4822	-0.0178	-0.0178
5.0	5.3087	5.3022	2.5	2.4865	2.4872	-0.0135	-0.0128
7.5	7.7952	7.7894	2.5	2.4870	2.4928	-0.0130	-0.0072
10.0	10.2822	10.2822	**Average:**			-0.0155	-0.0147
			Correlation factor:			**1.0151**	

Table G.11 Calibration data for LDS 1181

#10. LDS MG 1181 Model HS 10							
Micrometer	**LDS (up)**	**LDS (down)**	**(a)**	**(b) up**	**(d) down**	**(b) - (a)**	**(d) - (a)**
0.0	0.1248	0.1240	2.5	2.4761	2.4736	-0.0239	-0.0264
2.5	2.6009	2.5976	2.5	2.4771	2.4756	-0.0229	-0.0244
5.0	5.0780	5.0732	2.5	2.4807	2.4822	-0.0193	-0.0178
7.5	7.5587	7.5554	2.5	2.4748	2.4781	-0.0252	-0.0219
10.0	10.0335	10.0335	**Average:**			-0.0228	-0.0226
			Correlation factor:			**1.0227**	

Table G.12 Calibration data for LDS 0549

#11. LDS MG 0549 Model HS 10							
Micrometer	**LDS (up)**	**LDS (down)**	**(a)**	**(b) up**	**(d) down**	**(b) - (a)**	**(d) - (a)**
0.0	0.3060	0.3054	2.5	2.4759	2.4730	-0.0241	-0.0270
2.5	2.7819	2.7784	2.5	2.4794	2.4763	-0.0206	-0.0237
5.0	5.2613	5.2547	2.5	2.4815	2.4828	-0.0185	-0.0172
7.5	7.7428	7.7375	2.5	2.4814	2.4867	-0.0186	-0.0133
10.0	10.2242	10.2242	**Average:**			-0.0205	-0.0203
			Correlation factor:			**1.0204**	

Table G.13 Calibration data for LDS 0585

#12. LDS MG 0585 Model HS 10							
Micrometer	**LDS (up)**	**LDS (down)**	**(a)**	**(b) up**	**(d) down**	**(b) - (a)**	**(d) - (a)**
0.0	0.6538	0.6523	2.5	2.4808	2.4779	-0.0192	-0.0221
2.5	3.1346	3.1302	2.5	2.4898	2.4845	-0.0102	-0.0155
5.0	5.6244	5.6147	2.5	2.4904	2.4935	-0.0096	-0.0065
7.5	8.1148	8.1082	2.5	2.4879	2.4945	-0.0121	-0.0055
10.0	10.6027	10.6027	**Average:**			-0.0128	-0.0124
			Correlation factor:			**1.0126**	

Table G.14 Calibration data for LDS 12834

#13. LDS MG 12834 Model HS 10							
Micrometer	**LDS (up)**	**LDS (down)**	**(a)**	**(b) up**	**(d) down**	**(b) - (a)**	**(d) - (a)**
0.0	1.0015	0.9992	2.5	2.4858	2.4828	-0.0142	-0.0172
2.5	3.4873	3.4820	2.5	2.5001	2.4926	0.0001	-0.0074
5.0	5.9874	5.9746	2.5	2.4993	2.5042	-0.0007	0.0042
7.5	8.4867	8.4788	2.5	2.4944	2.5023	-0.0056	0.0023
10.0	10.9811	10.9811	**Average:**			-0.0051	-0.0045
			Correlation factor:			**1.0048**	

Table G.15 Calibration data for LDS 13553

#14. LDS MG 13553 Model HS 10							
Micrometer	**LDS (up)**	**LDS (down)**	**(a)**	**(b) up**	**(d) down**	**(b) - (a)**	**(d) - (a)**
0.0	0.3825	0.3762	2.5	2.4885	2.4849	-0.0115	-0.0151
2.5	2.8710	2.8611	2.5	2.4851	2.4885	-0.0149	-0.0115
5.0	5.3561	5.3496	2.5	2.4914	2.4917	-0.0086	-0.0083
7.5	7.8475	7.8413	2.5	2.4926	2.4988	-0.0074	-0.0012
10.0	10.3401	10.3401	**Average:**			-0.0106	-0.0090
			Correlation factor:			**1.0098**	